Università degli Studi di Ferrara

UCA Universidad de Cádiz

INTERNATIONAL DOCTORAL COURSE IN
"EARTH AND MARINE SCIENCES (EMAS)"

CYCLE XXXIV

COORDINATOR Prof. COLTORTI MASSIMO

# EVOLUTION OF RESTORATION PROJECTS OF COASTAL WETLANDS: FROM TIDAL FLAT TO SALT MARSH

Scientific/Disciplinary Sector (SDS) GEO/04


**Candidate**
Dott. Riccardo Brunetta

**Supervisor**
Prof. Paolo Ciavola


Years 2018-2022

## Acknowledgments

It is reductive to say that this was the most amazing piece of my existence. I strongly thank Prof. Paolo Ciavola for following me since the end of my master and for making me part of the COSTUF team. I truly appreciate his trust in me and, most importantly, his way of working and managing the job life, despite all the problems that occur continuously. I'd like to thank Eng. Guido Selvi for giving me the possibility to study such an incredible place like the Po River Delta; a huge thank should go to Vittorio Negri who escorted me with the boat during every survey I made and his immense patience. For the first part of my PhD, I'd like to thank Clara Armaroli for her suggestions that helped me to get started. I thank Silvia Cilli and Edoardo Grottoli for introducing me to this world and helping me during fieldwork and having a lot of fun. I am thankful to Prof. Gloria Peralta, Maria Aranda Garcia, and Juan Montes (Universidad de Cadiz) for sharing their knowledge and giving me important help to continue my thesis. For my second part of the PhD, I want to thank my adventure companions Enrico Duo, Stefano Fabri, and Paola Souto Checcon. They are not only a wonderful team but most importantly my friends; work was never a weight and I had so much fun with them. In particular, thanks for being who you are; Enrico, for your precision and patience; Stefano, for your sense of equity and resoluteness; and Paola, for making me a little less naive. An immense thank should go to all the CBWES group and the Geomorphology and Biology team of Saint Mary's University, starting with Prof. Danika van Proosdji (whose image of her kayaking inside 12 meters of tidal range will never go away) for allowing me to be part of the team, learn and improve incredibly my knowledge about tidal flats and salt marshes, and see a different world and way of thinking. Huge thanks should go to Emma Poirer, Sam Lewis, Chaz Garraway, Megan Elliot, Anna Murphy, Moire Fecteau, Prof. Jeremy Lundholm, and Camila Fisher for their help on the field and outside the field. I'd like to thank all the people that supported me during the fieldwork, like Lorenzo Franzoni, Asrat Asresu, and my graduated students Enrico Ferrari and Francesco Miricola. Special thanks go to the technicians: Umberto Tessari, (while talking with him I learned more about the Italian language, sedimentology, and many other things than anywhere else) and Francesco Droghetti for his ability on creating indestructible things (I am not talking about the Panda, no no). I am deeply grateful to the reviewers of this thesis Tom Spencer (University of Cambridge) and Denise Reed (University of New Orleans) who gave fundamental suggestions and critics that allowed me to largely improve the final discussions and give an identity to the whole work. A general thank you to everyone who gave me even the smallest help during my thesis. One last important thank must go to the people who made and set

up who I am, guess who, my family and my friends. I am infinitely grateful firstly to Moco, Pone, and Ico and our equilibrium that I consider the fundamental strength and part of our existence. I am so grateful to everyone in the family, starting with those who helped me here in Ferrara, like uncle Uccio, Dina, Lisa, and Michael, but also with Uncle Isa, Uncle Dario, and all the other thousand Uncles. Finally, thank you to all of my friends for being who you are, from south Italy to north Italy, from Spain to Wien, from the Netherlands to Lithuania, from Canada to India, from all over the world. Every drop of experience is a blessing. Turn your worst situation into knowledge and exploit everything you can.

# Table of contents

*Acknowledgments* ..... 3
*Summary* ..... 9
*Riassunto* ..... 11
*List of figures* ..... 14
*List of tables* ..... 19
1. *Introduction* ..... 21
*1.1 Coastal wetlands: Tidal flats and salt marshes* ..... 21
*1.2 Coastal defences and Building-With-Nature* ..... 23
*1.3 Human-induced coastal wetlands* ..... 25
*1.3.1 The tidal flat of the Barbamarco lagoon (Po River Delta, Italy)* ..... 25
*1.3.2 The Perkpolder restoration project (Scheldt Estuary, The Netherlands)* ..... 27
*1.3.3 The Converse restoration project (Bay of Fundy, Canada)* ..... 27
*1.4 PhD thesis structure* ..... 30
2. *Evaluating Short-Term Tidal Flat Evolution Through UAV Surveys: A Case Study in the Po Delta (Italy)* .. 34
*2.1 Introduction* ..... 34
*2.2 Study Site* ..... 36
*2.3 Materials and Methods* ..... 39
*2.3.1 Fieldworks* ..... 39
*2.3.2 Photogrammetric Tests* ..... 41
*2.3.3 Validation of the DSMs* ..... 43
*2.3.4 Comparisons between Photogrammetric Tests* ..... 43
*2.3.5 DEM of Difference: Evolution of the Area* ..... 44
*2.3.6 Significance of the Vertical Differences* ..... 44
*2.3.7 Integrated Geomorphological Interpretation* ..... 45
*2.4 Results* ..... 46
*2.4.1 Tidal Flat Morphology* ..... 46
*2.4.2 Differences due to DSM Resolution* ..... 47
*2.4.3 DSM Error Assessment* ..... 49
*2.4.4 Differences due to Flight Altitude* ..... 49
*2.4.5 Morphological Changes* ..... 53
*2.5 Discussion* ..... 57
*2.5.1 Morphodynamic Interpretation* ..... 57
*2.5.2 UAV-based Tidal Flat Monitoring* ..... 65
*2.6 Conclusions* ..... 73
3. *Sedimentary evolution of a young tidal flat in the Northern part of the Po Delta (Italy)* ..... 75

*3.1 Introduction* ..... 75
*3.1.1 Sedimentation in tidal flats and salt marshes* ..... 75
*3.1.2 Aims of the paper* ..... 76
*3.2 Study site* ..... 76
*3.2.1 The Po River Delta* ..... 76
*3.2.2 Geomorphology and Sedimentology of the Delta* ..... 79
*3.2.3 The Barbamarco Lagoon and study area* ..... 80
*3.3 Methodology* ..... 81
*3.3.1 Coring and sediment characterization* ..... 81
*3.3.2 Sediment traps for the analysis of deposition rates* ..... 83
*3.4 Results* ..... 88
*3.4.1 Granulometric and LOI distribution* ..... 88
*3.4.2 Sediment deposition* ..... 92
*3.5 Discussion* ..... 98
*3.5.1 Tidal flat formation* ..... 98
*3.5.2 Depositional patterns* ..... 102
*3.5.3 Sediment deposition in microtidal flats* ..... 105
*3.6 Conclusions* ..... 106
*4. Evolution of tidal flats in the Northern part of the Po Delta: a strategy for future building-with-nature management* ..... 108
*4.1 Introduction* ..... 108
*4.1.1 Building-with-nature approach* ..... 108
*4.1.2 Salt marsh and tidal flats* ..... 109
*4.2 Study site* ..... 110
*4.2.1 The story of the Po River Delta* ..... 110
*4.2.2 The tip of the Delta* ..... 111
*4.3 Methodology* ..... 114
*4.3.1 Orthophotos* ..... 114
*4.3.2 Tidal records and flow discharge analysis* ..... 115
*4.3.3 The tidal flat of the Barbamarco lagoon and vegetation distribution* ..... 116
*4.4 Results* ..... 116
*4.4.1 Historical evolution* ..... 116
*4.4.2 MHT variations and Spartina distribution* ..... 125
*4.5 Discussion* ..... 127
*4.5.1 The tidal flat of the Barbamarco lagoon* ..... 127
*4.5.2 From tidal flat to salt marsh* ..... 129
*4.6 Conclusions* ..... 133

5. Morphological Evolution of an Intertidal Area Following a Set-Back Scheme: A Case Study From the Perkpolder Basin (Netherlands) ..... 134
5.1 Introduction ..... 134
5.2 Study site ..... 137
5.3 Methodology ..... 139
5.3.1 Morphological analysis ..... 139
5.3.2 Particles Size Analysis (PSA) ..... 142
5.3.3 Measurement of sedimentation rate across the tidal flat ..... 142
5.3.4 Loss On Ignition analysis ..... 144
5.4 Results ..... 144
5.4.1 Morphological datasets ..... 144
5.4.2 Surface sediment characteristics ..... 148
5.4.3 Sedimentation rates ..... 149
5.4.4 Loss On Ignition ..... 150
5.4.5 Inlet morphology ..... 150
5.5 Discussion ..... 152
5.5.1 Sedimentological characteristics of the tidal flat ..... 152
5.5.2 Sediment budget of the tidal flat ..... 153
5.5.3 Salt marsh formation ..... 154
5.5.4 Comparison with other case studies in the North Sea area ..... 156
5.6 Conclusions ..... 159
6. Sedimentological characteristics of young marshes in the Bay of Fundy (Canada). ..... 160
6.1 Introduction ..... 160
6.2 Study site ..... 160
6.3 Methodology ..... 165
6.3.1 Converse ..... 165
6.3.2 Halfway River and Eldriken ..... 168
6.4 Results ..... 169
6.4.1 Sediment traps validation and rates of deposition ..... 169
6.4.2 Volumes and vertical changes of the tidal flat of Converse ..... 173
6.4.4 Granulometric distribution ..... 177
6.5 Discussion ..... 178
6.5.1 Sediment deposition ..... 178
6.5.2 Morphological evolution of the tidal flat of Converse ..... 180
6.5.3 Future evolution of the salt marshes ..... 181
6.6 Conclusions ..... 182
7. Evolution of coastal wetlands restoration projects: natural vs artificial tidal flats ..... 184

*7.1 Introduction* ..... *184*
*7.2 Study sites* ..... *185*
*7.2.1 Barbamarco lagoon (Po River Delta, Italy)* ..... *185*
*7.2.2 Perkpolder (The Netherland)* ..... *185*
*7.2.3 Converse (Bay of Fundy, Canada)* ..... *186*
*7.2 Methodology* ..... *187*
*7.2.1 Po River Delta (Italy) and the Converse tidal flat (Canada)* ..... *187*
*7.2.2 Perkpolder (The Netherland)* ..... *187*
*7.2.2 Tide gauge analysis and pioneer vegetation* ..... *189*
*7.3 Results* ..... *190*
*7.3.1 Deposition and accretion of young tidal flats* ..... *190*
*7.3.2 Sediment budget and inlets erosion* ..... *192*
*7.3.3 Tide gauges and Spartina spp. distribution* ..... *197*
*7.4 Discussion* ..... *198*
*7.4.1 Vertical variations and sediment deposition in human-induced tidal flats* ..... *198*
*7.4.2 Artificial morphologies affect the evolution of restoration projects* ..... *200*
*7.4.3 Morphological evolution of restoration projects* ..... *204*
*7.4.4 The transition from tidal flat to salt marsh* ..... *206*
*7.4.5 Final considerations* ..... *208*
*8. Final conclusions* ..... *210*
*8.1 Restoration in the Po delta system* ..... *210*
*8.2 The restoration project of Perkpolder (The Netherlands)* ..... *211*
*8.3 The restoration project of Converse (Canada)* ..... *211*
*8.4 Restoration projects from microtidal to macrotidal environments* ..... *212*
*8.5 Future improvements* ..... *212*
*9. References* ..... *214*

## Summary

The way we conceive coastal defences has profoundly changed during the last decades and, as a result, our approach to the coastal environment has been modified as well. New management realignment strategies are being explored, and natural-based solutions are preferred to traditional coastal structures, such as dykes, seawalls, and groins. Several restoration projects were applied in coastal wetlands nowadays focusing on landscape recovery and a new equilibrium between natural and anthropic structures.

This PhD thesis combines geomorphological and sedimentological analysis (i.e. drone surveys, sediment traps, sediment coring, historical orthophotos) with a multi-disciplinary approach to study the evolution of young tidal flats located worldwide, which origin was caused by human intervention, specifically due to the breach of a dyke or a channel excavation that has connected the sediment supplier with an intertidal area that was not a tidal flat. Three study sites were chosen based on their environmental characteristics and the tidal range: i) the tidal flat of the Barbamarco lagoon, located in the Po River Delta (microtidal) in Italy, ii) the artificial tidal flat of Perkpolder (macrotidal) located in the Scheldt Estuary in The Netherland, and iii) the management realignment of Converse (ultratidal) located in the Bay of Fundy in Canada. The analyses were improved by fieldwork carried out in the accidental marsh of Halfway River, and the marsh of Eldriken, which are other tidal flats located in the Bay of Fundy. The study aims to define the sedimentological evolution of different human-induced tidal flats, to discuss the processes that have led to their present conditions, and to understand whether and how the transition from flat to marsh will occurr, defining which factors should be considered for future restorations.

The first part of the PhD focused on fieldwork activities carried out on the tidal flat of the Barbamarco lagoon in the Po Delta (Italy). Several UAV (Unmanned Aerial Vehicle) surveys were performed between October 2018 and October 2020 and a collection of DSMs (Digital Surface Model) were processed. The granulometric distribution was achieved through core sampling and the rates of deposition were obtained using an innovative structure for Petri dish sediment traps that were built with a 3D printer. A historical review was accomplished using orthophotos acquired from the IGM (Istituto Geografico Militare Italiano) and the Veneto Region archives, from the 1950s until nowadays; the investigation was then extended to the lagoons of the whole tip of the Delta. Results gave important interpretations about the evolution of the tidal flat, indicating that the river is the sediment supplier, and during the last 20 years, it provided sediment for the

Barbamarco and other lagoons as well, like the Burcio lagoon, where a rapid marsh developed between 2011 and 2013, after a strong sediment injection.

Between fieldwork and data processing, the tidal flat of Perkpolder (The Netherland) was investigated using a dataset of Lidar provided by Rijkswaterstaat (Dutch Ministry of Infrastructure and the Environment) and rates of deposition that were obtained by the author during the master thesis (2017-2018). The results highlighted that, despite the rapid sediment accretion of the system, no vegetation has been established (until the last studies of 2018) and the tidal flat needs no less than a decade to meet the right conditions for a salt marsh to develop.

General knowledge regarding salt marshes and data processing were improved during a short period at the University of Cadice (Spain) (second year of the PhD). During the last year of the PhD, a period of three months at Saint Mary's University in Halifax (Nova Scotia, Canada) allowed investigating the evolution of the restoration site of Converse (Bay of Fundy). A field campaign was carried out between 23 and 26 July 2021 and several measurements were achieved (i.e. hydrodynamics, hydrology, sediment deposition, suspended sediment). The author participated actively in the measurements that regarded ADCP, ADV's, RBR turbidity sensor, M9 bathymetric surveys, sediment filter traps, suspended sediment collector, ISCO bottles; particle size analysis was then accomplished using the sediment collected by the traps. However, in this thesis, the results concern sediment deposition, particle size analysis, and water level variations. In addition, further analyses of sediment deposition were carried out in two different sites from the southern basin of the Bay of Fundy between 12 – 13 August 2021: Halfway River and Eldriken. The collected data were compared with the site of Converse and improved the final discussion.

The combination of the results from all study sites, which is discussed in the final part of the thesis, enhanced how artificial morphologies led to morphodynamic instability that alter the rates of deposition and, consequently, future insights. The strong erosion of the inlets and the strong accretion inside the tidal flats suggest that a cannibalization process might be ongoing, causing an increase in the rates of vertical variations for the short-term evolution. The analysis showed how vegetation growth is strongly linked to elevation with respect to the MHT (Mean High Tide) and the sediment supplier. From a morphological point of view, if the tidal flat is not located between the vertical range of any low marsh species, the surface needs to accrete and increase in elevation, but this can only happen if the sediment input is positive and constant in time. Salt marsh restoration can be a quick process (i.e. few years) but it can take longer periods (i.e. decades).

Future management realignments of coastal wetlands should consider how the design affects the future evolution of the morphology, the rates of sediment deposition, and the elevation of artificial tidal flats with respect to the MHT as a preliminary evaluation to predict the waiting time for salt marsh development.

## Riassunto

Negli ultimi decenni, la concezione di difesa costiera è profondamente cambiata e, come risultato, lo è anche il nostro approccio all'ambiente costiero. Nuove strategie di "riallineamento" si stanno esplorando e soluzioni "natural-based" sono preferibili alle tradizionali opere rigide, come argini, difese parallele e pennelli. Al giorno d'oggi, un'ampia varietà di progetti di restaurazione ambientale sono stati attuati nelle zone umide costiere con l'obiettivo di ripristinare il paesaggio e trovare un nuovo equilibrio tra strutture naturali ed antropiche.

La presente tesi di dottorato fonde analisi geomorfologiche e sedimentologiche (ad es. rilievo con drone, trappole per sedimento, carotaggi e studio di ortofoto storiche) con approcci multidisciplinari per studiare l'evoluzione di giovani piane tidali, localizzate in diverse parti del mondo, la cui origine è legata ad interventi umani, nello specifico, a causa della rottura di un argine o dello scavo di un canale che ha connesso il meccanismo di trasporto sedimentario principale con una zona intertidale che non era una piana tidale. Sono stati scelti tre casi studio in base alle loro caratteristiche ambientali e l'intervallo tidale: i) la piana tidale della laguna di Barbamarco, situata nel Delta del Po (microtidale), in Italia; ii) il progetto Perkpolder (macrotidale), localizzato nell'estuario dello Scheldt nei Paesi Bassi; e iii) a Converse (ultratidale), situato nella baia di Fundy in Canada. Le analisi sono state implementate da attività di campo effettuate nelle paludi salate (o barene) di Halfway River e Eldriken (Baia di Fundy, Canada). Lo scopo di questo studio è di comprendere l'evoluzione sedimentaria delle giovani piane tidali nate da interventi umani, discutere dei processi che hanno portato alle condizioni attuali, e comprendere se e come avverrà la transizione da piana tidale a palude salata, identificando i fattori che dovrebbero essere considerati nei progetti futuri.

La prima parte del dottorato è stata dedicata alle attività di campo presso la piana tidale della laguna di Barbamarco nel Delta del Po (Italia). Rilievi con UAV (Unmanned Aerial Vehicle) sono stati svolti tra Ottobre 2018 e Ottobre 2020 e sono stati processati diversi DSM (Digital Elevation Model). I carotaggi hanno permesso di ottenere la distribuzione granulometrica, mentre i tassi di deposizione sono stati acquisiti utilizzando le capsule Petri come trappole per sedimento e delle

strutture innovative sono state sviluppate (per le capsule) attraverso una stampante 3D. Una revisione storica è stata realizzata utilizzando ortofoto messe a disposizione dall' IGM (Istituto Geografico Militare Italiano) e gli archivi della regione Veneto, dagli anni 50 ad oggi; quindi, l'indagine è stata estesa alle lagune dell'intera punta del delta. I risultati hanno fornito importanti interpretazioni sugli eventi che hanno portato all'evoluzione della piana tidale, mettendo in evidenza che il fiume è il principale fornitore di sedimento e che durante gli ultimi 20 anni ha procurato sedimento alla laguna di Barbamarco e alle altre lagune, come per esempio la laguna di Burcio, dove una rapida colonizzazione da parte della vegetazione è avvenuta tra il 2011 e il 2013, subito dopo un forte accumulo di sedimento.

Contemporaneamente alle attività sul campo e il processamento dei dati, analisi più approfondite sono state completate presso la piana tidale di Perkpolder (Paesi Bassi), utilizzando il dataset di dati Lidar forniti da Rijkswaterstaat (Il ministero delle infrastrutture e dell'ambiente olandese) e i tassi di deposizione ottenuti dall'autore durante la tesi magistrale (2017-2018). I risultati hanno messo in evidenza come, nonostante il sistema si soggetto ad una rapida accrezione, la vegetazione non si è ancora stabilita (analisi riferite fino al 2018) e la piana tidale necessita di non meno di una decina di anni prima di raggiungere le condizioni ideali per lo sviluppo di una palude salata.

Durante un breve periodo presso l'Università di Cadice (Spagna) (secondo anno del dottorato) sono state migliorate le conoscenze relative alle paludi salate e il processamento di dati. Durante l'ultimo anno di dottorato è stato svolto un periodo di tre mesi presso l'Università di Saint Mary ad Halifax (Nuova Scozia, Canada) che ha permesso di includere nelle analisi il sito di Converse (Baia di Fundy). E' stata compiuta una campagna sul campo tra il 23 e il 26 Luglio 2021, ottenendo un elevato numero di dati (ad es. relativi all'idrodinamismo, alla deposizione e sospensione del sedimento); analisi granulometriche sono state svolte successivamente a partire dal sedimento raccolto dalle trappole. È importante far notare che i risultati della tesi riguardano unicamente la deposizione, le granulometrie del sedimento e le fluttuazioni del livello marino. Successivamente, le analisi relative ai tassi di deposizioni sono state implementate da una campagna effettuata tra il 12 e il 13 Agosto 2021 presso due siti localizzati nel bacino sud della baia di Fundy: Halfway River e Eldriken. I dati raccolti sono stati comparati al sito di Converse, migliorando le interpretazioni relative alla discussione finale.

I risultati ottenuti da tutti i casi studio, discussi nella parte finale della tesi, hanno messo in evidenza come morfologie artificiali portano ad una instabilità morfologica che altera i tassi di deposizione e conseguentemente future previsioni. La forte erosione localizzata nelle bocche e i forti tassi di accrezione riscontrati nella piana tidale suggeriscono che potrebbe essere in corso un processo di cannibalizzazione che aumenta i tassi di variazione verticale nell'evoluzione a breve termine. Le analisi hanno messo in evidenza come la crescita della vegetazione è fortemente legata all' elevazione della superficie rispetto al MHT (Mean High Tide) e il fornitore di sedimento. Da un punto di vista morfologico, se la piana tidale non è localizzata almeno tra l'intervallo verticale dove generalmente crescono le piante pioniere della parte bassa della palude salata, la superficie necessita di aumentare in elevazione, ma questo può avvenire solamente se l'accumulo di sedimento è positivo e costante nel tempo. La restaurazione di paludi salate può essere un processo veloce (ad es. pochi anni) ma può necessitare di periodo più lungo (ad es. decenni). Future strategie di "riallineamento" relative alle zone umide dovrebbero considerare come il design influenza l'evoluzione della morfologia, i tassi di deposizione e l'elevazione delle piane tidali rispetto al MHT per poter dare una valutazione preliminare e predire i tempi di attesa prima dello sviluppo della palude salata.

## List of figures

**Figure 1** - General structure of a salt marsh, based on inundation frequency. Source: De Vlas et al. (2013). 23

**Figure 2 -** Location of the principal study sites: a) the natural young tidal flat of the Barbamarco lagoon in the Po River Delta (Italy); b) the artificial tidal flat of Perkpolder, located in the Scheldt Estuary (The Netherlands); c) the restoration project of Converse, located in the Bay of Fundy (Canada). ..... 29

**Figure 3** - Graphical abstract that summarizes the key points of the thesis ..... 33

**Figure 4** - This (a) Po River Delta location and (b) main branches at the tip of the delta. (c) The tidal flat is located in the southernmost part of the Barbamarco Lagoon (orthophoto 1:35000 from 2015 made available by the Veneto region). ..... 38

**Figure 5** - (a) Orthophoto of October 2018 representing the study area (see Figure 3c) with the GCPs location of each survey. The blue area represents the cropped DSM of February 2019, while the red area represents the cropped DSM of February 2020. (b) DSM of October 2018 with GPS transect of February 2020. ..... 40

**Figure 6** - Tidal records from the tide gauge of Porto Garibaldi representing (a) the whole period of study, (b) the survey of 24 October 2018, (c) the survey of 18 February2019, (d) the survey of 7 July 2019, and (e) the survey of 7 February 2020. ..... 41

**Figure 7** –(a) Orthophoto developed by Agea in 2015. The arrow indicate the direction of the river flow that follows the channel that connects the Busa di Tramontana/Po della Pila with the Barbamarco lagoon. The Orthophotos on the right were produced by the authors after the survey of b) October 2018 and c) February 2020. In Figure b) the location of the crevasse splays are shown, as well as the creeks and how the sediment deposition occurs. In Figure c) three depositional areas are identified: the largest crevasse splay and its small creeks are shown in yellow: they formed after the flood of November-December of 2019; in light blue, the smallest crevasse located in the south-west section is shown; in white, a large depositional area located in the west part is shown. Orthophoto produced after the survey of b) October 2018 and c) February 2020. In Figure b) the location of the crevasse splays are shown, as well as the creeks and how the sediment deposition occurs. In Figure c) three depositional areas are identified: the largest crevasse splay and its small creeks are shown in yellow: they formed after the flood of November-December of 2019; in light blue, the smallest crevasse located in the south-west section is shown; in white, a large depositional area located in the west part is shown. ..... 47

**Figure 8** - Different resolutions of the DSM profiles at 80 m (D1) and 60 m (D2) of altitude from the survey of February 2020 (transect in Figure 5b). ..... 49

**Figure 9** - Orthophotos of February 2019 (a) and February 2020 (b) with GCP location. In figure c,d,e,f the DoEs are shown. (c) Variations between the B1 and the B3 of February 2019; (d,e,f) Variations between D1, D2, D3 of February 2020..... 51

**Figure 10** - (a) Profiles of the B tests of February 2019; (b) Profiles of the D tests of February 2020 and validation points of the GPS survey (transect in Figure 2b) ..... 52

***Figure 11*** *- Elevation changes between (a) October 2018 and February 2019; (b) February 2019 and July 2019; (c) July 2019 and February 2020; (d) the whole period from October 2018 to February 2020.* ..... 55

**Figure 12** - (a) Average flow discharge and (b) hydrometric level from the station of Pontelagoscuro. The dataset is provided by AIPO (Agenzia Interregionale per il fiume Po). The date of each survey is written in red..... 58

**Figure 13** - Rates of changes from October 2018 to February 2020 between DSMs at 80 m of altitude of the whole study area. ..... 61

***Figure 14*** *- GCP density compared with the RMSE from this and other studies in wetlands.* ..... 72

***Figure 15 -*** *(a, b) Location of the Po Delta. (c) The tidal flat is connected to the Po della Pila thanks to the Busa di Tramontana and it is located in the southernmost part of the Barbamarco lagoon. (Orthophoto 1:30000 of 2015 provided by Veneto region). (d) Orthophoto of October 2018 with core samples and traps stations location.* ..... 78

**Figure 16** - (a) Trap model used for sediment deposition collection. (b, c, d) The petri dish is inserted and locked with three bolts on a flat surface with 3 nails that allow to nails the trap on the mud. ..... 84

***Figure 17 -*** (a) Example of measurement station. Three traps were positioned per each station with a distance of 60 cm between each other. (b, c) Example of sediment deposition inside the traps, and (d) example of sedimentation influenced by a local disturbance (one trap collected less than the other two). (d) This image represents a test made before the surveys, while the traps were located during a river flood and they collected an overflowing amount of sediment, showing how river flood deposition is different compared to tidal controlled deposition in the Po Delta. ..... 86

***Figure 18*** *- Core samples extracted during the sampling of May 2019. Subfacies (1) presents grey colours, while Subfacies (2) is darker and sandier.* ..... 89

***Figure 19*** *- Granulometric distribution of (a) Subfacies (1) and (b) Subfacies (2). (c) Each sample was classified based on Stevens (1983) classification.* ..... 90

***Figure 20*** *- Spatial distribution of the subfacies. Subfacies (1) increases its thickness in the central section of the tidal flat but it decreases moving at the edges and moving north-westward.* ..... 91

***Figure 21*** *- Loss on Ignition (LOI) distribution between (a) Subfacies (1) and (b) Subfacies (2).* ..... 92

***Figure 22*** *- Tidal records registered by the tide gauge stations of Pila (AIPO), Porto Garibaldi (ARPAE), and the DLN during the surveys of (a) September 2019, (b) June-July 2020, and (c) March 2021.* ..... 97

***Figure 23*** *- Rates of deposition collected by the traps during (a) September 2019, (b) June-July 2020, and (c) March 2021.* ..... 98

***Figure 24*** *- Orthophotos of the study area provided by the Veneto region. (a) Before 1999, the west channel was the only connection to the Barbamarco lagoon and the study area was partially isolated from the Po della Pila. (b) between 1999 and 2003 the NE channel was dug and the river could flood in the study area. (c) In 2008 the levees of the east channel were not established by vegetation yet; (d) the channel shows a stabilized condition in 2012.* ..... 100

***Figure 25*** *- Timeline that describes the evolution of the tidal flat.* ..... 101

***Figure 26*** *- Comparisons between sediment amount collected by traps in grams and (a) average inundation, (b) total inundation, and (c) elevation above m.s.l..* ..... 104

**Figure 27** – (a) Location of the Po River Delta and (b) the village of Pila, in the municipality of Porto Tolle. (c) Orthophoto provided by the Veneto region (Agea2015) where three principal lagoons of the tip of the Delta are visible: the Barbamarco lagoon, in the north side of the Po della Pila; the Burcio lagoon is located on the East side of Busa di Tramontana; the Basson lagoon is in the southern side of the Po della Pila. ..... 113

**Figure 28** – The strong transgression of the Po Delta between 1949 and 1969. (a) In 1949 the Barbamarco lagoon was not a full lagoon and land reclamation continued until (b) 1955. (c) in 1962 and (d) 1969 river floods and coastal storms submerged most of the rice fields, giving birth to the recent configuration of the lagoons. ..... 118

**Figure 29** - The channel that connects the Po della Pila with the Barbamarco lagoon was first seen in 1962, but it stabilized its shape after 1977. ..... 119

**Figure 30** - A portion of the Basson lagoon experienced a "restoration project" dynamic. The dyke that was protecting the rice fields was breached and the area was submerged between (a) 1955 and (b) 1969. The new inlet allowed the freshwater to flood inside the lagoon and a salt marsh developed between (c) 1977 and (d) 2015..... 120

**Figure 31** – Between (a) 1983 and (b) 1990, the Bocca Sud mouth and the Porte Vinciane artificial mouth were opened. The vegetation of the southern channel decreased between (c) 1992 and (d) 1996. ..... 122

**Figure 32** – Between (a) 1999 and (b) 2003 a new channel was dug (NE direction) in the southern section of the Barbamarco lagoon. Strong sediment injection occurred after (c) 2008 and the levees were established by wild reeds, which is visible in the orthophoto of (d) 2012. ..... 124

**Figure 33** - The new tidal flat located in the southern part of the Barbamarco lagoon is visible in both orthophotos of (a) 2015 and (b) 2018. ..... 125

**Figure 34** – Sea level and tidal range variations between 2009 and 2019 obtained from the tide gauge of Porto Garibaldi. (MHT = Mean High Tide, MLT = Mean Low Tide). The tide gauge did not work between May and December 2012, hence the sea level values of 2012 could be unreliable. ..... 127

**Figure 35** – (a) The Burcio lagoon underwent a "restoration project" dynamic similar to the Basson lagoon. After (b) 2009, the wide inlet that formed in the previous years allowed high sedimentation in the Burcio lagoon and (c) a tidal flat formed in 2011. (d) In 2013, wild reeds covered the area and established a new system between (e) 2015, (f) 2017, and (g) 2020. ..... 132

***Figure 36.*** *(a) Map of the province of Zeeland and (b) the municipality of Hulst. (c) Location of the Perkpolder tidal basin within the Scheldt Estuary and (d) 1:15000 orthophoto from the Province of Zeeland of the area, captured in June 2017.* ..... 136

***Figure 37.*** *Orthophotos at 1:15000 scale of the Perkpolder basin from the maps of the province of Zeeland; (a) before works in March 2014, (b) shortly before the opening of the inlet in March 2015, (c) in March 2016, and (d) in June 2017.* ..... 139

***Figure 38.*** *DGPS cross-sections (C1-C4), inlet profile (A-B) and location of sediment samples*..... 141

***Figure 39*** *- Neap and Spring tides during the experiments. The first experiment is from 15 of May to 16 of June; the second experiment is from 13 to 27 of June. Data from the tidal station of Walsoorden.* ..... 143

**Figure 40** - Cross sections from North to South (a) C4, (b) C3, (c) C2, (d) C1 extracted from Lidars (2015 and 2016) and from DGPS surveys (June and December 2017). To notice that in the graphs the survey of June 2017 is presented (orange line) to qualitatively assess bed changes but this was not used for volume calculations as it was too close in time to the preceding and subsequent surveys. ..... 146

***Figure 41.*** *On the left and in the centre (a, b) elevation change computed from June 2015 to April 2016 and from April 2016 to February 2017; on the right (c, d) sedimentary budget computed for both periods considering errors of 0, 0.05, 0.10 and 0.15 m. See the text for further details on survey methodologies.* . 147

***Figure 42.*** *On the left (a) sediment granulometric distribution map derived from the analysis of 40 samples collected in Perkpolder. The map was produced using the natural neighbour interpolation. On the right (b) Shepard's diagram shows how all samples result from a mixture of end-members of dominant sand and silt fractions.* ..... 148

***Figure 43.*** *On the left (a) sedimentation rates from the 15 May to the 16 June 2017. In the centre (b) sedimentation rates from 13 June to 27 June 2017. On the right (c) Percentage of LOI distribution. All maps were produced using the "natural neighbour" algorithm.* ..... 149

***Figure 44.*** *(a) Scheme of the calculated parameters and (b, c, d, e, f, g, h) profile changes from the opening of the inlet in June 2015 to January 2017.* ..... 151

***Figure 45.*** *Variation of depth, width, and cross-section of the inlet expressed as the ratio between two-time intervals from June 2015 to January 2017.* ..... 152

***Figure 46.*** *- On the left (a) elevation changes from June 2015 to April 2016 and on the right (b) from April 2016 to February 2017.* ..... 156

**Figure 47** – (a) The restoration project is located in the northern basin of the Bay of Fundy (Canada). (b) The Converse marsh is next to the mouth of the Missaguash river, on the eastern side of the Cumberland basin. In Figure (c) are shown the value of the average deposited sediment calculated from the surveys of July 2021. The orthophoto was obtained during the surveys as well. ..... 162

**Figure 48** – (a) Location of the study sites in the southern basin of the Bay of Fundy. (b) The two case study are both situated in the Minas Basin, about 6 km far from each other. (c) Halfway River study area in detail. (d) Eldriken study area in detail. ..... 164

**Figure 49 –** Selected section for volumes and vertical changes analysis: the area concerning the inlet itself, the inlet area plus the channels and the nearby areas, the whole tidal flat area, and the highly vegetated area. ..... 168

**Figure 50** – Comparison between filter paper traps and Petri dish traps from the case study of Converse. 170

**Figure 51** – Rates of deposition of: (a) Halfway River, where P1-P1-P3 are located outside the river system; and (b) Eldriken ..... 170

**Figure 52** – Vertical variations of the study area: (a) from July 2019 to August 2021, (b) from August 2020 and July 2021, and (c) the whole study period, from July 2019 to July 2021. The calculations of (a) and (b) have a lower extension because the DSM of 2020 covers the central-eastern area of the tidal flat only. Note that the DSMs shown in these figures were not filtered, hence the red dots represent patches of vegetation. (d) Vertical variations of the inlet area, the channels, and the nearby areas from July 2019 and July 2021. ..... 175

**Figure 53 –** Sediment budget calculated from (a) July 2019 to August 2020, (b) August 2020 to July 2021, and (c) the whole study period, from July 2019 to July 2021. ..... 176

**Figure 54** – Granulometric distribution of (a) the site of Converse and (b) the site of Halfway River and Eldriken. ..... 178

**Figure 55** – (a) Rates of deposition of all study sites in comparison to the elevation; (b) Comparison between the rates of deposition and the submersion period of the tidal flat of Converse. ..... 179

**Figure 56 -** Division of the morphological relevant areas in the restoration project of Perkpolder. Zone 1 represents the proper tidal flat; Zone 2 concerns the pond that connects the inlet with the tidal flat; Zone 3 regards the inlet area only; and Zone 4 concerns the inlet area and the external nearby areas. ..... 189

**Figure 57** – Sediment deposition and average hours of submersion calculated from all traps of all surveys from the Po Delta, Perkpolder, and Converse..... 192

**Figure 58 –** (a) The net sediment budget of the whole restoration project of Perkpolder (Zone 1 and Zone 2). (b) Total sediment eroded from the external portion of the restoration project (Zone 3 and Zone 4). . 194

**Figure 59 –** Vertical changes of the restoration project of Perkpolder regarding the tidal flat (Zone 1) and the pond area (Zone 2) from (a) June 2015 to April 2016, (b) from April 2016 to February 2017, and (c) for the whole study period from June 2015 to February 2017. The DoDs shown in this figure are made with a TCD of 0.05 m. ..... 195

**Figure 60 –** Vertical changes of the restoration project of Perkpolder regarding the inlet area (Zone 3) and the external portion (Zone 4) from (a) July 2015 to April 2016, (b) from April 2016 to February 2017, and (c) for the whole study period from July 2015 to February 2017. The DoDs shown in this figure are made with a TCD of 0.05 m. ..... 196

**Figure 61** – Example of future trends for deposition in restoration projects under morphological instability. As tidal range increases, the average submersion period decrease next to the MHT, increasing the steepness of the linear regression. If the cannibalization process decreases in time, the linear regression will flatten, and the rates of deposition will drastically reduce. If the study site is characterized by high morphological complexities (i.e. channels, strong local elevation variations, and strong hydrodynamics next to the inlets) the dispersion of the datasets might increase, reducing the effect of the surface elevation, hence the submersion period. Combining datasets from different seasons or surveys dispersion as well. 204

## List of tables

***Table 1*** *- Summary of the photogrammetric test characteristics.*..... 42

**Table 2** - RMSE variations between DSM exported at varying resolutions..... 48

**Table 3** - Total Volume Variations (TVV) between DSM exported at different resolutions considering no threshold and with threshold (TCD). ..... 48

**Table 4** - Total Volume Variations (TVV) and Total Average Vertical Difference (TAVD) of DoEs of the February 2019 survey in an area of 4.7 ha and the February 2020 survey in an area of 1.8 ha; the values are calculated considering no threshold and with threshold (TCD) located in the Area with Significant Variation (ASV). ..... 52

**Table 5** - Summary of Total Volume Variations (TVV), Net Volume Variations (NVV) and Vertical Rates of Changes (VRC) for each time interval and DoD considering no threshold and with threshold (TCD) located in the Area with Significant Variations (ASV). ..... 56

**Table 6** - Statistical description of the flow discharge and the hydrometric level for the entire study period. ..... 59

**Table 7** - Summary of studies in microtidal wetlands worldwide. ..... 65

**Table 8** - Datasets and parameters from studies that were carried out in tidal flats and salt marshes using UAVs. ..... 71

***Table 9*** *- Distribution of water and sediment discharge of the Po branches according to Nelson (1970).* ..... 79

**Table 10** - Sediment amount collected by traps during the surveys. The depositional rates are calculated based on the tide gauge of Pila (AIPO). ..... 94

**Table 11** – Date and characteristics of the orthophotos. ..... 114

**Table 12** – Satellite images provided by SIO, NOAA, U.S. Navy, NGA, GEBCO, Maxar Technologies 2021, from Google Earth Pro 7.3.4.8248 (64-bit), between 2009 and 2020. The coordinates are referred to the location of the images. ..... 115

**Table 13** - Volume changes and rates of accretion of the study area considering different thresholds for error in the DTM. The last row derives from the comparison between Lidar and DGPS dataset and errors cannot be estimated due to non-heterogenous datasets. ..... 147

**Table 14** - Average rates of accretion of different study cases from the Western Scheldt (The Netherland) and South England. Next to each rate is expressed the elevation compared to the NAP in meters. *The total rate after 30 includes Lidar and DGPS surveys, so should be taken with attention as it might be overestimated for the last period. ..... 158

**Table 15** – Deposited sediment and rates of deposition of Converse (Bay of Fundy). ..... 171

**Table 16** – Deposited sediment and rates of deposition of Halfway River and Eldriken (Bay of Fundy). ..... 172

**Table 17** – Spartina spp. vertical distribution obtained from the study sites. ..... 197

# 1. Introduction

This introductive section presents the basic concepts and definitions of the environments under investigation, describing coastal wetlands, tidal flats, salt marshes, and their distribution. It follows an introduction of the Building-With-Nature approach and the study sites under research. Finally, it is introduced the structure of this PhD thesis.

## 1.1 Coastal wetlands: Tidal flats and salt marshes

Coastal wetlands are highly complex ecosystems that are strongly related to mean sea level; they include large intertidal areas (i.e. tidal flats, salt marshes, and mangroves) and non-tidal areas (i.e. swamps, non-tidal marshes, and fens). These environments were historically considered as non-productive habitats (i.e. unsuitable for agriculture) and carriers of unhealthy and insalubrious conditions (i.e. humidity, mosquitoes) (Boavida, 1999); reclamation, drainage, and strong anthropization of coastal areas caused a high reduction of these systems worldwide. However, several studies demonstrated that coastal wetlands provide numerous ecosystem services for nature and mankind. They improve the local economy through fisheries hosting important fish species (Boesch and Turner, 1984; MacKenzie and Dionne, 2008; Barbier et al., 2011); they shift the carbon sequestering from short-term to long-term (from 10-100 years to >1000 years), hence they have a fundamental role in the carbon cycle (Mayor and Hicks, 2009); they have an important role in local cultural aspects (Weis, 2016).

The most common and important intertidal coastal wetlands are tidal flats and salt marshes. These environments are highly dynamic due to the strong interactions between several biological, physical, and chemical factors. Typically, their evolution is controlled by tidal range and currents, waves, and river floods, since they control sedimentation, erosion, and morphology. Tidal flats are wide soft-sediment habitats, generally composed of mud and sand, characterized by the absence of vegetation (Dyer et al., 2000); they can be considered as slopes with low angles where surface elevation increases (compared to the mean sea level) moving landward. Due to this structure, the submersion period and the frequency of inundation caused by the tidal variations (i.e. hydroperiod) decrease as the elevation increase (French, 1993), which means that the sediment deposition decreases at higher elevations as well (Pethick, 1981). When tidal flats surface reaches a certain elevation compared to the m.s.l. (mean sea level), vegetation colonizes this intertidal area and a salt marsh is grown. Consequently, the transition of a tidal flat to a salt marsh is strongly dependant on the combination of several factors, which are the surface elevation,

sediment deposition, and vegetation patterns (Fagherazzi et al., 2006; Marani et al., 2007). A common general reference level that suggests the limit between the tidal flat and the salt marsh is the Mean High Tide (MHT) (De Vlas et al., 2013; Bakker, 2014) (Fig. 1). In turn, the vertical variation of the surface of coastal wetlands is controlled by a wide type of processes which concern sediment deposition (e.g. Temmerman et al., 2003; Butzeck et al., 2015), suspended sediment (e.g. Chen et al., 2005), compaction and consolidation (e.g. Brooks et al., 2018, 2022), subsidence (e.g. Fabris, 2019), waves action (e.g. Cortese and Fagherazzi, 2022), river and tidal currents (e.g. Lenstra et al., 2019), presence of vegetation (e.g. D'Alpaos et al., 2006).

Coastal wetlands worldwide are characterized by a similar range of geomorphological and hydrological factors; however, climatic differences and the dominance of specific processes in respect to others give unique shapes and characteristics. South European marshes, hence Mediterranean wetlands, develop under dry summer subtropical conditions. The most common pioneer plants are *Spartina maritima* and other higher elevation plants such as *Sarcocornia perennis* (Pratolongo et al., 2019). Most salt marshes are associated with deltaic environments, like the Rhône, Ebro, Nile, and Po Delta, due to their strong alluvial sediment supply (Vella et al., 2005). However, their evolution was highly driven by anthropic interaction and most Mediterranean systems are altered by intensive agriculture and human settlements (Benito et al., 2014); moreover, subsidence is particularly higher in these systems and the effect of sea-level rise is challenging these coastal wetlands (Day et al., 1995). North European marshes develop under oceanic climate, so they are characterized by cool summers and winters, with a relatively narrow range of annual temperatures. Precipitation is evenly distributed throughout the year, without a dry season. Typical vegetation pattern includes a pioneer zone with a sparse cover of *Spartina anglica* and *Salicornia dolichostachya/fragilis* (Pratolongo et al., 2019). Salt marshes from Eastern North America have similarities with the European ones, but a different structure, in particular since *Spartina alterniflora,* the most common species, grows in lower intertidal zone (Mckee and Patrick, 1988).

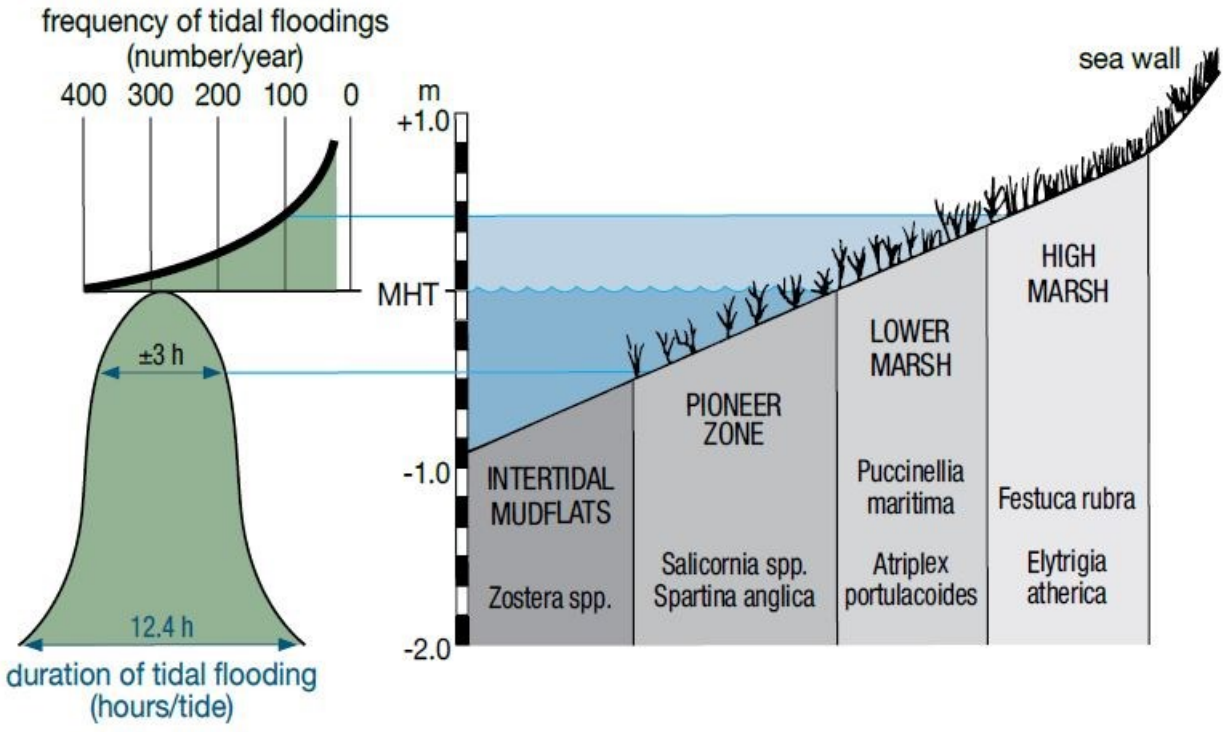


***Figure 1*** *- General structure of a salt marsh, based on inundation frequency. Source: De Vlas et al. (2013).*

## *1.2 Coastal defences and Building-With-Nature*

It is increasingly highlighted that traditional coastal structures, such as dykes, breakwaters, seawalls, and groins, are becoming inopportune choices (Temmerman et al., 2013) and several studies have shown how a pure engineering approach has unavoidable long-term effects. The increasing potential risk of casualties and damages in case the defences are broken (VanKoningsveld et al., 2008; Smits et al., 2006), or disturbances in sediment balance, an increase of land subsidence by soil drainage (Syvitski et al., 2009), and other human-induced alterations are changing the human approach to coastal environments and, in fact, short-term exploitation of natural resources (Capobianco and Stive, 2000) and the concept that defines sea and land as two different systems are now obsolete (Slobbe et al., 2013). A new concept of Building-with-Nature have been discussed and a new definition of coastal resilience is proposed:

"*Coastal resilience is the capacity of the socioeconomic and natural systems in the coastal environment to cope with disturbances, induced by factors such as sea-level rise, extreme events, and human impacts, by adapting whilst maintaining their essential functions*." (Masselink and Lazarus, 2019).

Basically, resiliency is the ability of a system to recover from a previously altered condition (Phillips, 2018). Coastal environments, thanks to their strong dynamism, are geomorphic systems that require strong resiliency (Masselink and Lazarus, 2019), and there are several examples, such as barrier islands, beaches, dunes, coral systems, and tidal wetlands. Tidal flats and salt marshes have the ability to cope with sea level rise maintaining the elevation with respect to the sea, thanks to the feedback between vegetation and sediment transport (Fagherazzi et al., 2012; Kirwan and Megonigal, 2013; Cahoon et al. 2016). Their evolution and resiliency are highly connected to the sediment supplier (Ganju et al., 2017; Thorne et al., 2018) which generally depends on the prevailing environmental processes, such as river floods or tidal currents. It is well recognized the ability of salt marshes to act as natural protection from coastal storms and river flooding (Bouma et al., 2014; van Loon-Steensma, 2014; Möller et al., 2014; Smolders et al., 2015; Stark et al., 2015; Vuik et al., 2016; Leonardi et al., 2018). Due to their resiliency and defensive capabilities, several restoration projects that aim to restore lost ecosystems dynamics and services were developed. In the case of coastal wetlands, several strategies were exploited to improve sediment introduction inside old and new systems (Cox et al., 2022), such as: i) river diversion, ii) tidal flooding, iii) sedimentation structures, and iv) vegetation planting. The first two main approaches (i.e. river diversion and tidal flooding) consist of improving the connection between the sediment supplier and the wetlands in order to improve sediment injection. In fact, coastal wetlands restoration projects are a peculiar strategy of coastal management based on a set-back scheme, which purpose is to make available portions of coastal inland to the sea in order to compensate sea level rise and restore the natural landscape, in particular where man intervention has deeply changed the original shape. This management choice consists of breaching an artificial structure, such as a dyke; then, the sea submerges several hectares of land, creating new tidal flats and, as the final goal, a salt marsh. The transition from tidal flat to salt marsh is the final aim of a management realignment since vegetation is the first line of defence against flood and storm events; in fact, one of the principal objectives of a restoration project is to reach this condition as soon as possible. The connection between land and sea through the dyke breach technique needs to be applied with criteria; in fact, the sediment injection into the system is one of the key points for the long-term survivance of coastal wetlands (e.g. Day et al., 2016; Verschelling et al., 2017; Cox et al. 2022). During the recent decades, the Building-with-nature approach has been used by several countries worldwide, in particular, in northern Europe, in the East coast of Canada, and the West coast of America.

## *1.3 Human-induced coastal wetlands*

The investigations that were carried out in this PhD thesis focus especially on human-induced young tidal flats. The study sites that are presented herein share the same origin: an intertidal area became a proper tidal flat after the breach of a dyke or a channel excavation that connected the sediment supplier with the system. Coastal wetlands are dominated by similar bio-physical processes which impact on the system changes based on their geographic location. For example, one of the most impactful factors is the tidal range, which defines the intertidal area (i.e. the extension of tidal flats), sediment transport and deposition, and vegetation distribution. Three study sites were chosen: i) the tidal flat of the Barbamarco lagoon (Po River Delta, Italy); ii) the artificial tidal flat of Perkpolder (Scheldt Estuary, The Netherlands); and iii) the restoration project of Converse (Bay of Fundy, Canada). These young tidal flats have the same origin in common (i.e. dyke or channel breach) and several other environmental conditions, such as the lagoonal structure (i.e. dyke or barrier island protection), low wave interaction, no vegetation, and strong sediment input. The aims of this PhD study are to define the sedimentological evolution of different human-induced tidal flats characterized by all ranges of tidal intervals, which means from microtidal to meso/macrotidal, to discuss the processes that have led to their present conditions, and to understand whether and how the transition from flat to marsh occurred, defining which factors should be considered for future restorations.

### *1.3.1 The tidal flat of the Barbamarco lagoon (Po River Delta, Italy)*

The first part of the thesis concerns the microtidal system of the Po River Delta (Italy) (Fig. 2a). The Po delta is a peculiar system extended for 700 $km^2$ along 90 km of coastline that has been strongly modified by both natural and anthropic processes (Cencini, 1998; Simeoni and Corbau, 2009). The recent evolution (i.e. last centuries) is highly influenced by human intervention, in fact, its current location was reached during 1604, when the Venetian Republic realized the 'Porto Viro' bypass, a massive operation that has diverted the delta southward (Stefani and Vincenzi, 2005), making it one of the largest anthropic deltas in the world (Maselli and Trincardi, 2013). The delta's beaches have been subjected to a generalized progradation from the 800 to 1945 (Visentini, 1940), until, between the 1930s-40s and the 1970s-80s, an erosional trend caused by heavy floods combined with human interventions (e.g. dams construction, material exploitation, agricultural reduction, etc. (Billi and Fazzini, 2017)) led to a consistent coastal regression. Most of the heavy landscape modifications were undertaken during 1870 – 1960 by the Italian Kingdom and continued by the Fascist Government and the Republican Government with the aim to improve economic

development and to contrast malaria (Cencini, 1998). During the following years, alternating phases of regression and progradation balanced the coastline, maintaining a significant stable condition. However, from 2010 till nowadays the delta is occurring accretion and a constructive process is ongoing (Ninfo et al., 2018). In short, the strong floods of the 1950s-60s submerged most of the agricultural fields located at the tip of the Delta and the recent progradation is giving birth to new tidal flats.

The formation and evolution of the Delta depend on the Po River, which is the longest Italian river and one of the largest of the Mediterranean sea from the freshwater fluxes viewpoint, considering that it is characterized by an average discharge of 1500 $m^3/s$ (Ludwig et al., 2009); it flows over 650 km into the Adriatic sea and it has a catchment area of over 70000 km2 (Bondesan et al., 1990). The river cleaves into five branches that cross the delta (from north to south, Po di Maestra, Pila, Tolle, Donzella or Gnocca, and Goro); wide lagoons develop behind the coastline, which is characterized by bars and sand spits. Each branch is associated with delta plain and delta front depositional systems. The predominant granulometry of the Delta is fine, from fine sand to mud (Dal Cin, 1983; Simoni et al., 2000a). A broad prodelta that extends to 6 km in the northern section and 10 km in the central-southern section defines the limit of the deltaic system (Simeoni et al., 2000b).

Human influence has caused vegetation loss in wetlands between the 1950s and the 2000s and despite environmental protection measures being carried out, the vegetation did not present a wide recovery, probably due to indirect anthropic interventions and natural factors (Gaglio et al., 2017). Between 1977 and 2011, the covering of the wild reeds that characterize the Delta reduced of about 48% (Verza and Catozzo, 2015). The delta regression and progradation have a similar evolution with the subsidence, whose origin is connected principally with tectonic, natural, and artificial sediment compaction. Anthropic subsidence was higher during the 1944 – 1977 period principally because of the draining of wetlands, land reclamation, and pumping of methane-rich water from Quaternary deposits, which operations are suspended nowadays (Colombo et al., 2009); the rate of subsidence has been reduced during recent years (Fabris, 2019). The tide is mixed, mostly semi-diurnal with a spring-tidal range of about 0.5 m.; the system was previously considered as river-dominated but during the last 50 years the trend was *wave-dominated* (Nelson, 1970); the trend could turn *river-dominated* once again if the progradation will continue. It is difficult to define a unique regime because each delta lobe within the same delta system is dominated by a different trend (Trincardi et al., 2003; Correggiari et al., 2005; Syvitski et al., 2005).

Although the events that have led to the recent configuration of the system are highly similar to the procedures of Building-with-Nature management, currently there are no restoration projects ongoing at the Po Delta. Three chapters were dedicated to this system since more analysis were necessary to understand its evolution and confirm that its development was related to human intervention. The study area is a ~8 ha tidal flat located in the most southern portion of the Barbamarco lagoon, which is situated on the northern side of the central branch of the Po River (i.e. Po della Pila).

### *1.3.2 The Perkpolder restoration project (Scheldt Estuary, The Netherlands)*

The tidal flat of Perkpolder (The Netherland) (Fig. 2b) is a 75-hectares artificial tidal flat located in the Scheldt Estuary (i.e. South-West of The Netherland). The system is 355 km long with a catchment area of about 22000 $m^3$ and it is characterized by a macrotidal range that varies from 3.8 m at the mouth to 5.2 m upstream (Claessens and Belmans, 1984). High amount of suspended material travels through the estuary thanks to the strong tidal and riverine currents; in fact, the sediment has both marine and terrestrial origin and the collision of these two processes cause strong resuspension, causing the Turbidity Maxima (ETM) (Swart, 1987; Wartel et al., 1993; Brinke, 1994; Chen et al., 2005). The tidal flat was created in 2015 as a cooperation project between Rijkswaterstaat (Dutch Ministry of Infrastructure and the Environment) and the regional government of Zeeland in order to recreate a tidally-dominated natural ecosystem (Boersema, 2016). The project includes the construction of recreational facilities and natural environments in order to prompt the socio-economic development of the area. Originally, the study area was dammed in 1210 and it was used for agricultural purposes and building new villages. However, due to strong subsidence, the area dropped below the mean sea level and despite new dykes were built in 1841, the continuing failure of the structures lead to a new rethinking of the protections. After the opening, the benthic macro fauna rapidly started to colonize the area, providing food for bird communities. This study was achievable thanks to the collaboration between the COSTUF team (University of Ferrara) and HZ University (Vlissingen).

### *1.3.3 The Converse restoration project (Bay of Fundy, Canada)*

The Bay of Fundy is a large bay located between New Brunswick and Nova Scotia on the East coast of Canada. This environment is characterized by a particularly high tidal range (i.e. from 5 to 16 m) that shapes the coast, leading to complex and diverse ecosystems; in fact, this system is principally composed by salt marshes, although 30,500 ha (~85% of initial area) were lost since European

colonization in the 17th century (Thomas, 1983). Most of wetland loss was caused by human intervention, which reclaimed areas were used for agricultural purposes (Ganong, 1903). Several management realignments have been started in order to recover the salt marshes; however most of them presented a different evolution and structure if compared with natural marshes (Virgin et al., 2020).

The collaboration between the author and Saint Mary's University (Nova Scotia, Halifax) allowed to participate in field surveys and obtain data from the Bay of Fundy. The Converse tidal flat (Fig. 2c) is a ~10 ha realignment project currently ongoing in the Missaquash River, which separates the provinces of New Brunswick and Nova Scotia. The river flows in the Cumberland Basin, a large basin (118 $km^2$) characterized by high sediment suspended concentrations (~0.3 g/L) (van Proosdji et al., 1999). The Tantramar Marsh is a large wetland system (2.3 $km^2$) that extends in this northern portion of the Bay (Chmura et al., 2001); it underwent a severe loss during the last 400 years due to human intervention as well. Sedimentation is highly controlled by tidal currents and seasonal variations and marshes are usually covered by snow and ice during winter; storms have a minor control on sedimentation (Greenberg, 1984).

The Converse tidal flat consists of a de-poldered area that was used for agricultural and grazing purposes; the dyke that separates the river from the inland was breached in December 2018. The project started due to several problems that include salt marsh loss, dyke failure and unfeasibility to maintain the protections. The main purposes are to protect the transportation route, the Parks Canada property and increase dyke sustainability. The project was developed by the CB Wetlands & Environmental Specialists Inc. (CBWES), in partnership with the Nova Scotia Department of Agriculture (NSDA), and the Environment and Climate Change Canada's National Wetland Conservation Fund (NWCF).

Two other study sites were under investigations, although they were not restoration projects, but they were highly influenced by human intervention, and they gave important information about altered wetland environments. The Halfway River and the Eldriken study site, which are proper salt marshes. The Halfway River is a small river located in Hantsport that flows into the Avon River (Minas Basin, south side of the Bay of Fundy). It was inundated in 2017 by sea water after the failure of the causeway that was protecting the river. This event resulted in a new salt marsh development and a new connection to the Bay of Fundy. However, a new dyke was built, in order to restore the previous condition. As a consequence, this "natural" realignment is now suffering

due to the strong reduction of the tidal range and water fluxes. The Eldriken site is a salt marsh located next to the Avon River, in the Southern Bight of Minas Basin of the Bay of Fundy (about 5 km far from Halfway River). This salt marsh is relatively young (i.e. >50 years) and it is still subjected to strong accretion.


***Figure 2*** *- Location of the principal study sites: a) the natural young tidal flat of the Barbamarco lagoon in the Po River Delta (Italy); b) the artificial tidal flat of Perkpolder, located in the Scheldt Estuary (The Netherlands); c) the restoration project of Converse, located in the Bay of Fundy (Canada).*

## *1.4 PhD thesis structure*

During the last three years (and a half), information and data from highly different natural and working environments were collected and this PhD thesis is the result of all the knowledge regarding tidal flats, salt marshes, and restoration projects that the author could combine. Field of studies from geology to biology, from geomorphology to hydrology, from sedimentology to coastal managing merged together to define the bio-physical processes that characterized these environments and how these processes drive their evolution in different parts of the world (Fig. 3).

The first three chapters are a collection of papers that concern the recent evolution of the Po River Delta (Italy). The papers separately take into account processes and environmental characteristics of the young tidal flat of the Barbamarco lagoon that is recently building up during the last decades and then extend the analysis to the other lagoons of the Delta. All these products derive from the efforts of the COSTUF team (University of Ferrara) and the collaboration with the Genio Civile of Rovigo, Eng. Guido Selvi, that gave important support for the analysis.

- Chapter 2: This is a peer-reviewed and published paper of a Special Issue "*UAV Application for Monitoring Coastal Morphology*" of the journal *Remote Sensing* (MDPI). This chapter investigates the recent evolution of the tidal flat of the Barbamarco lagoon between October 2018 and February 2020, analysing the rate of accretion and erosion, the morphology, and the deposition processes. Drone surveys were conducted, and the methodology of UAV analysis was discussed, in particular about the elevation of the drone sampling (i.e. photos) and the Ground Control Point (GCPs) location and distribution. This product derives from the collaboration between the author, E. Duo (COSTUF team), and P. Ciavola (COSTUF team).

  *Brunetta, R.; Duo, E.; Ciavola, P. (2021). Evaluating Short-Term Tidal Flat Evolution Through UAV Surveys: A Case Study in the Po Delta (Italy). Remote Sens., 13, 2322. https://doi.org/10.3390/rs13122322.*

- Chapter 3: This paper carries on with the previous analysis and investigates the sedimentary processes that have led to the formation of the tidal flat. Several cores sampling were carried out during May 2019 to define the granulometric distribution and the sediment source. Peculiar trap models were designed and three surveys were carried

out between September 2019 and March 2021 in order to measure the sediment deposition and calculate the rates of sedimentation. This work will be soon submitted to *Marine Geology* as:

*Brunetta, R.; Duo, E.; Ciavola, P. Sedimentary evolution of a young tidal flat in the Northern part of the Po Delta (Italy).*

- Chapter 4: This chapter represents the final part of the Po Delta analysis. The results and the observation of the previous papers are extended to the nearby lagoons of the Delta and a historical review based on orthophotos from the 1950s to 2018 was carried out. Combining time series of the tide gauge of Porto Garibaldi and vegetation analysis, this paper aims to describe the evolution of the whole tip of the Delta and where restoration is or is not taking place. The manuscript of this work is in preparation for submission to *Geomorphology* as:

  *Brunetta, R; Ciavola, P. Evolution of tidal flats in the Northern part of the Po Delta: a strategy for future building-with-nature management.*

The last chapters concern the proper restoration projects of Perkpolder (Chapter 5) and Converse (Chapter 6). The last chapter (7) combines all the final results and discussions.

- Chapter 5: This paper is peer-reviewed and published on *Frontiers in Earth Sciences*; it derives from the collaboration between the COSTUF team (the author and P. Ciavola) and J. S. Paiva (HZ University (The Netherland) in 2019); the data were made available by Rijkwaterstaat (Dutch Ministry of Public Works). In this chapter, the artificial tidal flat of Perkpolder (The Netherland) was investigated between June 2015 and January 2017. Three Lidars and Orthophotos were processed to estimate accretion and erosion rates in order to evaluate the tidal flat development. Sediment traps were used to measure rates of sedimentation and a comparison between similar restoration projects was discussed.

*Brunetta, R., de Paiva, J. S., and Ciavola, P. (2019). Morphological Evolution of an Intertidal Area Following a Set-Back Scheme: A Case Study From the Perkpolder Basin (Netherlands). Front. Earth Sci. 7, 228. doi:10.3389/feart.2019.00228.*

- Chapter 6: This chapter presents the data and the results that were achieved during a field campaign carried out in the Bay of Fundy (Canada) thanks to the collaboration between the author and Saint Mary's University (Nova Scotia, Halifax). This chapter focuses primarily on the sediment patterns and evolution of the restoration project of Converse, a young tidal flat located in the northern side of the Bay of Fundy (Cumberland Basin); then, the analysis focuses on two young wetlands located in the southern basin: i) Halfway River, which is a recent accidental restored marsh developed in the Minas Basin; ii) and the salt marsh of Eldriken, which is part of the Windsor marsh system, located in the Minas Basin as well. These analyses will be prepared for future publication.

  *Brunetta, R.; van Proosdji, D.; Ciavola, P. Sedimentological characteristics of young marshes in the Bay of Fundy (Canada).*

- Chapter 7: The final chapter of the thesis discusses the data obtained from all the study sites and introduces data analysis and results that were not presented in the other chapters (i.e. data correction, further morphological analysis, combination of datasets). The final discussion focuses on the rates of depositions in young tidal flats and their morphological behaviour; in particular, the discussion regards the unnatural processes that occur in the restoration projects in comparison with natural behaviours, and future trend that could be expected. Finally, the transition from tidal flat to salt marsh is discussed. The conclusions give important messages that regard the Po Delta recovery, and the future evolution of restoration projects. This chapter will be prepared for future publication and a future review on the methodology on rates of deposition calculation will be produced.

  *Brunetta, R.; Ciavola, P. Evolution of coastal wetlands restoration projects: natural vs artificial tidal flats.*

*Brunetta, R.; van Proosdji, D.; Ciavola, P. A review on sediment traps and rates of deposition calculation.*

All discussion is condensed in Chapter 8, where the discussion about the Po Delta, worldwide artificial tidal flats, and future improvements for restoration projects are summarized.

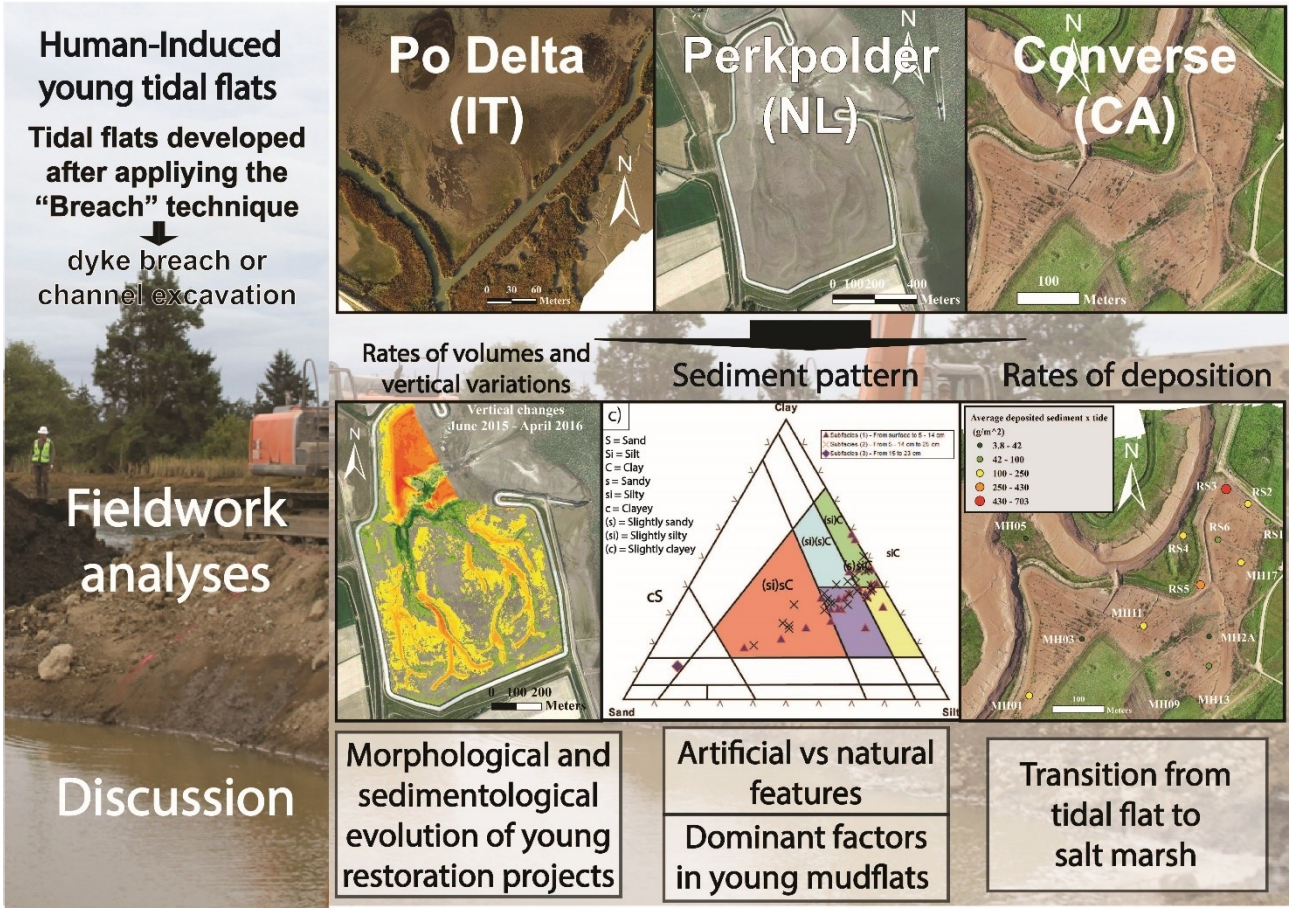


***Figure 3*** *- Graphical abstract that summarizes the key points of the thesis*

# 2. Evaluating Short-Term Tidal Flat Evolution Through UAV Surveys: A Case Study in the Po Delta (Italy)

## 2.1 Introduction

Coastal environments are continuously modified by intense processes like waves, wind, tidal currents combined with biological and, more often, anthropological, factors. Their interactions cause a very rapid evolution of these systems, making it necessary to acquire high-resolution data in short-time intervals in order to quantify and interpret the mechanisms behind morphological changes. Tidal flats are non-vegetated muddy or sandy surfaces located in the intertidal fringe (Dyer et al., 2000a); their upper portion (salt marsh) usually develops when saltwater vegetation grows at elevations around the mean high tide (Pratolongo et al., 2019) in low-energy and temperate coastlines (Adam, 1990; French et al.,1992), except for mangroves forests that develop in tropical coasts (Odum et al., 1982). The shape and extension of the flats are primarily connected to the tidal range and are typically characterised by tidal creeks that work as an exchange route for water and sediment between the main channels and the plain itself. The sediment grain size increases with proximity to the creek margin, depending on the intensity of the flood exceeding the elevation of the creek's levees (Christiansen et al., 2000; Leonard et al., 2002; Temmerman et al., 2004a). There are plenty of works and studies showing the importance of salt marshes from viewpoints as diverse as fishery (Boesch and Turner, 1984a; MacKenzie and Dionne, 2008a; Barbier et al., 2011), carbon sequestration (Mayor and Hicks, 2009), local cultural aspects (Weis, 2016) and the role of salt marshes as natural protection from coastal storms and river flooding (Bouma et al., 2014; van Loon-Steensma, 2014; Möller et al., 2014; Smolders et al., 2015; Stark et al., 2015; Vuik et al., 2016; Leonardi et al., 2018). Since wetlands usually cover wide regions and salt marshes have deteriorated during the last 50 years (Millennium Ecosystem Assessment (Program), 2005), there is an urgent need to both identify efficient methods of monitoring large areas and find new strategies to protect them. Unmanned Aerial Vehicle (UAV)-based photogrammetry is becoming a fundamental tool to achieve this objective (Eisenbeis, 2009), thanks to its low-cost and user-friendly techniques (Westoby et al., 2012; Moloney et al., 2018), which are well comparable with traditional topographic surveys (Mancini et al., 2013). A few simple steps can lead to an efficient survey strategy, based on the acquisition of high-quality data (Joyce et al., 2019). This methodology has been applied in a wide range of environments, from continental to coastal ones, such as in Arctic regions, rivers, and beaches (Javernick et al., 2014;

Ryan et al., 2015; Casella et al., 2016; Dąbski et al., 2017; Duo et al., 2018). However, few studies report on UAV applications in coastal wetlands.

As surveys are difficult to implement in these environments because of their morphology and their impracticability (i.e., sinking in mud, walking slowly, risk of getting stuck, etc.), remote sensing techniques are preferred. Satellite and aerial remote sensing have certainly improved our knowledge and assessment of coastal wetland dynamics (Klemas, 2014), but most of the studies focus on biomass evaluation (Adam et al., 2010; Ghosh and Mishra, 2017; Duffy et al., 2018; Doughty and Cavanaugh, 2019) rather than geomorphological changes. In these environments rates of accretion and elevation changes range from millimetric to centimetric, thus creating the need for high spatial and vertical resolutions able to perform reliable interpretations. Satellite images, with a spatial resolution from 0.5 m to 10-100 m (Campbell and Wang, 2019; Ozesmi and Bauer), are appropriate to monitor large portions (several square kilometres) of coastal areas, but they do not sufficiently capture small-scale evolution, which requires higher vertical accuracy. Lidar-based DEMs in vegetated areas are usually characterised by vertical errors from 0.1 to 0.45 m (Morris et al., 2005; Rosso et al., 2006; Cheng Wang et al., 2009; Millard et al., 2013) while Lidar products in bare mud can reach errors of 0.09 m (Fernandez-Nunez et al., 2017). Their reliability also depends on the rates of accretion and erosion affecting the intertidal area. Vertical changes are usually evaluated using marker horizons, sedimentation plates, or Sedimentation Erosion Tablets (SET) (Nolte et al., 2013), which are all very precise but are weak in spatial distribution representation. In this context, UAVs cannot cover such extended regions, but they can obtain very high-resolution images of smaller domains (several hectares), increasing the vertical resolution and accuracy of such final products as DEMs and orthophotos. Such precision becomes feasible when the flight plan is optimised as much as possible. It is widely recognised that drones are preferrable to other topographic tools for local-scale studies due to the potential resolution of UAV-derived products, their low cost, and feasibility; the potential of drone surveys in wetlands has come to the fore only in recent years (Green et al., 2017; Kalacska et al., 2017). Casella et al., (2020) made an interesting review of the accuracy in beach environments, with RMSEs (Root Mean Square Errors) of the elevation product ranging between 0.02 and 0.13 m. If this accuracy is achieved, the technique may also be suitable for monitoring tidal flats and salt marshes; however, the quality of a survey depends on many factors like ground control points (GCPs) location and distribution (James et al., 2017), weather conditions, water reflection (Mount, 2005), tide, and logistical issues. To implement an effective UAV survey on coastal areas, and in particular, on

wetlands, several favourable factors must be present simultaneously: the tide should be at the lowest possible daily level; the weather should allow the drone flight but, at the same time, the sunlight should not be too bright; moreover, the GCPs should be uniformly distributed across the study area and, most importantly, their placement must be practical. All these limitations combine to make surveys in wetlands more difficult than in other environments.

Global-scale analysis mostly considers salt marshes unable to keep up with relative sea-level rise (Nardin and Edmonds, 2014; Crosby et al., 2016; Spencer et al., 2016). On the other hand, local-scale assessments often result in an overestimation of the vulnerability of salt marshes (Kirwan et al., 2016). These tendencies suggest that both points of view should be taken into account, and large-scale studies should be accompanied by data obtained locally; as a consequence, UAV-based surveys can be a promising tool for monitoring the local scale evolution of salt marshes under the effect of a changing climate.

The current study aims to examine the morphology of a tidal flat in the Po Delta and to discuss UAV usage in coastal wetlands. In particular, this paper aims: (i) to describe the local morphological evolution of the tidal flat and interpret the system dynamics, making comparisons with other microtidal deltas; (ii) to quantify the accuracy of UAV-derived DSM (Digital Surface Model) products, and of the following morphodynamic analysis. The integrated analysis performed was useful in providing recommendations for the practical implementation of UAV surveys in wetlands as well as discussing the advantages and limitations of the general approach.

## *2.2 Study Site*

The Po Delta (Italy) is a unique system, extending for 691 $km^2$ along 90 km of coastline (Fig. 4a), that has undergone strong modification by both natural and anthropic processes (Bondesan' et al., 1990; Cencini, 1998; Simeoni and Corbau, 2009). Its formation and evolution depend on the Po River, which is the longest Italian river and, from the freshwater fluxes viewpoint, one of the largest in the Mediterranean Sea Basin. Indeed, it is characterised by an average discharge of 1500 $m^3/s$ (Ludwig et al., 2009), it flows over 650 km into the Adriatic Sea, and it has a catchment area of over 70,000 $km^2$ (Bondesan' et al., 1990). The river cleaves into five branches that cross the delta (from north to south, Po di Maestra, Pila, Tolle, Donzella or Gnocca, and Goro) and each ramification is associated with delta plain and delta front depositional systems (Fig. 4b); bars and sand spits characterise the coast bordering wide internal lagoons. The granulometry of the delta sediment is mostly fine, varying from fine sand to mud (Dal Cin, 1983; Simeoni et al., 2000). The

deltaic system terminates in a broad offshore prodelta that extends to 6 km in the northern section and 10 km in the central-southern section (Simeoni et al., 2000b). Its current location was established after heavy human intervention made under the Venetian Republic which, in 1604, completed the "Porto Viro" bypass, that diverted the delta southward (Stefani and Vincenzi, 2005), making it one of the largest anthropic deltas in the world (Maselli and Trincardi, 2013). Its beaches were subjected to a generalised progradation from the 1800s to 1945 (Visentini,1940) while most of the heavy landscape modifications, made to improve economic development and to combat malaria (Cencini, 1998), were begun by the Italian monarchy in 1870 and pursued under the Fascist regime and the Italian Republic until 1960. Between the 1930s-1940s and the 1970s-1980s, an erosional trend caused by heavy flooding, combined with human interventions (e.g., dam construction, resource exploitation, agricultural reduction, etc. (Billi and Fazzini, 2017)), led to a consistent coastal regression. A significantly stable condition was only reached years later, due to alternating phases of regression and progradation. However, from 2010 to today, the delta is the object of accretion and a constructive process is ongoing (Ninfo et al., 2018).

The tide is mixed, mostly semi-diurnal with an average spring-tidal range of about 0.5 m. The deltaic system was previously considered and classified as *river-dominated* but, over the last 50 years, the trend has become *wave-dominated* (Smith, 1966; Nelson, 1970; Galloway, 1975; Reineck, 1980); according to recent studies, if progradation continues, the trend could be inverted and the system could return to its *river-dominated* status once again. Because a different trend dominates each delta lobe, the definition of a single regime is particularly difficult (Trincardi, 2003; Correggiari et al., 2005; Syvitski et al., 2005).

The tip of the delta is part of the municipality of Porto Tolle, in the province of Rovigo (Veneto region, Italy). The area between Po della Pila, which is the central branch of the river, and the south-east part of the Barbamarco Lagoon, was the most affected by flooding. New tidal flats built-up during the last 50 years and hundreds of hectares of agricultural fields have been submerged; in fact, some artificial structures and houses are still underwater and abandoned nowadays. The study site concerns a young tidal flat of about 8 ha located between two artificial channels (Fig. 4c), connected to the Po della Pila branch; these channels are frequently crossed by hunters or fishermen who need to reach the two harbours located between the Po branch and the Barbamarco Lagoon. The channel levees are stabilised by freshwater vegetation. The rapid sediment deposition of the lagoon makes this tidal flat particularly suitable for this study.


***Figure 4*** *- This (a) Po River Delta location and (b) main branches at the tip of the delta. (c) The tidal flat is located in the southernmost part of the Barbamarco Lagoon (orthophoto 1:35000 from 2015 made available by the Veneto region).*

## 2.3 Materials and Methods

### 2.3.1 Fieldworks

The fieldwork campaigns were carried out between October 2018 and February 2020 using an aerial commercial drone (i.e., DJI Phantom Vision 3+; camera: FC300X; focal length: 3.61 mm; pixel size: 1.56 × 1.56 µm) and an RTK-GPS Trimble R8 (i.e., stop and go technique; horizontal accuracy of 8 mm and vertical accuracy of 15 mm).

During each survey, around 80 GPS points were collected throughout the tidal flat. In this paper, they will be referred to as "validation points", since they were used for comparison with the UAV-derived DSM products. The GCPs consisted of white and red wooden square targets, measuring 60 x 60 cm so as to be highly visible in the aerial photos; distributed around the tidal flat, their position was measured with the GPS antenna (Fig. 5a). They were located within, and at the edge of, the study area—where it was possible to safely walk on the mud flat—in order to support and optimise the photogrammetry reconstruction (see Section 2.3.2). Additionally, a transect (Fig. 5b) was surveyed along the entire study area (South-West North-East) during the last survey of February 2020. All GPS measurements (i.e., GCP and validation points) were then referenced in WGS84/UTM zone 33N (EPSG:32633). The average horizontal and vertical error associated with the measured GCP and validation points ranged between 3 and 4 cm, respectively.

In order to successfully complete a survey in coastal wetlands, many factors must combine due to water-saturated sediment surface and the reduced window of flight completion time; consequently, the surveys were carried out during spring-tides, when the moon and the sun are aligned and the lowest tides occurred and, during early morning or late afternoon, when the sun was not at its highest location in the sky; the wind speed ranged from 1.5 to 5.56 m/s during all fieldworks, thus its influence was considered negligible. Four surveys were carried out on the following dates: i) 24 October 2018; ii) 18 February 2019; iii) 9 July 2019; iv) 7 February 2020 (Fig. 6). In each drone survey, the front and the side overlap between each photo was ~70% and the flight speed was 8 - 10 m/s. The first survey was carried out at a height of ~80 m. During the survey of February 2019, two flights were completed, the first at ~80 m, and the second one at ~40 m. The survey of July 2019 was performed using a single flight at ~80 m. During the last survey of February 2020 two flights—at ~80 and ~60 m—were completed. The automated flights were prepared using the *"Drone deploy"* free application (https://www.dronedeploy.com/ access date: 11/06/2021), following parallel flight lines for all surveys.

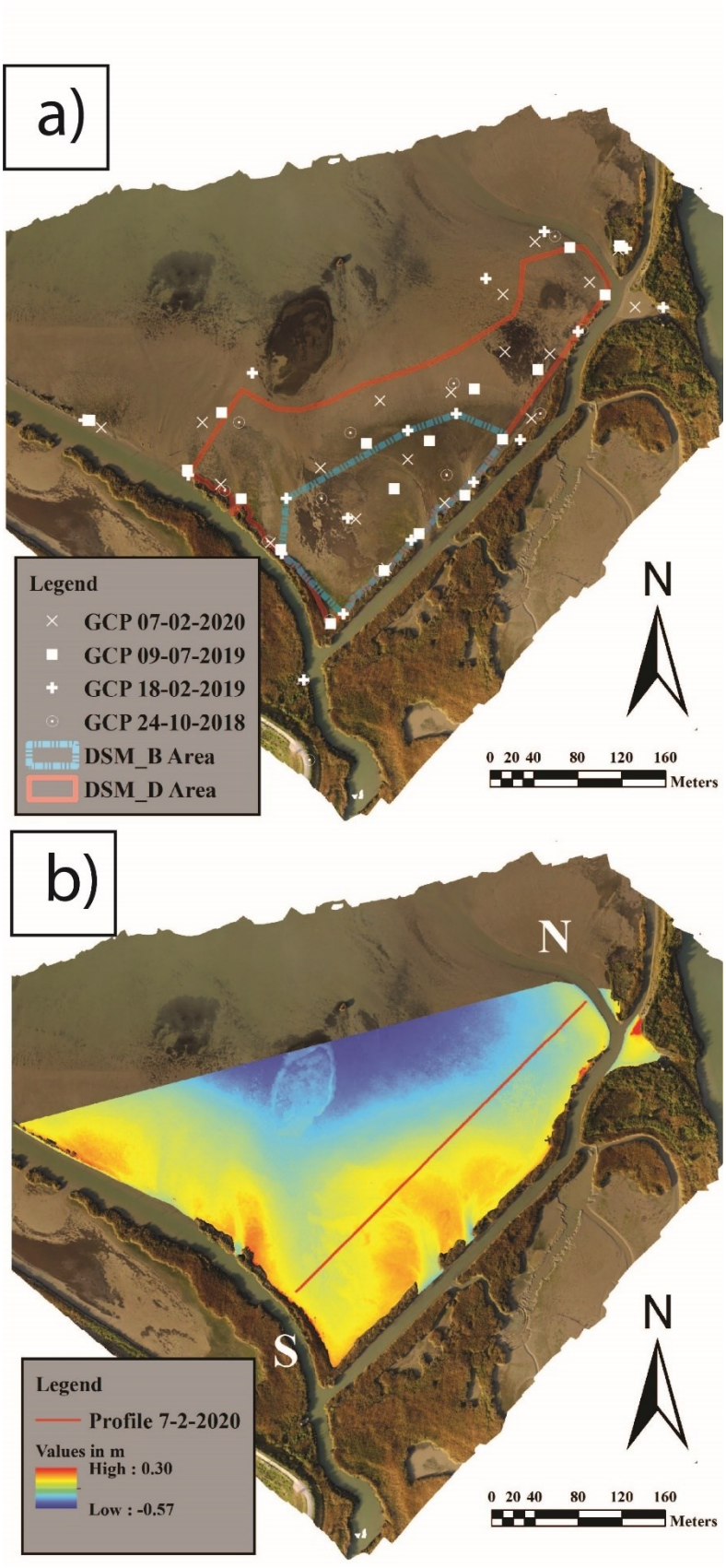


***Figure 5*** *- (a) Orthophoto of October 2018 representing the study area (see Figure 3c) with the GCPs location of each survey. The blue area represents the cropped DSM of February 2019, while the red area represents the cropped DSM of February 2020. (b) DSM of October 2018 with GPS transect of February 2020.*

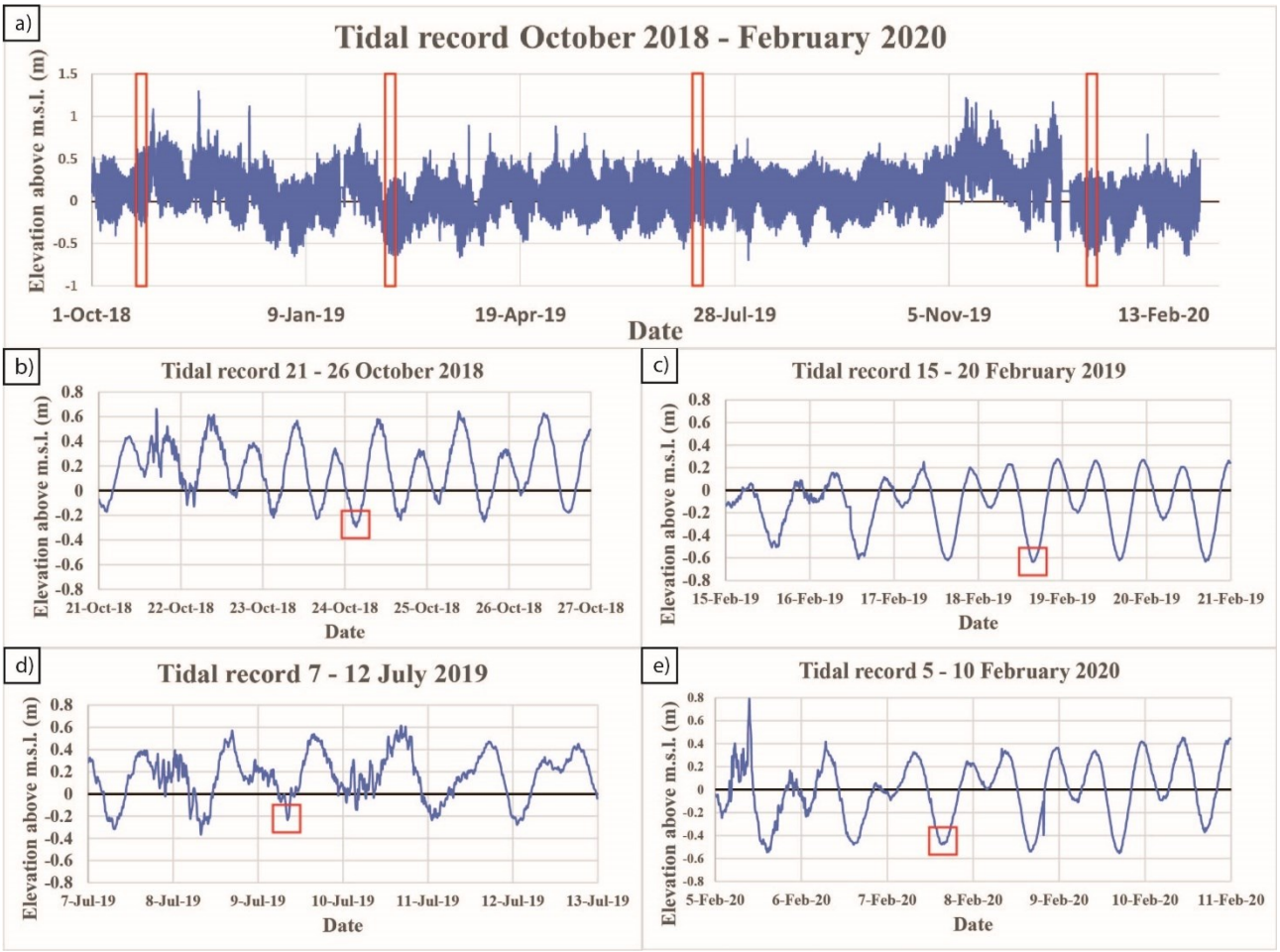


***Figure 6*** *- Tidal records from the tide gauge of Porto Garibaldi representing (a) the whole period of study, (b) the survey of 24 October 2018, (c) the survey of 18 February2019, (d) the survey of 7 July 2019, and (e) the survey of 7 February 2020.*

### *2.3.2 Photogrammetric Tests*

After each survey, the images were imported and processed using the *"Agisoft Metashape"* software (version 1.5.1 https://www.agisoft.com/ access date: 11/06/2021) which allows the generation of georeferenced DSMs and orthophotos by processing the drone images with the Structure-from-Motion (*SfM*) photogrammetric technique. The procedure followed previous UAV-based works, such as Fonstad et al. (2013), Casella et al. (2014, 2016), and Gindraux et al. (2017). In general, images were aligned, GCPs were manually detected, coordinates were imported and associated with each GCP, the camera alignment was optimised, a dense cloud was generated, and the DSMs and the orthophotos were processed and exported. It is important to note that the embedded GNSS position of the images was not used since the accuracy of the UAV GNSS was not appropriate for processing, hence the camera calibration was optimized through the GCP points and, consequently, the sparse cloud was georeferenced.

In total, eight photogrammetric tests were processed based on the combination of sets of photos taken at different altitudes. The details of the tests are given in Table 1. Notably, the tests cover the whole domain, or portion of it, depending on the processed set of images or their combination.

The DSM products were cropped, removing the portions outside the area covered by the GCPs and noises derived from water. For consistency, the analysis was performed exclusively on the same area. The vegetation at the edges and the wet areas of the domain were also excluded from the models. With the term "coverage" we mean the area that is contained by the polygon defined by the GCPs located at the edge of the study area. The DSMs cover the tidal flat only and there is no vegetation inside the study area, except for rare and erratic patches of *Spartina,* considered insignificant due to their small size and reduced distribution. It is important to note that the B3 test has the same coverage as B1, which means that 2 ha only were processed with two sets of photos at 40 and 80 m of altitude, while the rest of the area was processed with photos at 80 m of altitude.

The photogrammetric processes and their resulting products (i.e., the DSM and the orthophotos), were referenced in WGS84/UTM zone 33N (EPSG:32633).

***Table 1*** *- Summary of the photogrammetric test characteristics.*

| Test ID | Date of the surveys | Number of images | Ground Resolution (cm/pix) | GCP | Altitude (m) | Coverage (ha) | GPS points | Density GCP/ha | RMSE* vs GPS (m) |
|---|---|---|---|---|---|---|---|---|---|
| A | **24/10/2018** | 345 | 3.56 | 17 | 80 | 8.71 | 53 | 1.95 | 0.057 |
| B1 | | 198 | 3.47 | 19 | 80 | 6.49 | 77 | 2.93 | 0.034 |
| B2 | **18/02/2019** | 214 | 1.83 | 9 | 40 | 1.88 | 21 | 4.78 | 0.06 |
| B3 | | 412 | 2.58 | 18 | 80+40 | 6.49 | 77 | 2.77 | 0.031 |
| C | **09/07/2019** | 394 | 3.64 | 18 | 80 | 6.81 | 62 | 2.64 | 0.048 |
| D1 | | 205 | 3.46 | 20 | 80 | 7.11 | 103 | 2.81 | 0.037 |
| D2 | **07/02/2020** | 285 | 2.63 | 20 | 60 | 7.11 | 103 | 2.81 | 0.04 |
| D3 | | 490 | 2.97 | 20 | 80+60 | 7.11 | 103 | 2.81 | 0.041 |

** The RMSE is referred to DSMs with 0.1 m of spatial resolution.*

### 2.3.3 Validation of the DSMs

The elevation of the (GPS-based) validation points was compared with the UAV-derived DSM elevation in order to calculate the RMSE (Root Mean Square Error) (1) which, if the points are well distributed within the domain, represents a fair estimation of the accuracy of the drone-derived product:

$$\mathbf{RMSE} = \sqrt{\frac{\sum_{i=1}^{n}[(\boldsymbol{Z_{DSM}} - \boldsymbol{Z_{GPS}})^2]_i}{\boldsymbol{n}}} \quad (1)$$

where $Z_{DSM}$ is the vertical elevation of the DSM and $Z_{GPS}$ is the vertical elevation of the GPS point.

It should be noted that, in order to test the sensitivity of the RMSE to the variations in the resolution of the DSM, the tests C, D1 and D2 were exported at three different horizontal resolutions (0.1, 0.25, and 0.5 m) and compared with the GPS data.

### 2.3.4 Comparisons between Photogrammetric Tests

The pool of processed DSMs (Section 2.3.2) was compared by calculating the differences between couples of DSMs. Generally, this process is applied to evaluate the morphological changes between two DSMs representative of two instants in time, and its results are referred to as DEM of Difference (DoD). In the case of the current research, the comparisons were performed between DSMs representative of the same instant in time (i.e., same day of the survey) in order to understand the sensitivity of the DSM to changes in UAV flight altitude, GCP number, and distribution. The differences were evaluated in terms of vertical and volumetric variations. The DoD as defined in this paragraph will be referred to as DEMs of Error (DoE) in the following, in order to highlight that this product refers to the variation/error due to the field and photogrammetric input. It is important to understand that the DoEs do not provide information about the evolution of the study area.

The coverage between the 40 m DSM and the others is different, consequently, two areas were examined: one of about 4.7 ha and the other one of about 1.8 ha, so the DoEs are calculated separately.

### *2.3.5 DEM of Difference: Evolution of the Area*

As anticipated, a DoD represents the vertical variations of an area between two instants in time, as represented by two DSMs. For this study, four-time intervals were considered: i) from October 2018 to February 2019, ii) from February 2019 to July 2019, iii) from July 2019 to February 2020 and, finally, iv) the whole period from October 2018 to February 2020 (Fig. 6). DoDs were computed and analysed to understand the evolution of the tidal flat.

### *2.3.6 Significance of the Vertical Differences*

In order to evaluate the significance of the identified vertical variations, both DoEs (Section 2.3.4) and DoDs (Section 2.3.5) were computed with a tool developed by Wheaton et al. (2010) called Geomorphic Change Detection (GCD). This tool estimates vertical and volume variations between DEMs, and the related uncertainties considering a threshold for change detection (TCD) below which the variations are not considered significant; thus, the most significant changes are highlighted.

This is important as calculations between DSMs cause the propagation of individual errors. By not taking into account the propagated error, DoDs (or DoEs) might provide unreliable information on the vertical and volume variations. The GCD tool provides an effective way to account for the uncertainty of the results in terms of vertical and volume changes, considering the original uncertainty/error of the input DSMs.

In this study, it is assumed that the DoDs and DoEs have a spatially constant uncertainty which is assessed by linear propagation of the uncertainty/error of the original DSMs, using the following equation (2):

$$\delta Z_{DoD/DoE} = \sqrt{\delta Z_1^{\,2} + \delta Z_2^{\,2}} \qquad (2)$$

where $\delta Z_{DoD/DoE}$ is the propagated error, while $\delta Z_{1,2}$ are the individual errors of the DSMs used for the calculations. The spatial uniform TCD is considered equal to the propagated error. Notably, other studies applied a statistical coefficient to the propagated error (e.g., t-value [76-78]) to define the TCD, thus assigning a significance level to it. In the case examined here, due to the nature of the study area, and the entity of the monitored morphological changes, the applied t-value is 1, which corresponds to a significance level of 68%, while a t-value equal to 1.96

corresponds to a significance level of 95%. Although this ensures higher confidence in the results, doubling the TCD while assessing morphological changes in such tidal environments might lead to a massive loss of data.

The GCD provides information about areal, volumetric, and vertical changes that include areas of surface lowering or raising, total and net variations, definition of the area of interest (i.e., the entire study area) and the area with detectable changes (i.e., the area with changes above the TCD) with relative uncertainties.

The differences calculated through the DoEs (Section 2.3.4) are expressed as the sum of all volume variations, hereby referred to as the Total Volume Variations, which was calculated considering all vertical changes (TVV), and only the significant one (TVVtcd). In the latter case, by definition, the calculations refer to the Area with Significant Variations (ASV), which corresponds to the area with detectable changes. The calculated ratio between the TVV (TVVtcd) and the entire domain (the ASV) defines the Total Average Vertical Difference (TAVD and TAVDtcd, respectively) which represents the vertical difference between the tests.

The morphological differences, evaluated through DoDs, were used to assess—in addition to the TVV—the Net Volume Variation, as the difference between deposited and eroded volumes, calculated considering all vertical changes (NVV), and only the significant ones (NVVtcd). The Vertical Rate of Change (VRC) was calculated as the ratio between the NVV and the entire domain, over the time period analysed, reproportioning it over a year. The VRC was also calculated only considering the significant changes (VRCtcd), thus using the ASV as the reference area.

Note that, because of the different coverage of the photogrammetric tests (see Section 2.3.4), two reference areas were considered: one of about 4.7 ha and the other one of about 1.8 ha (see Fig. 5a). Thus, the GCD tool was applied accordingly (Section 2.4.3 and 2.4.4).

### *2.3.7 Integrated Geomorphological Interpretation*

The orthophotos, volumetric analysis, and on-field observations enabled interpretation of the recent evolution of this tidal flat. All of the results were compared with the hydrometric records and the average flow discharge of Pontelagoscuro obtained from AIPO (Agenzia Interregionale per il Fiume Po), which is the nearest station to the Po Delta.

The elevation changes were compared with other microtidal flats worldwide, in particular to man-made deltas or coastal wetlands that were heavily influenced by human intervention, and the

processes dominating these environments were discussed to find similarities or differences in their evolution.

## *2.4 Results*

### *2.4.1 Tidal Flat Morphology*

The tidal flat is protected northward by the barriers of the lagoon which prevent waves from influencing this area. The river and tidal currents are most probably the principal means of sediment transport (Fig. 7a). This observation is suggested by the presence of several crevasse splay structures that characterise the study area (Fig. 7b). During floods, the sediment is brought into the tidal flat, from south to north, by four mouths located in the channels (two in the east channel and two in the west channel). The largest crevasse splay is located in the central-east zone and it is built up by both east inlets (Fig. 7c in yellow); this sedimentary structure is particularly visible in the orthophoto of February 2020 after the strong flood of November-December of 2019. A second one is in the central-west zone, next to the first western mouth (Fig. 7c in azure). One last large area of deposition is in the most western part, where vegetation did not completely colonise the channel levee (Fig. 7c in white). Two central creeks are visible next to each inlet (except for the farther west part) where the current velocity exerts its strongest effect. The creeks are not very developed, and their length ranges from 30 to 100 m. It is notable from both orthophotos and DSMs that the creeks are developing following a NNW direction; this irregular (curved) creek shape suggests that flood influence could be higher than tidal currents alone. During high tide, the whole tidal flat is covered by water. The only vegetation able to grow in the area, excepting the levees, consists of sporadic patches of *Spartina* and algae. During the study period, the tidal flat did not undergo consistent alteration and the principal changes were observed in the crevasse splays.

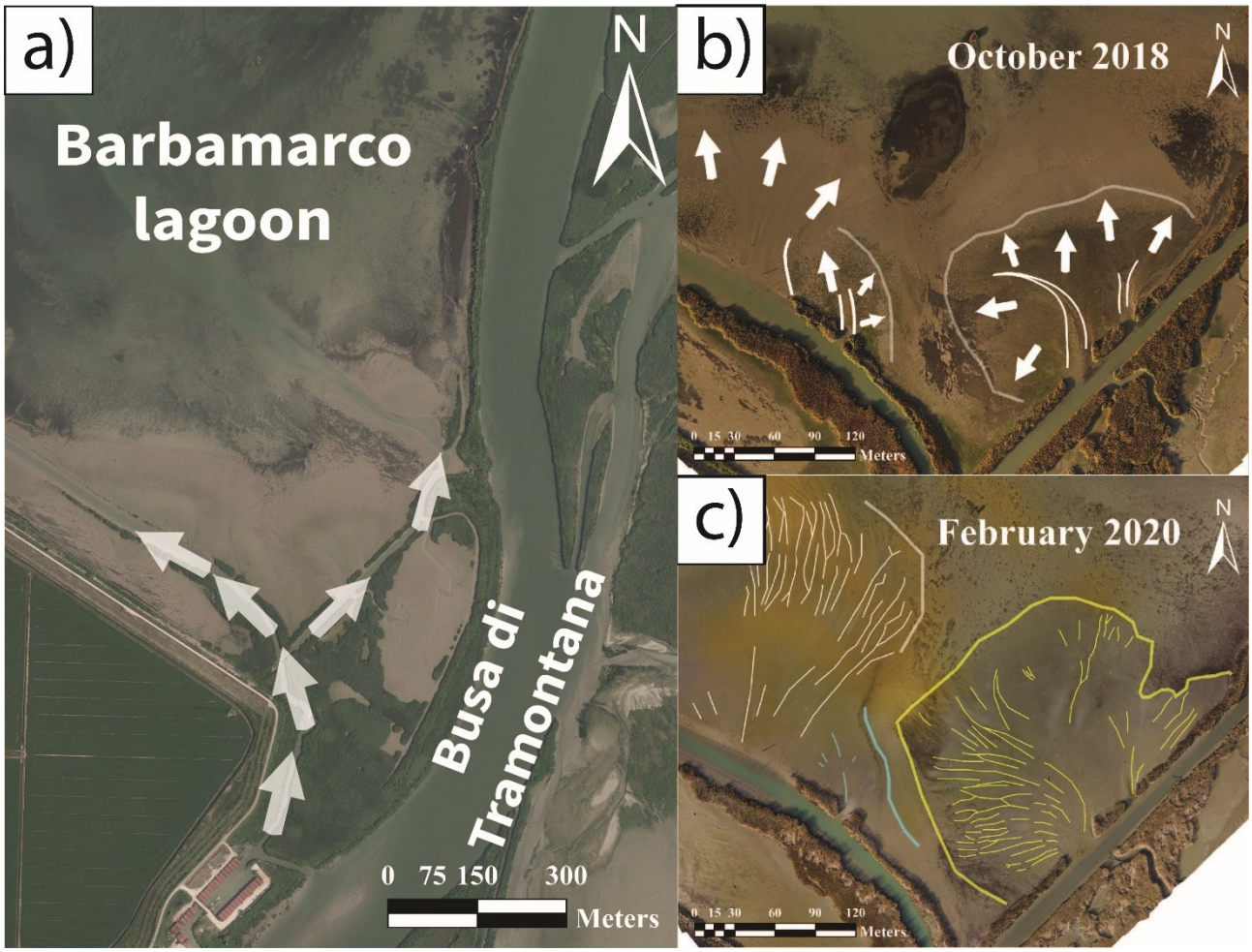


***Figure 7*** *–(a) Orthophoto developed by Agea in 2015. The arrow indicate the direction of the river flow that follows the channel that connects the Busa di Tramontana/Po della Pila with the Barbamarco lagoon. The Orthophotos on the right were produced by the authors after the survey of b) October 2018 and c) February 2020. In Figure b) the location of the crevasse splays are shown, as well as the creeks and how the sediment deposition occurs. In Figure c) three depositional areas are identified: the largest crevasse splay and its small creeks are shown in yellow: they formed after the flood of November-December of 2019; in light blue, the smallest crevasse located in the south-west section is shown; in white, a large depositional area located in the west part is shown. Orthophoto produced after the survey of b) October 2018 and c) February 2020. In Figure b) the location of the crevasse splays are shown, as well as the creeks and how the sediment deposition occurs. In Figure c) three depositional areas are identified: the largest crevasse splay and its small creeks are shown in yellow: they formed after the flood of November-December of 2019; in light blue, the smallest crevasse located in the south-west section is shown; in white, a large depositional area located in the west part is shown.*

## *2.4.2 Differences due to DSM Resolution*

The spatial resolution of the elevation model does not significantly affect the error calculations. The variations between the RMSEs of the same tests with 0.1, 0.25, and 0.5 m resolutions are millimetric, or sub-millimetric (Table 2). Overall, the RMSE decreases for the DSMs with a

resolution of 0.5 m and it is higher for the DSM with the 0.1 m resolution; however, this variation is lower than 1 mm and might be mostly due to the smoothing process. Indeed, as expected, lower resolutions (e.g., 0.5 m) generate smoother profiles (Fig. 8). While the variations arising from the different resolutions appear negligible, differences in volume estimations based on the different resolution of the input DSMs are also contained (Table 3); for example, the DoEs calculated between the D1 and D2 tests with different resolutions show volume differences in the order of 20-30 $m^3$, which consistently decrease when only considering the significant changes (i.e., higher than the TCD), while the DoDs calculated between C and D1 or D2 show volume variations around 50 $m^3$, which increase to ~70 $m^3$ for the significant changes. This means that the spatial resolution of the extracted DSMs does not influence the results. The results reported in the following sections were produced using DSMs with a spatial resolution of 0.1 m.

***Table 2*** *- RMSE variations between DSM exported at varying resolutions.*

| Photogrammetric Test | Resolution [m] | RMSE [m] |
|---|---|---|
| **C** | 0.1 | 0.048 |
| | 0.25 | 0.047 |
| | 0.5 | 0.046 |
| **D1** | 0.1 | 0.037 |
| | 0.25 | 0.037 |
| | 0.5 | 0.036 |
| **D2** | 0.1 | 0.039 |
| | 0.25 | 0.039 |
| | 0.5 | 0.038 |

***Table 3*** *- Total Volume Variations (TVV) between DSM exported at different resolutions considering no threshold and with threshold (TCD).*

| Comparison between: | Resolution [m] | TCD [m] | TVV [$m^3$] | TVVtcd [$m^3$] |
|---|---|---|---|---|
| **D1 - D2** | 0.1 | 0.05 | 668 | 13.9 ±11.4 |
| | 0.25 | 0.05 | 652 | 13.5 ±10.6 |
| | 0.5 | 0.05 | 641 | 15.1 ±9.3 |
| **C - D1** | 0.1 | 0.06 | 2196 | 1194.7 ±839.7 |
| | 0.25 | 0.06 | 2182 | 1175.8 ±831.1 |
| | 0.5 | 0.06 | 2150 | 1124.8 ±802.2 |
| **C - D2** | 0.1 | 0.06 | 2469 | 1507.9 ±1069.6 |
| | 0.25 | 0.06 | 2469 | 1503.3 ±1069.5 |
| | 0.5 | 0.06 | 2417 | 1438.3 ±1038.9 |

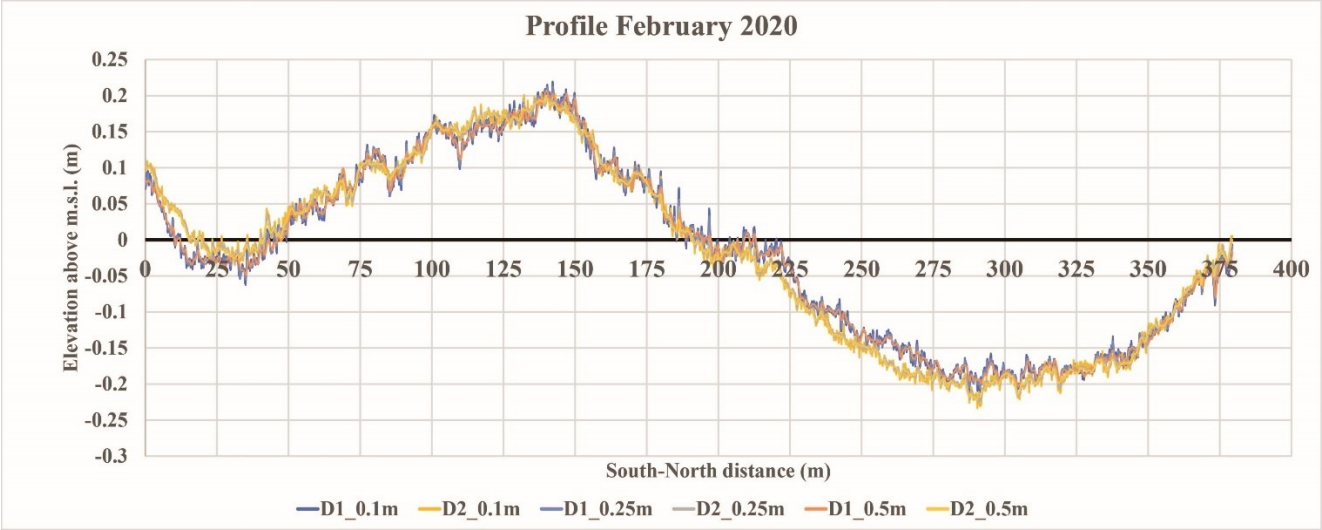


***Figure 8*** *- Different resolutions of the DSM profiles at 80 m (D1) and 60 m (D2) of altitude from the survey of February 2020 (transect in Figure 5b).*

### *2.4.3 DSM Error Assessment*

Overall, the RMSEs of the analysed tests vary between 3.1 and 6 cm (Table 1). The A test based on images taken at an altitude of 80 m is characterised by one of the highest RMSE (5.7 cm), the highest coverage (8.7 ha), and the lowest density of GCPs. The B1 and the B3 tests of February 2019 have the lowest RMSE (~3 cm). It is notable that the B2 test has a higher error (6 cm) despite its showing the highest GCP density. The C test of July 2019 is based on images taken at an altitude of 80 m and shows an RMSE of 4.8 cm. This test has a higher GCP density when compared to the A test. The two flights of the last survey of February 2020 cover the same area at different altitudes (80 m and 60 m) with the same number of GCP (20 GCPs in 7.1 ha). In all D tests, the RMSE does not significantly vary more than 4 cm although it is slightly lower in the D1 test and slightly higher in the D3 test. The RMSE of the D tests is calculated using all validation points, including the transect (see Section 2.3.1). The accuracy does not change significantly (i.e., variations of ~1-2 mm) if the GPS points of the transect are excluded.

### *2.4.4 Differences due to Flight Altitude*

The results of the analysis of the DoEs are shown in Table 4. It is notable that the volume differences (TVV) between all tests on the 4.7 ha area range between ~475 and ~1000 $m^3$ without applied threshold, and decreases (overall ≤ 380 $m^3$, maximum, including uncertainty) when considering significant differences (i.e., with applied TCD) only. These values concern tests with

RMSE of 3 – 4 cm (i.e., B1, B3, and D). The TVV increase for the DoEs concerning the B2 test (i.e., B1_B2, B2_B3): by reproportioning based on the covered area, the volume variation is ~2050 $m^3$ (no TCD) and ~1460 $m^3$ (with TCD, maximum, including uncertainty). Conversely, the AVDs with an applied threshold (AVDtcd) are generally higher for the D tests compared to the B ones. This is mostly due to the fact that the AVD is calculated based on the ASV, and not on the entire covered area used for regular AVD computation.

Most of the DoE values are below the threshold (Fig. 9c, 9d, 9e, 9f), but higher values can be observed where the GCP density decreases. For example, in the northern area, where there is the largest gap in the GCP distribution, the DoE B1_B3 shows values of vertical differences between 0.1 – 0.15 m. The D tests are characterised by lower vertical variations, reaching a maximum of 0.05 – 0.1 m. Patterns can be highlighted for all the tests shown in Fig. 9: there is an increase of (absolute) vertical differences moving northward, and closer to the vegetation at the borders of the south-west channel. This suggests that other factors, besides GCP distribution, may cause an increase in variations, such as, for example, the increased presence of water on the tidal flat surface moving towards the internal part of the lagoon, and the shadows due to the vegetation located at the borders of the channel.

An observation of the tests on the transect surveyed in February 2020 brings to light other details. First, the DSMs values of February 2019 were extracted based on the track of the transect surveyed one year later (Fig. 10a): the vertical differences in the order of 0.1 m are visible between the B2 test and the others. The B1 and B3 tests are very similar in the first 150 m of the profile, which coincide with the B2 extension; from 150 m to 300 m the B3 test shows higher elevations with respect to B1. However, the vertical difference is about 0.05 m. The differences amongst the D tests are generally lower than 10 cm (Fig. 10b); in the same figure, it is notable that most of the validation points are lower than the D tests, indicating that the DSMs generally overestimate (RMSEs ≤ 4.1 cm) the elevation of the surface when compared with GPS measurements. These lower GPS values, in particular, are probably due to a systematic error occurring during the survey when the tip of the GPS pole sinks in the mud, which is a common problem in a soft-sediment environment (Casella et al., 2020).

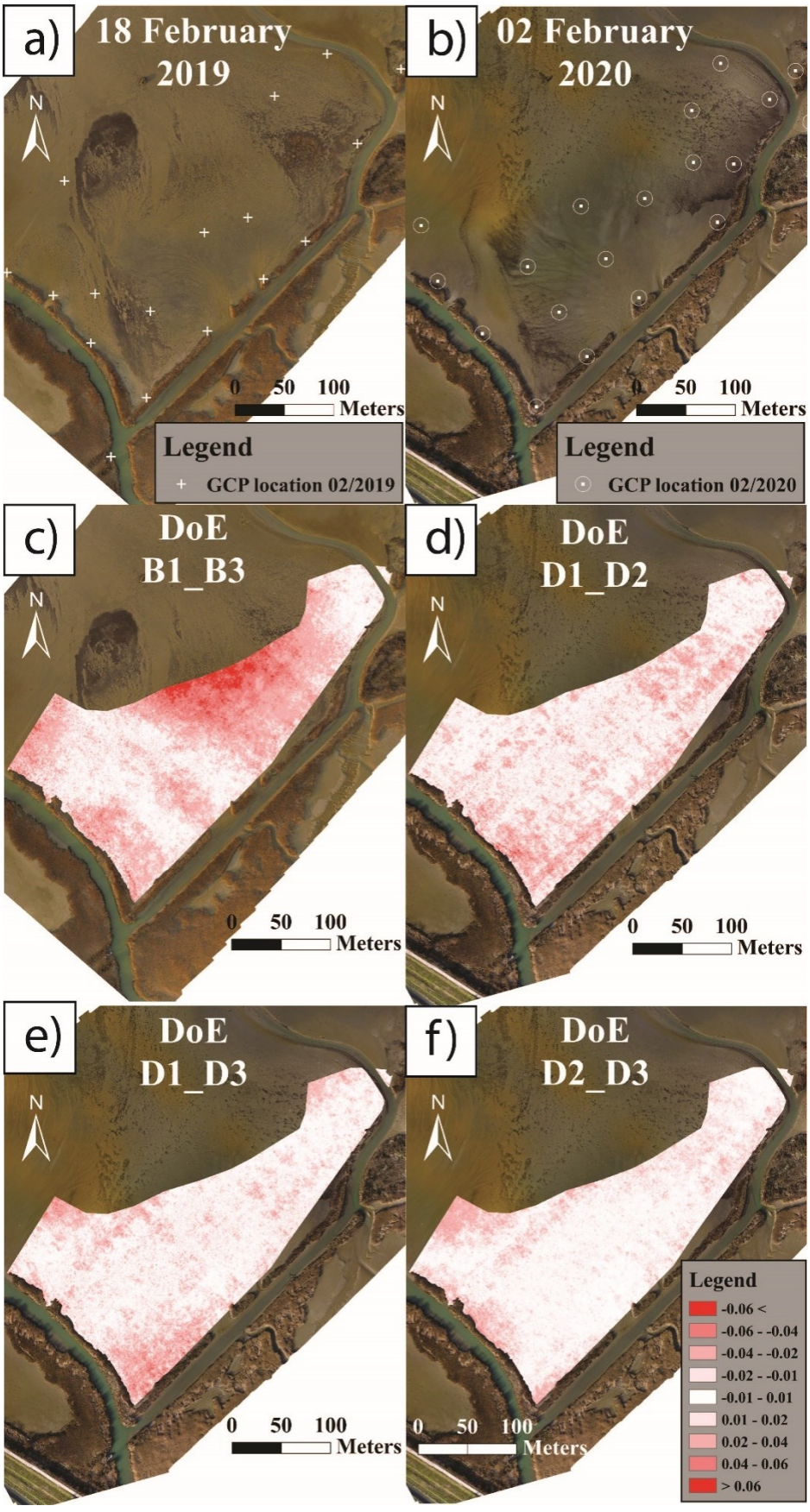


***Figure 9*** *- Orthophotos of February 2019 (a) and February 2020 (b) with GCP location. In figure c,d,e,f the DoEs are shown. (c) Variations between the B1 and the B3 of February 2019; (d,e,f) Variations between D1, D2, D3 of February 2020.*

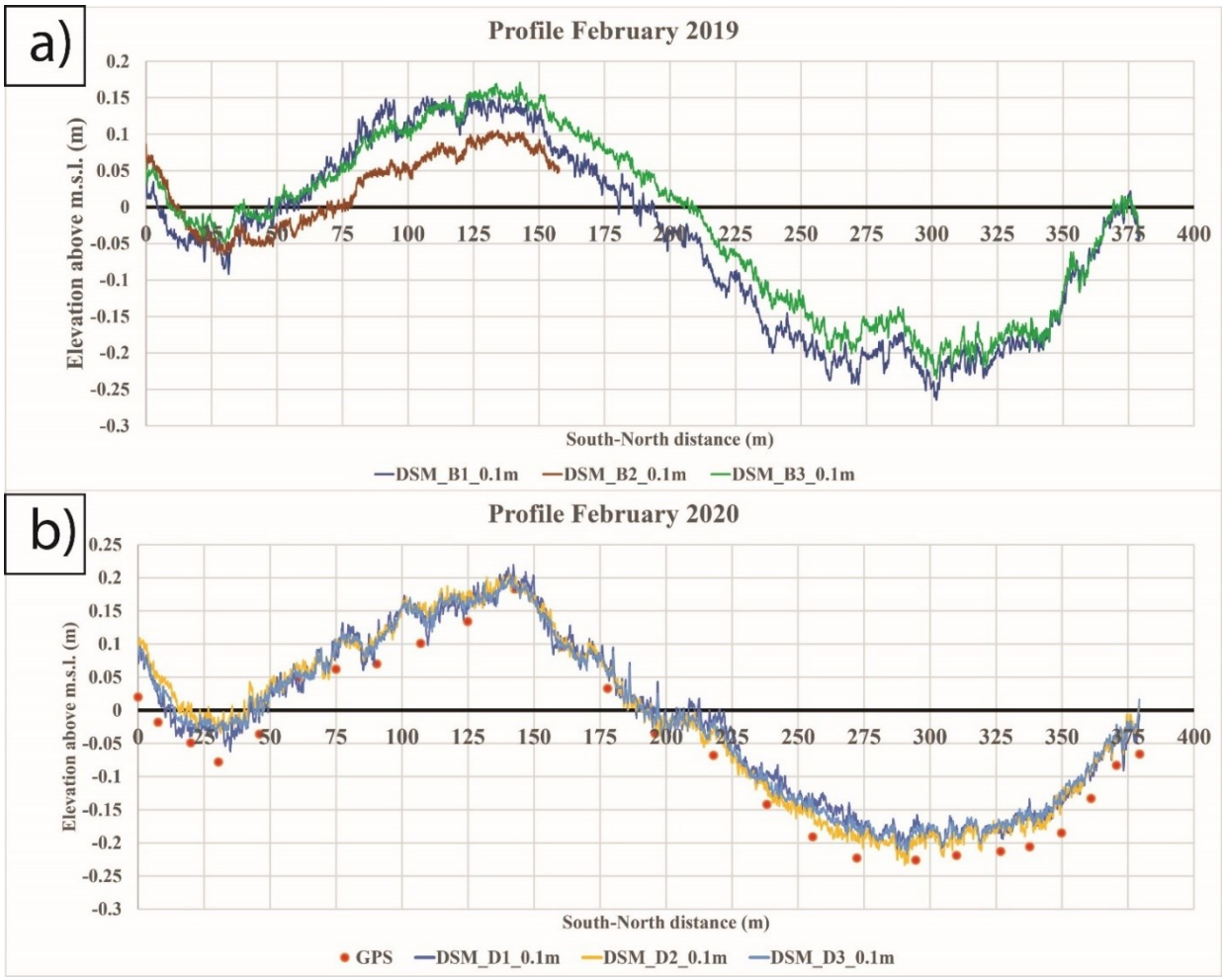


***Figure 10*** *- (a) Profiles of the B tests of February 2019; (b) Profiles of the D tests of February 2020 and validation points of the GPS survey (transect in Figure 2b)*

***Table 4*** *- Total Volume Variations (TVV) and Total Average Vertical Difference (TAVD) of DoEs of the February 2019 survey in an area of 4.7 ha and the February 2020 survey in an area of 1.8 ha; the values are calculated considering no threshold and with threshold (TCD) located in the Area with Significant Variation (ASV).*

| DoE ID | Area [ha] | TCD [m] | TVV [$m^3$] | TVVtcd [$m^3$] | TVVtcd / TVV [%] | ASV [$m^2$] | TAVD [m] | TAVDtcd [m] |
|---|---|---|---|---|---|---|---|---|
| **B1_B3** | 4.72 | 0.05 | 1062.3 | 208.6±173.3 | 20±16 | 3546.3 | 0.02 | 0.06±0.05 |
| **D1_D2** | | 0.05 | 668.3 | 13.9±11.4 | 2±2 | 227.1 | 0.01 | 0.06±0.05 |
| **D1_D3** | | 0.06 | 588.3 | 3.5±2.4 | 1±0 | 39.6 | 0.01 | 0.09±0.06 |
| **D2_D3** | | 0.06 | 475.3 | 0.9±0.4 | 0±0 | 6.1 | 0.01 | 0.14±0.06 |
| **B1_B2** | 1.77 | 0.07 | 765.8 | 299.1±251.9 | 39±33 | 3599 | 0.04 | 0.08±0.07 |
| **B1_B3** | | 0.05 | 310.9 | 6.5±5.9 | 2±2 | 117.7 | 0.02 | 0.06±0.05 |
| **B2_B3** | | 0.07 | 778 | 110.3±103.5 | 14±13 | 1478.7 | 0.04 | 0.07±0.07 |

### *2.4.5 Morphological Changes*

The morphological changes were analysed using DoDs (see Section 2.3.5) and the GCD tool (see Section 2.3.7), thus identifying significant vertical changes (i.e., higher than the TCD). The results are presented in the maps in Fig. 11 and in Table 5. The area of interest of the analysis is ~4.72 ha. The morphological changes are analysed considering four-time intervals: i) from October 2018 to February 2019 (Fig. 11a); ii) from February 2019 to July 2019 (Fig. 11b); iii) from July 2019 to February 2020 (Fig. 11c); and iv) the whole period from October 2018 to February 2020 (Fig. 11d). The morphological changes are presented here below by focusing on net volume variations (NVV) and vertical rate of change (VRC), calculated by considering the NVV.

During the first time interval—from October 2018 to February 2019 (117 days)—the study area does not show remarkable changes. The DoDs B1-A and B3-A show—without applying TCD—two different scenarios (Table 5): one is characterised by a sediment loss of ~ 400 $m^3$, the other shows a sediment gain of ~ 170 $m^3$. The same DoDs analysed only considering significant changes (i.e., with applied TCD) show in both cases a sediment loss, but considering the uncertainty, the trend is not established. These values make it unclear if there is an overall erosive or accretional trend, suggesting that in these few months the tidal flat did not experience considerable changes. Nevertheless, the maps (Fig. 11a) show that the sediment is moving, causing accretion in the central-northern area reaching values of 12 cm, and erosion in the south-west area, with even higher values of up to 15 cm.

The pattern is confirmed for the second period analysed, from February 2019 to July 2019 (141 days). In this case, the DoDs C-B1 and C-B3 show an erosion of ~ 95 $m^3$ and ~ 680 $m^3$, considering all changes, while if only significant changes are considered, then a positive sediment budget is highlighted. However, once again, the uncertainty ranges are large and include almost null sediment budget as well as erosive trends. The erosion is quite extended throughout the central area (up to ~15 cm), while the accretion is concentrated in the northern area (up to 20 cm) (Fig. 10b).

During the third time interval—from July 2019 to February 2020 (213 days)—significant changes occurred. After the period presented above, the previously described trends were reversed and the central area presented high elevation changes (up to 25 cm), while the northern area demonstrates erosion (up to 20 cm) (Fig. 11c). The sediment budget is positive for all DoDs, with an average deposit of ~1300 $m^3$ considering all changes. The evaluation of the significant changes

confirms the positive pattern (average volume ~950 $m^3$). In addition, all tests (C-D1, 2, 3) show uncertainty ranges which, although wide, do not include null or negative budgets, thus confirming the positive pattern.

Considering the whole study period—from October 2018 to February 2020 (471 days)—the tidal flat gained ~790 $m^3$ on average when considering all changes, and ~420 $m^3$, on average when calculating the significant changes. Although the uncertainty ranges widely diverge and do not allow incontrovertible considerations, overall the study area shows a positive trend where the principal area of accretion is located in the central-northern part characterised by vertical changes ~15 cm, while the south-west part is eroding with a similar trend that is particularly high next to the channel (>30 cm) (Fig. 11d).

The net rates presented (VEC and VECtcd, Table 5) reflect the volume variations and are highly variable, since they show different trends based on the period, ranging from -3.3 to 4.6 cm/year, considering all changes. The values of VECtcd present high variability that ranges between -7.8 to 9.7 cm/year, excepting for the B1-A tests that show a higher value due to localised erosion of the mouth of the west channel (Fig. 11a). The corresponding uncertainty range falls between 16.8 and 4.4 cm/year (19.8 cm/year for the B1-A test), suggesting that the evaluation is highly uncertain.

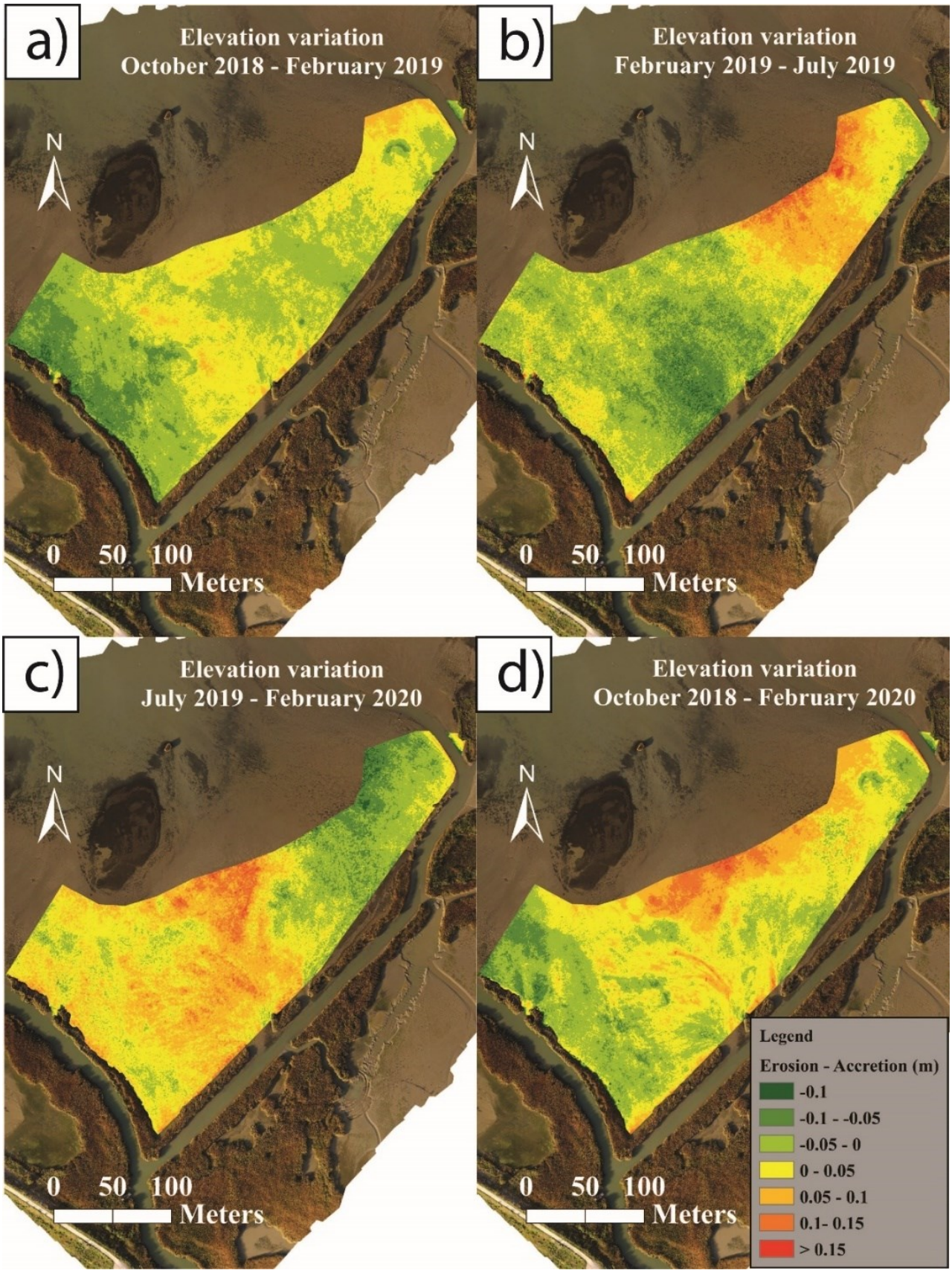


***Figure 11*** *- Elevation changes between (a) October 2018 and February 2019; (b) February 2019 and July 2019; (c) July 2019 and February 2020; (d) the whole period from October 2018 to February 2020.*

***Table 5*** *- Summary of Total Volume Variations (TVV), Net Volume Variations (NVV) and Vertical Rates of Changes (VRC) for each time interval and DoD considering no threshold and with threshold (TCD) located in the Area with Significant Variations (ASV).*

| **Time interval** | | **DSMs** | **TCD** | **TVV** | **TVVtcd** | **NVV** | **NVVtcd** | **ASV** | **VRC** | **VRCtcd** |
|---|---|---|---|---|---|---|---|---|---|---|
| Period | Days | | [cm] | [$m^3$] | [$m^3$] | [$m^3$] | [$m^3$] | [$m^2$] | [cm/year] | [cm/year] |
| Oct. 2018 / Feb.2019 | 117 | B1-A | 7 | 1298 | 229±173 | **-418** | **190±157** | 2476 | -2.8 | -23.9±2 |
| | | B3-A | 7 | 1587 | 482±165 | **167** | **90±262** | 5260 | 1.1 | -5.4±15.5 |
| Feb. 2019 / Jul. 2019 | 141 | C-B1 | 6 | 1856 | 920±647 | -94 | 191±388 | 7633 | -0.5 | 6.5±13.2 |
| | | C-B3 | 6 | 1764 | 686±529 | -680 | -300±416 | 8816 | -3.7 | -8.8±12.2 |
| Jul. 2019 / Feb.2020 | 213 | D1-C | 6 | 2197 | 1195±840 | **1187** | **818±718** | 13996 | 4.3 | 10±8.8 |
| | | D2-C | 6 | 2497 | 1508±1070 | **1296** | **946±887** | 17827 | 4.7 | 9.1±8.5 |
| | | D3-C | 6 | 2415 | 1439±1011 | **1438** | **1087±889** | 16848 | 5.2 | 11.1±9 |
| Oct. 2018 / Feb. 2020 | 471 | D1-A | 7 | 1717 | 605±435 | 674 | 421±381 | 6210 | 1.1 | 5.3±4.8 |
| | | D2-A | 7 | 1630 | 554±409 | 783 | 355±350 | 5843 | 1.3 | 4.7±4.6 |
| | | D3-A | 7 | 1745 | 661±471 | 925 | 496±425 | 6728 | 1.5 | 5.7±4.9 |

## 2.5 Discussion

### 2.5.1 Morphodynamic Interpretation

#### 2.5.1.1 Tidal Flat Evolution

Tidal flats are known as dynamic environments. Nevertheless, they usually do not show remarkable morphological variations in short intervals of time (e.g., shorter than 6 months) unless a significant event occurs. Indeed, during the first 3 months of the analysed period (i.e., October 2018 – February 2019), and the following 5 months (i.e., February 2019 – July 2019), the Pila tidal flat did not show notable changes. The analysis was not able to clearly identify a morphodynamic trend, because of the high variability of the calculated net volumes and related uncertainty. Furthermore, the area with significant changes (i.e., exceeding the TCD) is limited (ASV max ~1.8 ha, over an area of interest of 4.7 ha). These observations do not mean that the results are uninterpretable; they suggest that it is unclear if the tidal flat underwent sediment loss or a stable condition. In both cases, during the spring–summer season, the central zone of the study area seems to have experienced sediment loss while the northern part accreted, which infers that the sediment is moving northward, inside and outside the study area.

During the remaining 8 months (Jul. 2019 – Feb. 2020), the variations become more evident. In all cases, a positive trend is shown with high vertical rates of change (4.7 cm/year and 10.1±8.8 cm/year, considering all and only significant changes, respectively), in particular in the central-northern zone.

Two principal trends seem to be followed: erosion/stability during the spring–summer season, when the tidal flat loses sediment or maintains a stable condition; and accretion during the autumn–winter season. These trends seem to coincide with the river discharge peak seasons: the most important floods caused by rainfall during winter, and weaker floods due to ice melting during the spring season (Tesi et al., 2011). In fact, it is mandatory to compare these tendencies with the hydrometric records and the average flow discharge of Pontelagoscuro obtained from AIPO (Agenzia Interregionale per il Fiume Po) (Fig. 12a, 12b).

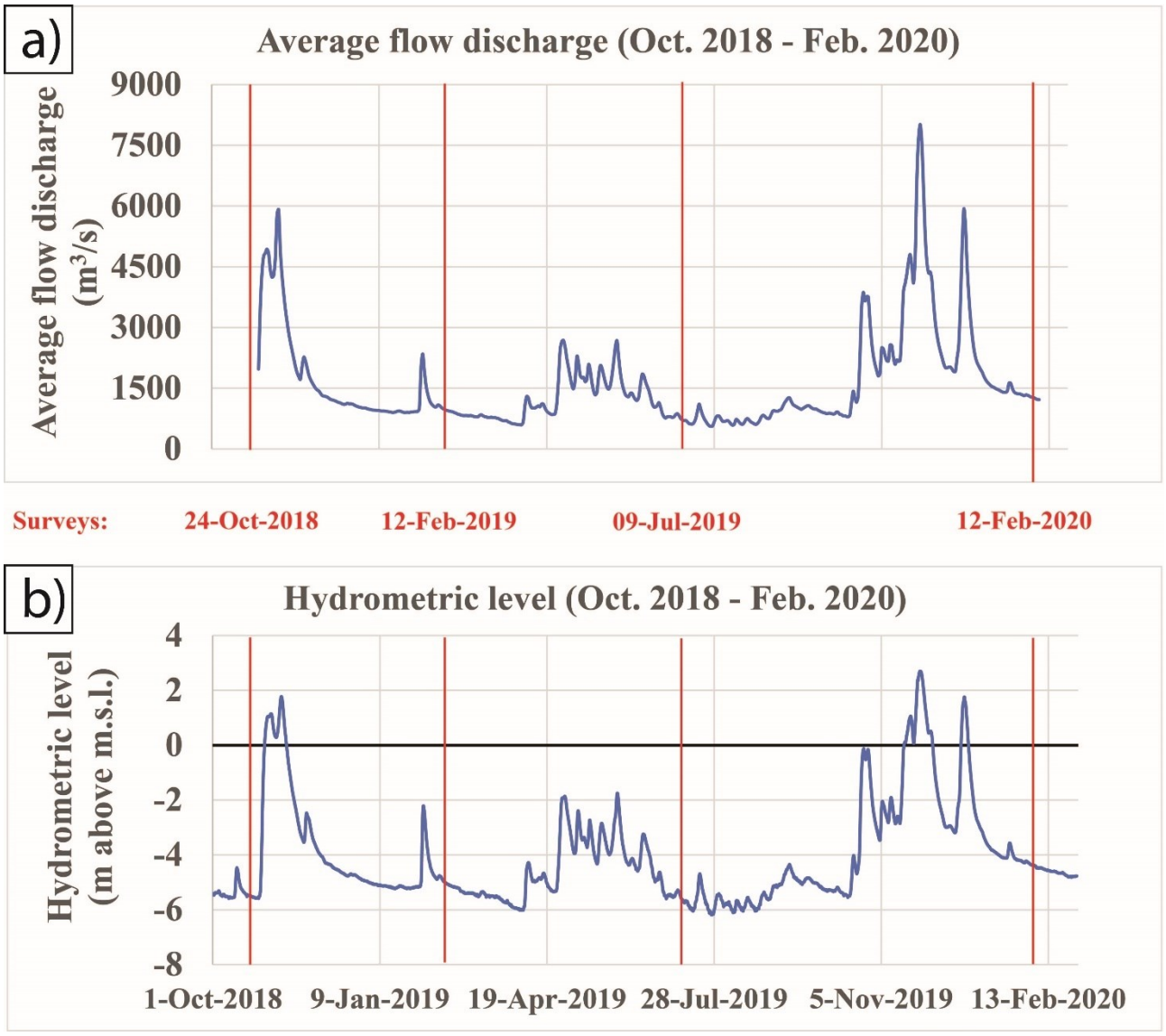


***Figure 12*** *- (a) Average flow discharge and (b) hydrometric level from the station of Pontelagoscuro. The dataset is provided by AIPO (Agenzia Interregionale per il fiume Po). The date of each survey is written in red.*

As shown in Table 6, the mean flow discharge and the mean hydrometric level for the whole study period were respectively about 1600 $m^3/s$ -4.1 m. In November 2018 only, there was a flood with a higher average flow discharge compared to the usual flow; the discharge peak was lower than 6000 $m^3/s$ and it lasted around 10 days. After February 2019, there were no significant floods; a few spikes are visible between April and July, probably due to small floods caused by snow melting (Palikas et al.,2005; Tesi et al., 2011). On the contrary, between November and December 2019, the Po River underwent heavy flooding (> 6000 $m^3/s$) that persisted for two months and caused a high volume of sediment transport. These events corresponded to the evolutionary trends of the tidal flat, thereby supporting the hypothesis that sediment transport is determined by river floods rather than by tides. In fact, Tesi et al. (2011) showed that significant deposition in this part of the

delta occurs only during large flood events; instead, only a small portion of material delivered by ordinary floods (~4000 – 6000 $m^3/s$) reaches the prodelta.

***Table 6*** *- Statistical description of the flow discharge and the hydrometric level for the entire study period.*

| **Average flow discharge ($m^3/s$)** | |
|---|---|
| **Mean** | 1592.6 |
| **St. Deviation** | 1191.8 |
| **Min** | 556.7 |
| **Max** | 8011.8 |
| **Hydrometric level (m)** | |
| **Mean** | -4.07 |
| **St. Deviation** | 1.84 |
| **Min** | -6.19 |
| **Max** | 2.7 |

Similar interpretations can be assessed for the vertical variations. The sediment loss caused an average lowering of the tidal flat of about 1.5 cm/year with significant values of 7.9±15.2 cm/year during the first 8 months, followed by 4.7 cm/year with significant accretion values of 10.1±8.8 cm/year during the last 8 months. Overall, the sediment budget of the tidal flat is positive for the entire analysed period, and sediment transport is particularly active in this part of the delta. The central crevasse splay is widening northward and the river seems to deposit ~800 $m^3$/year (~420±385 $m^3$/year by considering the significant changes only) with an average vertical change rate of 1.3 cm/year (5.2±4.8 cm/year by considering the significant changes only) for the whole tidal flat.

As previously explained, the DoDs were calculated reducing the domain of the DSMs to cover the same area and keep the validity of the DoDs. Unfortunately, this excludes most of the western part of the tidal flat from the analysis; hence, in order to show the vertical variations of the whole domain, the DoD between October 2018 and February 2020 was produced without filters, and it is shown in Fig. 13. It is important to note that in the north-west part of the domain the GCP density is lower and the vertical variations tend to increase, as previously shown; however, these errors do not influence the reliability of a qualitative interpretation.

The small creeks are not characterised by high rates of accretion, a common behaviour expected for creeks located in natural tidal flats, which are, in themselves, in a very young stage of development. The mud platform resists flow, causing it to be concentrated into the creeks which, typically, undergo an enlarging phase (D'Alpaos et al., 2006). Usually, the process is caused primarily by tidal currents but, in this study case, creek formation is probably owed to both river floods and ebb currents. The latter exert a greater influence on the morphology than flood tides do (Geng et al., 2020). Moreover, this research area is characterised by river floods and ebb tide direction both moving from south to north. The sedimentological analysis of sediment samples, collected during the period covered by this study but not reported in this paper, suggests that coarser sediment is located in the internal part of the crevasse splay, while finer sediment is found moving peripherally to these areas; judging from the low amount of deposited sediment during tidal cycles, it is possible to conclude that the tide reshapes the tidal flat and moves the sediment around the lagoon, while the hydrometric and flood discharge records suggest that the river is the principal sediment source.

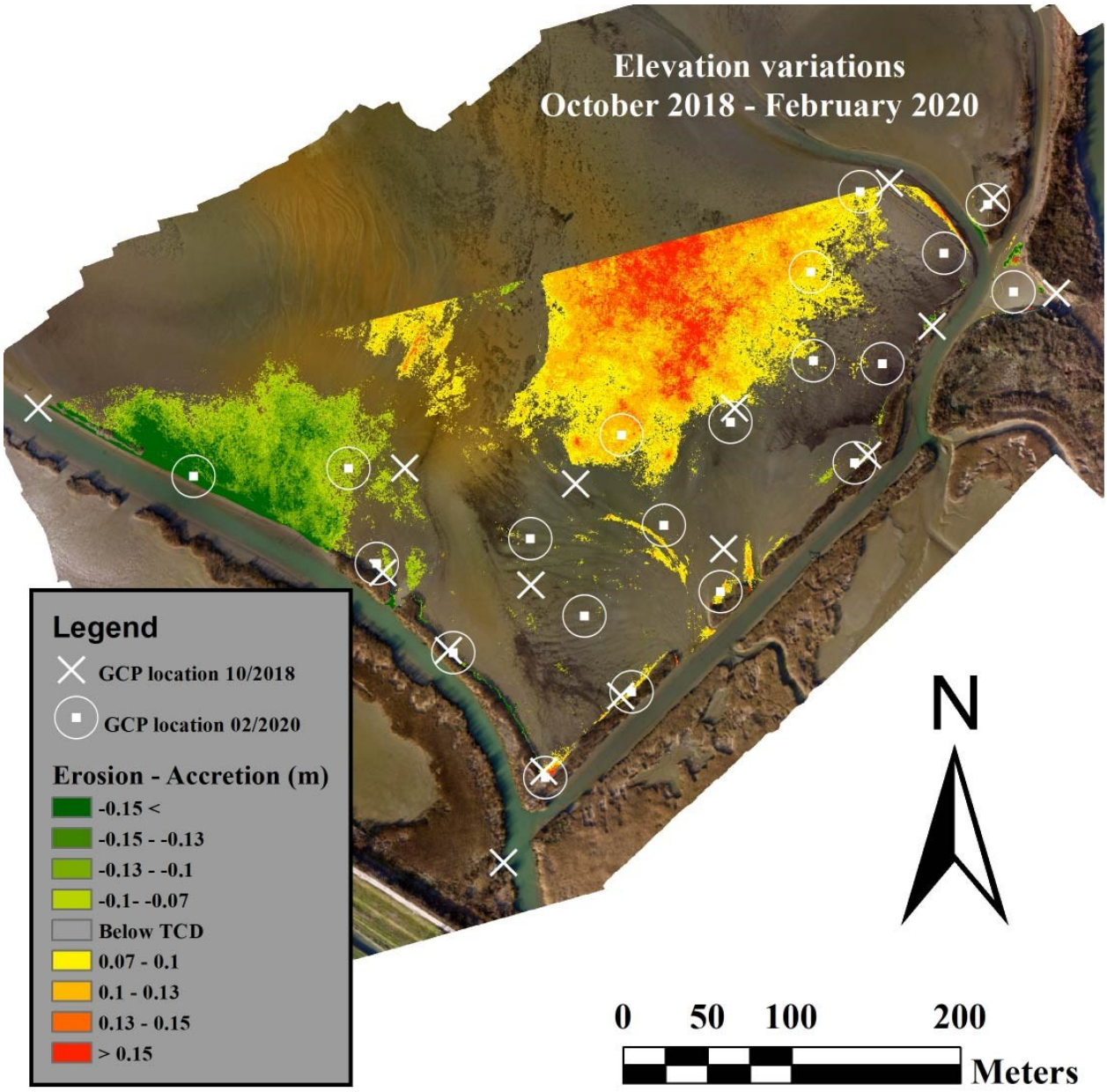


***Figure 13*** *- Rates of changes from October 2018 to February 2020 between DSMs at 80 m of altitude of the whole study area.*

Notably, the central-north part of the tidal flat is the section gaining sediment, with values of accretion higher than 0.15 m; conversely, the south-west section is still subject to erosive action with high values of erosion (higher than 0.3 m) principally next to the channel levees, which, when present at all, are very low compared to the other levees. This strong erosion could be caused by fishermen boats sailing across the channels. In fact, the west channel is frequently crossed by workers needing to move through the lagoon; the waves generated influence and erode the levees, in particular, on the west side. In this section, the vegetation is absent and cannot protect the levees as it does along the other channel. This is a common problem in tidal flats or salt

marshes situated close to harbours (Verney et al., 2007) or subject to intense boat traffic. Another possible reason for this strong erosion could be the formation of a new tidal creek—such as the ones seen in the inlets of the east channel—since the lack of vegetation could enable the floods and ebb tidal currents to exert a strong influence in this portion of the tidal flat.

#### *2.5.1.2 Comparisons with Other Microtidal Flats*

Seasonal variations are strictly connected to the driving process dominating tidal flat evolution. As an example, the Kongsmark tidal flat in Rømø Bight (Denmark) (Andersen et al., 2006), a temperate microtidal environment, shows similar rates of accretion (1.5 cm/year) compared to those observed for this study case. There the controlling processes for sediment transport are the tide and the waves. However, the sediment deposition is caused by algae binding, which grows during the spring–summer period (Frostick and McCave, 1979), while erosion occurs during the rest of the year. A different evolutionary trend is found in the Pila tidal flat since, as this study suggests, the sediment deposition is due to river floods rather than to other processes like vegetation sediment entrapment, hence accretion is higher during the autumn–winter flood periods. Despite this difference, both tidal flats show that microtidal basins are highly dynamic environments and they present high rates of accretion in short periods, reaching more than 3 – 4 cm/year.

A similar trend is found in the Waccassa Bay in Florida (US) (Wood and Hine, 2007). This coastal wetland seems to be characterised by higher sediment deposition during summer, rather than winter, because of higher biological activity. However, sediment deposition during winter seems to be controlled by storms (Goodbred and Hine, 1995; Wood and Hine, 2003). Like the previous site, these marshes seem to indicate an opposite trend compared to river-dominated marshes, since the seasonality of the processes that act as a sediment supplier is different; however, in all these environments, the sediment deposition occurs during specific periods and depends on episodic events.

The Venice Lagoon (Italy) does not show very high rates of accretion/erosion (~ 0.3 cm/year) (Day et al., 1998; Scarton et al., 2000; Ciavola et al., 2002) even though it is characterised by tidal and environmental conditions similar to the Po Delta. The lack of an important sediment supplier combined with the age of the wetland (the Venice Lagoon was formed by older consolidated salt marshes, whose higher elevation entailed decreasing sediment deposition (Pethick, 1981)) does

not allow the lagoon to undergo significant change, which is quite the contrary with respect to a tidal flat as young as the Pila one.

This important difference in sedimentation is also found in other American fluvial–deltaic landscapes such as the tidal flats of North Carolina (Dora et al., 2014), or in the Texas marshes (White et al., 2002), or in the Mississippi Delta in Louisiana (Hatton et al., 1983; Paola et al., 2011; Jankowski et al., 2017) where the accretion rates are millimetric due to a sediment deficit caused by human activities.

There are some cases in which tidal and fluvial sediment supply are complementary, like in the marshes and tidal flats of the Hudson River in New York (Yellen et al., 2021). These microtidal wetlands are characterised by rates of accretion of 0.6 – 1.1 cm/year. The sediment is brought into the tidal flats and marshes by both river discharges and high tides. Still, the river confirms its role as the principal sediment input.

Other deltas around the Mediterranean Sea Basin present similarities to the Po Delta, such as the Rhone River Delta in Southern France (Hensel et al., 1999). This large Mediterranean delta is characterised by a microtidal range of 0.3 m and river floods strongly influence the wetland evolution. Even if the delta is a wave-dominated type, the average elevation changes are quite high (1.1 cm/year), as in the Po case. The Ebro Delta in Spain suffers from sediment budget reduction due to the construction of dams, artificial levees, dikes, and canals, just like other sites previously mentioned. This activity is impacting the resilience capability of the marsh (accretion rates between 0.1 – 0.6 cm/year) (Ibáñez et al., 2010).

The results of this study are in line with Day et al. (2011), who measured and compared the vertical surface changes of the previously mentioned Mediterranean deltas (i.e., Po, Rhone, and Ebro deltas) with a SET. They discovered that the highest values were located next to river channels (i.e., 1 – 2 cm/year for all deltas), while the non-riverine sites had lower rates (few millimetres). The accretion rates of the study area confirm these observations and, most importantly, they show that river floods can cause a very high vertical surface increase in a very short period (4.2 cm/year). They also point out how important riverine inputs contribute to salt marsh survival.

Overall, microtidal wetlands are characterised by average vertical rates of accretion that range from a few millimetres to ~1.5 cm/year. Each microtidal wetland behaviour depends on a variety of factors (i.e., tidal range, river inputs, storm occurrences, wave influence, etc.) so it is

fundamental to understand the sediment transport mechanism and elevation changes in order to represent the tidal flat trend, focusing, in particular, on long-term vertical variations more than on just accretion (Cahoon, 1995; Cahoon et al., 2011). It appears evident that microtidal wetlands are highly dynamic and, in most cases, their sediment transport is dominated by episodic events (i.e., storms, floods) occurring during specific seasons; the influence of these factors on the morphology seems to be higher than in meso and macrotidal environments. In fact, although tidal flats and salt marshes in high tidal regimes are influenced by seasonal variations as well, the amount of deposited sediment is more impactful (e.g., (van Proosdij et al., 2006; Brunetta et al., 2019). Microtidal wetlands need these events in order to survive. In Table 7, the previously cited studies' vertical changes are summarised.

Despite these considerations, it is important to remember that vertical changes are strictly linked to the elevation above the mean sea level (Pethick, 1981), which means that different portions of the wetlands present different vertical rates. The averages of the vertical variations of whole systems are useful when comparing different environments but they are inaccurate when considering the capability of marshes to keep pace with Relative Sea Level Rise (RSLR). Kirwan et al., (2016) demonstrated that a static topographic representation, where the landscape does not modify with the RSLR, leads inevitably to marsh drowning; they suggest focusing the analysis on lower elevation areas because these are the most frequently flooded areas. Basically, studies should focus on distinguishing elevation changes in different vertical ranges. For example, the northern portion of the Pila tidal flat that ranges between -0.4 and -0.2 m above m.s.l. has elevation rates of 6 - 7 cm/year, which is a very high value compared to the whole tidal flat. Quite a different case is presented by the Lippenbroek tidal flat (NL)—an artificial tidal flat with controlled tidal amplitude (tidal range of 1.3 m), which had > 8 cm/year around 0 and 0.3 m above m.s.l. (Oosterlee et al., 2017). These sites are an example of how river-dominated transport can be just as important as tidal-driven sediment transport.

***Table 7*** *- Summary of studies in microtidal wetlands worldwide.*

| Location | Author | Average vertical rate of change [cm/year] | Mean tidal range [m] | Monitoring/monitored period [year] |
|---|---|---|---|---|
| Pila (Po Delta) (IT) | This study | 1.3 (5.2±4.8)* | 0.5 | 1.3 |
| Venice lagoon (IT) | Day et al. (1998)<br>Scarton et al. (2006)<br>Ciavola et al. (2002) | 0.3 | 0.8 | - |
| Kongsmark, Rømø Bight (DNK) | Andersen et al. (2006) | 1.5 | 1.8 | 8 |
| North Carolina, Orgeon inlet, Jacob's creek (US) | Craft et al. (1993) | 0.5 | 0.3 | 25 |
| Texas Bayhead plain (US) | White et al. (2002) | 0.51 - 0.33 | 1< | >100 |
| Louisiana Deltaic plain (US) | Hatton et al. (1983)<br>Jankowsky et al. (2017) | 1.3 - 0.4 | 1< | >6 |
| Waccassa bay (US) | Wood and Hine (2007)<br>Goodbred and Hine (1995) | 0.2 | 1.2 | >100 |
| Hudson river, New York (US) | Yellen et al. (2020) | 0.6 - 1.1 | 1.2 | >100 |
| Rhone Delta (FR) | Hensel et al. (1999) | 1.1 | 0.3 | 4 |
| Ebro Delta (ES) | Ibanez et al. (2010) | 0.1 - 0.6 | 0.2 | 3 - 9.5 |

**This range is representative of the significant changes occurring on the ASV, as defined in Section 2.3.7.*

## *2.5.2 UAV-based Tidal Flat Monitoring*

In this section, the main aspects of the approach are discussed, based on the photogrammetric tests and error assessment analysis of the UAV-based DSMs, and morphodynamical assessment. Suggestions will be given throughout this section to help researchers and practitioners in planning future field activities in tidal flats, taking into account the strengths and limitations of UAV-based surveys.

### *2.5.2.1 Field Implementation and DSM Error Assessment*

The quality of a UAV-based photogrammetric product (e.g., DSM) relies on several factors, most of which are linked to environmental conditions (e.g., sunlight, presence of water on observed surfaces, etc.) and field implementation (e.g., flight planning, GCPs positioning, etc.). In this study, all of the surveys were carried out under similar environmental conditions and using the same procedure. In particular, all drone surveys were performed at the reference flight altitude of 80 m. Moreover, for some of the surveys, additional altitudes were tested (i.e., 40 and 60 m). This allowed investigation into the influence of flight altitude—and indirectly, into the number and position of the GCPs—on the accuracy of the photogrammetry-based DSMs. These parameters are all strictly correlated, and they had to be taken into account when considering the spatial and

vertical accuracy of the photogrammetric products. The sensitivity analysis of the horizontal resolution (0.1, 0.25, 0.5 m) of the (exported) DSM product showed no variability in terms of error assessment (Table 2, 3). The following discussion concerns DSM error assessments implemented using DSMs with 0.1 m horizontal resolution. It was found that lowering the altitude of the reference flight (i.e., 80 m), or combining sets of photos taken at different altitudes during the same day of the survey, did not necessarily reduce the error (i.e., RMSE) of the photogrammetric product (i.e., DSM), which ranged between 3 and 6 cm. For example, in both surveys of February 2019 and February 2020, the RMSEs of the B2 (40 m) and the D2 (60 m) DSMs were higher than the error of the model produced with images from an 80 m altitude (i.e., B1 and D1, respectively). The difference between B2 and B1 might have been influenced by the different coverage and GCP distribution, but for D1 and D2 the GCP density was the same. The B3 DSM (February 2019, 40 + 80 m) had the best accuracy (RMSE = 3.1 cm), but the D3 (February 2020, 60 + 80 m) presented greater error (RMSE = 4.1 cm) than the D1 (80 m). Overall, a density of ~2.8 GCP/ha enabled the error estimation (i.e., RMSE) to be limited to around 3 – 4 cm. Notably, higher errors were found for lower (1.9 GCP/ha) and higher (4.8 GCP/ha) density of GCPs as well. These results suggest that 80 m (but also 100 m (Jaud et al., 2016), see Section 2.5.2.3) is a sufficient altitude to document tidal flat morphologies with UAV flights, and therefore to generate accurate photogrammetric elevation models. This reduces the flight time compared to 60 or 40 m altitude flights, and thus speeds up the field activities. However, tidal flats are commonly wide (e.g., several km), and consequently, UAV surveys can prove impracticable; therefore, it is important to find the right compromise between the required resolution and the extent of the study area.

The research herein confirmed that the number and distribution of GCPs are very important and must be considered in relation to the area being under surveyance. These findings are in line with previous works on UAV surveys (Sadeghi and Sohrabi, 2019; Sanz-Ablanedo et al., 2020); Sanz-Ablanedo et al. (2020) found that neither adding higher vertical imagery nor increasing the vertical photo overlap and mixing a higher number of crossed images (in flat environments) improved the accuracy. A possible explanation of these results for this type of environment could be that the lower the flight is, the harder it will be for the *SfM* algorithm to identify common (i.e., tie) points between images, considering that tidal flats are quite homogeneous in terms of texture and colours. This is particularly evident in the lowest flight (B2) where, despite the high density of GCPs (i.e., 4.8 GCP/ha), the RMSE is the highest (i.e., 6 cm) (Fig. 9a).

*2.5.2.2 UAV-based Morphodynamic Assessment and Uncertainty*

The differences in terms of total average vertical (TAVD) and total volume (TVV) variations highlighted for the tested DSMs (Table 4), which, on the contrary, showed similar results in terms of error assessment (RMSE; Table 1), raise questions on the reliability of the UAV-derived DSMs to perform morphodynamic assessments in such environments. For example, in terms of total volume change on the 4.7 ha area, the total average vertical difference amongst the DSMs B and D were 2 and 1 cm, respectively, while the (average) total volume difference resulted to be ~1000 $m^3$ and ~550 $m^3$, respectively. By only considering the significant vertical changes (i.e., higher than the TCD), the volume differences decrease, while the total average vertical difference increases. The uncertainty of these results is high.

These variations highlight that UAV-based elevation models are accompanied by a certain degree of uncertainty—due to the fieldwork implementation (i.e., flight altitude)—that must be expected and that propagates to the results of the morphodynamic assessment. This uncertainty is contained within the overall uncertainty of the elevation model (assessed through RMSE; Table 1), but the effect on the DoD results is not known *a priori*: it can be either irrelevant or important depending on the expected volumetric variations. The previously mentioned values of total volume variations of the D tests (TVV; Table 4), compared to the total volume variations (TVV) calculated for the morphodynamic analysis (Table 5), show that the differences in volume between D1, 2 and 3 (~550 $m^3$) represent 25-30% of the TVV calculated for the DoDs referring to February 2020. While considering the same comparison for the B test (TVV ~1000 $m^3$; Table 4), the percentages increase to 55-75%. This result is expected since the B2 test has a higher RMSE (6 cm). Note that these percentages do not represent the error of the calculated morphodynamic volumes, but indicate that the input DSMs have a certain degree of uncertainty (hereby expressed as TVV) that is comparable to (i.e., in the order of) the results of the morphodynamic assessment on volumes, performed by considering all changes. On the other hand, if similar comparisons are made considering the significant changes only—and thus between the TVVtcd in Table 4 and Table 5, only considering the mean value, excluding the uncertainty range—the percentages referring to the D tests decrease below 1%, while for the B tests they generally decrease, but never below 22%.

This suggests that in order to reduce the uncertainty of the final study case results—thus increasing the reliability of the assessment—UAV flights should always be performed at the same altitude (e.g., 80 m) to ensure field consistency, and consecutive surveys should be planned

sufficiently distant in time so that the expected changes in elevation and volume are higher than the uncertainty generated by the field implementation (e.g., differences in flight altitude).

Indeed, as coastal wetlands slowly modify their surfaces, the vertical variations need time to occur and to be detectable via monitoring instruments depending on their characteristics. The changes depend on the entity of the accretion/erosional trend. Since each environment has different evolutionary trends, the optimal timing for a survey depends on when important morphological variations will be detectable. For example, in the Po Delta sediment is mainly transported by the river [70–72], so morphological variations become evident when important floods occur; hence, surveys should be carried out before providing the forecast is available ahead of time—and after the event. On the other hand, tidal currents take a much longer time to influence tidal flats, so that the time interval between one survey and the consecutive one should be longer.

Similar conclusions can be reached by considering that if the expected average vertical variations are lower than the (accepted) error of the DoD—which is assessed by propagating the (accepted) errors (i.e., RMSEs) of the analysed DSMs—it is very likely that most of the calculated vertical and volume variations are not significant, having assumed that the original DSMs are a correct representation of the reality, with acceptable errors. Thus, in general, the period between two consecutive surveys should be calibrated based on the expected variations and the expected error of the DSMs. As a simplified example, the case documented here assumes that the representative expected rate of variation can be assessed by calculating the TAVD (Section 2.3.6) with the TVV in Table 5 for the entire analysed period (Oct. 2018 – Feb. 2020), reproportioning it over one year, and dividing it by 2 (thus assuming null NVV, i.e., equal eroded and deposited volumes), producing a result of ~1.4 cm/year; since the average error (i.e., RMSE) of the UAV-based DSMs was ~5 cm and, the propagated DoD error between two DEMs is ~7 cm, the shortest period between consecutive UAV surveys, can be roughly estimated as 7 [cm]/1.4 [cm/year] = 5 [years]. This is, of course, unfeasible. However, if the calculation takes into account the uncertainty, meaning that non-significant changes are excluded from the analysis (e.g., using the methods applied for this study), this period decreases. For the previous example, considering the TVVtcd—which is representative of the areas with significant changes only (ASV)—the representative expected variation is 3.8 (± 2.7) cm/year, thus, the previous assessment leads to 1.8 (± 2.6) years needed between one UAV survey and the consecutive one. Notably, this range is comparable with the entire period analysed in this study (~1.3 years). If the representative expected variations are calculated for all the other periods considered in this study, and the mean values, including

uncertainty, are considered, the representative expected variation results 11.4 (± 7.1) and it leads to 0.6 (± 1.0) years. Indeed, the seasonal variations of the Pila tidal flat were documented through sub-annual surveys.

This experimentation demonstrates that the UAV is a suitable tool to monitor tidal flat morphodynamics when sub-annual variations are expected to be higher than the error propagation. However, this is only valid if the accuracy is assessed and monitored throughout the entire process. Notably, the morphodynamic interpretation (Section 2.5.1) of the case study documented here and the considerations collected in this section were made possible because the elevation model uncertainty was thoroughly analysed and tracked throughout the entire process. This research feature, in particular, made it possible to evaluate the effect of some aspects of the field implementation on the DSM accuracy and to detect significant changes to perform accurate and reliable morphodynamic interpretations. It is therefore suggested to take uncertainty into account while processing UAV surveys for morphodynamic monitoring on tidal flats, and other environments.

#### *2.5.2.3 Comparisons with Other Studies with UAV in Wetlands*

Fieldwork in tidal flats and salt marshes is usually very challenging and needs to be well organised. Beyond its mere feasibility, a survey should be organised considering two principal aspects: the extension of the study area, and the significance of the expected vertical changes. It is very important to consider the rates of changes because they determine the resolution needed for the study which would, otherwise, produce unreliable data. However, a longer time interval between surveys can correct the imbalance among these rates of change. For example, the Venice Lagoon (Italy) has a very low rate of accretion ranging between millimetres and a few centimetres per year [90,91] which means that even UAV surveys would have difficulty evaluating volume and vertical changes; this is the reason why different on-field methodologies, like sedimentation plates, are used in the Venetian lagoon. The opposite situation can be found in the Perkpolder tidal basin (Netherlands) where the sedimentation rates are very high (> 6 cm/year) and constant; wide vertical changes allow Lidar methodology to be quite accurate with a time interval of one year (Brunetta et al., 2019). As explained in the previous section, it is necessary to find a compromise between the extent of the study area and the resolution of the survey. An overview of datasets for similar intertidal environments from the literature is shown in Table 8.

In producing a reliable survey, flying at a low altitude (e.g., 20 – 30 m) seemed less important (Sanz-Ablanedo et al., 2020) compared to GCP density, spatial distribution, and flight plan which, by contrast, appeared to be driving factors. Other salt marsh research with UAVs has been carried out at very low heights with a GCP distribution and density comparable to this study; we recall here Kalacska et al. (2017) and Brunier et al. (2020). They flew, respectively, at 18 and 30 m of altitude, with a GCP density of 4.6 and 2.8 GCP per hectare. Their estimation of RMSE is very low (2.7 and 3.4 cm) but it is no more precise than the error calculations of this study at higher altitudes (i.e., 60 - 80 m). Furthermore, in this study as well, the lowest flight at 40 m with 4.8 GCP/ha did not achieve higher accuracy. The same RMSE can also be achieved at higher altitudes, as shown in the Jaud et al. (2016) case. They conducted a very similar survey in an area of ~10 ha flying at 100 m and with a GCP density of 1.5 GCP/ha and were able to reach an error ranging between 3.9 and 2.7 cm. In other studies where the UAVs flew at higher altitudes, between 80 to 180 m, and the GCP density was very low (below 0.2 GCP/ha), the error increased to 10 - 20 cm till 5 m (Long et al., 2016; Dai et al., 2018; Kim et al., 2019). The relation between GCP density and RMSE from the previously cited researches is shown in Fig. 14. These comparisons suggest that centimetric errors (e.g., 2.7 – 6 cm) can be achieved with UAV flight altitudes from 20 to 100 m. Even though it could be possible to increase accuracy at heights lower than 20 m, either the fieldwork would prove extremely long or the area would have to be highly restrained; nevertheless, proper foresight can simplify the survey and ensure it achieves a very good quality. The distribution of the GCPs for Jaud et al. (2016) and Brunier et al. (2020) was homogeneous and the distance between each GCP was mostly coherent, which probably resulted in achieving a low RMSE (i.e., 3 – 4 cm). In studies with greatly extended areas, the GCP distribution was neither dense (Dai et al., 2018) nor homogeneous (Long et al., 2016; Kim et al., 2019), causing higher RMSE (i.e., > 10 cm). The best GCP distribution seems to be around ~ 2.5 and 3 GCP/ha, which is 2 - 3 GCP every 100 m homogeneously and equally spaced around the tidal flat.

***Table 8*** *- Datasets and parameters from studies that were carried out in tidal flats and salt marshes using UAVs.*

| Author | Drone model | Camera | Focal [mm] | Coverage [ha] | Number of images | GCP | Speed [m/s] | Altitude [m] | RMSE [cm] | DGPS [m] | Overlap (front - side) | Density [GCP/ha] |
|---|---|---|---|---|---|---|---|---|---|---|---|---|
| This study | DJI Phantom visual 3+ | FC300X | 3.61 | 8 | 198 - 490 | 17-19-18-20 | 8 - 10 | 40 – 60 - 80 | 3 – 6 | 0.03 | 70 | 1.9 – 2.8 – 4.9 |
| Brunier et al. (2020) | DJI F550 | RICOH GR | 18.3 | 3 | 265 | 14 | - | 18 | 2.7 | 0.03 | 90-60 | 4.667 |
| Dai et al. (2018) | DJI MATRICE 600 | Zenmuse X5 | 15 | 26 - 37 | 1219-1360 | 6-4 | 5 | 80 | 9.79-17.30 | 0.005-0.01 | - | 0.231-0.108 |
| Jaud et al. (2016) | DroneSys DS6 DRELIO | Nikon D700 | 35 | ~ 10 | 316-168-247 | 12-15-15 | 3 | 100 | 3.9-2.7-3.5 | 0.03 - 0.04 | 60 | 1.2-1.5 |
| Kalacska et al. (2017) | DJI Inspire 1 | X3 FC350 | 20 | 4.26 - 5.49 - 8.46 | 274-182-390 | 12-6-9 | 1.16 | 30 | 3.4 | 0.02 | 90-80 | 2.817-1.093-1.064 |
| Kim et al. (2019) | Vision-1000 | Canon 6D DSLR | 17 | 250 | 305 | 11 | Automatic | 180 | 5 m | - | 60-70 | 0.044 |
| Long et al. (2016) | eBee flying wing | Canon ELPH110HS RGB | 4.3-21.5 | 400 – 33 | 672-643-301 | 46-56-24 | 6-10-2 | 150-150-50 | 9.44 - 17 | - | 75-60 | 0.115-0.140-0.727 |

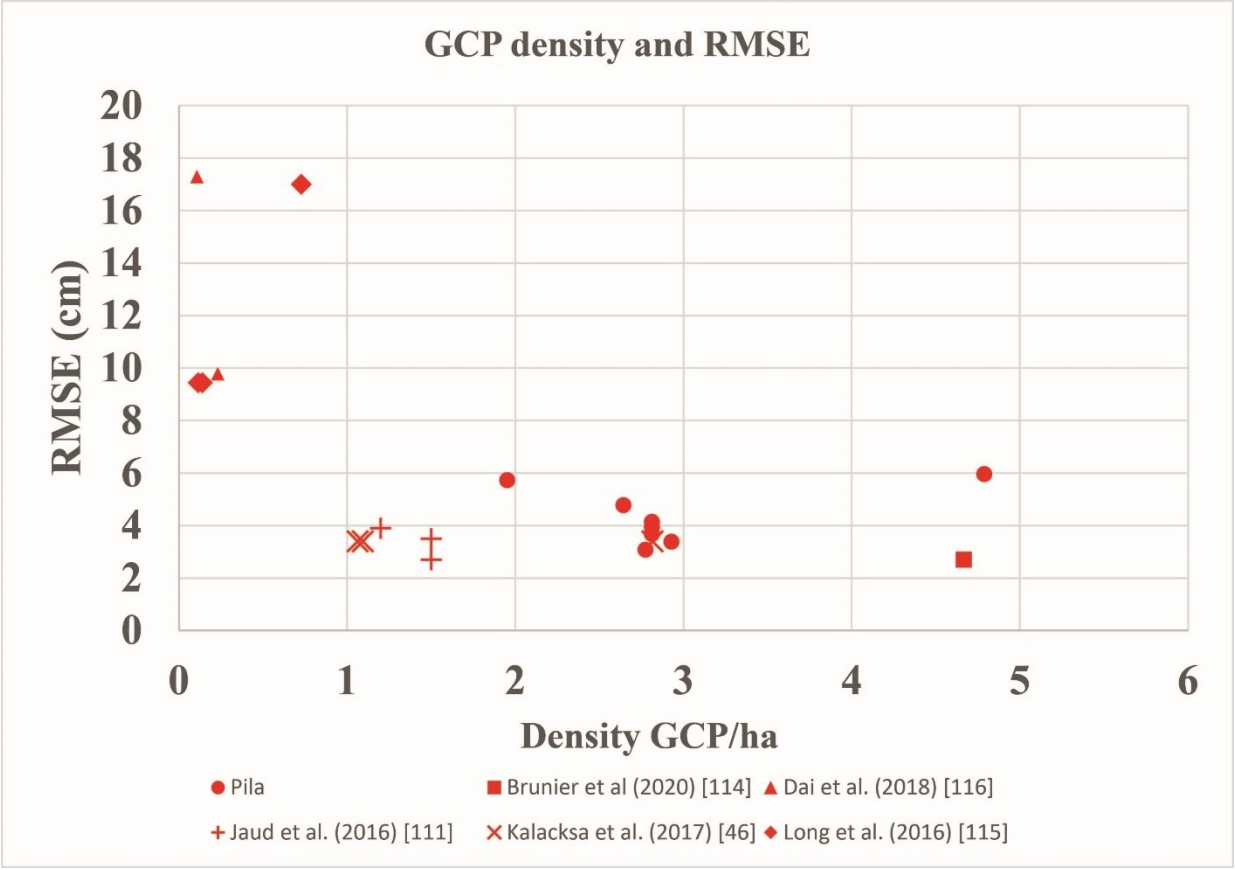


***Figure 14*** *- GCP density compared with the RMSE from this and other studies in wetlands.*

### *2.5.2.4 Recommendations for UAV surveys in wetlands*

The discussion of the results and the limitations of the general approach brought us to make considerations about UAV surveys in wetlands and thus recommendations are proposed to optimize the data acquisition. The following points are suggested:

- The fieldwork should be planned in the function of the expected rate of changes and the time between each survey based on the knowledge of the area;
- A comparison with ground-truthing (e.g., vs. GPS) is always recommended;
- 2 – 3 GCPs should be located every 100 m homogeneously and equally distributed in order to reach centimetric RMSE;
- The flight can be carried out at 80 - 100 m altitude to save time but the altitude must be kept constant for the whole monitored period;

- The fieldwork should be carried out during the early morning or late afternoon time slots, and with cloudy weather when a spring low tide occurs.

These guidelines can help researchers and practitioners in planning field activities in such environments, taking into account the strengths and limitations of UAV-based surveys. Notably, such guidelines must be considered non-definitive since additional research on UAV applications should be envisaged, particularly with regard to developing thorough uncertainty assessments.

## *2.6 Conclusions*

Over the last 50 years, the Po River Delta has been subjected to alternating phases of erosion and progradation. During the last decade, the delta has been accreting, and new tidal flats are forming. This study concerns an 8 ha young tidal flat that stretches northward from the southern part of the Barbamarco Lagoon to the Po della Pila branch in the Po Delta (Fig. 4). From October 2018 to February 2020, four UAV surveys were carried out at different altitudes and with different GCP numbers and distribution. Eight photogrammetric tests were performed in order to evaluate the uncertainty and accuracy of the elevation models and related morphodynamic assessments. The volumetric and elevation changes were evaluated considering the whole study area and the area with significant changes, which are defined as the vertical changes higher, in the module, than an established threshold. The threshold was evaluated on the basis of the propagation of the error of the input DSMs.

The principal conclusions of this research on the morphodynamics of the analysed portion of the Pila tidal flat are the following ones:

1. During the last phase part of the winter season and the spring–summer season of 2018 - 2019, the study area experienced erosion while in the autumn–winter season of 2019 – 2020 an accretion trend was predominant. Timewise, the increase and the widening of the tidal flat coincide with the heavy flood events occurring in the Po River during November – December 2019;

2. Overall, the sediment budget is positive, and the tidal flat is gaining ~800 $m^3$/year with an average accretion rate of 1.3 cm/year (by considering the significant variations those values become 420±385 $m^3$/year and 5.2±4.8 cm/year, respectively);

3. The accretion trends of the tidal flat of Pila are similar to other microtidal deltas worldwide; most of them are characterised by seasonal variations that depend on episodic events (i.e., floods, storms) and do not present constant trends like tide-dominated deltas.

The above points were supported by a thorough assessment of the accuracy of the UAV-based DSMs and of the calculated volume changes. In regard to this, the RMSE (vs. GPS measurements) of the DSMs ranged between 3 and 6 cm. The accuracy of the DSMs was not dependant on the altitude of the UAV flight, but rather on the number and distribution of the GCPs.

# 3. Sedimentary evolution of a young tidal flat in the Northern part of the Po Delta (Italy)

## 3.1 Introduction

### 3.1.1 Sedimentation in tidal flats and salt marshes

The combination of geomorphic and biotic factors in deltas and estuaries leads to the formation of peculiar wetlands located in the intertidal interval, such as tidal flats, which are wide unvegetated surfaces characterized by mud or sand (Dyer et al., 2000), and salt marshes, characterized by halophyte vegetation located at higher elevations (Pratolongo et al., 2019). Although tidal flats cover about 7% of all coastal areas (Stutz and Pilkey, 2002), they offer numerous ecosystem services, such as supporting fisheries (Boesch and Turner, 1984a; MacKenzie and Dionne, 2008a; Barbier et al., 2011), carbon sequestration (Mayor and Hicks, 2009), and leisure activities (Weis, 2016); furthermore, tidal flats that become salt marshes have a fundamental role as natural protection against coastal storms and river floods (Barbier et al., 2008; Gedan et al., 2011; Shepard et al., 2011; Bouma et al., 2014; Möller et al., 2014; Smolders et al., 2015; Stark et al., 2015; Vuik et al., 2016; Leonardi et al., 2018), and to keep up with sea-level rise (Kirwan et al., 2010; Fagherazzi et al., 2012).

These transitional environments are affected by a great number of factors that interact with each other. The morphology is one of the most important since tidal flats are slopes with highly low angles that increase in elevation moving landward; this shape leads to a decrease in submersion period and frequency of inundation (hydroperiod) (French, 1993). Tidal currents move sediment continuously through the tidal flats, which means that as the elevation increase and the hydroperiod is reduced, the sediment deposition decreases as well (Pethick, 1981). Several other factors influence the evolution of a tidal flat, such as tidal and wave processes (Bassoullet and Bacher, 2000; Coco et al., 2013; Green and Coco, 2014), sediment supply, fluvial inflow, organic and anthropic activities (Murray et al., 2008; Wang et al., 2015; de Vet et al., 2017). The most important process for tidal flats and salt marshes is sediment deposition and how fast it occurs in respect to sea level rise (Redfield, 1972; Orson et al., (1985); Schuerch et al., 2012), which is in turn controlled by seasonal conditions (Reef et al., 2018), sediment availability and grain size distribution (Schuerch et al., 2014), storm frequency and intensity (Schuerch et al., 2012).

The Italian region presents two principal coastal wetland systems: the Venice Lagoon and the Po River Delta, located both in the Adriatic Sea. Although they are characterized by a similar tidal range (microtidal), the evolutionary processes that dominate are different. The Po Delta is controlled principally by the Po River and anthropic influence that have shaped the Italian north-east coast, in particular during the last 400 years. During the 1950-60s several strong floods have submerged most of the tip of the Delta, giving birth to new sections of the lagoon and new tidal flats. Most works have studied the evolution of the Delta at large-scale (e.g. (Dal Cin, 1983; Ramirez and Imberger, 2002; Ninfo et al., 2018), but few have discussed the sedimentological evolution of the internal part of the lagoon at small-scale and its recent evolution.

### *3.1.2 Aims of the paper*

This paper focusses on the southernmost tidal flat of the Barbamarco lagoon that has been developing during the recent years. The main aims are: i) to quantify the granulometric distribution and depositional rates on the area; ii) to identify sedimentation patterns and the most important processes that drive the tidal flat evolution; and iii) to define a conceptual model of the origins and evolution of the tidal flat.

The objectives are pursued by means of an integrated analysis of field observations collected between 2019 and 2021, and interpretation of orthophoto from the period 2000-2019.

## *3.2 Study site*

### *3.2.1 The Po River Delta*

The tidal flat that is under investigation is located at the tip of the Po River Delta (Italy), in the municipality of Porto Tolle (Rovigo, Veneto region) (Fig. 15a, 15b, 15c). This Delta system is one of the largest anthropic Delta in the world (Maselli and Trincardi, 2013); in fact, its actual location was stabilized after the “Porto Viro” bypass in 1604, a massive human operation made under the Venetian Republic that diverted the river natural path southward (Stefani and Vincenzi, 2005). Progradation occurred between the 1800s and 1945 (Visentini et al., 1940) until the heavy human interventions of the Fascist regime and the Italian Republic caused an erosional trend between the 1930s-1940s and 1970s-1980s (Billi and Fazzini, 2017). This regression phase stopped years later and a stable condition was reached. After 2010, a constructive process is ongoing and the Delta is experiencing progradation once again (Ninfo et al., 2018; Bezzi et al., 2021).

Five principal branches called, from north to south, Po di Maistra, Pila (the central one), Tolle, Donzella or Gnocca, and Goro define the structure of the Delta, which extends for 691 km along 90 km of coastline. Its evolution is tightly connected to the anthropic interventions of the last century (Bondesan et al., 1990; Cencini et al., 1998; Simeoni and Corbau, 2009), and to the Po River, which is the longest Italian river (it flows for 650 km into the Adriatic sea and it has a catchment area of 70000 $km^2$ Bondesan et al., 1990). In fact, the system was considered as *river-dominated* due to the large amount of sediment supply of the Po River (average discharge of 1500 $m^3/s$ (Ludwig et al., 2009)); during the last 50 years the trend shifted to *wave-dominated* (Smith et al., 1966; Nelson, 1970; Galloway et al., 1975). However, it is difficult to define a single dominant regime, since each ramification has its own depositional system and each lobe has a different evolutionary trend (Trincardi et al., 2003; Correggiari et al., 2005; Syvitski et al., 2005).

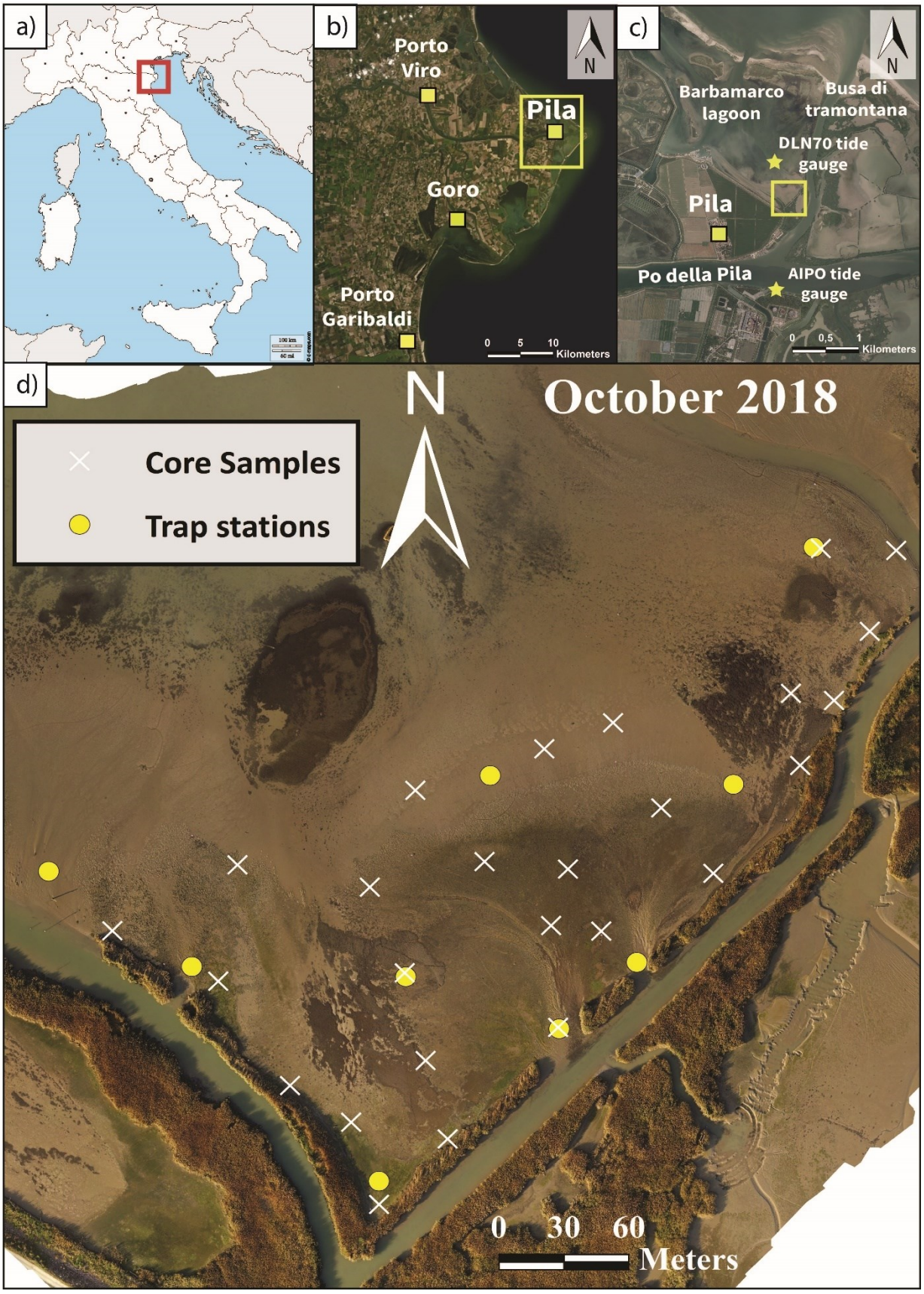


***Figure 15 -*** *(a, b) Location of the Po Delta. (c) The tidal flat is connected to the Po della Pila thanks to the Busa di Tramontana and it is located in the southernmost part of the Barbamarco lagoon. (Orthophoto 1:30000 of 2015 provided by Veneto region). (d) Orthophoto of October 2018 with core samples and traps stations location.*

### *3.2.2 Geomorphology and Sedimentology of the Delta*

A wide lagoon delimited by bars and sand spits characterize the external part of the Po Delta. The depositional system extends offshore for 6 km in the northern section and 10 km in the central-southern section (Simeoni et al., 2000 (bacile)). Several authors estimate that bedload is about 12 – 20 % of the suspended portion (Visentini, 1940; Canali and Allodi, 1963; Nelson, 1970; Idroser, 1994). Measures carried on by Maicu et al., (2018) show how the central branch (Po della Pila) is the one with the highest discharges while the others are subjected to lower discharges (Tab. 9). However, the Po di Tolle is the branch that transports the courser sediment (Dal Cin and Simeoni, 1984).

***Table 9*** *- Distribution of water and sediment discharge of the Po branches according to Nelson (1970).*

| River branch | Water discharge (%) (Nelson, 1970) | Sediment discharge (%) (Nelson, 1970). | Water discharge (%) (Maicu et al., 2018) |
|---|---|---|---|
| **Maistra** | 3 | 1 | 2 - 5 |
| **Pila** | 61 | 74 | 38 - 56 |
| **Tolle** | 12 | 7 | 15 - 25 |
| **Donzella or Gnocca** | 16 | 11 | 10 - 17 |
| **Goro** | 8 | 8 | 5 - 14 |

The Po River regime is mixed and it is highly affected by its tributaries. Two principal regimes dominate: strong floods occur during June due to snow melting and in particular during November due to rain (Marchi et al., 1996; Palinkas et al., 2005) where significant deposition in the prodelta takes place during large flood events (>6000 $m^3/s$) (Tesi et al., 2011); low water periods occur in January and August (Marchi et al.,1996) where a reduced portion of material delivered by ordinary floods reaches the delta (~4000 - 6000 $m^3/s$) (Tesi et al., 2011).

The Delta is characterized by fine sediment, which varies from fine sand to mud (Dal Cin, 1983; Simeoni et al., 2000). However, there are a few works that describe the sedimentology of the Po Delta. One of the most important is from Dal Cin (1983), which describes the granulometry of the coastline. Here, the sand percentage is predominant (100 – 85%), decreasing with the increase in depth. Pelitic sediment is high next to fluvial inlets (>20 – 30%) in particular next to secondary tributaries. The mud is principally represented by silt and is highly poor in clay content. The coarser sand (medium sand) is located between the northern side of the Po della Pila (Busa dritta) and the Busa di Tramontana, but the predominant granulometric class is very fine sand. The Po della Pila is the only branch able to deliver limited amounts of medium sand; the rest of the ramifications distribute appreciable quantities of fine sand.

The granulometry of the lagoon presents different classes in respect to the Delta coastline, ranging between silty sand and sandy silt (Zonta et al., 2019) according to Shepard's classification (Shepard, 1954). The highest percentage of fine sediment is found in the Barbamarco Lagoon, northward the Po della Pila central branch, possibly due to high suspension load from the Busa di Tramontana (Ramirez and Imberger, 2002), which is a small ramification of the central branch.

### *3.2.3 The Barbamarco Lagoon and study area*

The study is located in the southernmost part of the Barbamarco Lagoon. This inland water body is located northward to the Po della Pila branch and it extends for 7 km in NW direction. A 3 km long sand bar defines the limit of the lagoon where two inlets (Bocca Nord and Bocca Sud) separate it from the Adriatic Sea. The southern section of the lagoon is connected to the Po della Pila through the Busa di Tramontana branch thanks to two small channels. The tide is mixed, principally semi-diurnal with an average range of 0.5 m; the highest spring-tide can reach 1 m. The structure of the lagoon prevents waves to affect this section of the Delta; in fact, the tide and the river are the two principal mechanisms of sediment transport and water mixing.

During the last 50 years, the tip of the Delta was hit by several severe floods that have submerged hundreds of hectares of agricultural fields; some anthropic structures and houses are underwater presently. This gave birth to the actual Barbamarco lagoon and the birth of new tidal flats that started to build-up in particular during the last decades. The tidal flat at issue is an ~8 ha young tidal flat that has been developing seemingly in the last 20 years. The mudflat is located between two channels that develop in opposite directions (NE and NW direction) (Fig. 15d); both channels are separated from the tidal flat by the presence of wild reeds that have established on the

channels levees, except for two inlets on the east channel and one on the west channel. The study area is characterized by several crevasse splays that originate from the inlets that connect the channels to the Barbamarco Lagoon (Brunetta et al., 2021). A large crevasse splay develops in NW direction from the two inlets located on the east channel where two small creeks cut through the tidal flat; a smaller crevasse deposit develops from the inlet of the west channel. A large depositional area is located northward to the west channel, where vegetation disappears. Brunetta et al. (2019) suggest that these morphological forms are caused by floods and the river is the principal sediment supplier; besides morphological analysis, no sedimentological proof has been provided to support this hypothesis. This theory was taken into account and investigated in order to demonstrate its validity.

## *3.3 Methodology*

Fieldwork activities were carried out between May 2019 and March 2021. Sediment samples were collected by means of coring (May 2019) in order to analyse the recent subfacies and to characterize the sediment by means of Particle Size Analysis (PSA) and Loss on Ignition (LOI) analysis. Sediment traps were placed (autumn 2019, summer 2020, spring 2021) to evaluate sediment deposition rates. A tide gauge was placed in the lagoon (March 2021) to collect a timeseries of water levels as reference for the local hydrodynamics of the study area.

### *3.3.1 Coring and sediment characterization*

Twenty-six cores were collected in May 2019 by means of manual coring using PVC tubes with a length between 18 and 32 cm and with a diameter of 3.5 cm. The size of the PVC tubes was considered sufficient for the analysis since great vertical changes were not expected (Brunetta et al., 2021). Despite physical compaction, sediment thinning, and sediment bypassing affect the sample causing core shortening, low depth coring (i.e. <30 cm) poorly alters the sediment column (Morton and White, 1997); for example, a fluvial wetland core of 25 cm reaches a shortening of 0.8 cm, which is acceptable for this study. The PVC tubes were inserted vertically into the mud and then locked using a cap on the top of the upper part; the tubes were extracted, and another cap was used to lock the lower part. The cores were transported and opened using a small circular saw. Due to (i) the reduced length of the tubes, (ii) the strongly consolidated mud and (iii) the

necessity to study the surficial sediment distribution, the possible alteration of the sediment column was considered negligible.

Based on visual analysis (i.e. colours, evident granulometric differences), two subfacies were distinguished and 51 samples (i.e. at least one for each identified subfacies, for each core) were collected from the 26 cores. These samples were further analysed as presented in the following.

#### *3.3.1.1 Particle size analysis (PSA)*

The adopted procedure for the Particle Size Analysis (PSA) is set by ICRAM (2004) which represents the guidelines for the Italian national standard.

The sediment samples were treated with 120 ml of Hydrogen Peroxide at 16 volumes for several days to remove the organic matter. The sand and the mud were distinguished based on the Wentworth scale (Wentworth, 1922); the two fractions were separated by wet sieving using a mesh of 63 microns. The sand fraction was dried at 105 °C and all the extraneous material (e.g., shell fragments, non-sediment particles, etc.) was removed using another sieve of 1 mm. The sand quantity was limited to a few grams (less than 20% for most of the samples) and no further analysis was necessary. The mud was stored in large pitchers and left to decant for several days allowing the fraction to deposit on the bottom of the containers. Then, the water was removed from the pitchers and the mud was displaced into smaller beakers and weighted. Part of the mud was moved into glass Petri dishes and dried at 105 °C to calculate the water content and the real mud quantity. Finally, a Micromeritics Sedigraph Analyzer was used to discriminate the percentages of silt and clay. The PSA results were represented using the most suitable classification for this type of environment: Stevens' diagram (Stevens, 1983, 1991) using the Triplot software (McHone, 1977). In this case, Shepard's diagram (Shepard, 1954) is not considered because even if it is a standard representation of sediment granulometry, it does not distinguish the differences between restricted grain-size ranges, such as mud-dominated grains; Stevens' diagram discerns these subclasses and represents with higher details the granulometric distribution; in fact, it uses a nomenclature that places more emphasis upon clays content. Both diagrams were plotted into ArcGIS to develop a sediment distribution map.

#### *3.3.1.2 Loss on Ignition (LOI) analysis*

A portion of the 51 sediment samples (of each subfacies) was used to evaluate the Loss on Ignition (LOI) content, following the Heiri et al. (2021) method. The samples were located in ceramic cups and dried for a week at 105 C° in order to remove the water and determine the dry weight. Once weighted, the content was burnt at 500 C° for 6h and weighed once more to evaluate the LOI.

### *3.3.2 Sediment traps for the analysis of deposition rates*

Measuring sediment deposition can be achieved through a high variety of techniques, which have different strengths and weaknesses (Nolte et al., 2013). They can vary from simple filters (usually positioned for the duration of one tidal cycle) to metal or plastic plates and cylinders (generally deployed for days, weeks, or months). These traps are widely employed for the last 40 years thanks to their inexpensiveness, practicability, and good spatial resolution (Marion et al., 2009). However, the design of a trap, from a practical point of view, depends on many factors, such as the sediment accretion rate itself, the purpose of the study, the occurrence of precipitation, re-suspension, or other disturbances. Each type of trap has pros and cons which depend on these variables; for example, some authors used flat traps that are supposed to minimize the disturbance on the measurement because they have no edges. However, they cannot feature friction and adhesion, preventing the particles to deposit on the traps and causing serious difficulties during the phase of traps collection. Another common methods is using filter papers left on the surface of the tidal flat/salt marsh for a period of a few hours or several days (Reed, 1989; Frencht et al., 1995; Leonard et al., 1995; Leonard, 1997; Brown, 1998; Culberson et al., 2004; Neumeier and Ciavola, 2004; van Proosdij et al., 2006; Price). Other studies were carried out using plastic cylinders as traps, such as Petri dish, generally deployed for several days or weeks (Temmerman et al., 2003; Butzeck et al., 2015). For this study, the type of trap selected is the Petri dish, which represents a cylinder trap.

#### *3.3.2.1 Trap model*

The adopted trap is a 4.7 cm diameter sterile Polystyrene Petri dish with an edge of 1 cm, produced by Merck KGaA (Darmstadt, Germany). In order to insert and secure the Petri dish on the mud, a structure was designed (Fig. 16a) and printed in series using a 3D printer (Fig. 16b, 16c, 16d). The structure is a Polylactic Acid (PLA) plate with a diameter of 8 cm; the plate has three 15 cm long pins that allow the trap to be easily anchored to the mud. The Petri dish is fixed in the centre of the upper part of the plate using a cover. The cover has the same diameter of the plate,

and it has a hole in the centre that allows to insert the cover on the Petri dish and lock it at its border. The plate and the cover are fastened using three bolts.

The Petri dish itself acts as a trap and can be pulled out of the structure so that the model can be used again. The choice of this type of trap was based on the vertical accretion expected during the survey (Brunetta et al., 2021), the weather condition normally experienced in this area (e.g. rainfall), and the seasonal conditions.

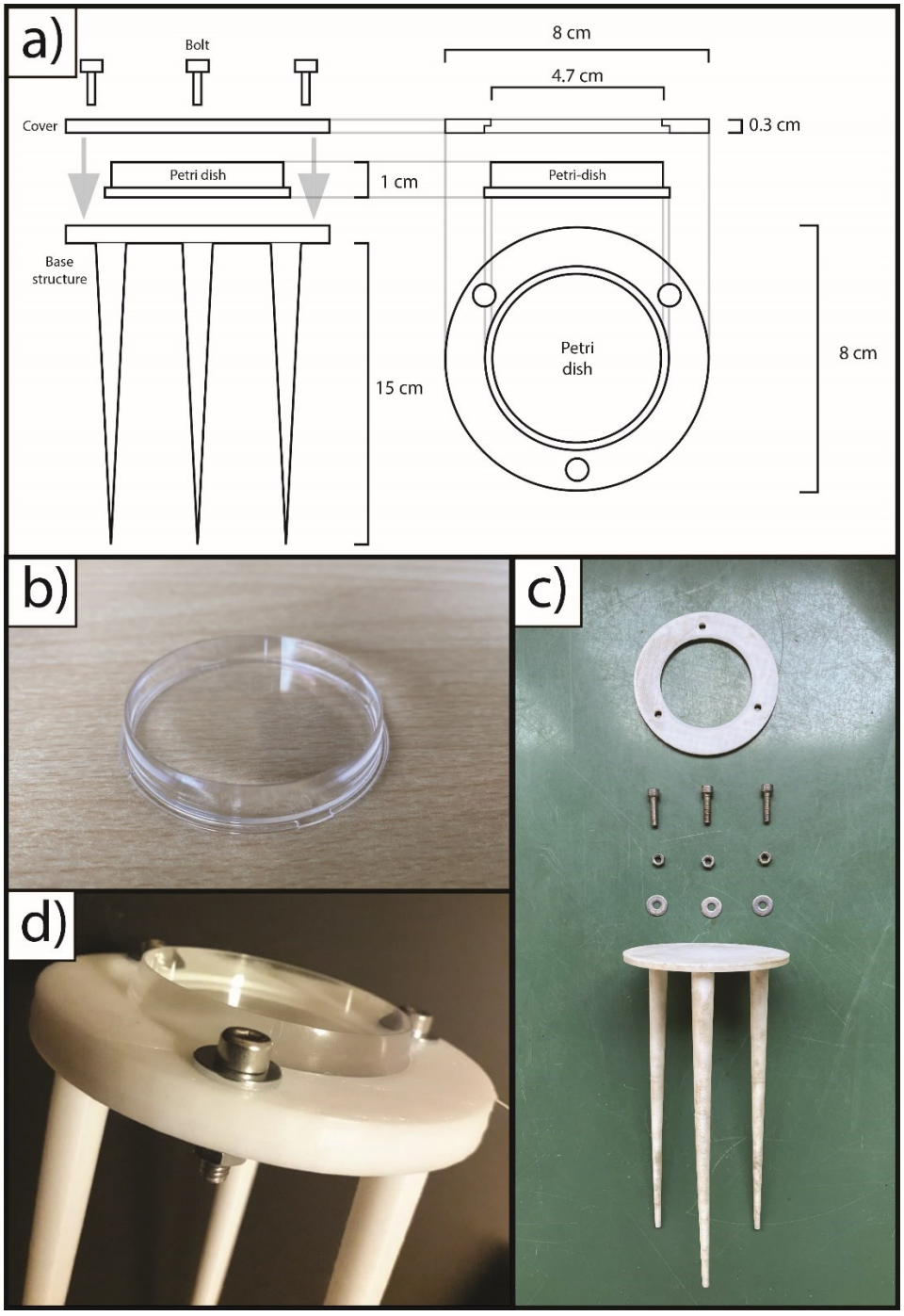


***Figure 16*** *- (a) Trap model used for sediment deposition collection. (b, c, d) The petri dish is inserted and locked with three bolts on a flat surface with 3 nails that allow to nails the trap on the mud.*

*3.3.2.2 Measurement stations and quality control of the measurements*

Nine measurement stations were distributed around the tidal flat (see Fig. 15d); at each station, 3 traps were positioned (27 in total), each one located at one of the vertices of an equilateral triangle with a side of 60 cm (Fig. 17a, 17b, 17c); the traps were positioned ensuring that one of the vertices was pointing Northward, as such the other two were laying on the West-East parallel.

Three measurements were carried out between September 2019 and March 2021:

i. from 17 to 27 September 2019;
ii. from 26 June to 10 July 2020;
iii. and from 12 to 25 March 2021.

The Petri dishes were therefore deployed during spring-neap tidal cycles. After 10 to 15 days the traps were recollected, the Petri dishes were detached from the PLA structure, closed with their caps and catalogued registering the identifier of the station and the position of the trap (i.e. N, E, W). The sediment samples were then transported to the lab, dried at 105 °C in glass beackers, and weighed.

The design of the measurement station was chosen to ensure a quality check on the measurements (e.g., identification of outliers due to local disturbances). Indeed, although cylindrical traps with appropriate aspect ratio are considered efficient for sediment trapping (Bloesch and Burns, 1980), there are several factors that can affect the deposition measurements, such as, the waves generated by boats passing nearby, or animal disturbances (e.g. birds, crabs). This design allows to identify possible incorrect or incoherent measurements of the sedimentation by directly comparing the sediment captured by the three traps of the same station. A high variability between the observations (i.e. the three measured weights of trapped sediment) indicates the possible presence of incorrect measurement. Filtering is therefore applied, and measurements discarded when necessary. As an e.g., during the third survey (03/02/2021), the area next to station P8 (fig. 17d) was denoted by the presence of marks left by boats on the mud surface; the traps showed a clear distinction on sediment amount and less sediment deposited inside the trap that was nearer the boat signs. As a consequence, the data collected by these traps were discarded. Another example of discarded data is shown in figure 17e. These traps were not located during the listed surveys but it was a test made in order to verify the traps behaviour during floods. They collected the sediment deposited during the flood of May 2019 and as

expected, the sediment overflowed. No trap was buried by the sediment deposited during the presented surveys (i.e. no floods occurred during the fieldwork, see 3.4.2).

The average of the sediment weights collected by the three traps, excluding outliers or incorrect measurements, was considered here to represents the sediment deposited during the measurements period at each measurement station, and it is assigned to a single point located at the centre of the equilateral triangle, which was geolocated using the RTK-GPS (i.e. Trimble R8, stop and go technique with a horizontal accuracy of 8 mm and a vertical accuracy of 15 mm) during field activities.

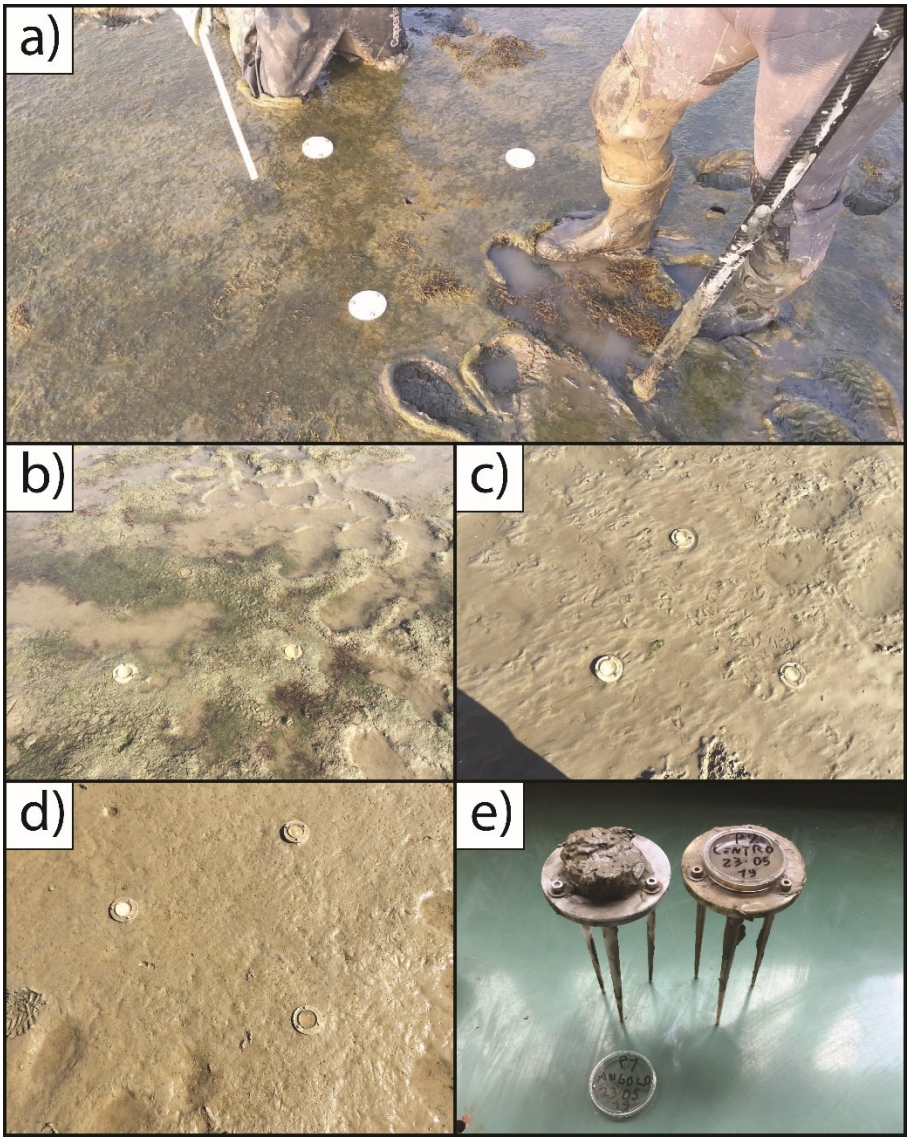


***Figure 17 -*** (a) Example of measurement station. Three traps were positioned per each station with a distance of 60 cm between each other. (b, c) Example of sediment deposition inside the traps, and (d) example of sedimentation influenced by a local disturbance (one trap collected less than the other two). (d) This image represents a test made before the surveys, while the traps were located during a river flood and they collected an overflowing amount of sediment, showing how river flood deposition is different compared to tidal controlled deposition in the Po Delta.

*3.3.2.3 Sedimentation estimation and tide gauge validation*

There are in the literature a large variety of ways to estimate the rate of sediment deposition. The most common is to calculate a daily rate in g/m$^2$ per day (Brown, 1998; Culberson et al., 2004; Butzeck et al., 2015); in other cases, a tide event-based rate in g/m$^2$ per tide event (e.g. Leonard et al., 1995; van Proosdij et al., 2006) or in g/m$^2$ per Spring-Neap tide event (Temmerman et al., 2003) is preferred.

In this paper, the sediment deposition rate (S) is estimated for each station, under the assumption that it is constant in time, using the following Equation (3):

$$S = \frac{w}{(\pi r^2) \cdot B} \quad (3)$$

where w is the average weight of sediment collected by the three traps of the station (see Section 3.2.2), r is the ray of the Petri dish, and B changes depending on the estimation method. In particular, in this case, three estimates are considered and rates are calculated:

a) on a daily basis, where B is the number of days during which the traps were deployed in the tidal flat; ,
b) based on submersion events, where B is equal to T/t, with T the total submersion time in hours, and t the average submersion time in hours, during high tides;
c) based on the hours of submersion, where B equals T.

Estimates a) and b) are considered less reliable when compared with c) in case of asymmetric tides, when high and low tides do not occur twice every single day and single tidal events are difficult to distinguish. In order to implement estimates b) and c), water levels observed as close as possible to the area of interest must be analysed to calculate the submersion time considering the measured elevation (i.e. GPS) of the station.

The observed water levels of the tidal gauge of the Po della Pila, provided by AIPO (Agenzia Interregionale Per il Fiume Po), and of the Porto Garibaldi tide gauge, provided by ARPAE Emilia-Romagna, were analysed to identify the submersion events, and the hours of submersion (i.e. T and t) for each station (i.e., based on its measured elevation). A tide gauge (DLN70) was installed inside the Barbamarco lagoon in March 2021 in order to measure the water elevation in comparison to the institutional data.

## *3.4 Results*

### *3.4.1 Granulometric and LOI distribution*

The granulometric classes of the tidal flat consist of fine sediment, as expected. In agreement with Stevens (1983), 5 principal classes are identified: **(si)C** (Slightly Silty Clay), **siC** (Silty Clay), **(si)(s)C** (Slightly Silty and Slightly Sandy Clay), **(s)(si)C** (Slightly Sandy and Slightly Silty Clay), **(si)sC** (Slightly Silty Sandy Clay). Only one sample (P21(3)) is characterized by a sixth class of **cS** (clayey Sand). Two principal subfacies are distincted (Fig. 18): the first one (called as subfacies (1)) extends from the surface of the tidal flat to ~5 – 14 cm; it is characterized by a grey to brown/yellow sediment with an average sand content of 14 %, a silt content of 50 % and a clay content of 36 %. The second subfacies (called subfacies (2)) is similar from the granulometric point of view (sand content 16%, silt content 47%, clay content 37%), however, the coarser sediment increase deepening, following a fining-upward sequence, and the sediment colour is predominantly dark (black). Furthermore, only two samples present different characteristics; the sample P20 has the last 2.5 cm rich in sand, while the sample P21 has the last 8.5 cm characterized by grey sand (76%) which can be considered as a third subfacies (subfacies (3)).

In both subfacies, the coarser sediment is overall located in the central part of the larger central crevasse splay that develops from the inlets of the eastern channel (Fig. 19a, 19b). Instead, the finer sediment is found at the edges of the tidal flat, except at the north-east end, next to the eastern channel. The two Subfacies have a similar granulometric distribution, but in the deepest part of Subfacies (2) the **(si)sC** (the coarser class) is slightly shifted to the levees of the east channel. Overall, the sediment of subfacies (2) is sandier than subfacies (1) next to the eastern channel.

Besides the granulometric classes, it is interesting the vertical distribution of the two subfacies. The profile in Fig 20 that cut through the whole tidal flat in NE direction shows that Subfacies (1) increases in thickness moving from the edges of the tidal flat to the centre of the crevasse splay (from 2 to 14 cm). This organization of layers is visible moving in NW direction as well, but the thickness of Subfacies (1) decreases (from 3.5 to 8.5 cm) and the vertical variation becomes flatter. It is evident the difference in sand content between the two subfacies next to the eastern inlets, moving from ~20 % of Subfacies (1) to ~30% of Subfacies (2).

As for the granulometric distribution, the LOI distribution is similar between the two subfacies. Subfacies (1) is characterized by values between 3.6 and 10.7 %, while Subfacies (2) has a smaller

range of values between 4.6 and 8.9 %. The lowest content of Subfacies (1) is located in the centre of the study area, inside the largest crevasse splay (Fig. 21a); the LOI content increase moving to the edges of the tidal flat. The deeper Subfacies (2) present a similar behaviour, but the lowest organic content is next to the east channel instead of the centre of the crevasse splay (Fig. 21b).


***Figure 18*** *- Core samples extracted during the sampling of May 2019. Subfacies (1) presents grey colours, while Subfacies (2) is darker and sandier.*

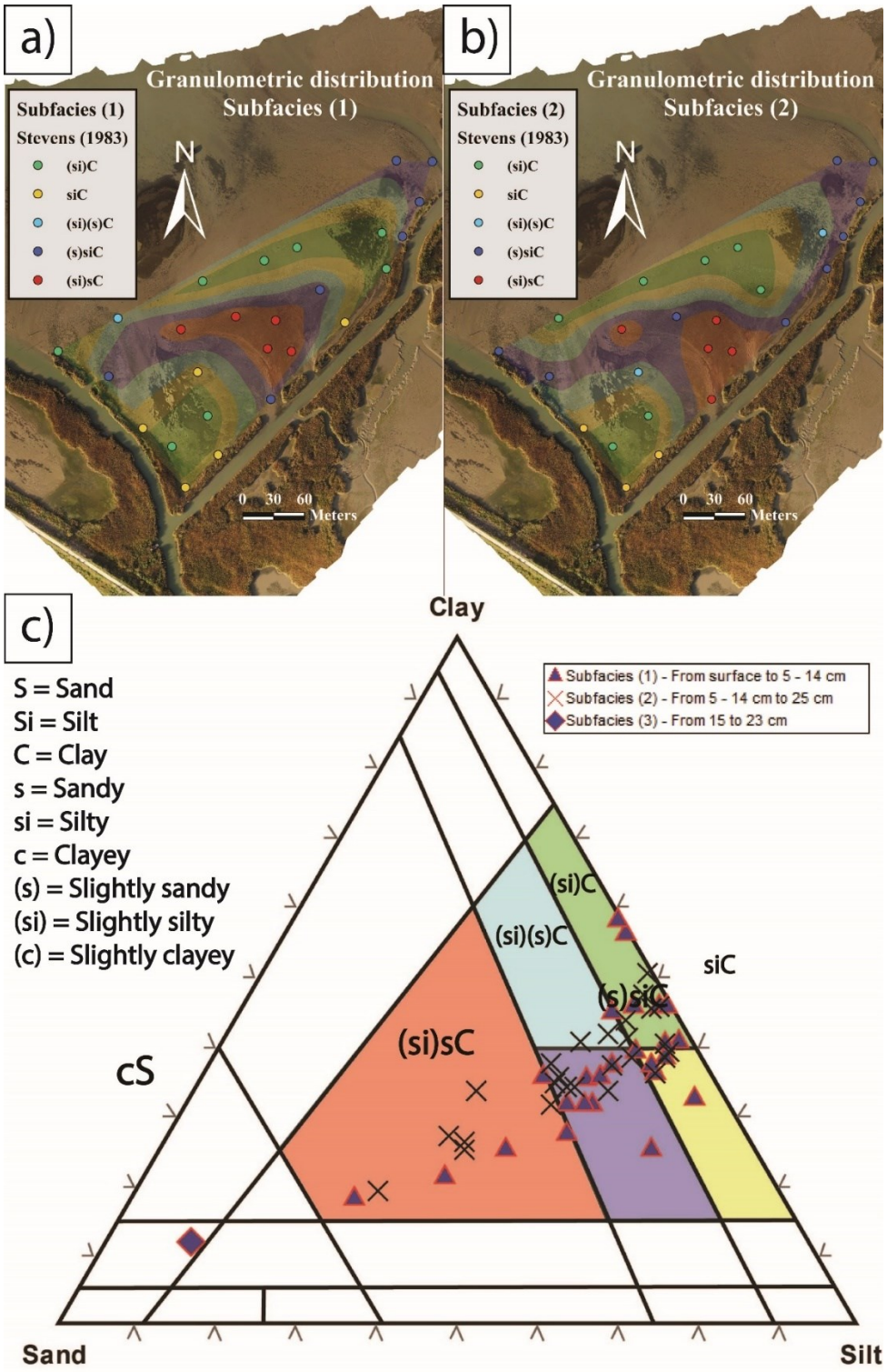


***Figure 19*** *- Granulometric distribution of (a) Subfacies (1) and (b) Subfacies (2). (c) Each sample was classified based on Stevens (1983) classification.*

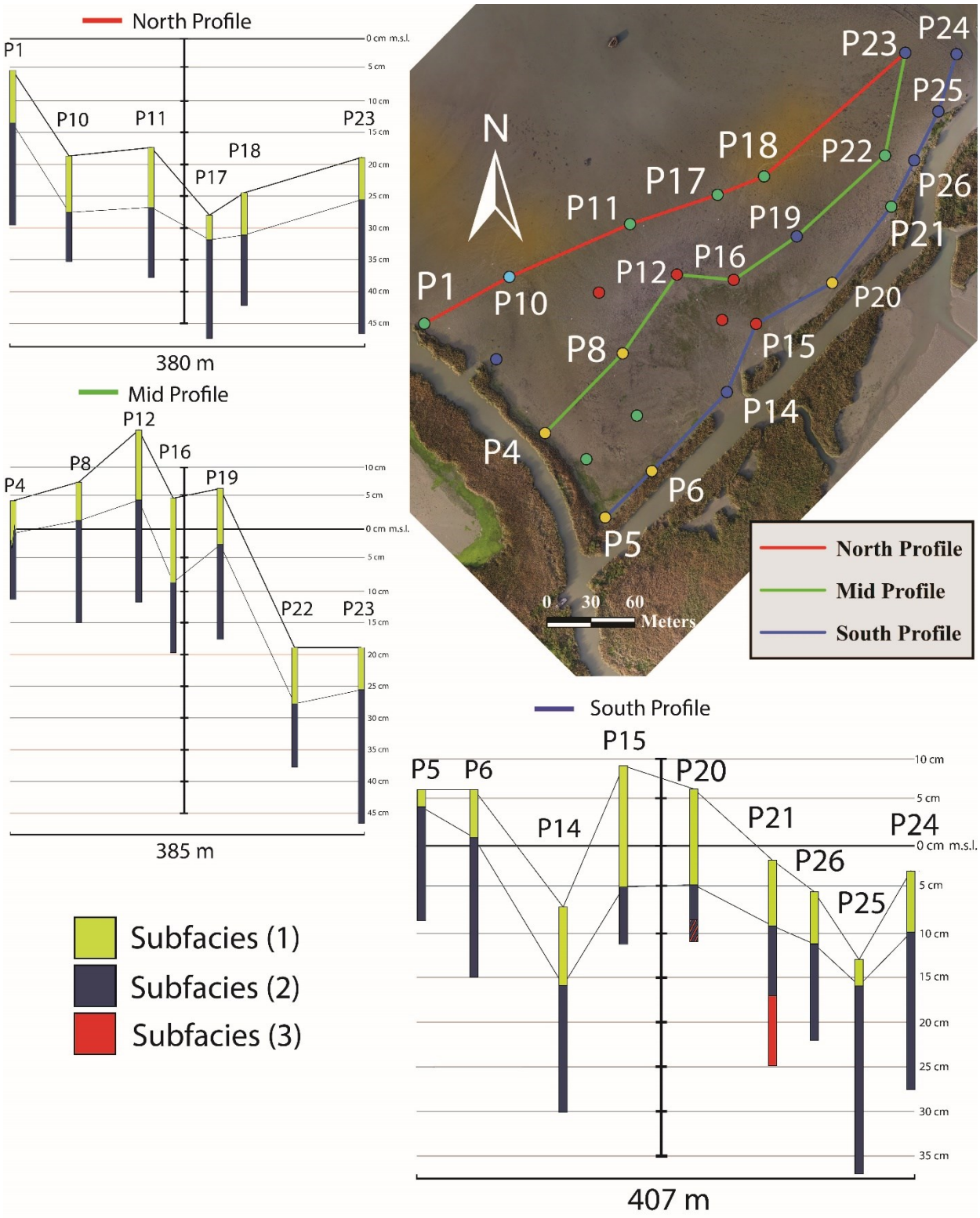


***Figure 20*** *- Spatial distribution of the subfacies. Subfacies (1) increases its thickness in the central section of the tidal flat but it decreases moving at the edges and moving north-westward.*

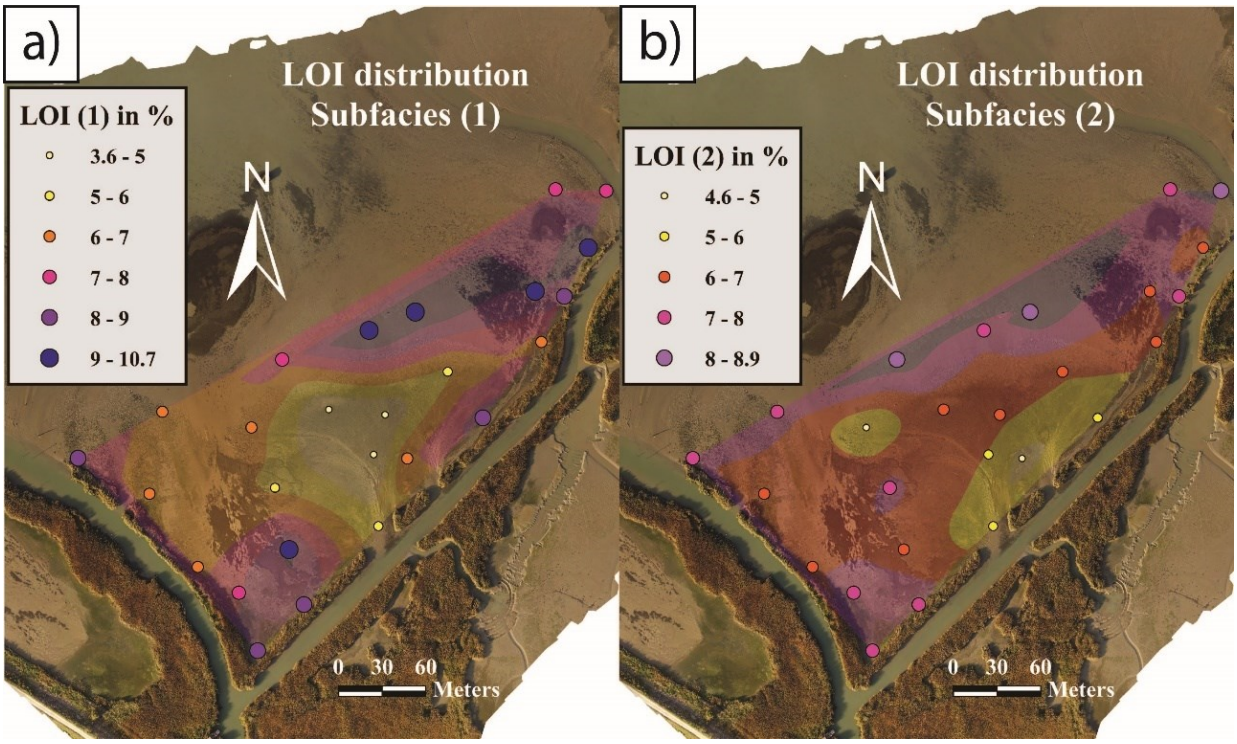


***Figure 21*** *- Loss on Ignition (LOI) distribution between (a) Subfacies (1) and (b) Subfacies (2).*

### *3.4.2 Sediment deposition*

The depositional rates were calculated using all three tide gauge timeseries (i.e. ARPAE, AIPO and DLN70) and the results were compared. The variation of these rates between traps of the same station was highly limited (few grams); only one station of the first survey and one of the last surveys were ignored because they collected highly different amounts of deposited sediment and showed other signs that indicate the influence of external factors (i.e. boat trespassing at low tide). In most cases, the tide gauge of Porto Garibaldi recorded higher values in respect with the Pila tide gauge (Fig. 22a, 22b, 22c), in particular during surge events. This discrepancy can be related to several factors, such as wave setup (Duo et al., 2021), the distance from the Po della Pila and Porto Garibaldi (~40 km) that causes a delay of the tidal vertical variation, and no river influence. The rates calculated from the DLN and the Pila tide gauges showed a similar linear correlation (R=0.6) and the results are highly comparable, indicating that the Pila tide gauge can be used for all three surveys. Consequently, the following rates (Tab. 10) are referred to the Po della Pila tide gauge provided by AIPO (Agenzia Interregionale del fiume Po).

Sediment deposition has varied during the three surveys. The first survey of September 2019 lasted for 10 days; during this period, the tidal flat was submerged for an average of ~14 hours

(with a total submersion of 155 hours) and it had an average rate of deposition of 19.7 g/m$^2$ per tidal event. As shown in Fig. 22a, the tide has shifted from symmetric to asymmetric with a minimum range between low and high tide of 0.48 m (from -0.25 m to 0.23 m) and a maximum range of 0.8 m (from -0.32 m to 0.5 m). A surge event occurred after 5 days, affecting the tidal signal for 2 days. Overall, the average sediment collected by the traps is between 7 and 15 g/m$^2$ per tide around the tidal flat, except next to the west inlet (25 g/m$^2$ per tide) and the north section (60 g/m$^2$ per tide) (Fig. 23a).

The second survey was carried out between June and July 2020 for 15 days. In this case, the sediment collected was remarkably higher, with an average rate of deposition of 66.9 g/m$^2$ per tide and an average submersion of ~13 hours (total submersion of ~216 hours). Only three traps were submerged for less than 8 hours, while the others were submerged for more than 16 hours. The tide was mostly asymmetric, and the maximum tidal range was similar to the first survey (~0.8 m), but it included an entire spring-tidal cycle and the tidal range remained between 0.8 and 0.6 m (Fig. 23b). The highest deposition rates were found next to both inlets and overall, in the southern part of the tidal flat (Fig. 23b) with values between 20 and 50 g/m$^2$ per tide, and notable values higher than 100 g/m$^2$ per tide at the western and northern edges of the study area.

The final survey (March 2021) lasted for 14 days with an average submersion of ~6 hours (total submersion of ~130 hours). The traps collected an amount of sediment similar to the first survey, with an average rate of deposition of 18.9 g/m$^2$ per tidal event. During the spring-tide, the highest tidal range was observed, with 1.1 m (from -0.62 m to 0.52 m) during the first 7 days, then the neap-tide occurred and the tidal range reduced to 0.4 m (-0.26 m to 0.15 m) (Fig. 22c); the tide was mostly asymmetric. In this case, the higher sedimentation occurred in the central and the northern part of the tidal flat, with values between 20 and 60 g/m$^2$ per tide, while few grams (between 5 and 15 g/m$^2$ per tide) were collected in the southern edges (Fig. 23c).

Rain occurred during a few days of the first and the last survey but we consider that even if the rain can splash the sediment outside the trap, it can also cause the opposite (besides the fact that the rain itself is a mechanism of sediment transport), which means that the rain effect can be considered as negligible. Based on the data retrieved by the station of Pontelagoscuro provided by AIPO the hydrometric level of the Po River remained constant between its average value (-4.1 m) during all surveys. No strong flood occurred, since common floods are characterized by average hydrometric level higher than -3 m and strong floods can reach values higher than 0 m above m.s.l. .

***Table 10*** *- Sediment amount collected by traps during the surveys. The depositional rates are calculated based on the tide gauge of Pila (AIPO).*

| | | | | (a) Daily rate | (b) High tide rate | (c) Submersion rate | | |
|---|---|---|---|---|---|---|---|---|
| **Survey** | **ID** | **Weights** | **Avg. Weight** | **g/m² per day** | **Average g/m² per tide** | **g/m² per hour of submersion** | **Average submersion period (hours)** | **Total submersion period (hours)** |
| **September 2019 (10 days)** | **P1** | 0.349<br>0.396<br>1.248 | 0.664 | 38.31 | 25.54 | 2.94 | 8.70 | 130.5 |
| | **P2** | 0.288<br>0.407<br>0.852 | 0.516 | 20.04 | 15.42 | 1.12 | 13.77 | 179 |
| | **P3** | 0.254<br>0.228<br>0.457 | 0.313 | 18.05 | 12.03 | 1.43 | 8.43 | 126.5 |
| | **P4** | 0.918<br>0.973<br>0.992 | 0.961 | 55.42 | 61.58 | 2.54 | 24.22 | 218 |
| | **P5** | - | - | - | - | - | - | - |
| | **P6** | 0.414<br>0.507<br>- | 0.793 | 26.56 | 18.97 | 1.77 | 10.71 | 150 |
| | **P7** | 0.27<br>0.205<br>0.251 | 0.242 | 13.96 | 9.30 | 1.37 | 6.80 | 102 |
| | **P8** | 0.266<br>0.151<br>0.186 | 0.201 | 11.59 | 7.24 | 0.95 | 7.63 | 122 |
| | **P9** | 0.21 | 0.164 | 12.28 | 7.68 | 1.01 | 7.63 | 122 |

| | | | | | | | | |
|---|---|---|---|---|---|---|---|---|
| | | 0.216<br>- | | | | | | |
| | **Average** | | **0.880** | **39.75** | **19.72** | **1.64** | 13.4 | 152.9 |
| **June-July 2020 (15 days)** | **P1** | 1.436<br>1.712<br>1.651 | 1.600 | 61.50 | 46.12 | 4.59 | 10.05 | 201 |
| | **P2** | 4.766<br>3.624<br>4.556 | 4.315 | 165.90 | 207.38 | 9.15 | 22.67 | 272 |
| | **P3** | 0.664<br>1.069<br>0.961 | 0.898 | 34.52 | 23.54 | 2.76 | 8.52 | 187.5 |
| | **P4** | 0.386<br>0.453<br>0.687 | 0.509 | 19.56 | 18.33 | 1.23 | 14.94 | 239 |
| | **P5** | 2.257<br>2.982<br>2.904 | 2.714 | 104.35 | 130.88 | 5.23 | 25.04 | 299.5 |
| | **P6** | 1.226<br>0.886<br>0.797 | 0.970 | 37.28 | 37.28 | 2.25 | 16.57 | 248.5 |
| | **P7** | 1.444<br>1.926<br>0.882 | 1.417 | 54.49 | 34.06 | 5.19 | 6.56 | 157.5 |
| | **P8** | -<br>-<br>2.532 | 7.946 | 305.49 | 73.01 | 7.28 | 10.03 | 200.5 |
| | **P9** | 1.522<br>1.376<br>1.025 | 1.308 | 50.27 | 31.42 | 5.22 | 6.02 | 144.5 |
| | **Avera** | | **2.41** | **92.60** | **66.89** | **4.77** | 13.4 | 216.7 |

| | | | | | | | | |
|---|---|---|---|---|---|---|---|---|
| | **ge** | | | | | | | |
| **March 2021 (14 days)** | **P1** | 2.7<br>12.7<br>3.8 | 0.222 | 9.16 | 6.41 | 1.64 | 3.90 | 78 |
| | **P2** | 9.4<br>9.1<br>13.0 | 0.382 | 15.75 | 10.50 | 1.00 | 10.45 | 219.5 |
| | **P3** | 19.0<br>15.4<br>24.6 | 0.818 | 33.68 | 19.65 | 4.69 | 4.19 | 100.5 |
| | **P4** | 26.2<br>21.7<br>25.5 | 0.976 | 40.19 | 24.46 | 3.08 | 7.93 | 182.5 |
| | **P5** | 64.9<br>50.0<br>60.2 | 1.924 | 79.27 | 58.41 | 4.12 | 14.18 | 269.5 |
| | **P6** | 13.1<br>22.3<br>21.9 | 0.794 | 32.72 | 19.09 | 3.56 | 5.35 | 128.5 |
| | **P7** | 8.5<br>7.4<br>10.7 | 0.200 | 8.25 | 8.89 | 2.92 | 3.04 | 39.5 |
| | **P8** | - | - | - | - | - | 4.19 | 100.5 |
| | **P9** | 1.7<br>5.1<br>3.7 | 0.091 | 3.75 | 3.50 | 0.95 | 3.67 | 55 |
| | **Average** | | **0.578** | **26.03** | **18.86** | **2.75** | 6.3 | 130.4 |

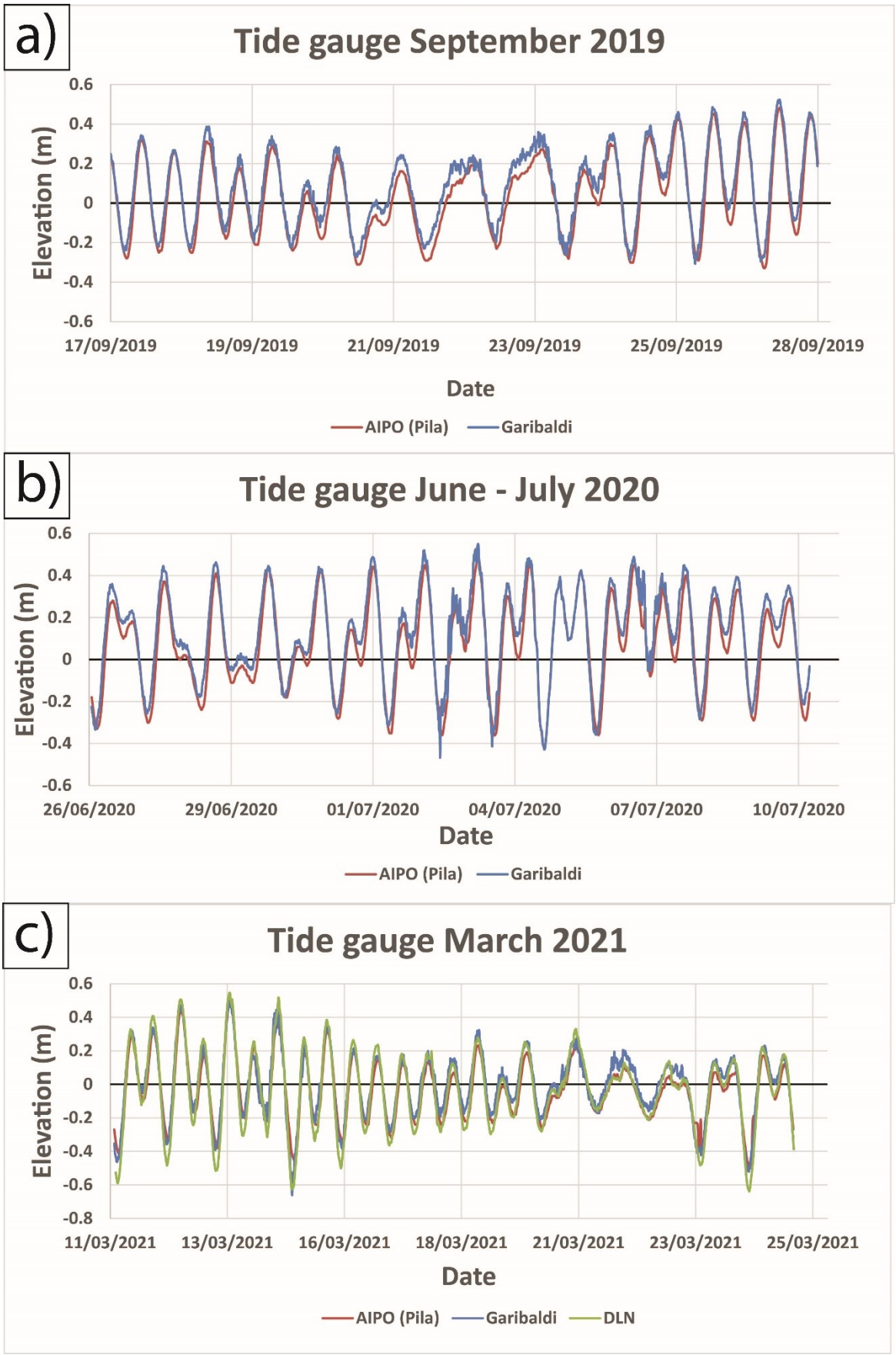


***Figure 22*** *- Tidal records registered by the tide gauge stations of Pila (AIPO), Porto Garibaldi (ARPAE), and the DLN during the surveys of (a) September 2019, (b) June-July 2020, and (c) March 2021.*

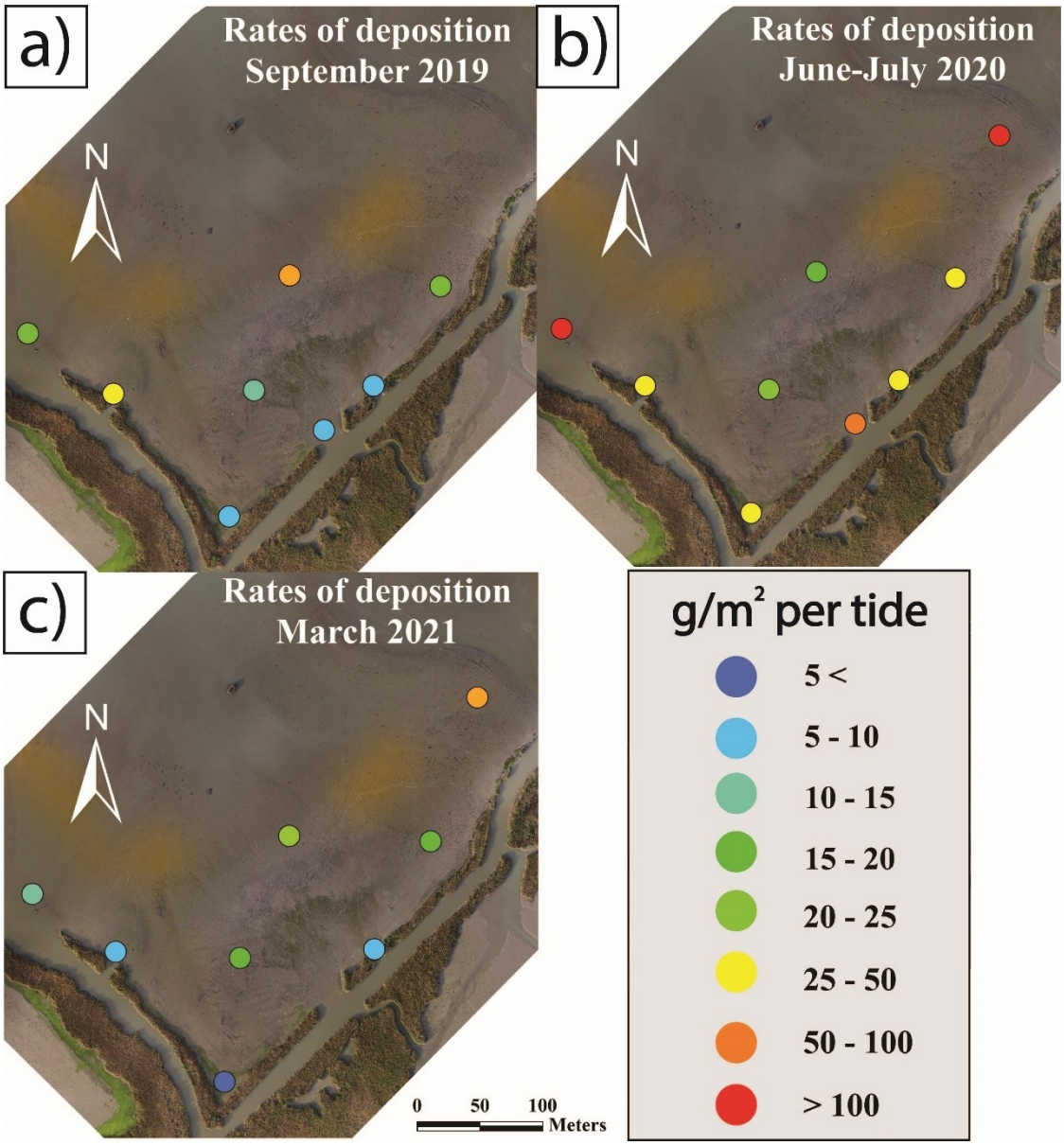


***Figure 23*** *- Rates of deposition collected by the traps during (a) September 2019, (b) June-July 2020, and (c) March 2021.*

## *3.5 Discussion*

### *3.5.1 Tidal flat formation*

The granulometric distribution of the tidal flat presents a clear organization primarily affected by the hydrodynamic patterns of the study area. Overall, the coarser sediment (**(si)sC**) is located in the central section of the tidal flat, in particular next to the inlets or where there is a lack of vegetation (wild reeds). This sandier layer reflects an area characterized by higher hydrodynamic energy in respect to the edges of the tidal flat (next to the channels), which consist predominantly of finer sediment. This organization indicates that water fluxes flow from the channels inside the

tidal flat in NW direction. Furthermore, the sand content is located principally on the mentioned crevasse splays described by Brunetta et al., (2021). This distribution supports the hypothesis that the river has a strong influence inside the tidal flat.

More information can be obtained considering the vertical distribution of the layers. Considering Subfacies (1), it is notable that the granulometric distribution reflects the modern morphodynamic. However, in Subfacies (2) the sandier layer is shifted next to the east channel, besides the fact that the whole subfacies is sandier than the surficial one. This distribution could indicate that the coarser layer is prograding following a NW direction and the crevasse splay had a different location in the past. This observation is supported by a collection of orthophotos provided by the Veneto region. These orthophotos show that before 1999, the NE channel was missing (Fig. 24a) and the southern section of the Barbamarco lagoon was partially separated by the Po della Pila. Between 1999 and 2003, the eastern channel was dug, allowing the river to directly flood the study area. It is highly probable that the tidal flat began its developments during that period (Fig. 24b). Before 2008 the levees of the east channel were not stabilized and there were no inlets (Fig. 24c). In this condition, the river floods were able to spread and overflow inside this section of the lagoon without any restriction. After 2012, the levees were stabilized by vegetation and the only connection between the tidal flat and the channel were the “new” inlets, which forced the river to flow through, generating the modern crevasse splay (Fig. 24d).

This interpretation leads to another interesting hypothesis. As previously shown, Subfacies (1) thickness increases (~14 cm) on the location of the central crevasse splay and decreases (~5 cm) on the edges of the tidal flat, in every direction. Brunetta et al., (2021) calculated the average rate of accretion of the whole tidal flat around 1.3 cm/year. If we consider this esteem, and the river as the principal and constant sediment supplier, under the hypothesis that the depositional trend was stable, the river could have deposited an average vertical sediment column between 9.1 - 14.3 cm in 7 - 11 years (since the vegetation established between 2008 and 2012). This value is included in the range of sedimentation of Subfacies (1), suggesting that this surficial subfacies represents the sedimentation of these last ~10 years, while Subfacies (2) represents a different condition (before ~2010) when sedimentation occurred next to the east channel since vegetation was not established and the river was flooding into the north-east section of the tidal flat (next to the channel). Since the river was able to flood this section of the lagoon after early 2000, Subfacies (2) could have formed between ~2000 and ~2010. These hypothesis is summarized in figure 25.

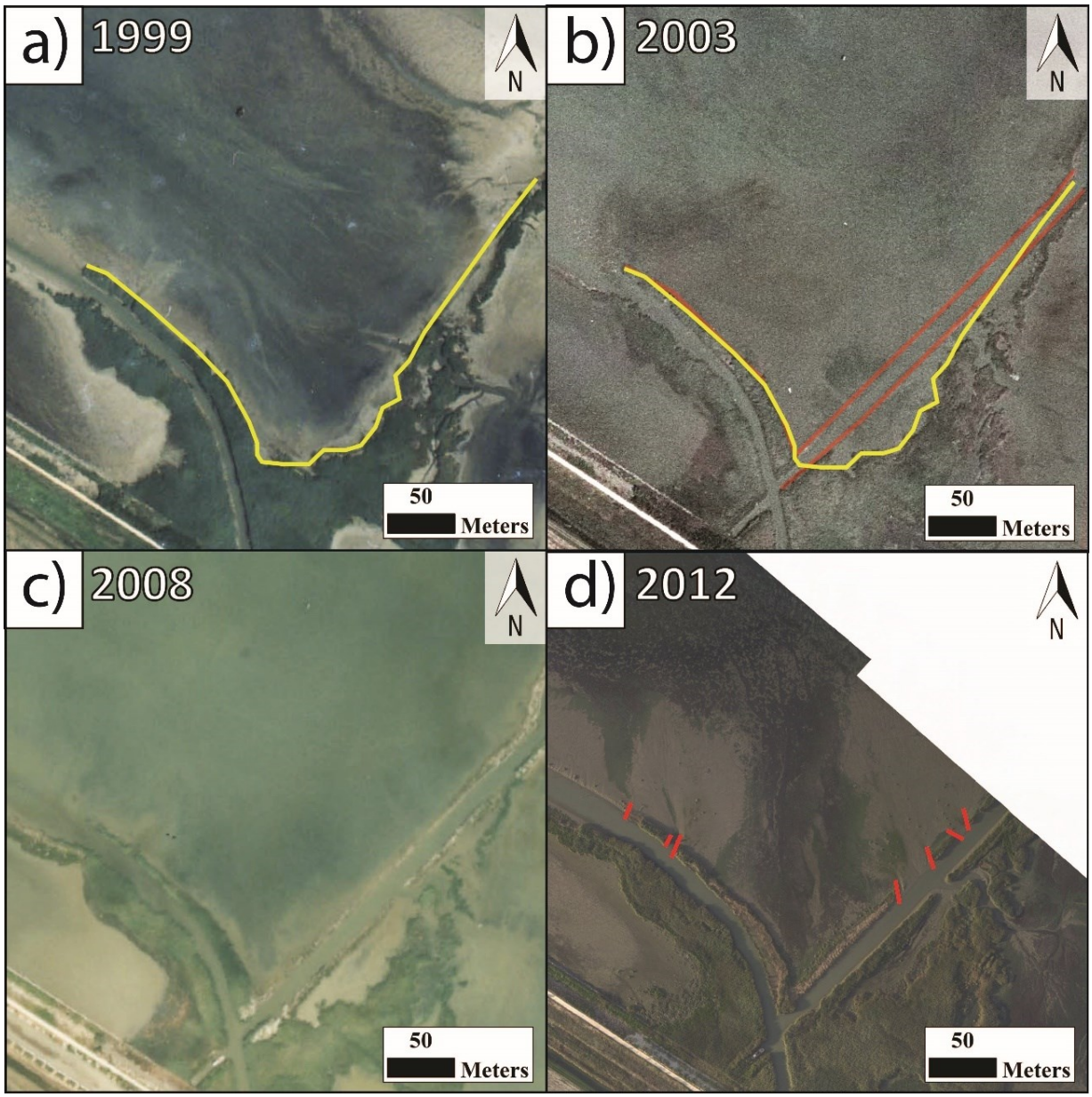


***Figure 24*** *- Orthophotos of the study area provided by the Veneto region. (a) Before 1999, the west channel was the only connection to the Barbamarco lagoon and the study area was partially isolated from the Po della Pila. (b) between 1999 and 2003 the NE channel was dug and the river could flood in the study area. (c) In 2008 the levees of the east channel were not established by vegetation yet; (d) the channel shows a stabilized condition in 2012.*

However, the low limit of Subfacies (2) is undefined (only two samples are characterized by a third Subfacies), hence it is not clear if Subfacies (2) represents the condition before the vegetation establishment (between ~2000 and ~2010) or it is older than 10 years. If this is the case and Subfacies (2) represents the condition before ~2000, Subfacies (1) could have been deposited during the last 16 - 19 years. In this condition, the rate of accretion would be around ~0.3 - ~0.8 cm/year (for 5 to 14 cm of vertical column), which is slightly lower than the previously calculated one (i.e. suggesting that this interpretation could be less reliable), but not implausible given the

uncertainty of the evaluations (see Brunetta et al., 2021). Furthermore, the coarser sediment increases deepening, which could indicate that the sand could come from a mix between the previous soil condition (e.g. sandier agricultural fields).

It is important to note that the difference between the two Subfacies is caused by the different colour and the increase in sand content moving downward. However, in the previous interpretations, it was assumed that the colour change coincides with two different sedimentation conditions. It is more probable that the progradation of the crevasse splay was slow and gradual, which means that the colour change could depend on a different factor. Despite Subfacies (2) being darker than Subfacies (1), the LOI content decreases in the deeper subfacies. This condition does not surprise since granulometry increases in Subfacies (2); the darker tones could indicate that the organic matter has not been oxidated.

Besides which interpretation is correct, the opening of the channel, the establishment of the levees, and the consequent tidal flat formation occurred after ~2000, when the Po della Pila mouth gave the first signs of recovery around 2002 (Ninfo et al., 2018).

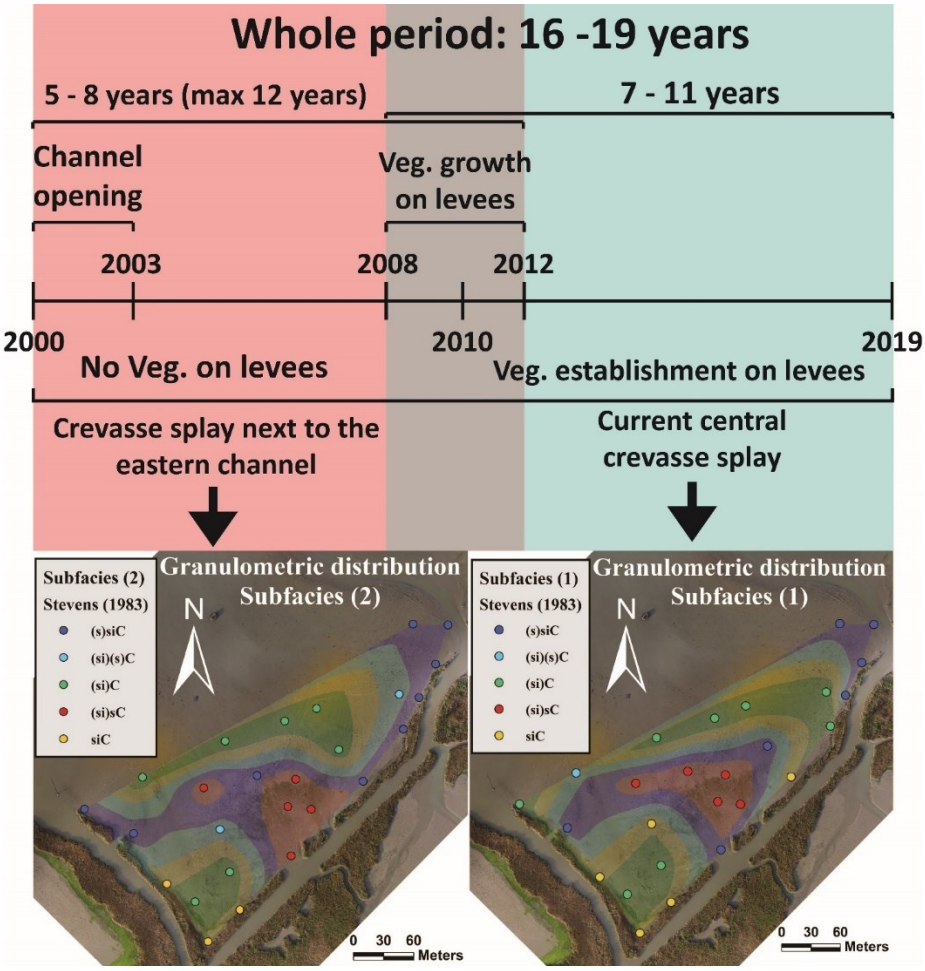


***Figure 25*** *- Timeline that describes the evolution of the tidal flat.*

### *3.5.2 Depositional patterns*

The deposited sediment collected by the traps shows that the tidal flat follows common depositional patterns due to tidal influence. During all analyzed periods, sedimentation increases when the hydroperiod increases (Fig. 26a, 26b) and decreases when elevation above m.s.l. increases (Fig. 26c). This is a common behaviour for tidal flats (Pethick, 1981; French, 1993). Overall, the highest rates of deposition occurred in the external part of the study area, moving westward and northward, since these stations are located in the most depressed areas; lower rates are found southward, next to channels levees and in the middle of the inlets, probably due to higher hydrodynamic conditions. However, spatial patterns changed between surveys. During June and July, notably higher rates of deposition occurred in the whole tidal flat (>50 g/m$^2$ per tide), in comparison with the surveys of September 2019 and March 2021, where the deposition was highly similar (~20 g/m$^2$ per tide). Since important floods did not occur (i.e. average daily discharge of ~1000 m$^3$/s), rain and wave interactions were negligible, the sediment transport can be mainly attributed to the tide and average river condition. The results show that the tidal flat experienced seasonal trends that affect the depositional rates in different periods during the year. Low sedimentation occurred during the first and the last surveys, hence at the beginning of autumn and spring seasons, while high sedimentation occurred during summer. This trend is not driven by the river, since only important floods cause high sedimentation (Tesi et al., 2011), which is dominant during winter (Palinkas et al., 2005; Brunetta et al., 2021). Furthermore, if an important flood had occurred, it would have buried the traps (based on early tests with the traps and field observation). These seasonal trends can be assigned mostly to the tide, although no analysis of tidal current velocities was carried on in order to increase the reliability of this interpretation. The variation in sedimentation could be related to the difference in tidal range since the summer survey was characterized by a constant range between 0.6 and 0.8 m, which is higher than the other two surveys, although there is no available evidence at this moment supporting this hypothesis. There are other factors that could influence depositional patterns. Biological interaction can increase deposition, such as in the case of Frostick and McCave (1979), and Andersen et al. (2006) where they described a microtidal mudflat characterized by high sedimentation during spring-summer seasons due to algae binding. At this moment, *Spartina maritima* is the only salt marsh pioneer plant able to grow inside the tidal flat, but its distribution is highly restrained to a few patches. The presence of algae is found in some areas of the study area, but their location is not stable and it changes between the years. Bioturbation is another

possible reason that could increase sediment deposition, like Temmerman et al. (2003) described in the Scheldt estuary (Netherlands), where deposition was amplified during summer due to bioturbation of bottom sediment. Wave influence is to consider negligible inside the lagoon as well, in particular since sheltered marshes with fetch that is lower than 10 km are not highly impacted by this process (Cortese and Fagherazzi, 2022). Another factor that influences deposition is coastal storm occurrence (e.g. Goodbred and Hine, 1995; Wood and Hine, 2003), but it is not the case of the Po Delta. Despite small surge events that occurred during the surveys (Fig. 23), the structure of the lagoon and the rates of deposition do not suggest storm influence. The results suggest that river and tide control opposite trends of sedimentation, with the river floods increasing deposition during winter, while the tide during summer; however, the river is the dominant factor. This interpretation is supported by comparisons with accretion and depositional trends found in other tidal flats. For example, the Perkpolder tidal flat (Netherland) is a macrotidal young mudflat characterized by an average 6 cm/year of accretion and rates of deposition (with similar average submersion period to the tidal flat at issue) between 60 and 70 g/m$^2$ per tide (Brunetta et al., 2019); in this case, the proximity of the tidal flat to the turbidity maximum, which is where sea and freshwater fluxes collide and mix, leads the tide to be the principal factor that controls sedimentation. Since the Pila tidal flat has an average of 1.3 cm/year of accretion and sediment deposition varies between 20 and 60 g/m$^2$ per tide, sedimentation due to tidal influence is reduced and probably the tide re-distributes sediment around the lagoon. Opposite seasonal trends are found in other tidal flats, such as for the Waccassa Bay case in Florida, where biological factors increase sedimentation during summer (Wood and Hine, 2007), but storms are the most dominant one during winter (Wood and Hine, 2003). More considerations about sediment deposition between tidal flats are described in paragraph 5.3.

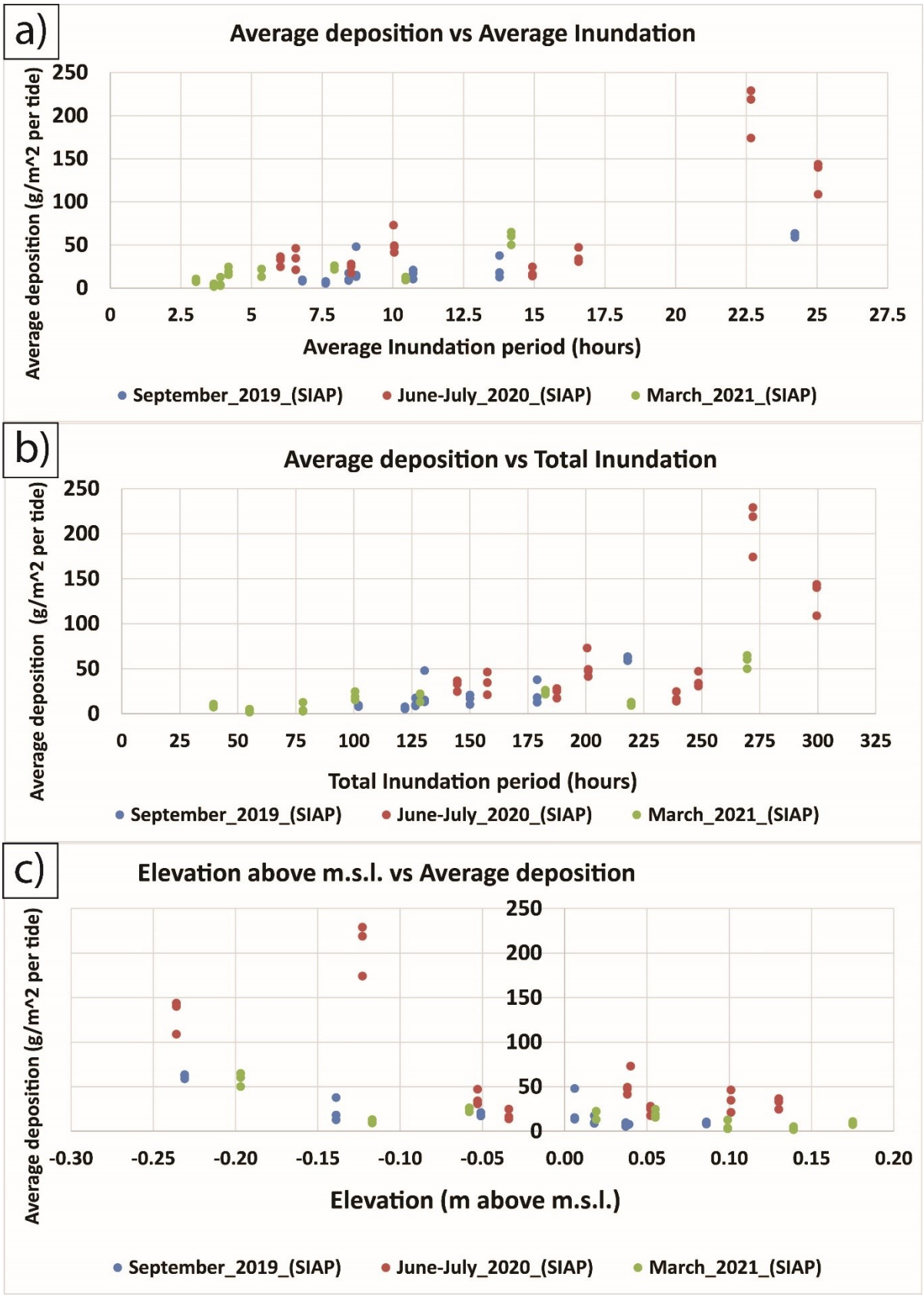


***Figure 26*** *- Comparisons between sediment amount collected by traps in grams and (a) average inundation, (b) total inundation, and (c) elevation above m.s.l..*

### *3.5.3 Sediment deposition in microtidal flats*

Although microtidal flats are commonly subjected to limited changes compared to meso and macrotidal wetlands, their vertical evolution can be appreciable, in particular in short periods, such as for Andersen et al. (2006) and the Po Delta case; however, in most cases, the tide is not the principal sediment supplier and it is assisted by other processes that cause high sediment transport and deposition, such as waves resuspension (Duvall et al., 2019), storm occurrence (Wood and Hine, 2003), river input (Brunetta et al., 2021). According to studies of microtidal wetlands, the average deposition is mostly between a few grams to ~50 g/m$^2$ per tide (Reed, 1989; Leonard et al., 1995; Leonard, 1997; Culberson et al., 2004; Duvall et al., 2019)

American microtidal marsh systems have some similarities with the present study area (e.g. Letzsch and Frey, 1980; Reed, 1989; Leonard, 1997). For example, Leonard et al. (1995) studied a marsh system located next to Crystal River in Florida (US) with similar tidal characteristics to the Po Delta (average semi-diurnal tidal range of 0.9 m), and similar methodology (i.e. traps) and conditions (i.e. inundation period, marsh elevation). Using filter papers on Petri dishes, they measured sediment deposition next to the creek and the internal part of the mudflat; the values are between 5.8 and 35 g/m$^2$ per tidal cycle. They pointed out that deposition was higher during summer rather than winter and that proximity to creeks increases sedimentation; furthermore, deposition is higher when storms occurred during winter, but it is still comparable to normal deposition during summer. These events are relatively similar to the presented study site and the seasonal difference in deposition is ascribed to bioturbation due to fiddler crab's activity, such as disaggregating surficial sediment and providing fecal pellets (Harrison and Bloom, 1977). Moreover, the increase in water temperature may enhance sedimentation due to a decrease in water viscosity and, consequently, an increase in settling velocities (Blatt et al., 1981). Since in both studies the sediment deposition is caused mostly by the tide, the tidal flat of the Barbamarco lagoon seems to be subjected to higher rates of deposition, in particular during summer; however, this could be related to different elevation and location of the traps, since the study area of this study is a tidal flat and the one from the Crystal River is a marsh, so vegetation could have changed sedimentation patterns.

It is worth noticing that higher importance should be given to the estimation of the rates of deposition since inaccurate calculations can lead to incorrect interpretation of the dynamics of the environment under investigation. The paper from Mfikili et al. (2022), for example, shows some

inaccuracies that undermine the appropriateness of the interpretation. Similarly to this study, the authors analysed a microtidal marsh located in Keurbooms Estuary (South Africa); they used Petri dish traps to evaluate the rates of deposition and they obtained the rates of accretion, following the same methodology of Butzeck et al. (2015). However, the rates of deposition that they report range between 0.085 and 0.267 g/cm$^2$ per tide, which represent 850 – 2670 g/m$^2$ per tide. These values appear to be extremely high for a microtidal environment analysed in the paper (the values are higher than macrotidal wetland such as in the Bay of Fundy, see paragraph 6.4), in particular if when these are considered in relation to the reported rates of accretion, which average value is about 0.8 mm/year. Additionally, during the period analysed by Mfikili et al. (2022), the average river discharge (between 3 to 150 m$^3$/s) was low compared to the Po River (i.e. average 1500 m$^3$/s) and, overall, floods are relatively rare (1 every 2 – 5 years) for the Keurbooms Estuary. This suggests that the river is not the factor that caused deposition while the sediment traps were deployed. Since the marsh under investigation by Mfikili et al. (2022) is located inland and is defended by a large sand barrier, the wave influence is expected to be negligible as well. Additionally, the authors state that the suspended sediment is low during non-flooding periods. All these considerations suggest that there might be an oversight in the order of the rates of deposition; however, the authors do not specifically report about the calculations of the rates, and it is not possible to identify the source of the identified inaccuracy.

## *3.6 Conclusions*

This paper focuses on the sedimentological evolution of the southernmost tidal flat of the Barbamarco lagoon, in the Po River Delta (Italy). Granulometric distribution, sediment deposition, and orthophotos, allowed to study the recent evolution of the tidal flat and to interpret the events that have led to the recent framework. Twenty-six cores sampled using PVC tubes were analysed to distinguish stratigraphical differences and sediment classes. Twenty-seven sediment traps distributed in nine different stations were located around the tidal flat during September 2019, June-July 2020, and March 2021 in order to estimate sediment deposition. Orthophotos from 1999 to 2012 were interpreted. The most relevant conclusions are the following:

- Two subfacies were identified in the first 25 cm below the surface; both are characterized by fine granulometric classes, which are **(si)C** (Slightly Silty Clay), **siC** (Silty Clay), **(si)(s)C**

(Slightly Silty and Slightly Sandy Clay), **(s)(si)C** (Slightly Sandy and Slightly Silty Clay), **(si)sC** (Slightly Silty Sandy Clay);

- The coarser classes are located in the centre of the tidal flat while the finer sediment is located at the edges;
- Granulometric and LOI distribution enhance the presence of a crevasse splay that develops from the inlets of the eastern channel in the NW direction, and suggest that the river flood influence is important on the tidal flat formation;
- The distribution of the subfacies and orthophotos highlight that the tidal flat started its evolution in early 2000, after the birth of the eastern channel due to human intervention that allows the river to flow directly inside this section of the Barbamarco lagoon;
- The levees of the channel were not established before 2008, causing sedimentation mostly in the north-eastern part of the tidal flat;
- After 2008, the inlets directed the floods in NW direction, leading to the recent crevasse splay and recent shape;
- Sediment deposition surveys pointed out that sedimentation is higher during summer (average 66.89 $g/m^2$ per tide) and lower during winter (18-20 $g/m^2$ per tide);
- Waves influence is not relevant, due to the lagoon morphology, and no floods, storms, or other events occurred during the surveys, hence deposition can be addressed to the tide itself;
- Comparisons with other microtidal flats suggest that other factors (i.e. bioturbation) could cause seasonal differences and that in most cases the accretion and erosion of microtidal flats are controlled by other processes rather than tidal currents alone;
- Tidal influence seems to be higher during summer, but higher rates of accretion occur during winter, suggesting that the river is the principal sediment supplier;
- Both granulometric distribution and sediment deposition strengthen the hypothesis that tidal flat accretion is controlled by river floods rather than tidal currents alone.

# 4. Evolution of tidal flats in the Northern part of the Po Delta: a strategy for future building-with-nature management

## *4.1 Introduction*

### *4.1.1 Building-with-nature approach*

During the last decades, the conception of coastal defences has profoundly changed and, consequently, our approach to the coastal environment has also been modified. The policy of the last decades based on short-term exploitation of natural resources (Capobianco and Stive, 2000) where sea and land were considered as two different systems are now obsolete (Slobbe et al., 2013) and new key concepts of coastal resilience and Building-with-Nature have been defined (Masselink and Lazarus, 2019). Although dykes, sea walls, and other artificial protections are commonly perceived as the best solution, conventional coastal engineering is becoming unsuitable (Temmerman et al., 2013). Several studies have shown how these structures have unavoidable long-term effects, not only because of the increasing potential risk of casualties and damages in case the defences are broken (Van Koningsveld et al., 2008; Smits et al., 2006) but also because of disturbances in sediment balance, an increase of land subsidence by soil drainage (Syvitski et al., 2009) and other human-induced changes. Instead, it is well known that coastal ecosystems such as marshes, mangroves, dunes, coral reefs, and shellfish reefs are fundamental in coastal protection thanks to their ability to reduce storm waves (Barbier et al., 2008; Gedan et al., 2011; Shepard et al., 2011; Bouma et al., 2014), storm surges (Temmerman et al., 2012; Zhang et al., 2012; Boutwell and Westra, 2015; Stark et al., 2015; Leonardi et al., 2018), and to keep up with sea-level rise (Kirwan et al., 2010; Fagherazzi et al., 2012). Natural-based solutions are to be considered rather than traditional approaches and several restoration projects are now conducted worldwide. The purpose of these projects is to restore coastal zones allowing the sea to flood inland areas using a set-back scheme, which consists of giving the ecosystem the possibility to establish a new equilibrium without human intervention. Several countries worldwide have already started using this approach, in particular, north European ones, in the East coast of Canada and the West coast of America. Despite this, we need more information about the evolution and the consequences of this method, and the floods of the 1950s – 60s of the Po River have given an interesting opportunity to study new strategies for Building-with-Nature management.

### *4.1.2 Salt marsh and tidal flats*

A proper salt marsh consists of herbaceous halophytes that have adapted to tolerate regular saltwater inundation (Pratolongo et al., 2019) in low-energy and temperate coastlines (Allen and Pye, 1992; Adam, 2011), except for the mangroves forests (Odum et al., 1982). The location of a salt marsh is strictly related to its elevation with respect to the m.s.l. and the tidal range. If the surface of the flat is located below a certain elevation, the vegetation will not be able to grow; this condition is typical of tidal flats, which are non-vegetated intertidal habitats mainly composed of sand or mud (Dyer et al., 2000a). A perfect level that separates tidal flats from salt marsh does not exist, but a reference threshold that is commonly considered is the Mean High Tide (MHT), which is the average high tide; generally, a tidal flat needs to reach this elevation (in respect to m.s.l.) to allow vegetation to grow (De Vlas et al., (2013); Bakker, 2014). This means that salt marshes are critically dependent on how fast sediment deposition occurs with respect to sea-level rise (Redfield, 1972; Orson et al., (1985); Schuerch et al., 2012); in turn, sediment deposition is controlled by several different factors, such as seasonal conditions (Reef et al., 2018), sediment availability and grain size distribution (Schuerch et al., 2014), storm frequency and intensity (Schuerch et al., 2012). Nowadays, great knowledge of physical (e.g. Pethick, 1981), morphological (e.g. Cahoon, 1995), and ecological processes (e.g. MacKenzie and Dionne, 2008) comes from studies that focussed on established salt marshes that are evolving or deteriorating. Moreover, several studies discussed the ability of salt marshes to adapt and keep pace with sea-level rise (Stevenson et al., 1986; van Wijnen and Bakker, 2001; Schuerch et al., 2013; Crosby et al., 2016; Kirwan et al., 2016; Spencer et al., 2016). However, Building-With-Nature approach concerns new environments that turn into salt marshes; despite our great understanding of processes that characterize well-developed salt marsh, there is a strong need for information about the mechanisms that lead to salt marsh transition (Gunnell et al., 2013). The “set-back” approach (i.e. to let the environment develop without human intervention, in this case giving back to the sea part of coastal areas) is a strategy implemented in different environments worldwide, such as in the Perkpolder tidal basin located in the Scheldt estuary (Zeeland, Netherland) (Brunetta et al., 2019; Cao et al., 2021), or in the Bay of Fundy (Nova Scotia, Canada). The current study focuses on the evolution of the tip of the Po River Delta, in particular on the Barbamarco lagoon and a young tidal flat that is developing in the last 20 years. The principal aims are: i) to define the evolution of the Barbamarco lagoon during the last century; ii) to discuss the evolution of tidal flats, salt

marshes and their possible future evolution; iii) to compare the study area with other building-with-nature projects and discuss the feasibility in the Po Delta context.

## *4.2 Study site*

### *4.2.1 The story of the Po River Delta*

Before human intervention, the structure of the Po River Delta was highly influenced by strong rainfall, climatic fluctuations, tectonics and subsidence (Bondesan' et al., 1995). After the last glacial phase (18000 years ago), where an extended fluvial plain was located 300 km south-eastward compared to the actual location (basically inside the recent Adriatic sea), the system was subjected to a strong transgression caused by a warmer climatic period where the sea level rise set the coastline approximately to the recent configuration (Colantoni and Galliniani, 1985). The "Little Ice Age" that occurred between 1500 – 1850 was characterized by a high fluvial solid discharge and an extended salt marsh system developed (Veggiani, 1994). The most important human intervention took place in 1604 (Simeoni and Corbau, 2009; Cencini; Bondesan, 1990) when the Venetian Republic concluded the "Porto Viro" bypass that diverted the Po River course (Stefani and Vincenzi, 2005), starting the evolution of the modern delta. During the last 400 years, the river divided into five principal branches that cross the delta, which are from north to south Po di Maistra, Pila, Tolle, Donzella or Gnocca, and Goro. Po di Maistra was the most important branch (Ciabatti, 1967) until 1872, when the Po della Pila became the main branch. A generalized progradation occurred between 1800 and 1945 (Visentini, 1940), while human interventions increased their role in the evolution of the Delta. The most important landscape modifications were started by the Italian monarchy in 1870 to meet human requirements, in particular, to improve the economy and contrast malaria (Cencini, 1998), and afterwards by the Fascist regime and the Italian Republic until 1960. Dam construction and river bed material exploitation (Billi and Fazzini, 2017), combined with strong floods, caused a strong erosional trend between the 1940s and the 1980s, with an overall shoreline regression of 224 m (Bezzi et al., 2021); several agricultural fields were submerged, giving birth to new lagoons. Overall, during the last century, strong vegetation loss occurred in all the lagoons of the delta, reaching values of about 48% compared to their maximum extension (Verza and Catozzo, 2015; Corbau et al., 2022). This erosional trend is highly reduced between the 1980s and the 2000s and a process of stabilization

took place. The first signs of a slow recovery occurred after 2002 and an evident constructive process started after 2010 (Ninfo et al., 2018).

Nowadays, with an extension of 700 $km^2$ and a coastline of 90 km, the Po Delta can be considered as one of the major anthropic Delta in the world (Maselli and Trincardi, 2013) (Fig. 27a, 27b). The Delta structure depends on the Po River, which flows into the Adriatic sea for 650 km and an average discharge of 1500 m/s (Ludwig et al., 2009) and a catchment area over 70000 $km^2$ (Bondesan, 1990). Due to the strong dependency on the river, the Delta was considered *river-dominated* and it probably shifted to *wave-dominated* after the strong anthropic influence of the 1950s (Smith et al., 1966; Nelson, 1970; Galloway et al., 1975). It is important to note that each ramification is associated with peculiar delta plain and delta front depositional systems that are dominated by different trends, hence there is no principal regime (Trincardi et al., 2003, Correggiari et al., 2005; Syvitski et al., 2009). The Delta is characterized by a microtidal range of about 0.5 m (spring-tidal range about 1 m); the tide is mixed, mostly semi-diurnal. The Po della Pila is the branch with the highest water and sediment discharge (61% of water and 74% of sediment) while the Po di Maistra is the lowest one (3% of water and 1% of sediment) (Nelson, 1970). Seasonal floods differences occur between summer and winter: June is commonly characterized by snow melting and November is subjected to rain (Marchi et al., 1996; Palinkas et al., 2005); summer floods between January and August are usually weaker than winter floods, with a discharge of about ~4000 - 6000 $m^3/s$ (Tesi et al., 2011), and do not deliver a high amount of sediment (Marchi et al.,1996). Large floods occur between October and December (>6000 $m^3/s$) causing significant deposition (Tesi et al., 2011). The coastline of the Delta consists predominantly of sandier component (Dal Cin, 1983; Simeoni et al., 2000) while the internal part of the lagoon is characterized by finer sediment, principally mud, and silt.

### *4.2.2 The tip of the Delta*

The Barbamarco lagoon is located between the mouth of the Po di Maistra and Po della Pila, which means on the northern side of the tip of the Delta, and it develops for 7 km in NW direction and can reach 3 km of width (Fig. 27c). The Po River flows inside the lagoon through two small channels of the Busa di Tramontana and the water reaches the Adriatic Sea via two inlets called Bocca Nord (North side) and Bocca Sud (South side). Waves interaction is highly restrained by the sand bar that separates the lagoon from the sea and the most important processes that influence sediment transport is the river and the tide.

The study area of this paper concerns the Burcio lagoon and the northern portion of the Basson lagoon as well. The Burcio lagoon is a smaller lagoon located between the Busa di Tramontana and the Po della Pila; protected by 3.5 km of sand barriers and extended for a maximum of 3 km, it represents the most north-eastern extension of the Delta. Vegetation covers the limit of the lagoon and old dikes that persisted from previous fields. Few underwater human structures (i.e. probably farms and houses) are what remain in the southern part. The southern tip of the Delta is characterized by the presence of the thermoelectric power plant (built by Enel Productions), which is inactive nowadays, and the Bassoon lagoon, that extends for about 5 km in SW direction between the Po della Pila and the Busa di Scirocco, which is a small channel that develops southward.

The Barbamarco lagoon and the other areas of the tip of the Delta reached their recent condition after the strong floods of the last century; nowadays, hundreds of hectares of agricultural fields, houses, and other anthropic structures are underwater. Strong changes occurred to the eco-geomorphology of this part of the Delta as well. Human influence has caused vegetation loss in wetlands, but even after environmental protection measures, the vegetation did not recover, probably due to indirect anthropic interventions and natural factors (Gaglio et al., 2017). Thanks to the complex forcing that controls the delta, the vegetation is highly variable but it is composed principally of marsh plants such as the associations of *Spartinetum maritimae, Puccinellietum palustris, Salicornietum radicantis, Salicornietum fruticosae, Agropyro-Inuletum crithmoidis, Halimionetum portulacoidis* (Ferrari et al., 1985). Most of these plants share their habitats with wide common marsh grass, such as reeds (*Phragmites australis*), which mainly cover the channels levees (Verza and Catozzo, 2015).

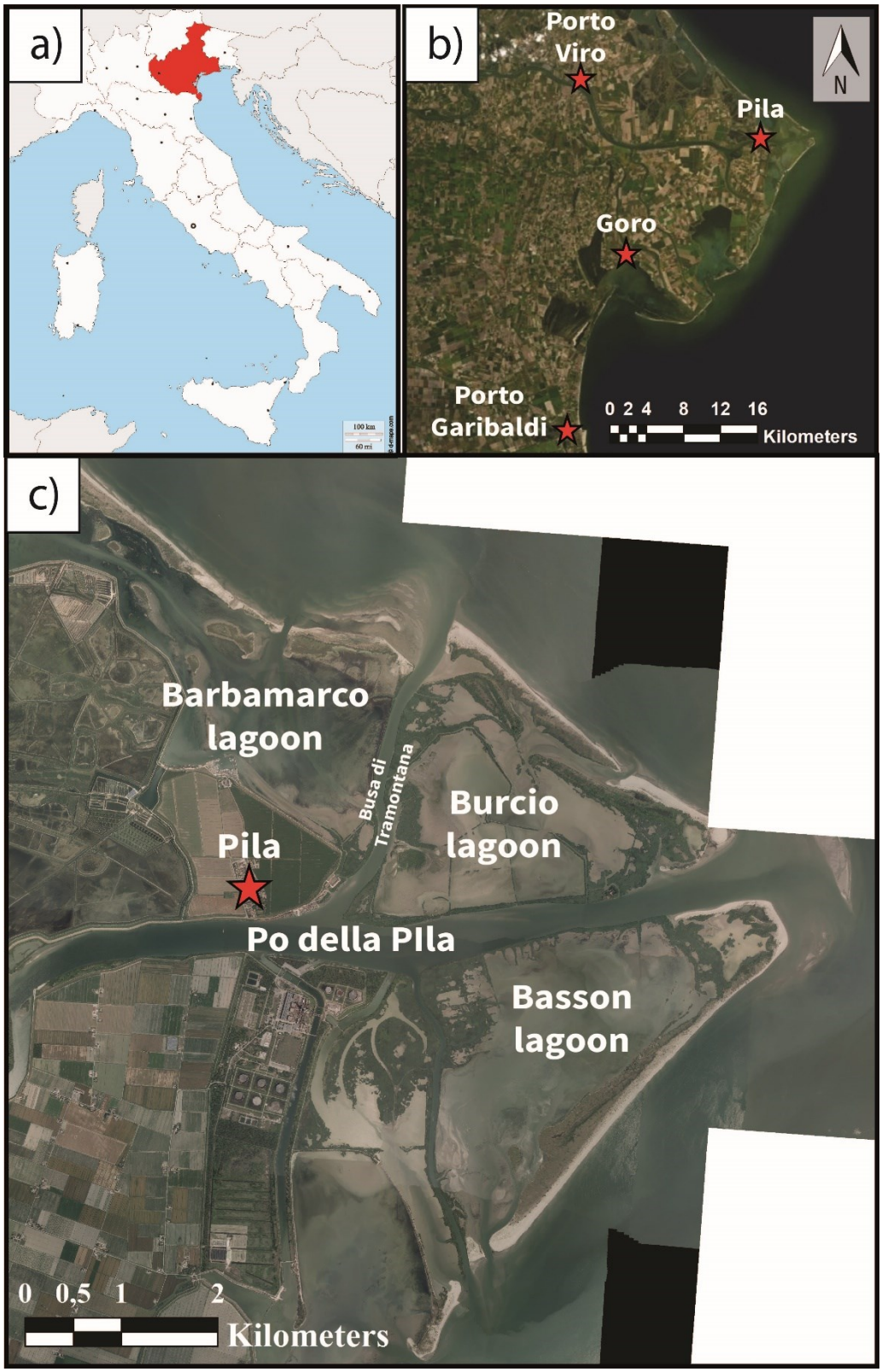


***Figure 27*** *– (a) Location of the Po River Delta and (b) the village of Pila, in the municipality of Porto Tolle. (c) Orthophoto provided by the Veneto region (Agea2015) where three principal lagoons of the tip of the Delta are visible: the Barbamarco lagoon, in the north side of the Po della Pila; the Burcio lagoon is located on the East side of Busa di Tramontana; the Basson lagoon is in the southern side of the Po della Pila.*

## *4.3 Methodology*

### *4.3.1 Orthophotos*

The reconstruction of the history of this tidal flat and the nearby areas requires high-resolution images. Satellites cannot reach the temporal and spatial detail needed for this analysis; consequently, the photographic archives are the best source of historical data. Eighteen Orthophotos from 1949 until 2018 were available from the IGMI (Istituto Geografico Militare Italiano) and the Veneto region archives (Tab. 11). The photogrammetric correction was not necessary because no displacements were expected in a flat territory such as a Delta and also because of the qualitative analysis. The oldest orthophotos were necessarily georeferenced in the WGS 1984 Zone 33N coordinate system. A short time period was investigated using satellite images provided by SIO, NOAA, U.S. Navy, NGA, GEBCO, Maxar Technologies 2021, from Google Earth Pro 7.3.4.8248 (64-bit), between 2009 and 2020 (Tab 12).

***Table 11*** *– Date and characteristics of the orthophotos.*

| Date | Scale | Altitude | Archives | Resolution |
|---|---|---|---|---|
| 10/07/1949 | 18000 | 3600 | IGM | / |
| 14/10/1955 | 33000 | 5000 | IGM | / |
| 11/07/1962 | 33000 | 3600 | IGM | / |
| 17/07/1969 | 35000 | 5400 | IGM | / |
| 10/08/1977 | 29000 | 4500 | IGM | / |
| 04/06/1983 | / | 2600 | Veneto region | / |
| 06/07/1989 | 35000 | 5400 | IGM | / |
| 03 – 07/1990 | / | 3000 | Veneto region | 90 cm |
| 01/07/1991 | 36000 | 5500 | IGM | / |
| 03/09/1992 | 35000 | 5940 | IGM | / |
| 14/09/1996 | 38000 | 5800 | IGM | / |
| 05/10/1999 | / | 2500 | Veneto region | 70 cm |
| 2003 | / | / | Veneto region | 50 cm |

| | | | | |
|---|---|---|---|---|
| 2006 | / | / | Veneto region | 50 cm |
| 06/2006 – 09/2007 | 10000 | / | Veneto region | 50 cm |
| 21-22/08/2008 | / | 1250/2500 | Veneto region | 70 cm |
| 17/09/2012 | / | / | Veneto region | 20 cm |
| 2015 | / | / | Veneto region | 20 cm |
| 14/04/2018 | / | / | Veneto region | 20 cm |

***Table 12*** *– Satellite images provided by SIO, NOAA, U.S. Navy, NGA, GEBCO, Maxar Technologies 2021, from Google Earth Pro 7.3.4.8248 (64-bit), between 2009 and 2020. The coordinates are referred to the location of the images.*

| **Date** | **Coordinates** |
|---|---|
| 13/04/2009 | 44° 58’ 26.52” N<br>12° 30’ 12.95” E |
| 06/03/2011 | |
| 16/08/2013 | |
| 28/03/2015 | |
| 22/06/2017 | |
| 03/04/2020 | |

## *4.3.2 Tidal records and flow discharge analysis*

Complementary information, such as flow discharge and tidal variations, are needed for a correct interpretation of the delta dynamics and the evolution. Ninfo et al. (2018) provided data of the effective flow discharge ($Q_k$) from 1925 to 2015, which is represented by the following equation (4):

$$\boldsymbol{Q_k = Q_{max} * Q_{10d}/(Q_{max} - Q_{10d})} \quad (4)$$

where $Q_{10d}$ is the average of the highest discharges occurred in 10 days per year and $Q_{max}$ is the highest discharge of the year. This calculation considers the most representative and impactful floods of the Po River since these cause higher sedimentation and changes in the Delta (Tesi et al.,

2011). The time series derive from the station of Pontelagoscuro, provided by AIPO (Agenzia Interregionale del fiume Po).

For tidal measurement, the station of Porto Garibaldi was taken into account, which is located ~40 km southward the Delta. The tide gauge of Po della Pila was not chosen for this analysis since the influence of the river would not allow a correct calculation of the variation of the local Mean High Tide (MHT) and mean sea level. The time range chosen for the data collected by the Porto Garibaldi tide gauge was from 2009 to 2019.

### *4.3.3 The tidal flat of the Barbamarco lagoon and vegetation distribution*

This study is combined with the results of Brunetta et al. (2021) and the previous chapter, which concerns the evolution of the recent tidal flat of the southernmost part of the Barbamarco lagoon. In these papers, morphology, rates of accretion and erosion, rates of sediment deposition, granulometry distribution, and historical interpretation are discussed, and they will assist and support the discussion of this study.

In addition, a small dataset of *Spartina maritima* distribution was collected the 29 October 2020 in order to measure the elevation and location on the tidal flat surface. The position was measured using an RTK-GPS Trimble R8 and referred to the WGS84 – UTM 33N coordinate system.

## *4.4 Results*

### *4.4.1 Historical evolution*

#### *4.4.1.1 Land reclamation: the first time interval (1949 – 1955)*

The oldest orthophoto available of the Po delta was realized in 1949 (Fig. 28a). The Po della Pila branch, which is the larger one, brings the river water from the West to the East; this tributary splits to the North into the Busa di Tramontana branch. At this moment in time, the Po della Pila and the Barbamarco lagoon were separated. Although the photo is damaged, it is visible that agricultural fields (in particular in the area of the recent Burcio lagoon) and other anthropic structures covered most of the territory. The southern section of what will become the Barbamarco lagoon presented several parallel artificial channels that develop in NW direction. However, in the central-northern section, a natural large tidal channel extended from the sand barrier inside the land, suggesting that most of the lagoon was not perpetually underwater and

indicating the presence of a tidal flat. Some smaller tidal creeks developed on the channel east side and darker areas indicate the presence of vegetation, hence salt marsh. Furthermore, The Porto Tolle harbours were very small, and the thermoelectric power plant located southward to the Po della Pila branch was not built yet. The flow discharge during these years was not above the average ($Q_k$ = 6000 – 7000 $m^3/s$) and this condition was almost stable for the next decade, although during 1953 an important flood of about 30000 $m^3/s$ occurred. Some of the features described previously are clearer and visible in the orthophoto of 1955 (Fig. 28b), since it has a better quality. The agricultural fields were not covered by the water and a new harbour next to Porto Tolle in the South was under new developments. The photo, which probably shows high tide conditions, confirms that the levees of the tidal creeks were covered by vegetation, suggesting that salt marsh species were present in this central part of the "not yet" lagoon. During the 1940s-50s, the presence of complex tidal creek systems has been seen in other lagoons of the Po Delta as well (Corbau et al., 2022). A well-developed salt marsh (with an extension of more than 200 hectares) and its tidal creeks covered the tip of the Delta between the Busa di Tramontana and the Po dell Pila (i.e. recent Burcio lagoon); the salt marsh developed on the other side of the Po della Pila as well (i.e. recent Basson lagoon), despite new agricultural fields were reclaimed from the marsh between 1949 and 1955. Between 1951 and 1955, an important storm occurred, characterized by wind speed between 12 and 15 m/s, and mean sea level higher than 0.9 and 1.5 m (Perini et al., 2011); however, the structure of the tip of the Delta did not change.

#### *4.4.1.2 Extreme events: the second time interval (1955 – 1969)*

The most severe events and changes took place during the following decade. In 1960 the most important floods occurred, characterized by 67000 $m^3/s$, and the consequences of this heavy discharge are visible in the orthophotos of 1962 (Fig. 28c), where the whole Barbamarco lagoon was completely submerged; this event gave birth to the recent configuration of the lagoon. The agricultural fields of the recent Burcio lagoon and the Basson lagoon were also covered by water and the tidal creeks were not visible anymore. A new channel connected the Po della Pila with the Barbamarco lagoon, probably developed due to human intervention to allow the boats from the harbour in the south to move to the north-west one which was under construction (Fig. 29). On the coastline, the sand barriers that were protecting the internal area underwent a breakup and the back-barrier vegetation was submerged as well. The lagoon is now established, and this severe reduction and destabilization continued for the following years, as shown by the orthophoto of 1969 (Fig. 28d). In this period, the small channel of the south part of the lagoon became deeper

and vegetated; its westward evolution was probably related to boats transition and levees establishment due to vegetation. Between the 60s-70s submersion did not occur due to river floods alone; several heavy storms characterized by wind speed between 10 and 18 m/s and mean sea level higher of 1.1 and 1.2 m caused strong erosion and enormous damages to human structures. In particular, in 1966 an extreme storm demolished the dikes and 150 hectares of the territory of Porto Tolle went underwater (Perini et al., 2011). These substantial changes occurred concurrently with the highest subsidence rates ever recorded in the Delta (between 3.7 to 25 cm/year) (Fabris, 2019).

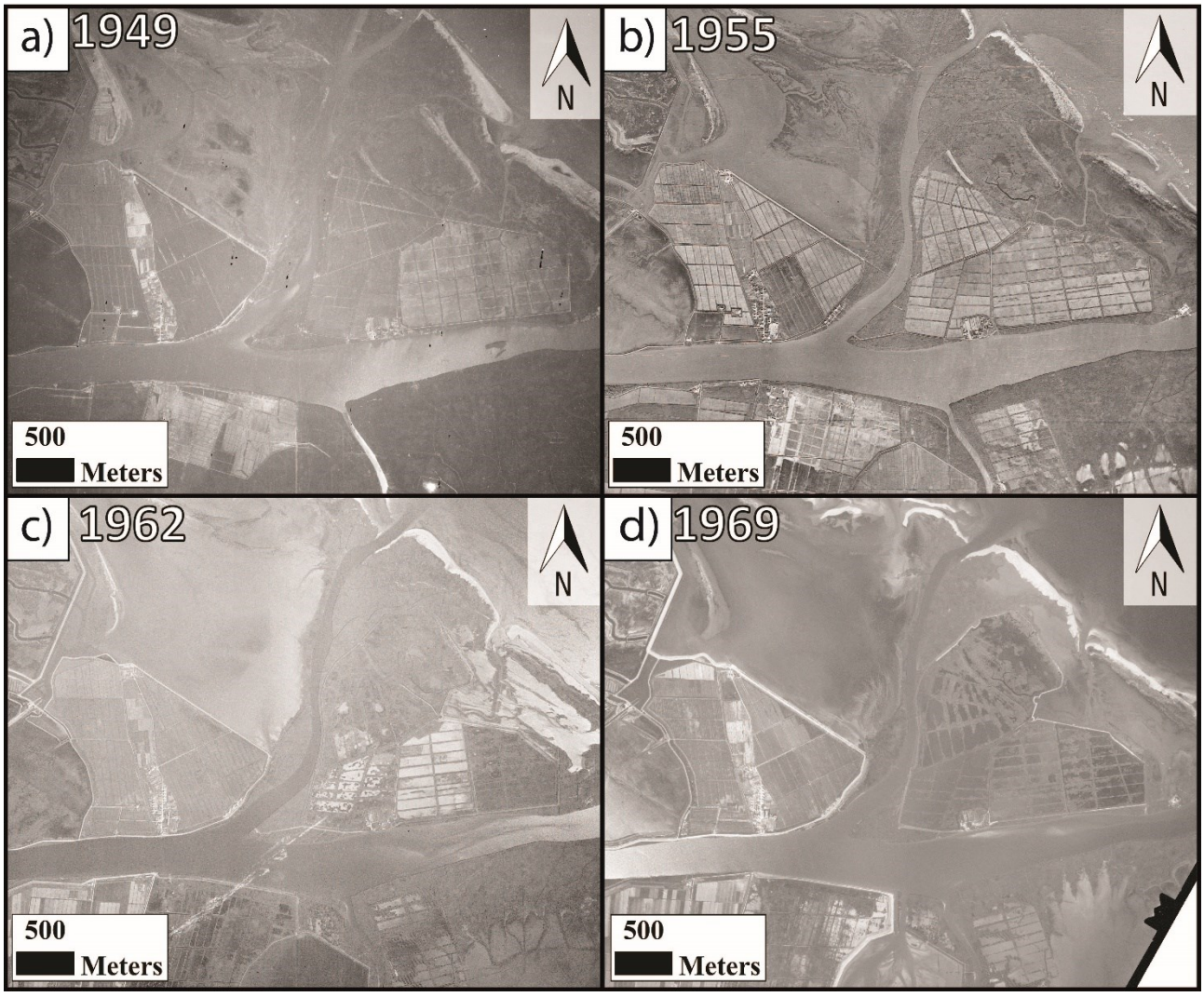


***Figure 28*** *– The strong transgression of the Po Delta between 1949 and 1969. (a) In 1949 the Barbamarco lagoon was not a full lagoon and land reclamation continued until (b) 1955. (c) in 1962 and (d) 1969 river floods and coastal storms submerged most of the rice fields, giving birth to the recent configuration of the lagoons.*

In 1977 a thermoelectric power plant was built southward to the Po della Pila branch. During this last period, a slight recovery of the marsh occurred in a few sections of the Delta. Vegetation kept on growing next to the levees of the channel that connects the Barbamarco lagoon to the Po della Pila branch for about 150 m, and the sand barriers on the west side of the Busa di Tramontana seemed to recover as well, but the differences in thickness are noticeable compared to the previous condition (1955). It is highly interesting to note that the reclaimed areas next to the power plant experienced a "restoration project" dynamic; in fact, in 1955 this area consisted of rice fields that were protected by dykes (Fig. 30a). Between 1955 and 1969 the floods submerged this area, and the new inlet allowed the freshwater to flood inside the lagoon (Fig. 30b). A salt marsh developed during the following years until nowadays (Fig. 30c, 30d).The trend of the whole Delta between 1950 and 1977 was highly negative and most of the littoral suffered strong erosion with a mean shoreline shift of more than -200 m (Bezzi et al., 2021).

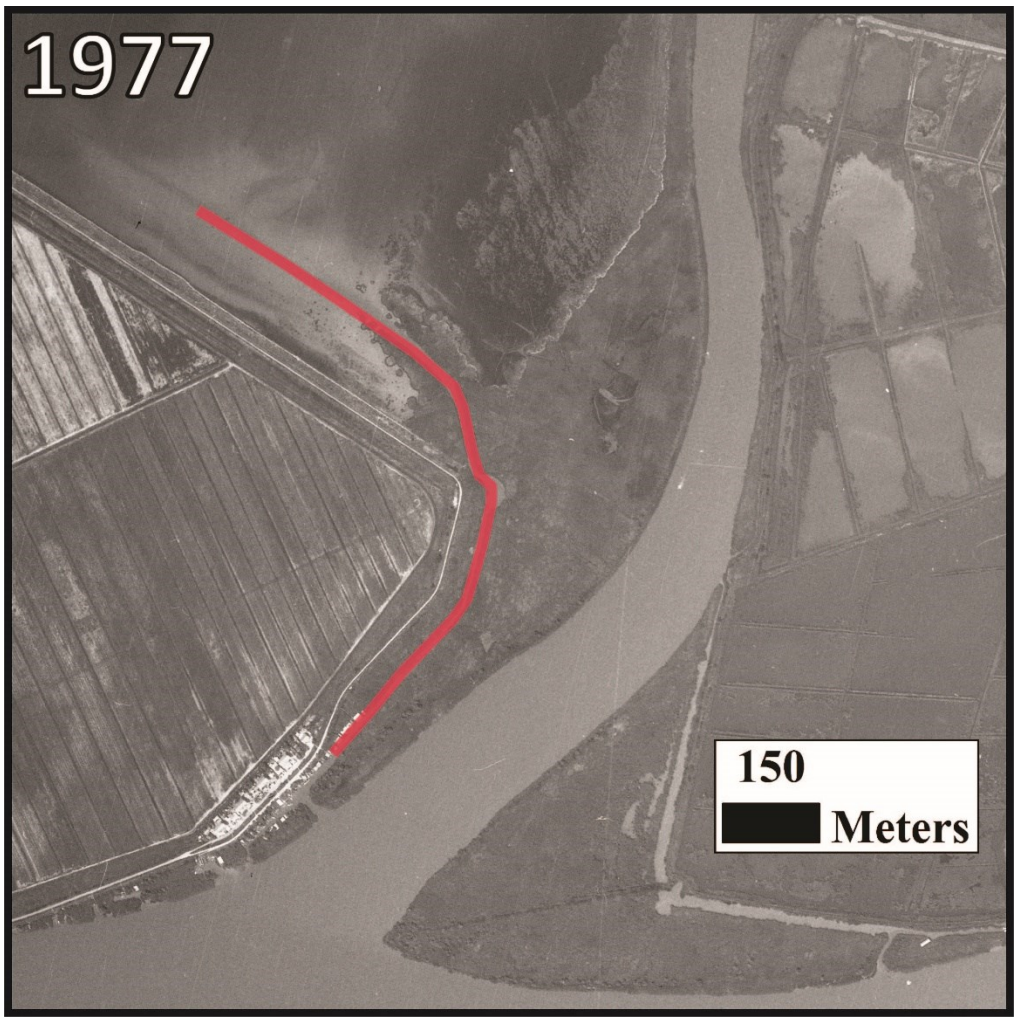


***Figure 29*** *- The channel that connects the Po della Pila with the Barbamarco lagoon was first seen in 1962, but it stabilized its shape after 1977.*

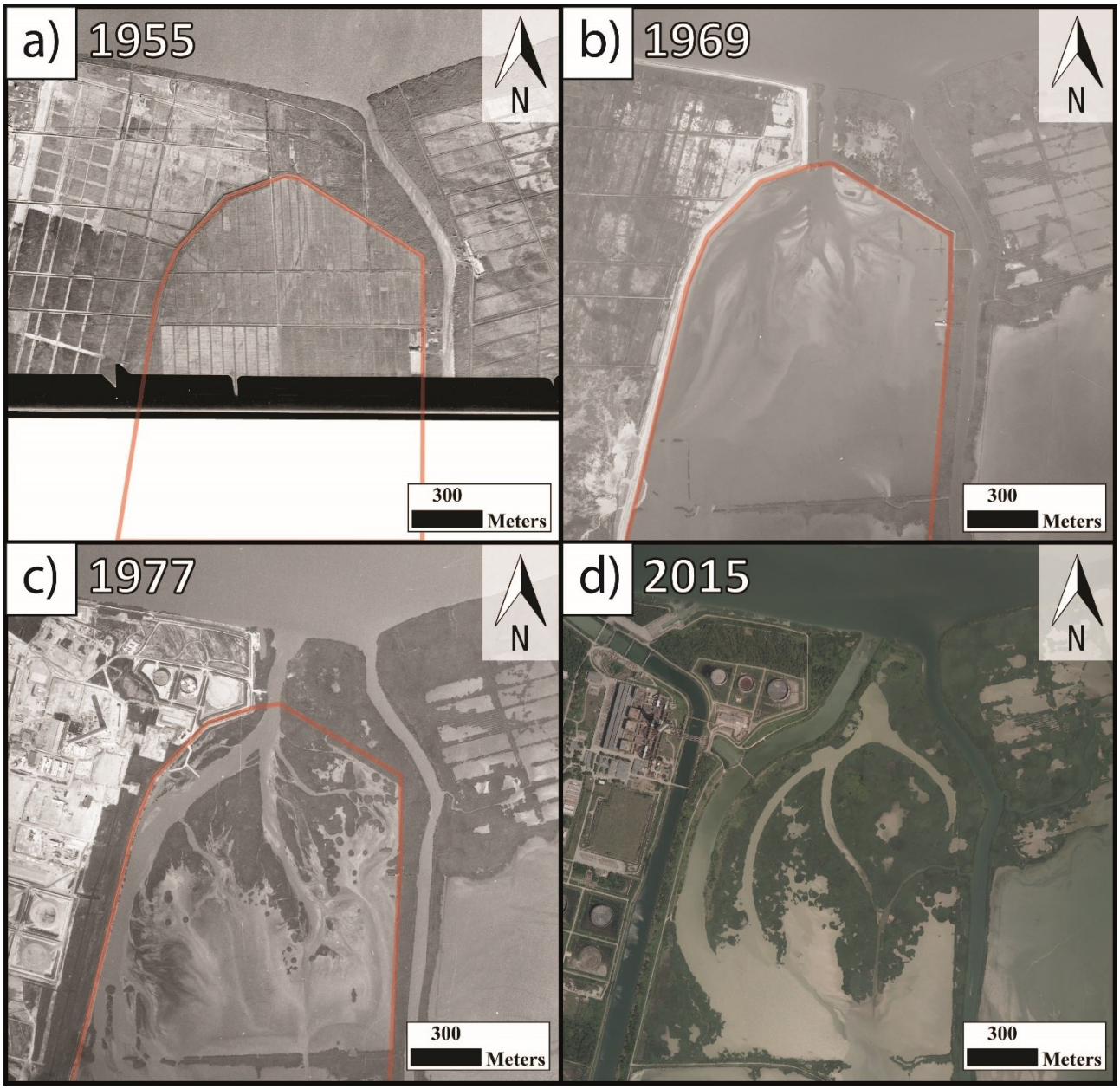


***Figure 30*** *- A portion of the Basson lagoon experienced a "restoration project" dynamic. The dyke that was protecting the rice fields was breached and the area was submerged between (a) 1955 and (b) 1969. The new inlet allowed the freshwater to flood inside the lagoon and a salt marsh developed between (c) 1977 and (d) 2015.*

### *4.4.1.3 Small recovery: third time interval (1977 – 1999)*

In 1983 the barriers of the Barbamarco lagoon seemed to recover and accrete on both sides of Busa di Tramontana and a sand lobe was separated from the west side creating a small barrier island. This year was characterized by a high flood discharge (43000 $m^3/s$). Vegetation developed and grew along the small channels of the lagoon, but the green wall that separates the lagoon itself from the eastern branch was losing thickness. After 1989 the tip of the delta reached a state

that is similar to the current one. The area between Busa di Tramontana and Po della Pila became the Burcio lagoon and the salt marsh next to the power plant and the Basson lagoon developed along the tidal creeks levees, reaching its highest extension of about 130 hectares. The sea transgression was remarkable and a new mouth that connected the lagoon to the sea was opened (Bocca Sud) (Fig. 31a, 31b); it is visible a perpendicular sand bar next to the east side of the mouth that was going to disappear during the next years until 1992. On the east side of Busa di Tramontana (seaward section) a small tidal creeks system developed while the mouth of the branch became larger. In front of this section, a large sand spit that extended up to the tip of the delta was developing.

Other anthropic interventions were carried out; works in both harbours were progressing and a new artificial mouth called Porte Vinciane was opened next to the southern part of the west side of Busa di Tramontana (Fig. 31c). However, this small mouth was closed in 1996 and a smaller dam was built 70 meters southward (Fig. 31d). River floods can now enter from this side of the small branch; during 1990 and 1996, a progressive reduction of vegetation is visible on the channel that connects Po della Pila with the Barbamarco lagoon, with regression of about 80 m that will persist during the following years. A small in-place narrowing of the barriers occurred on the west side of the Busa di Tramontana branch, while the large sand barrier at the east side was widening. In 1996, on the opposite side of the Porte Vinciane (east side of Busa di Tramontana) a new inlet of about 150 m connected the branch with the Burcio lagoon, which was isolated from 1989; this inlet could have been caused by the failure of the dikes since the vegetation wall was thinning since 1990. Overall, from 1977 to 1996, a process of stabilization occurred in the whole Delta, and erosion rates decreased significantly (Bezzi et al., 2021).

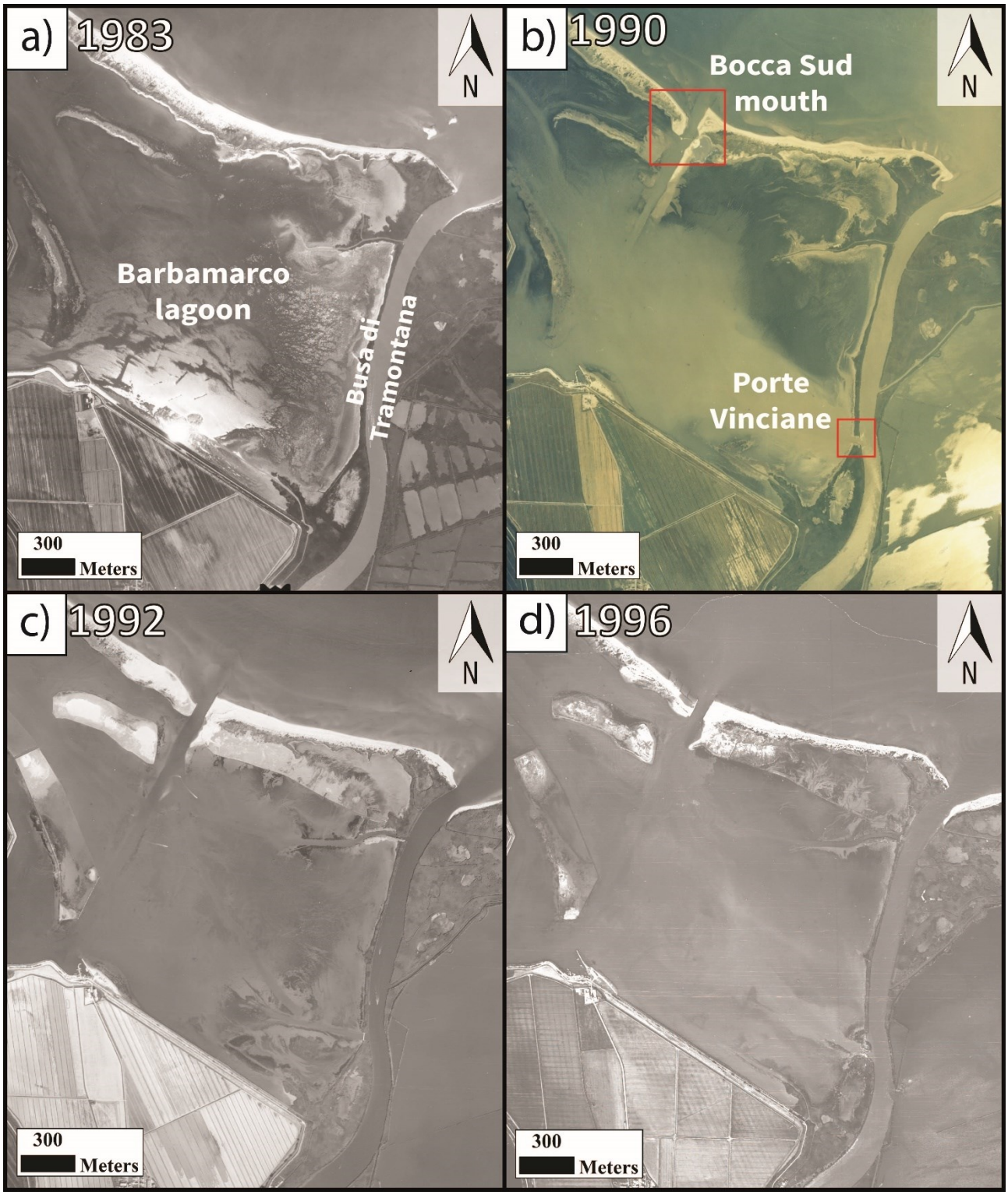


***Figure 31*** *– Between (a) 1983 and (b) 1990, the Bocca Sud mouth and the Porte Vinciane artificial mouth were opened. The vegetation of the southern channel decreased between (c) 1992 and (d) 1996.*

#### *4.4.1.4 Accretion of the Barbamarco lagoon: fourth time interval (1999 – 2018)*

In the early 2000s new inlets and channels development improved the connection between the Po della Pila branch and the lagoons. The orthophoto of 2003 shows a new channel that was dug artificially in the most southern part of the Barbamarco lagoon perpendicularly to the small channel that was dug in 1977 to connect the harbour of Porto Tolle and the other one of the Barbamarco lagoon (that has reached its maximum extension in 2003), probably to enable boats to reach the Bocca Sud mouth. This event is important because this channel allowed the sediment transported by the floods to reach the southern internal part of the lagoon which was inaccessible before. In the same years, the inlet of the Burcio lagoon underwent an important enlargement, reaching its maximum extension of about 450 m.

This last period was characterized by high sedimentation and a general progression occurred among the delta (Ninfo et al., 2018; Bezzi et al., 2021). After 2010, strong sedimentation is visible in the southernmost part of the Barbamarco lagoon and, in particular, on the west side of the Burcio lagoon; in this last section, a wide area of more than 10 hectares emerged. Vegetation stabilized several morphological forms between 2012 – 2013, such as the levees of the channel dug in 2003 of the Barbamarco lagoon (which was also larger) (Fig. 32a, 32b, 32c, 32d), the back-barrier area of the sand barriers, and the new tidal flat of the Burcio lagoon. A new tidal flat was forming in the southernmost part of the Barbamarco lagoon thanks to high deposition delivered by the river (Brunetta et al., 2021); it is important to note that several patches of Spartina are visible for the first time in the young tidal flat and in the back-barrier areas, although they disappeared in 2015 (See 4.4.2 and 4.5.1 for more details).

In the orthophotos of 2015 and 2018 (Fig. 33a, 33b), the sediment deposition in the southern part of the Barbamarco lagoon is evident; the tidal flat progressed developing several crevasse splays (Brunetta et al., 2021) and enlarging next to the channel that connected the harbours of the Barbamarco lagoon; it is visible a recovery structure that was built to protect the west side of the Busa di Tramontana and improved vegetation establishment on the levees; the Burcio western salt marsh was widening as well. However, compared to 1989, the Basson lagoon has lost several hectares of salt marsh. In particular, the salt marsh that has developed next to the thermoelectric powerplant reduced its extension of about 30 hectares.

After 1990 the storm frequency increased remarkably (Perini et al., 2011), but none of them changed drastically the landscape as in the previous periods. Overall the last period, from 1996

until nowadays, was characterized by a positive trend where the shoreline moved seaward, despite the Delta didn't reach the position of the 1950s (Bezzi et al., 2021).

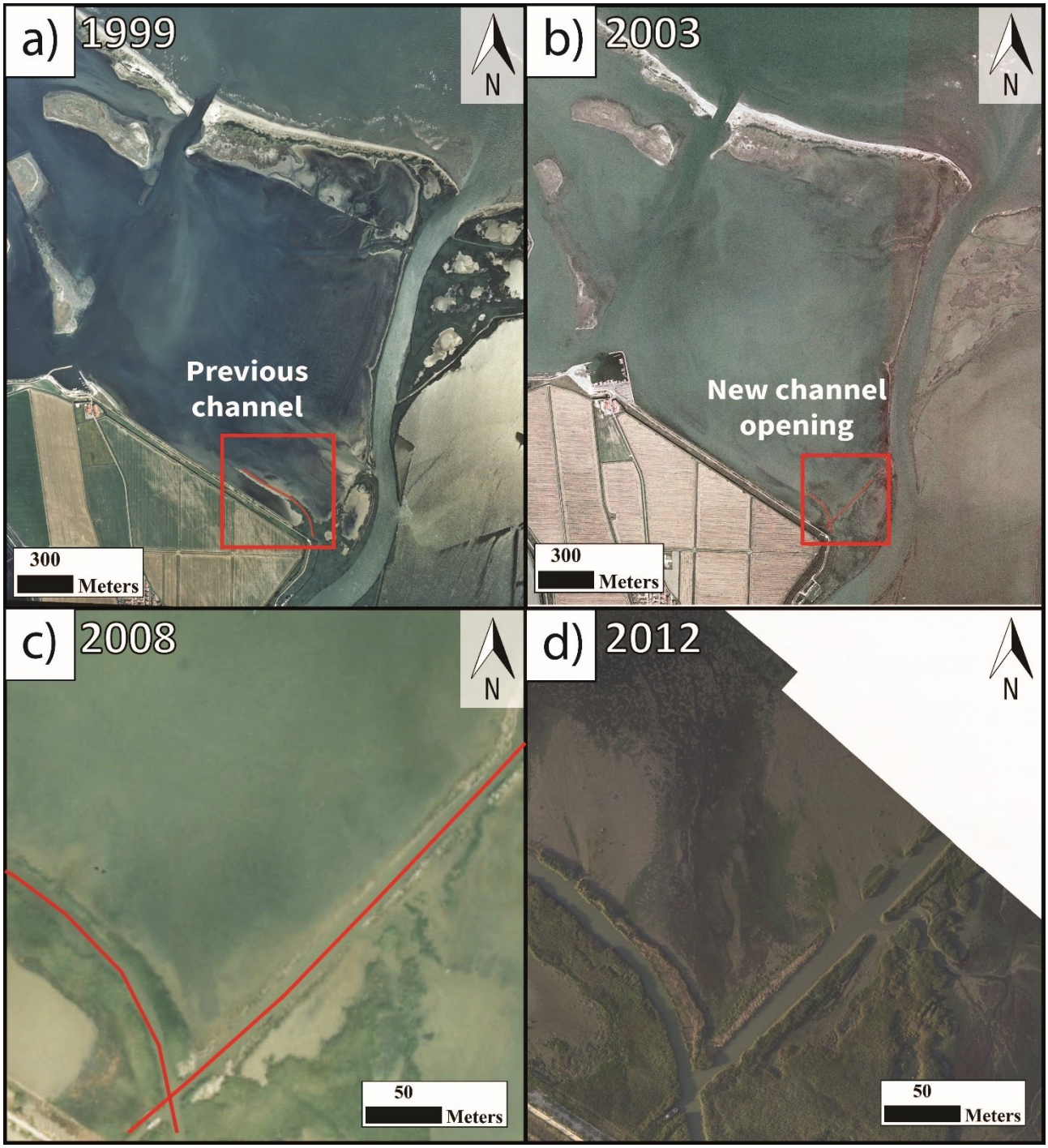


***Figure 32*** *– Between (a) 1999 and (b) 2003 a new channel was dug (NE direction) in the southern section of the Barbamarco lagoon. Strong sediment injection occurred after (c) 2008 and the levees were established by wild reeds, which is visible in the orthophoto of (d) 2012.*

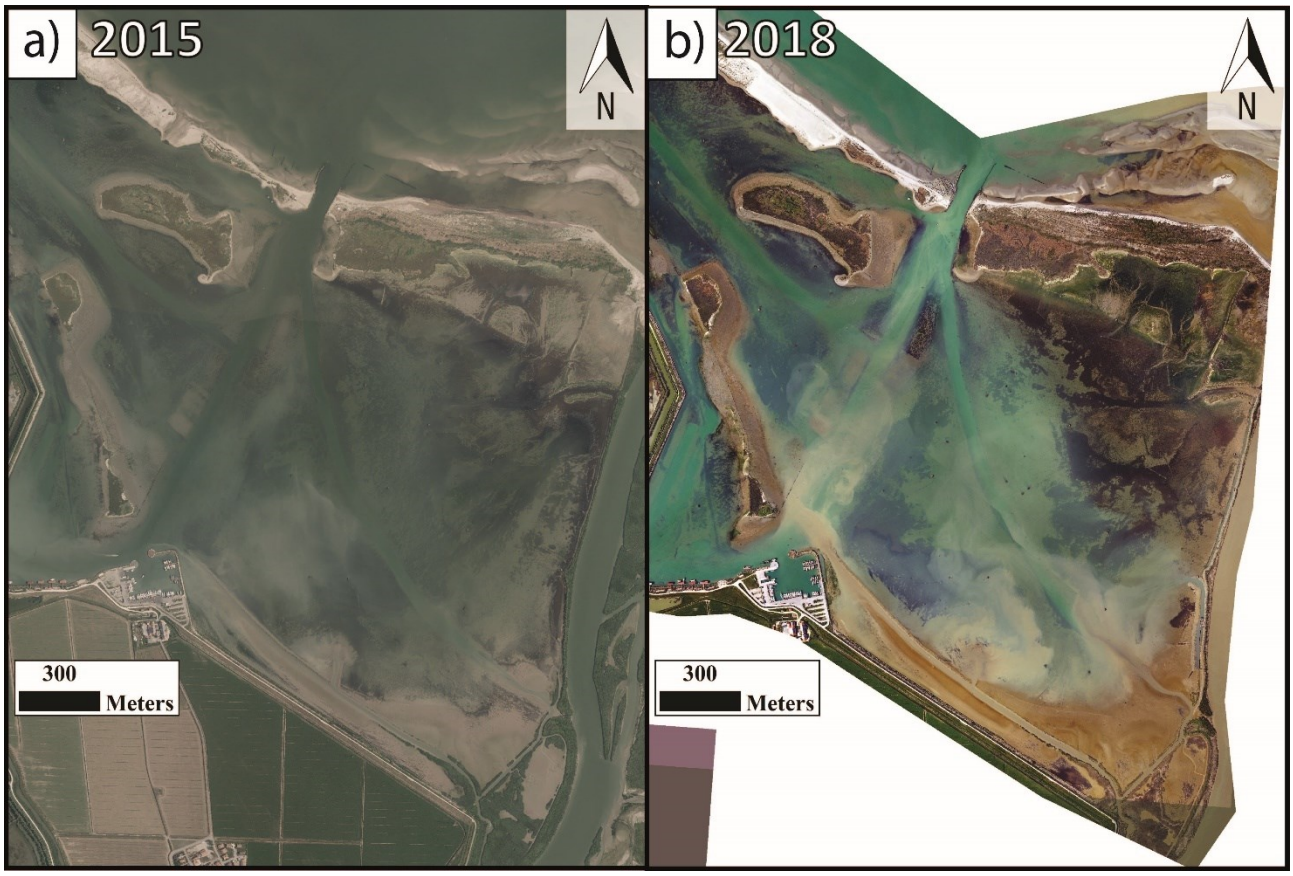


***Figure 33*** *- The new tidal flat located in the southern part of the Barbamarco lagoon is visible in both orthophotos of (a) 2015 and (b) 2018.*

### *4.4.2 MHT variations and Spartina distribution*

Based on the tidal records of Porto Garibaldi, from 2009 to 2019 the local mean sea level underwent a wide range of variations, from -0.17 to 0.16 m (Fig. 34). In particular, from 2011 to 2013 the m.s.l. was between -0.7 and -0.17 m, which is the period with its lowest level; then the values increased until 2019, reaching 0.14 m above m.s.l.. These variations affected the MHT as well, changing from 0.24 m in 2009 to 0.4 m in 2019. The tidal range has never changed between the years, and it maintained a stable value of 0.48 m. It is important to state that during 2012 the tide gauge did not work between May and December, which means that the sea level values of 2012 could be unreliable.

The young tidal flat that is developing in the southernmost part of the Barbamarco lagoon is characterized by two species, which are: i) the halophyte pioneer plant *Spartina maritima*; ii) and the common freshwater plant of the Po Delta *Phragmites australis*.

*Spartina maritima* grows as small patches around the tidal flat, but the location of the patches is not stable; they grow during spring-summer and die during autumn-winter, without keeping the same colonized place. The GPS survey showed that its location is between 0.03 and 0.25m above m.s.l., with an average distribution of 0.12 m above m.s.l.. This distribution is confirmed by other studies carried out in the Venice lagoon (Silvestri et al., 2005; Scarton et al., 2004). Old orthophotos (1950 – 2000) does not allow to clearly distinguish vegetation distribution and typology, but the recent ones (2012 – 2018) show that patches of Spartina had a high distribution during 2012 in the most elevated areas of the tidal flat, which are next to the levees; however, they disappeared in 2015 and although their presence is found during the next years, their location changed recurrently. *Phragmites australis* grows on the levees that separate the tidal flat of the Barbamarco lagoon from the channels, and it is highly common all over the Delta, despite its distribution has reduced during the last century. Their distribution in the Southern part of the Barbamarco lagoon did not change from the early 2000s till nowadays and it did not colonize the tidal flat. However, it colonized most of the areas next to the new inlets that opened during the years, such as in the Burcio lagoon (i.e. 2011 – 2013) and in the Basson lagoon (i.e 1969 – 1977).

The Lidar of 2018 shows that no section of the Barbamarco lagoon reached the MHT level, except for the sand barriers. The Burcio lagoon presents wider vegetated areas above 0.3 m in the back-barriers, but probably it derives from a mixture of back-dune and salt marsh vegetation. The Basson lagoon presents a similar condition as the Burcio lagoon, but the elevation interval for a salt marsh development is highly restrained and the vegetation that established the barrier is probably composed of back-dune plants.

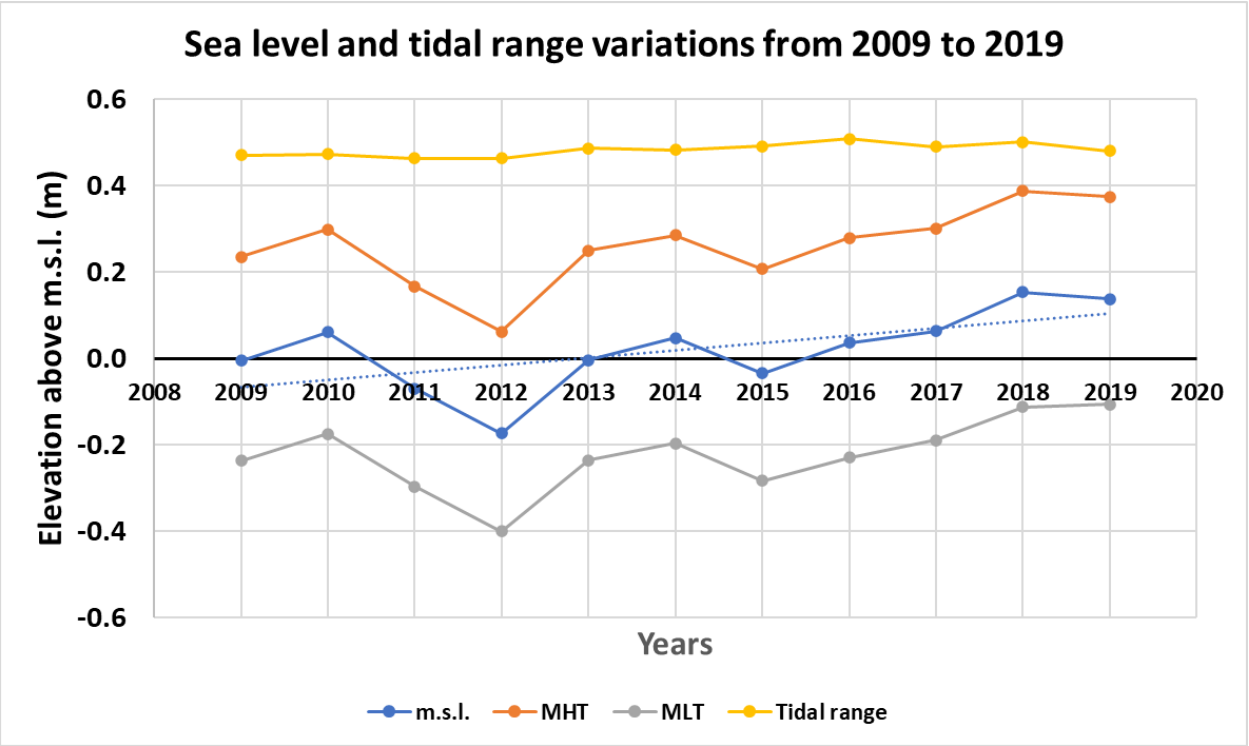


***Figure 34*** *– Sea level and tidal range variations between 2009 and 2019 obtained from the tide gauge of Porto Garibaldi. (MHT = Mean High Tide, MLT = Mean Low Tide). The tide gauge did not work between May and December 2012, hence the sea level values of 2012 could be unreliable.*

## *4.5 Discussion*

### *4.5.1 The tidal flat of the Barbamarco lagoon*

The delta underwent high modifications during the last century due to direct and indirect human intervention. The photos showed how land reclamation persisted before 1960 and how the lack of sediment supply and other factors due to human interaction (i.e. dam, material exploitation, subsidence, etc (Billi and Fazzini, 2017)) caused a forced transgression of the system that has not recovered yet. The tidal system of the Barbamarco lagoon disappeared completely and no tidal flats have been seen before 2010. The only restoration project that was carried out inside the Barbamarco lagoon consisted of two sandy islands artificially built in the 1990s. However, Brunetta et al., (2021) showed that the increase in river sediment supply and the opening of new connections between the lagoon and the branches (i.e. next to the Busa di Tramontana) caused the birth of a new tidal flat, that is following a positive trend with an average rate of accretion of about 1.2 cm/year (between 2018 – 2020). The river floods control sediment deposition and several crevasse splays cover the tidal flat. These studies pointed out that accretion is higher at

the northern-western border of the mudflat, suggesting that the tidal flat is widening, besides building-up; this behaviour is visible in the recent orthophotos as well (i.e. 2015 – 2018). Furthermore, several dredging has been made at the southern mouth of the Barbamarco lagoon (i.e. Bocca Sud) during the last decades, due to high sediment deposition that prevents ships to travel across the mouth. If the river sediment injection is constant in time, the tidal flat could slowly cover the lagoon, possibly leading to the previous situation before 1950.

However, a salt marsh has still not developed after 20 years in this section of the lagoon and only two species are present (i.e. *Spartina maritima* and *Phragmites australis*). It is important to underline that Italian salt marshes are mostly located in the Venice lagoon (i.e. usually called as "Barene") and *Phragmites australis* is commonly not considered as part of the Italian marsh. However, in several studies *Phragmites* is included as a freshwater marsh species (e.g. Silliman and Bertness, 2004; Smith, 2013), and most importantly it is a common and autochthonous species of the Po Delta (Verza and Catozzo, 2015); hence, this species is considered as part of the low marsh in this study as well. There are several possible reasons that explain why the salt marsh did not developed in the southern part of the Barbamarco lagoon:

i) the MHT is high compared to the elevation of the tidal flat surface; in fact, salt marshes use to develop when tidal flats reach these values (De Vlas et al., (2013); Bakker, 2014), at least from a sedimentological point of view. The MHT of 2019 is about 0.38 m above m.s.l. and the highest values of the surface range between 0.2 and 0.3 m. From a mere morphological point of view, considering an average rate of accretion constant in time (i.e. 1.2 cm/years) and the highest elevation of the surface (i.e. 0.2-0.3 m above m.s.l.) the tidal flat needs around 15 years to reach a feasible elevation for salt marsh development. Based on the sea level records of Porto Garibaldi, future MHT fluctuation could influence vegetation establishment and prolong the time for a salt marsh establishment. However, long time series of tidal records (1875-2017 from Trieste tide gauge) show that the Relative Sea Level Rise (RSLR) is about 1.3 mm/year, while the short time series (1992-2017) have higher rates of 3.8 mm/years (Da Lio and Tosi, 2019); these results suggest that the rates of accretion of the tidal flat should be able to cope with sea level rise. Besides the MHT, it is important to note that these vertical ranges are included in the common *Spartina maritima* vertical distribution (Scarton et al., 2004). In fact, this pioneer species is able to grow in small patches, but its location changes every year, meaning that the plant is not able to establish. Strong colonization of *Spartina* occurred between 2011 and 2013 only (visible in the orthophoto of 2012); this event could be related to lower levels of MHT and m.s.l. that

characterized these years (0.17, 0.06, 0.25 m). This limitation in colonization is not visible on this species only; *Phragmites australis* is stable on the levees of the channels, but it was not able to increase its extension during the last 20 years. Furthermore, it did not colonize the tidal flat. These observations suggest that, in the case of the tidal flat of Barbamarco lagoon, vertical elevation is important, but there is a secondary factor that is limiting the evolution of the low marsh species.

ii) The salinity fluctuation is high for both species to spread. Although no salinity measurements were carried on during this study, it is well known that the wild reed needs freshwater to develop and grows only around the tip of the delta, mostly next to the levees (Verza and Catozzo, 2015). *Spartina*, instead, is able to survive at high ranges of salinity (Adams and Bate, 1995), however a long submersion period (i.e. >6 hours) can decrease photosynthetic activity (Duarte et al., 2014). It is important to note that the elevation of the levees colonized by the wild reed is higher than the elevation of the tidal flat and this factor could affect the plant establishment as well. This factor is discussed in detail in paragraph 4.5.2.

Other important factors are: iii) Excavations and boat crossings. The channel that connects the Po della Pila with the Barbamarco lagoon is commonly used by fishermen to move between the two harbours. The waves generated by the boats are a possible cause of erosion in the southern-western part of the tidal flat (Brunetta et al., 2021) and vegetation reduction on the levees; furthermore, this channel is regularly dredged in order to avoid the boats to get stuck. iv) other biochemical factors, such as nutrients, or the drainage (Cao et al., 2021).

### *4.5.2 From tidal flat to salt marsh*

After 2010, the whole delta was subjected to a strong sediment injection. New tidal flats were born around the whole tip of the Delta (i.e. the Burcio). The analyses on the tidal flat of the Barbamarco lagoon gave an example on how these tidal flats evolved; however, different behaviours were found. In 2011, the large inlet of the Burcio lagoon that developed during the 2000s (Fig. 35a) allowed the deposition of a large tidal flat on the East side of the Busa di Tramontana (Fig. 35b, 35c). In 2013, this section was covered by *Phragmites* and its expansion continued till nowadays (Fig. 35d, 35e, 35f, 35g). As a consequence, a river-tidal system is developing inside the internal part of the lagoon. Similar behaviour is found in the Basson lagoon, where a full river-tidal system covered by wild reeds developed between 1955 and nowadays. The orthophotos show how the different phases of its evolution are highly similar to the steps followed by recent restoration projects (i.e. land, dikes breaching, submersion of the land,

vegetation establishment). Most importantly, both cases from the Burcio and the Basson lagoon enhance how vegetation can quickly recover the natural landscape (i.e. around 10 years for Basson, and around 3 years for Burcio). This behaviour is at odds with the tidal flat of the Barbamarco lagoon. Wild reeds represent one of the most common marsh plants that can be found among the delta; as discussed in 5.1, the growth of this plant is strictly connected to the channel location, since they need both freshwater flux and a sufficient elevation in respect to the mean sea level. The colonized areas of the Burcio and Basson lagoon are located next to the Po della Pila branch, which means that they have direct access to freshwater, and they are protected by the lagoon itself from the sea water. Maicu et al. (2018) showed that the Burcio and the Basson lagoon are characterized by freshwater (with stable psu values lower than 10±2). *Phragmites* is commonly found with salinity values between 0 and 13 psu (Packett and Chambers, 2006), suggesting that the concentration is favourable for the species. In fact, the colonized areas are located next to the principal river branch. A different condition is found in the Barbamarco lagoon. Freshwater floods only through the small channel that connects the Busa di Tramontana with the lagoon, while seawater moves inside the lagoon from the Bocca Sud inlet. This low hydrodynamic mixing cause sharp gradients where freshwater is confined in the southern part of the Barbamarco lagoon (i.e. where the tidal flat is located) with variable psu values between 10-15±10, and higher salinity is found in the northern section, with variable psu values from 17 to 25±10. Since *Phragmites* have specific salinity requirements and the *Spartina* submersion is high at these elevations (Duarte et al., 2014), vegetation distribution could be limited; it is possible that the condition of the Barbamarco lagoon is allowing both plants to grow but not to colonize and extend their domain. Instead, the Burcio and the Basson lagoon present a better condition for the wild reeds to establish. Overall, the historical review showed that marsh zones that have not a direct connection with the river and, as a consequence, low deposition tend to regress, instead new channels that connected the lagoons to the Po dell Pila branch developed vegetation. It is important to state that salinity measurements were not carried out during this thesis and these observations must be taken with caution. Furthermore, no sedimentological and morphological analyses were carried out on the lagoons of Burcio and Basson).

It is important to consider the shape of the lagoons and the sediment distribution as well. The Barbamarco lagoon is highly larger and deeper than the Burcio lagoon and the restored section of the Basson lagoon. Due to this morphology and since the only connection to the river is a small channel, it is plausible that the tidal flat of the Barbamarco lagoon is slowly extending north-

westward without vegetation establishment. Furthermore, this lagoon is highly influenced by boats crossing and the presence of the harbours. On the other side, the Burcio lagoon is basically an empty shallow basin that has a direct connection to the river, and it is not exploited by man. This condition is highly convenient for a future salt marsh restoration of the Po Delta. The opening of new inlets that connect the river to the lagoons could increase deposition, give birth to new tidal flats, help salt marsh formation and restore the landscape. However, more aspects need to be investigated in order to verify the conditions for salt marsh formation. In fact, new inlets can change water circulation, which means salinity variations and sediment transport as well. Furthermore, they will change the sediment budget distribution between the lagoons and outside the Delta system, which could mean higher sediment deposition inside the lagoon and lower transport outside.

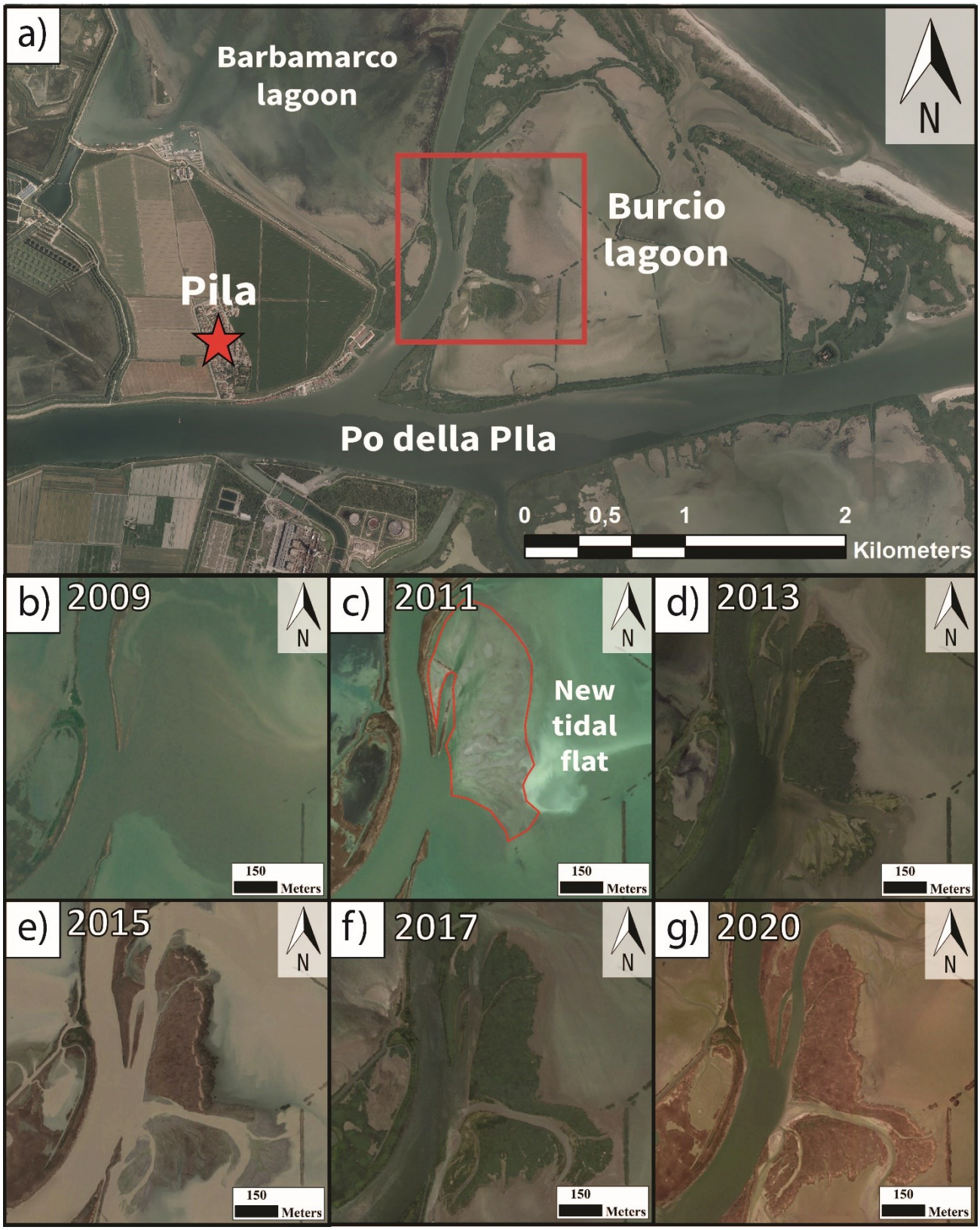


***Figure 35*** *– (a) The Burcio lagoon underwent a "restoration project" dynamic similar to the Basson lagoon. After (b) 2009, the wide inlet that formed in the previous years allowed high sedimentation in the Burcio lagoon and (c) a tidal flat formed in 2011. (d) In 2013, wild reeds covered the area and established a new system between (e) 2015, (f) 2017, and (g) 2020.*

## *4.6 Conclusions*

This paper focuses on the evolution of the lagoons of the Po River Delta (Italy) from the 1950s until nowadays, and a historical review was accomplished through orthophotos provided by the IGM (Istituto Geografico Militare Italiano) and the Veneto Region. The review showed how, between 1949 and 1955, the Barbamarco lagoon was not regularly submerged and it presented a well developed tidal system characterized by tidal channels, tidal flats, and salt marshes; on the other side, land reclamation occurred in the lagoon of Burcio and Basson, where several hectares were used as rice fields. Several flood events submerged most of the agricultural fields and other areas of the Delta between 1955 and 1969, causing a strong marine transgression and the disappearance of the tidal system. A relatively stable condition occurred between 1977 and 1999; several connections between the river branch and the lagoons were opened due to human intervention and erosive processes. A new tidal system evolved in the lagoon of Basson and a salt marsh composed of *Phragmites australis* covered the submerged old rice fields. During the last decades (1999-2018) a slow progradation began, and new tidal flats developed. The channel between the Po della Pila and the Barbamarco lagoon gave birth to a tidal flat that is building up and extending north-westward; however, vegetation (*Spartina maritima*) is not permanently colonizing the surface. The Burcio lagoon was subjected to strong sedimentation as well, and a 10 hectares marsh of *Phragmites* has developed between 2011 and 2013. The lagoon of Burcio and Basson presented a similar evolution to worldwide restoration projects, showing how targeted heavy sediment injections are fundamental for vegetation recovery for the Po Delta. This approach could be exploited to restore abandoned portions of lagoons that have no purpose to man, such as the Burcio lagoon.

Future studies should investigate the recently vegetated tidal flats (e.g. Burcio lagoon) under a morphological and biological point of view to verify if a restoration project is feasible, recover the unused section of the Po Delta and increase low marsh cover. It is important to not forget that analysis should consider how the opening of new breaches, or the closure of channels, could influence sediment transport in and outside the Delta.

# 5. Morphological Evolution of an Intertidal Area Following a Set-Back Scheme: A Case Study From the Perkpolder Basin (Netherlands)

## 5.1 Introduction

Tidal flats are intertidal, non-vegetated, soft sediment habitats generally composed of mud and sand (Dyer et al., 2000b), often backed by salt marshes that grow at higher elevations within the intertidal fringe. Coastal salt marshes are usually found along low-energy and temperate coastlines (Allen, 1992; Adam, 2011) except for the extensive mangroves forests that are located at tropical latitudes (Odum et al., 1982). Salt marsh plants, mostly herbaceous halophytes, are adapted to tolerate regular saltwater inundation, especially the species that colonize the low-elevated parts (Pratolongo et al., 2019). Despite the fact that salt marshes were historically considered as a source of insalubrious conditions (humidity, mosquitoes) and as land unsuitable for agriculture (Boavida, 1999), they can offer numerous ecosystem services. Several studies have discussed the benefits derived from these environments to nature and mankind: i) they support fisheries as they host economically and ecologically important fish species (Boesch and Turner, 1984; MacKenzie and Dionne, 2008; Barbier et al., 2011); ii) they play a role in the carbon cycle as they are able to shift carbon sequestering from the short-term (10–100 years) to the long-term (1000 years) (Mayor and Hicks, 2009); iii) they can host leisure activities and have an important role in local cultural aspects (Weis, 2016). The decline of these environments during the last 50 years has caused an important loss of ecosystem services (Millennium Ecosystem Assessment, 2005). Nevertheless, recent assessments on the future of salt marshes are quite controversial. In fact, global-scale predictions suggest that the capacity of marshes to recover against sea-level rise is overestimated (Nardin and Edmonds, 2014; Crosby et al., 2016; Spencer et al., 2016), but local-scale assessments concluded the opposite prediction (Kirwan et al., 2016). The reason behind this discrepancy is that large-scale assessments do not consider the biophysical feedback mechanisms that are included instead in local-scale models (Kirwan et al., 2016). Several local-scale studies demonstrated that coastal wetlands loss can be avoidable using nature-based adaptation in coastal management solutions (Schuerch et al., 2018).

One of the most important roles of salt marshes is coastal protection as they are able to attenuate wave energy and consequently reduce the flood hazard (Bouma et al., 2014). Many studies demonstrated the effect of vegetation and wetlands on wave impact reduction (Möller et al.,

2014; Smolders et al., 2015; Vuik et al., 2016) and storm surge (Stark et al., 2015; Leonardi et al., 2018). Nature-based solutions are to be preferred to conventional coastal defences because they are effective and have a reduced cost if compared to traditional approaches (Koch et al., 2009; Borsje et al., 2011; Temmerman et al., 2013). In order to support the efficient design of nature-based solutions, a deep understanding of feed-back effects between biotic (e.g. vegetation) and non-biotic factors is needed. Previous studies focussed on established, evolving or deteriorated salt marshes; few works analysed the processes acting on newly developed salt marshes. Several works defined how hydrological and sedimentological processes influence the topographic evolution of the marsh in response to sea level rise, with surface growth following an asymptotic law (Pethick, 1981) and how the hydroperiod changes spatially and temporally sediment accretion and accumulation (Cahoon and Reed, 1995). Furthermore, several studies discussed the adaptation capacity of salt marshes to keep pace with sea level rise (Stevenson et al., 1986; van Wijnen and Bakker, 2001; Schuerch et al., 2013; Crosby et al., 2016; Kirwan et al., 2016; Spencer et al., 2016; Schuerch et al., 2018). Mathematical models have been implemented to describe sediment transport inside salt marshes and tidal creeks (Kirwan et al., 2010; Green and Hancock, 2012; Reimer et al., 2015) and biological parameters have been introduced to explain how the eco-geomorphological state of marshes influences their contribution to sediment budgets (Stark et al., 2017). In this type of environment, sediment deposition is influenced by a number of factors, such as seasonal conditions (Reef et al., 2018), sediment availability and grain-size distribution (Schuerch et al., 2014), and storm frequency and intensity (Schuerch et al., 2012).

Despite our current knowledge of hydrological and sedimentological processes on well-developed salt marshes, there have been few observations and experiments concentrating on the mechanism of salt marsh creation (Gunnell et al., 2013). A better understanding of how a salt marsh develops is necessary to estimate the future distribution of vegetation as well as the time required to observe the transition from tidal flat to marsh environments, natural or artificial. The capacity of predicting salt marsh development is also important to understand if a ‘‘set-back’’ approach is feasible, i.e. the environment is free to develop without any human intervention, such as building new coastal structures to control the process. The existence of salt marshes is critically dependent on how fast sediment accumulates with respect to sea level rise (Redfield, 1972; Orson et al., 1985; Schuerch et al., 2012). Using 40 years of study of salt marshes in the Wadden sea (Netherland), Bakker (2014) put in evidence that a natural salt marsh forms when a mud or sand

flat rises through vertical accretion until it lies just below the Mean High water Tide level (MHT), so that it is submerged twice a day for several hours and it is dry the rest of the time.

In the current study, this concept will be applied to verify the possibility to predict the future evolution of a young, artificially-created, tidal flat at Perkpolder (Zeeland, NL) (Fig. 36a, 36b, 36c, 36d). The overall aims of the study are: (i) to understand the patterns of morphological variation of the tidal flat; (ii) to describe patterns of sediment accretion across the most elevated parts of the flat; (iii) to predict where and when an optimal elevation will be reached for the establishment of permanent vegetation; (iv) to define the morphological evolution of an artificial inlet that was dredged to establish communication with the estuary.

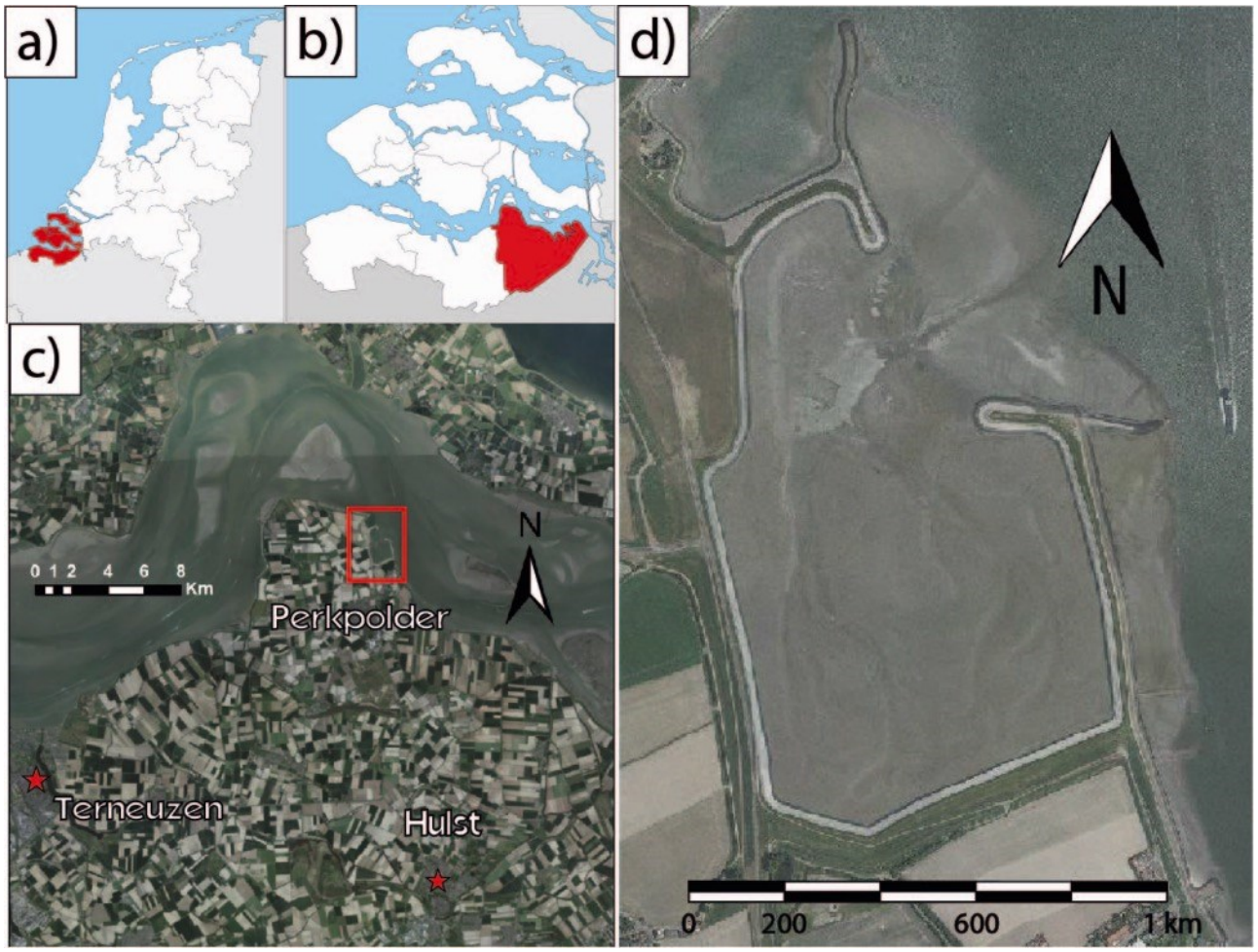


***Figure 36.*** *(a) Map of the province of Zeeland and (b) the municipality of Hulst. (c) Location of the Perkpolder tidal basin within the Scheldt Estuary and (d) 1:15000 orthophoto from the Province of Zeeland of the area, captured in June 2017.*

## *5.2 Study site*

The study area is located in Perkpolder, a previously reclaimed area in the municipality of Hulst, in the province of Zeeland (The Netherlands). This site is part of the Scheldt Estuary, characterized by a length of 355 km from source to mouth, with a total catchment area of 21863 km². About 10 million people live in the river basin (Meire et al., 2005). According to the geometry of the estuarine channel and its hydraulics, the Scheldt is divided into three different zones: a narrow part dominated by freshwater from Gentbrugge to Rupelmonde, an intermediate zone from Rupelmonde to Hansweert, and a wide and well-mixed part from Hansweert to the mouth (Nihoul et al., 1978). The mud of the Scheldt Estuary has both marine and terrestrial origins; the ratio between these two muds of different sources is highly variable, partially due to the variation in the location of the turbidity maximum (ETM), and partially due to changes in sediment load of the tributaries of the Scheldt (Swart, 1987; Wertel et al. 1993; Brinke, 1994; Chen et al., 2005). The sediment transport rates depend on the seasons and on the tidal cycles. The suspended concentration is usually higher during the flood and during Spring tides than during ebb and Neap tides. In winter, the suspended concentration and the tidal amplitude are better correlated than during the summer and the maximum concentration occurs one tide after the highest tide. These seasonal variations are connected to several processes like changes in freshwater discharge, temperature, land erosion, and, in a less significant way, wave-induced resuspension (Fettweis et al., 1998). The study area falls in the mid-part of the estuary, the most important for sediment transport. The strong tidal currents, combined with the occurrence of flocculation, due to the mixing of tidal and riverine water masses, as well as residual currents, increase the residence time of the suspended material, reaching values from hundreds of milligrams per liter to a few grams per liter (Chen et al., 2005). The mean tidal range of the estuary varies from about 3.8 meters at Vlissingen (at the mouth) to about 5.2 meters at Antwerp (78 km upstream); thus, most of the Western Scheldt is meso-tidal. Current velocities are up to 1-2 m $s^{-1}$ in the main channels, for an average tidal range. The mean Spring tidal range of the study area is about 5 meters (Claessens and Belmans, 1984).

The study area is a 75-hectares tidal flat (Fig. 37a), created as a cooperation project between Rijkswaterstaat (Dutch Ministry of Infrastructure and the Environment) and the regional government. This project, started after the closure in 2003 of the ferry service between Kruiningen (Zuid-Beveland) and Perkpolder (Zeeuws-Vlaanderen), was named Plan Perkpolder and it aims at prompting the socio-economic development of the area, by combining the construction of

recreational facilities and natural environments. One of the most important objectives of this plan was to recreate a tidally-dominated natural ecosystem (Boersema, 2016). This polder was originally dammed in 1210 and the land was reclaimed for crop growth and for building small villages. Subsequently, the land behind the dike subsided, dropping to an elevation below mean sea level. Due to the proximity of the Schaar van Ossenisse, a deep channel in the Western Scheldt, the coast was susceptible to dike failure. In 1841 a new dyke of about 1 km was built along the coast, but half of it was quickly lost.

The Perkpolder tidal flat is divided into three zones: the foreshore outside the basin, the pond, and the inner part, where several creeks were dug during the restoration project. There are two main creeks of about 40 meters in width; they divide southwards into narrower branches of about 30 meters in width, reaching a total length of about 800 m. On 25 June 2015, the dyke was breached (Fig. 37b) and the salt water of the Western Scheldt started to flow in the basin covering the whole tidal flat. The inlet has a width of about 300 m and its bottom is located at a height of about 0 – 1 m NAP. The inlet is submerged during high tide only, except for the central part, which is deeper, being at – 0.8 m NAP. This deeper permanent channel has a width of about 10 m and allows continuous water exchange between the pond and the open estuary.

Field observations, the basin structure, and the presence of a dyke ring support the idea that the flood and ebb currents were the principal agents causing morphological changes as wave action is negligible given the small internal fetch and the unlikely penetration across the shallow inlet (Fig. 37c, 37d). Field observations after the opening also suggest that benthic macro fauna rapidly started to colonize the area, providing food for bird communities.

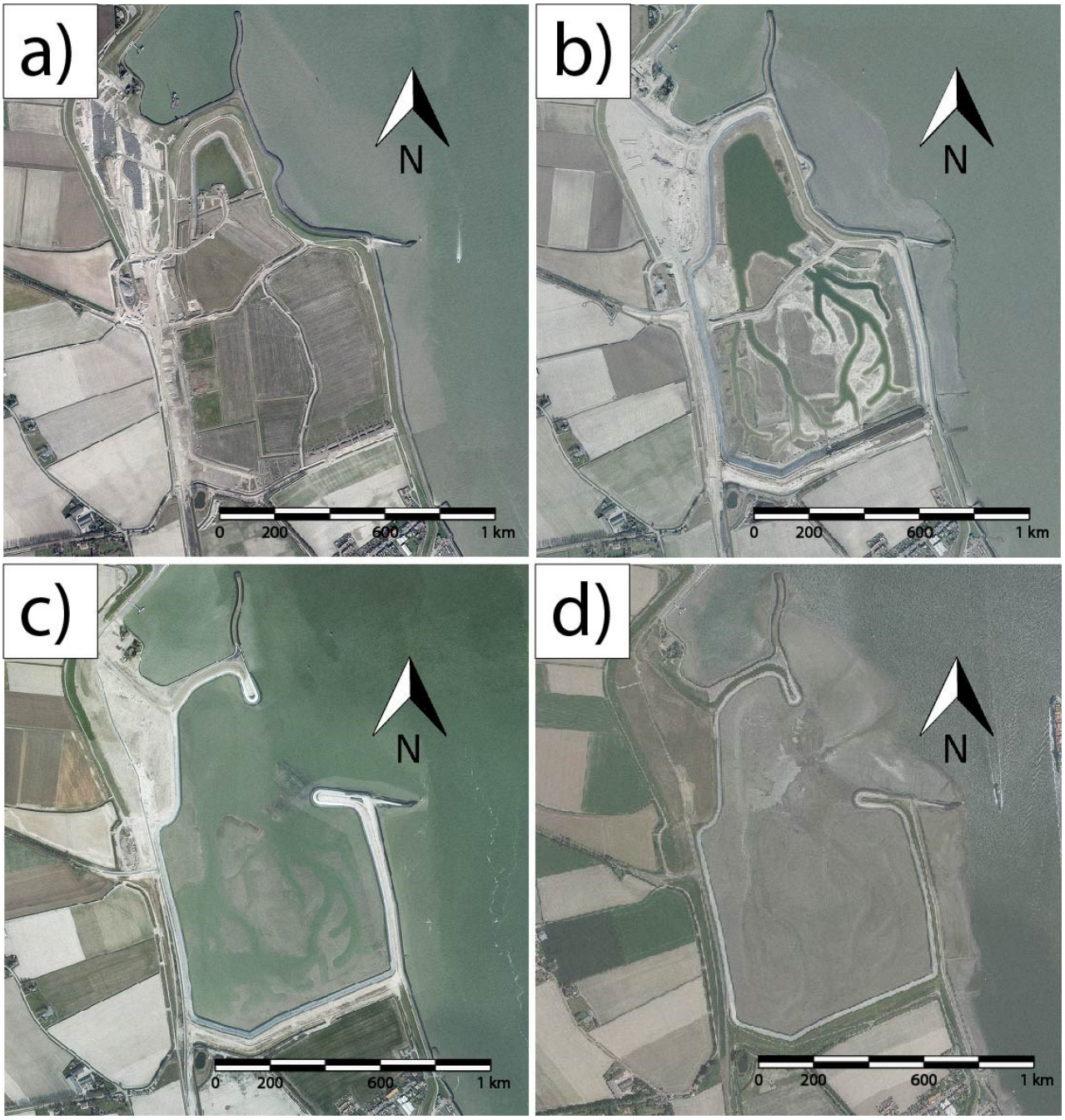


***Figure 37.*** *Orthophotos at 1:15000 scale of the Perkpolder basin from the maps of the province of Zeeland; (a) before works in March 2014, (b) shortly before the opening of the inlet in March 2015, (c) in March 2016, and (d) in June 2017.*

## *5.3 Methodology*

### *5.3.1 Morphological analysis*

The monitoring strategy aimed at identifying the evolution of the area immediately after the opening of the inlet. Following previous authors (Thomas and Ridd, 2004; Nolte et al., 2013), sedimentation patterns are analysed in a short-time interval, to obtain data from a spring-neap

tidal cycle (15 days) as well as over a longer-period (32 days). Additionally, from June 2015 to January 2017, seven multi-beam datasets were obtained from surveys undertaken by Rijkswaterstaat of the inlet area. A cross-section was digitized across the inlet to see its evolution through time, assessing changes in width, depth, and wetted area.

In order to assess the morphological evolution of the tidal flat through time, three Lidar surveys, with a 2x2 m resolution, were used. The surveys were performed by Rijkswaterstaat. As the unprocessed point clouds were not supplied, a direct evaluation of the vertical accuracy could not be undertaken. To notice that accuracy depends on the Lidar sensor resolution (Wehr and Lohr, 1999), the landscape features of the intertidal environment (Evans et al., 2019), and the presence of vegetation (Hladik and Alber, 2012). In low and high marshes, the vegetation clearly influences the accuracy, causing errors from 0.1 to 0.45 m (Morris et al., 2005; Rosso et al., 2006; Wang et al., 2009; Schmid et al., 2011; Millard et al., 2013), requiring corrections to DTMs.

As in Perkpolder the tidal flat is completely un-vegetated and with no large bed features, it was considered unnecessary to re-process further the DTMs. As shown by Fernandez-Nunez et al. (2017), bare mud in Lidar surveys is represented with very high accuracy (0.04 – 0.09 m) and the effects of corrections in these kinds of environments can be meaningless or even increase the error. The first survey was undertaken in June 2015, in correspondence with the opening of the inlet; the second survey was undertaken in April 2016 and the third one in February 2017. Two RTK-DGPS fieldwork campaign were performed on 12-15 June and 6-8 December 2017 (Fig. 38); the DGPS survey of June was not taken into account for morphological analysis because of its proximity with the Lidar survey of February. Four cross-sections were prepared in advance on ArcGIS software and uploaded on the GPS datalogger to collect the points along selected orientations; during the successive surveys the points of measurements were repeated with absolute care. The spacing between the surveyed points was about 10 meters, except inside the creeks, where the spacing was about 5 meters or less; the horizontal and the vertical accuracy was sub-centimetric. . The adopted datum is the NAP (Normaal Amsterdam Peil), while the coordinate system is the Amesrsfoort/RD new. Data was manipulated in the ArcGIS software using “natural neighbour” as algorithm of interpolation to create the DTMs. To evaluate the rate of sediment accretion, volume gain/loss, the datasets were processed with the Geomorphic Change Detection (GCD) tool of Wheaton et al. (2010). The tool performs an analysis of vertical variations and volume gain and loss including an evaluation of uncertainty. According to Brasington et al. (2003), the individual errors of DTMs when a Dod (Dem of Difference) is made can be propagated as:

$$\delta u_{DoD} = \sqrt{(\delta z_{new})^2 + (\delta z_{old})^2} \quad (5)$$

In equation (5), $\delta u_{Dod}$ is the propagated error, while $\delta z_{New}$ and $\delta z_{Old}$ are the individual errors of each DTM. Because no vertical accuracy was set-up as the unprocessed point clouds were not available, the best option was to consider a range of the individual error in this type of environment (0.04 – 0.09 m), implying that the error of the new DTMs ranged between 0.06 – 0.12 m. The GCD tool also allows to choose the threshold below which lower variations are considered meaningless: in this case, the calculations were made considering thresholds of 0.05, 0.10, and 0.15 m and no threshold at all, as previously done by Duo et al. (2018). Because of different vertical accuracy in the datasets (e.g. Lidar vs DGPS), the interpretation of DTM changes has higher reliability only when the same types of datasets are compared. This means that the most consistent data intervals are from the first two years after the inlet opening (June 2015 – February 2017). To study the additional period from February 2017 to December 2017 a comparison between datasets was made (i.e. Lidar vs DGPS), but the interpretation must be taken with extreme caution.

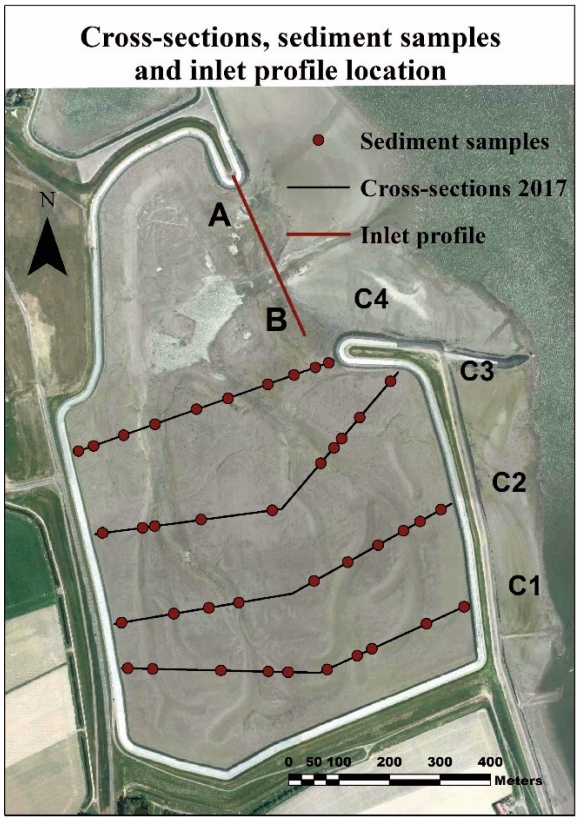


***Figure 38.*** *DGPS cross-sections (C1-C4), inlet profile (A-B) and location of sediment samples*

### *5.3.2 Particles Size Analysis (PSA)*

As the same time as topographic measurements, 40 sediment samples were collected (10 samples distributed in each cross section) to characterize the particle size distribution across the tidal flat. The adopted procedure for Particle Size Analysis (PSA) follows the Italian national standard set by ICRAM (2004). The sediment samples were treated with 120 ml of Hydrogen Peroxide at 16 volumes for several days to remove the organic matter. As the Wentworth scale (Wentworth, 1922b) was used to distinguish the sand from mud, the two fractions were separated using a mesh of 63 microns by wet sieving (Widdows et al., 2000). The mud was stored in large pitchers to decant while the sand was dried at 105 °C. Then, all the extraneous material (e.g. whole shells or fragments, etc) was removed using another sieve of 1 mm and the sand content was quantified. No further analysis on the sand fraction was carried out, considering the small quantity (e.g. a few grams, less than 30 % for most of the samples). After several days, the water in the pitchers was removed and the mud was displaced into smaller beackers and weighted. Part of the mud was then moved into glass petri dishes and dried at 105 °C. Finally, a Micromeritics Sedigraph Analyzer was used to discriminate the percentages of silt and clay. The results of the PSA were plotted onto the Shepard's diagram (Shepard, 1954) using the Triplot program (McHone, 1977b) and a map of sediment distribution was prepared.

### *5.3.3 Measurement of sedimentation rate across the tidal flat*

Sediment deposition was measured using traps built with Perspex Petri dishes with a diameter of 9 cm and a height of 1.5 cm, placed along each cross section at 10 different spots, at the same location of the sediment samples. This kind of sediment traps has been widely used since the 1980s (Reed, 1989; Leonard, 1997; French et al., 1995; Brown, 1998; Culberson et al., 2004; Neumeier and Ciavola, 2004; van Proosdij et al., 2006). This method is highly economical and provides a good spatial resolution of sedimentation (Marion et al., 2009). Despite the fact that this technique is commonly used, there is no settled standard; the structure of the Petri dishes differs from author to author, depending on the purpose of the study, the sediment accretion rate, the occurrence of precipitation, re-suspension or other considered variables or disturbances. The technique principally varies from using pre-weighted filters for small time periods, to the petri dish itself as trap, left in the tidal flat for many days or weeks, like Butzeck et al. (2015) or Temmerman et al. (2003) have done. The choice of this type of Petri dish was based on the seasonal period chosen for our study (winter-summer), the weather conditions normally experienced at the site (for example absence of torrential rainfalls), and the vertical accretion expected on this type of

tidal flat from literature studies. All the traps were covered by the tide for the same time period and by all the tides, since neap tides during experimentation were high enough to cover the whole basin. The vertical accretion did not completely bury the traps, with the exception of 2 Petri dishes. These Petri dishes were located in the southern part of the area (cross-section C1) inside the creeks, where the accretion was observed to be the highest even from the analysis of the topographic surveys. Consistent rainfall was absent while traps were operating, so it did not influence the sediment deposition. In order to avoid that near-bed tidal currents displaced traps, the Petri dishes were nailed into the ground using pickets glued in the centre of the dish. One spring-neap tidal cycle (15 days) and a long-period tidal cycle (32 days) were measured in two different time intervals (Fig. 39).

The first measurement campaign employed 40 Petri dishes (10 per cross section) which were deployed from 15 May 2017 to 16 June 2017. A second measurement campaign employed 40 Petri dishes from 13 to 27 June, therefore covering a shorter time interval that represents a spring-neap tidal cycle. Only 57 traps over 80 deployed were recollected after the two campaigns. The samples were dried, weighted, and the recovered sediment amount was normalized according to the days each Petri dish was left in the tidal flat to obtain values in grams day$^{-1}$. The normalization was made assuming a constant rate of deposition per day.

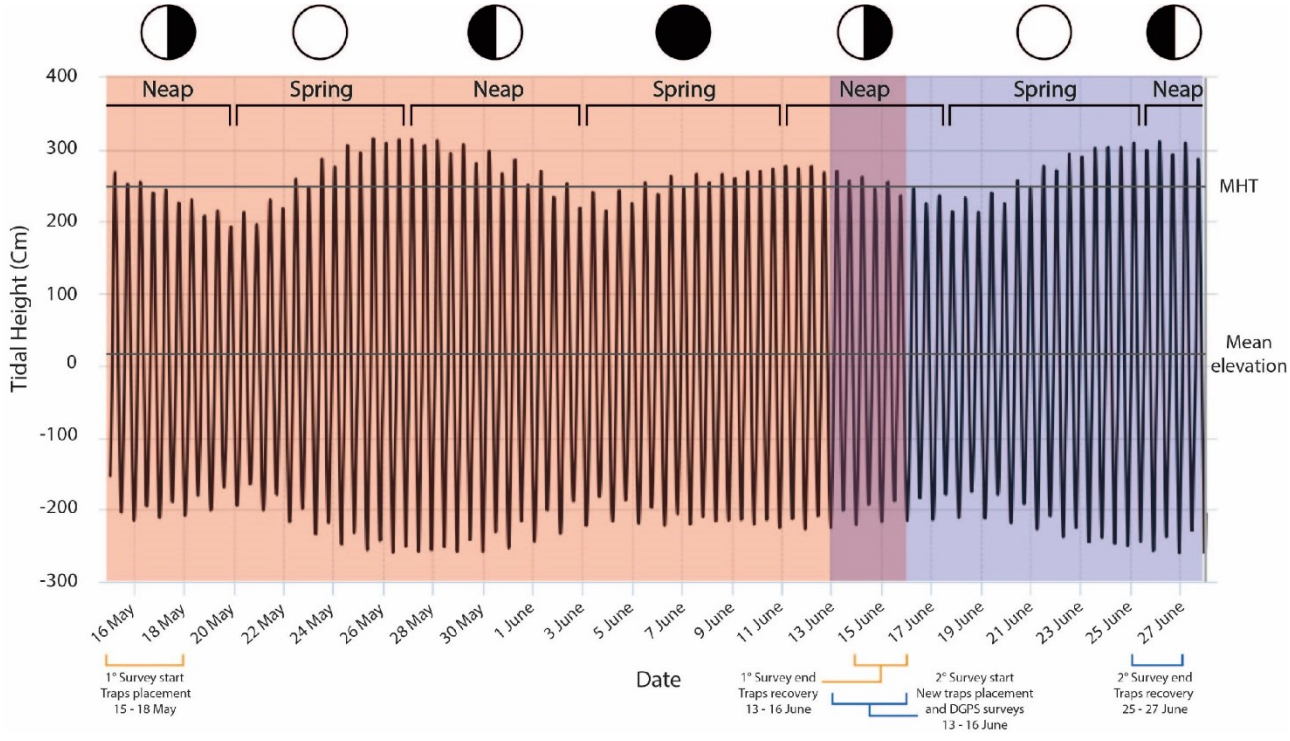


***Figure 39*** *- Neap and Spring tides during the experiments. The first experiment is from 15 of May to 16 of June; the second experiment is from 13 to 27 of June. Data from the tidal station of Walsoorden.*

### *5.3.4 Loss On Ignition analysis*

Part of the bed samples was used to determine the LOI content (Loss On Ignition) according to the method of Heiri et al. (2001). The analytic procedure was divided into two phases: 1) each sediment sample was placed in an aluminum cup and then dried for a week in an oven at 80 C° to remove water and determine the dry weight; 2) the dried sediment was moved into ceramic cups and weighted. The samples were then burnt at 550 C° for six hours and weighted once again to define the LOI.

## *5.4 Results*

### *5.4.1 Morphological datasets*

Four time intervals of morphological evolution could be considered: (i) from June 2015 to April 2016; (ii) from April 2016 to February 2017; (iii) from February 2017 to December 2017; (iv) the whole period, from 2015 to December 2017. In Fig. 40 the profiles from Lidar surveys and also from DGPS surveys are shown.

For what concerns the first interval between June 2015 and April 2016 (Fig. 41a, 41b), the accretion is centred principally in the areas adjacent to the creeks. Overall, the accretion increases moving southwards on the tidal flat; the highest and the lowest values are located in the western creek, while the lowest parts of the creek show erosion (reaching approx. 115 cm of erosion, 11.5 cm month$^{-1}$). The accretion is not stable along the creeks, in fact in some areas, in particular in the centre of the eastern creek and in the further western creek, the elevation changes are inhomogenous. On the other hand, the upper part of the flat (the southernmost part of the polder) gained a large quantity of sediment (approx. 125 cm of accretion, 12.5 cm month$^{-1}$).

During the first 10 months after the opening of the inlet, the tidal flat experienced a great sediment gain. If we use the different error thresholds we observed changes in the order of thousands of cubic meters: (i) with a threshold of 0.05 m the net sediment gain is 19300 ± 8400 m$^3$; (ii) with a threshold of 0.10 m the value is about 16900 ± 10400 m$^3$; (iii) with a threshold of 0.15 m the net gain is around 13800 ± 10000 m$^3$ and (iv) considering no threshold at all the total sediment budget is 20000 m$^3$. It is clear that even considering the highest threshold, the tidal flat is gaining sediment.

From April 2016 to February 2017 accretion and erosion have a similar trend; both maximum erosion and accretion reach 60 cm in 10 months, 6 cm month$^{-1}$. The highest values are concentrated in the western creek with the maximum erosion at the beginning of the creek, while the maximum accretion occurs in the central-southern part of the creek. As shown in Fig. 41b, the rate of accretion seems to become stable in the whole tidal flat, with the exception of the creeks that have the highest rates. This influenced the volume calculations: during these 10 months, the total sediment budget was: (i) with a threshold of 0.05 m, 14000 ± 8800 m³; (ii) with a threshold of 0.10 m, 4800 ± 4200 m³; (i) with a threshold of 0.15 m, 850 ± 1100 m³ and (iv) with no threshold at all 17000 m³. However, it is notable that the tidal flat continues to experience sediment accumulation. in a homogeneous way, with no evident morphological changes. In the last time interval, between February 2017 and December 2017, the sediment gain estimation is about 16200 m³.

The net sedimentation rates are: i) from June 2015 to April 2016, ~ 1800 m³ month$^{-1}$; ii) from April 2016 to February 2017, ~ 1400 m³ month$^{-1}$; iii) from June 2017 to December 2017, ~ 1600 m³ month$^{-1}$. Thus, the first two analysed periods result to have quite similar sedimentation rates, characterized by a reduction of sediment gain as the tidal flat builds up. The last period is characterized by a higher rate of sediment accumulation but this last calculation derives from the DGPS surveys and the value is probably overestimated. Considering the whole period since the opening of the inlet in June 2015 (Fig. 41c, 41d), the total sediment gain on the whole tidal flat was about ~ 30000 m³ from June 2015 to February 2017, of which over than 16000 m³ was estimated from February to December 2017.

The same logic of error thresholds was employed to find the most reliable sediment accretion rate (Tab 13). The rate of accretion calculated over the whole study area (i) from June 2015 to April 2016 was 6 ± 2.5 cm year$^{-1}$ (averaged using all thresholds); (ii) from April 2016 to February 2017 was 4.8 ± 3 cm year$^{-1}$ (using only the 0.05 threshold as data variability was smaller); (iii) from February 2017 to December 2017 only an estimation of 5.7 cm year$^{-1}$ can be produced. No quantification of the error can be performed as two heterogeneous datasets (DGPS *vs* Lidar were used).

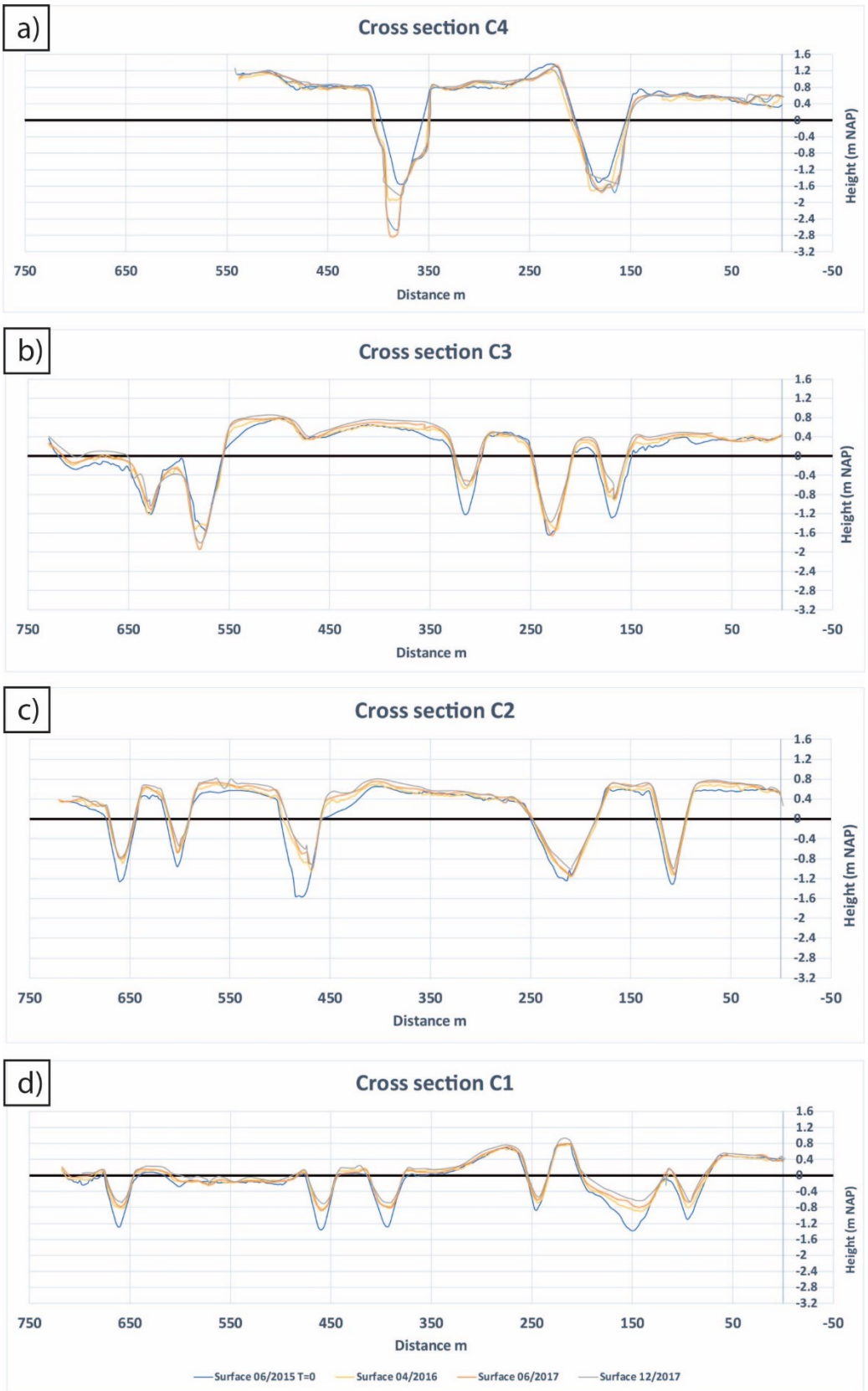


***Figure 40*** *- Cross sections from North to South (a) C4, (b) C3, (c) C2, (d) C1 extracted from Lidars (2015 and 2016) and from DGPS surveys (June and December 2017). To notice that in the graphs the survey of June 2017 is presented (orange line) to qualitatively assess bed changes but this was not used for volume calculations as it was too close in time to the preceding and subsequent surveys.*

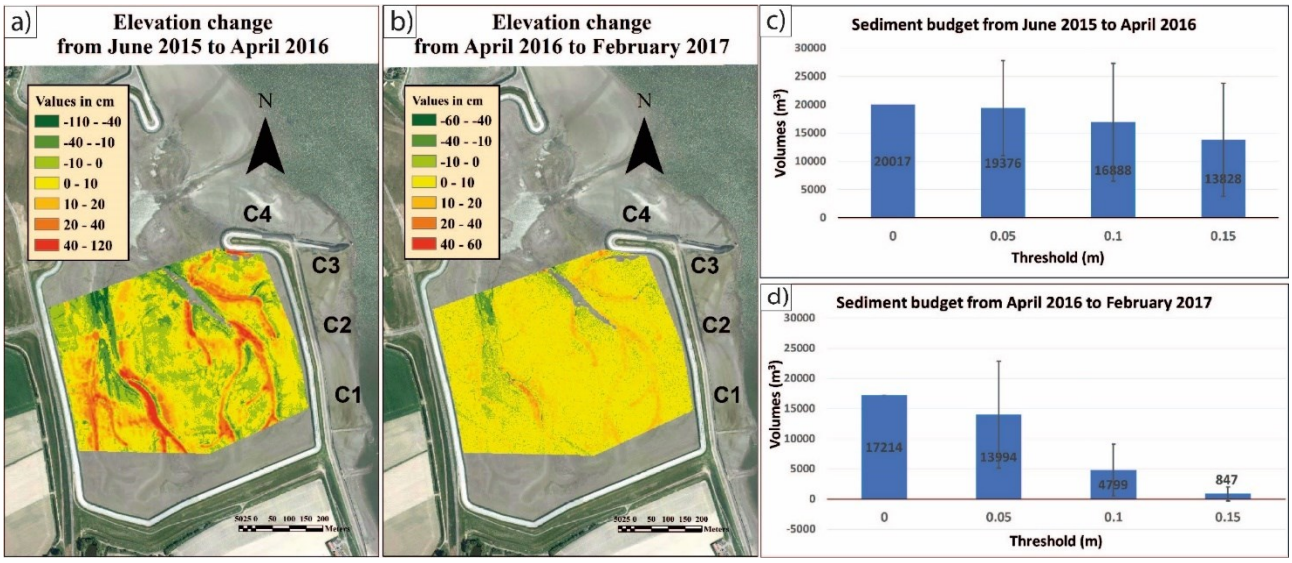


***Figure 41.*** *On the left and in the centre (a, b) elevation change computed from June 2015 to April 2016 and from April 2016 to February 2017; on the right (c, d) sedimentary budget computed for both periods considering errors of 0, 0.05, 0.10 and 0.15 m. See the text for further details on survey methodologies.*

***Table 13*** *- Volume changes and rates of accretion of the study area considering different thresholds for error in the DTM. The last row derives from the comparison between Lidar and DGPS dataset and errors cannot be estimated due to non-heterogenous datasets.*

| DTM Error Threshold (m) | Time interval | Volumes ($m^3$) | Volume Error ($m^3$) | Rate of accretion (cm $year^{-1}$) | Error (cm $year^{-1}$) |
|---|---|---|---|---|---|
| 0 | June 2015 – April 2016 | 20000 | / | 6.8 | / |
| 0.05 | June 2015 – April 2016 | 19300 | ± 8400 | 6.6 | ± 2.9 |
| 0.1 | June 2015 – April 2016 | 16900 | ± 10400 | 5.7 | ± 3.5 |
| 0.15 | June 2015 – April 2016 | 13800 | ± 10000 | 4.7 | ± 3.4 |
| 0 | April 2016 – February 2017 | 17000 | / | 5.9 | / |
| 0.05 | April 2016 – February 2017 | 14000 | ± 8800 | 4.8 | ± 3 |

| | | | | | |
|---|---|---|---|---|---|
| 0.1 | April 2016 – February 2017 | 4800 | ± 4200 | 1.6 | ± 1.5 |
| 0.15 | April 2016 – February 2017 | 850 | ± 1100 | 0.3 | ± 0.4 |
| / | February 2017 – December 2017 | 16200 | / | 5.7 | / |

### *5.4.2 Surface sediment characteristics*

The granulometric classes in which the sediment samples fall are sand, silty sand, sandy silt, loam, and clayey silt. Overall, the samples that contain a significant amount of sand were found next to the channels; the sand content decreases moving southwards, as shown in Fig. 42a. In Fig. 42b the collected samples are classified using Shepard's diagram. To notice that pure silt and clay fractions are generally under-represented.

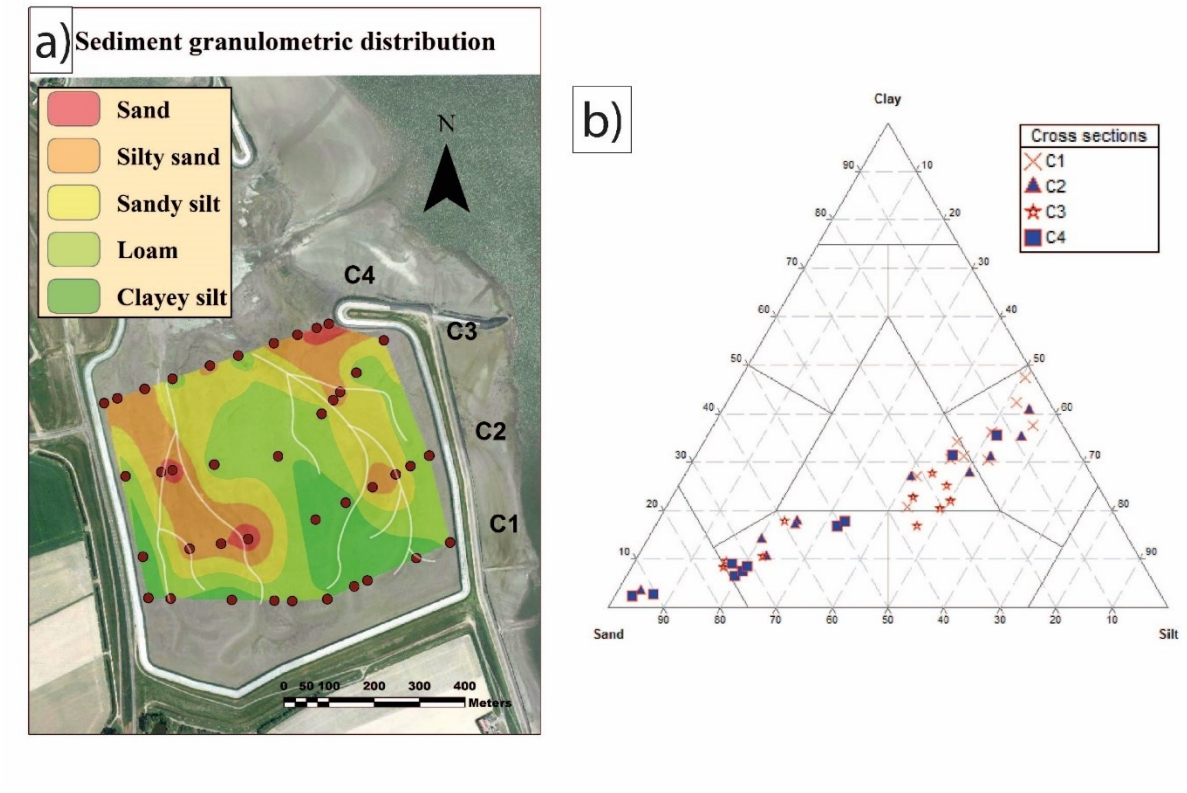


***Figure 42.*** *On the left (a) sediment granulometric distribution map derived from the analysis of 40 samples collected in Perkpolder. The map was produced using the natural neighbour interpolation. On the right (b) Shepard's diagram shows how all samples result from a mixture of end-members of dominant sand and silt fractions.*

### *5.4.3 Sedimentation rates*

No traps were completely buried, except two, implying that the collected sediment was a realistic measure of the total sediment flux. These Petri dishes were located in the southern part (cross-section C1) and inside the creeks, where the accretion measured by topographic surveys was highest.

The data from the surveys are shown in Fig. 43a, 43b, where values of sedimentation rates are presented in grams/m$^2$ day$^{-1}$. Due to the strong tidal flow during the first survey, only 18 Petri dishes out of 40 were recovered. Subsequently, because of the reduced density of measurements, it was decided to not interpolate the data.

From 15 May to 17 June 2017 (Fig. 43a), the amount of sediment trapped ranges from 6.3 g/m² day$^{-1}$ to 355.5 g/m² day$^{-1}$. The sediment amount increases moving southwards on the tidal flat.

After the second survey, performed after the Spring tide of June 2017, 39 petri dishes were collected and analysed (Fig. 43b). The amount of deposited sediment per day is in the same range of the first sampling, i.e. between 4.7 g/m² and 460.8 g/m². The southernmost areas are characterized by larger accumulation, especially next to the creeks and at the border of the tidal flat. The average sediment deposition across the flat is about 111.9 g/m² day$^{-1}$ in the first survey and about 117.6 g/m² day$^{-1}$ in the second one.

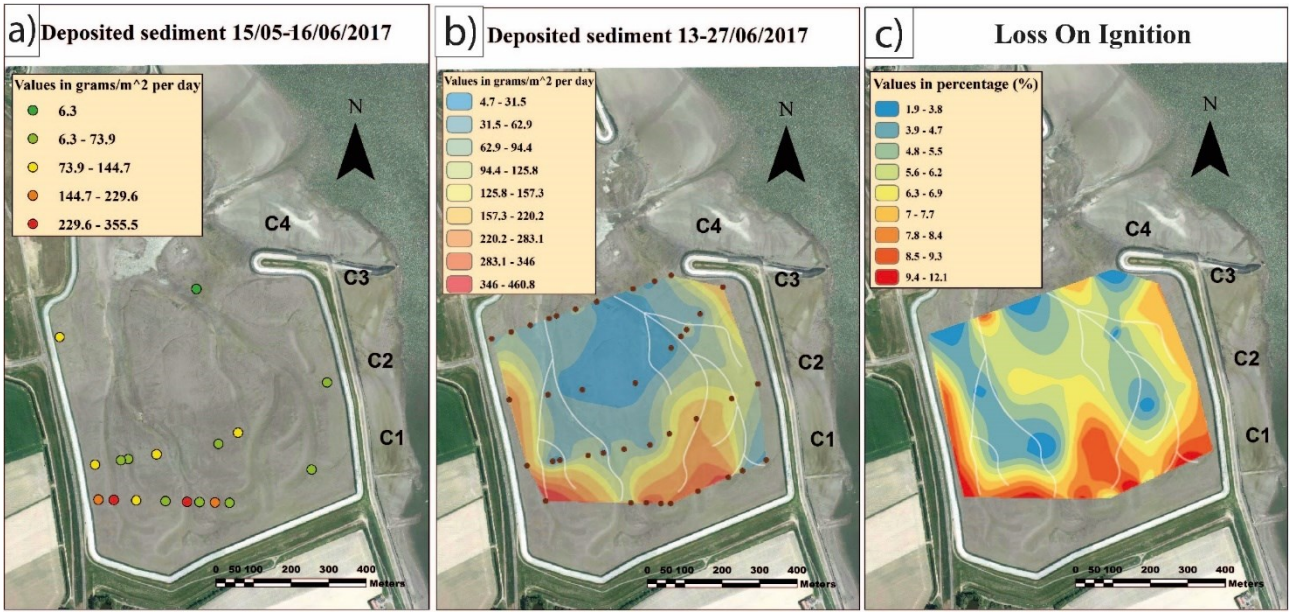


***Figure 43.*** *On the left (a) sedimentation rates from the 15 May to the 16 June 2017. In the centre (b) sedimentation rates from 13 June to 27 June 2017. On the right (c) Percentage of LOI distribution. All maps were produced using the "natural neighbour" algorithm.*

### *5.4.4 Loss On Ignition*

The distribution LOI is presented in Fig. 43c. Overall, the organic carbon content increases moving southwards across the basin. The greatest amount is distributed around the edges, next to the dyke, and in the central area. Clayey silts contain the highest concentration of organic carbon, reaching values around 8.39 – 12.07 %. The lowest values of 1.85 – 4.74 % are located next to the creeks, associated to sandy sediments.

### *5.4.5 Inlet morphology*

The Dutch Ministry of Public Works (Rijkswaterstaat) supplied eight multi-beam surveys, with a cell size of 1x1 m, performed between June 2015 and January 2017 (respectively 25 June 2015, 30 July 2015, 17 September 2015, 8 January 2016, 19 April 2016, 20 July 2016, 31 October 2016, 27 January 2017). For each survey, the rate of change of the width, depth, and area of the cross-section of the inlet was calculated. The width was calculated as the bankfull choosing as boundaries the points of increasing slope as shown in Fig. 44a. The depth was measured considering the differences in heights between the vertical position of two-time intervals. Changes in inlet characteristics were calculated by dividing one observation by the previous one. Therefore no change equals to 1, width or depth reduction is represented by values <1, and width or depth increase by values >1. In Fig. 44b, 44c, 44d, 44e, 44f, 44g, h the profile changes from June 2015 to January 2017 are presented. As shown in Fig. 45, after 2 - 4 months the rate of change slowly decreased, and after 6 - 8 months the inlet became almost stable.

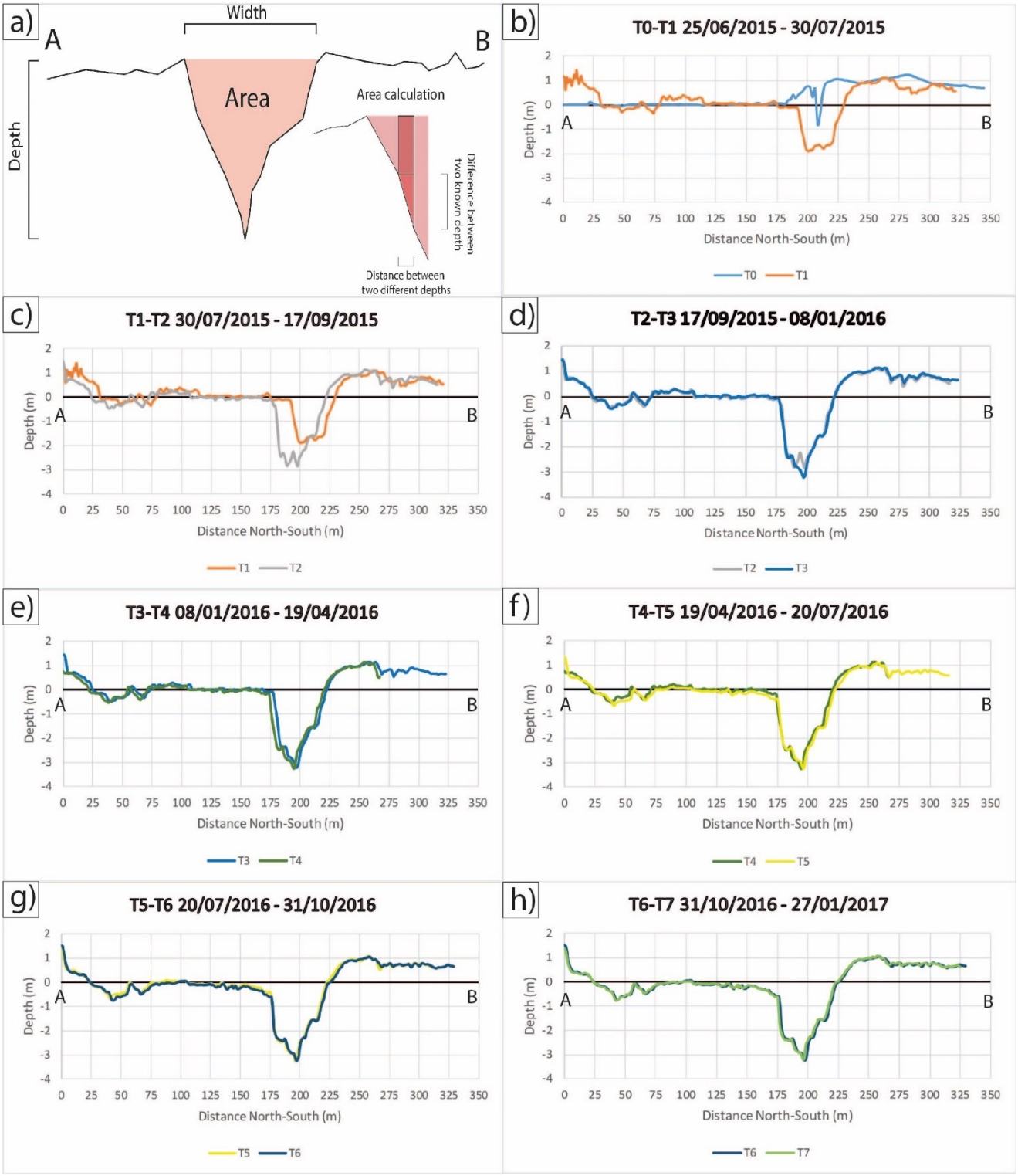


***Figure 44.*** *(a) Scheme of the calculated parameters and (b, c, d, e, f, g, h) profile changes from the opening of the inlet in June 2015 to January 2017.*

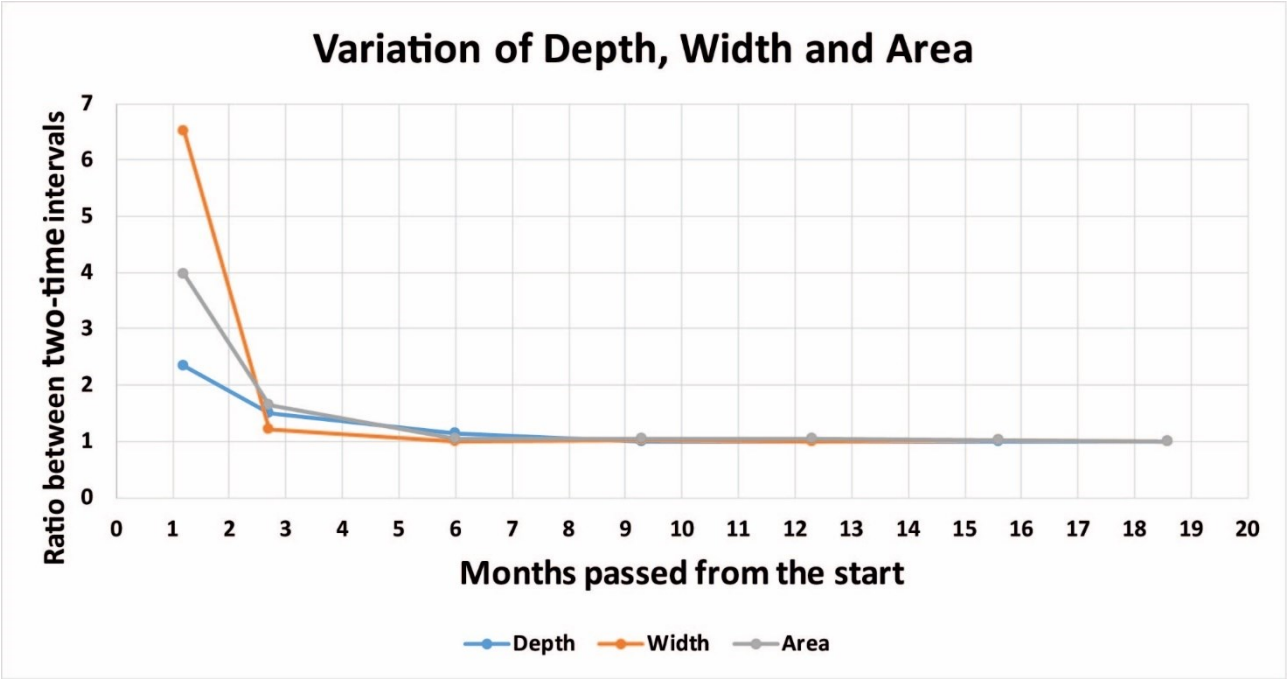


***Figure 45.*** *Variation of depth, width, and cross-section of the inlet expressed as the ratio between two-time intervals from June 2015 to January 2017.*

## *5.5 Discussion*

### *5.5.1 Sedimentological characteristics of the tidal flat*

From a sedimentological point of view, the conditions found on this reconstructed tidal flat reflect the typical characteristics of back-barrier flats as outlined by Friedrichs (2011); the pattern of the sediment distribution, defined by coarser sediment in the creeks and on lower flats grading to finer sediment on upper flats reflect the hydrodynamic energy level and sediment supply (Mai and Bartholomä, 2000). As the dominant grain size is silt and clay, defining this as a muddy flat, the presence of coarser sediment in the creeks could be exclusively related to higher peak tidal velocities (Grabemann et al., 2004). In turn, the dominance of muddy sediment in the upper flat may depends on the location of the maximum flood line compared to the tidal flat elevation (Gadow, 1970). Because of the high tidal range, the tidal flat of Perkpolder is completely covered by the water and completely dried every day, with the exception of the northern part of the creeks. Consequently, the proximity to the creeks reflects the higher energy of the flow, allowing the transport of the coarser (sand) sediment as bedload, while the other parts of the tidal flat are characterized by fine suspended sediment due to a lower hydrodynamic regime. Furthermore, due to the reduced fetch of the basin enclosed by the dyke, it is conceivable to consider wave action not very significant, therefore the distribution of the grain size can be directly related to the peak

tidal flow (Amos, 1995). Another important aspect to consider is the source of the sediment deposited inside the polder. The increasing sediment budget and the quick equilibrium state reached by the inlet strongly support the hypothesis that the sediment derives from outside the basin, also favoured by the proximity of the tidal flat to the tide-dominated ETM (Nihoul et al., 1978; Chen et al., 2005). However, it must be taken into account that before the opening of the inlet, the nature of soils used for agriculture was indeed predominantly sandy. As erosion rates resulted to be more pronounced in the Northern part of the tidal flat, the higher percentage of sand in the samples could derive from the reworking by tidal currents of the original agricultural soils. It is also noticeable, as expected, the similarity in the distribution of LOI with the particle size distribution. Low values of LOI coincide with the location of coarser sediment, an indicator of higher tidal currents. The association between fine sediments and high values of organic matter is found in locations with low hydrodynamic regimes.

### *5.5.2 Sediment budget of the tidal flat*

Overall, the sediment budget of the tidal flat is positive and the speed of accretion, after a very rapid onset immediately after basin opening, seems to have slightly decreased towards the end of the monitored period. During the first period of monitoring, the vertical changes were remarkable, meaning that all error thresholds could be considered as they were smaller than the order of change. Thus, the sediment budget was obtained as the average between the volumes calculated using all thresholds, resulting in ~ 22000 $m^3$ $year^{-1}$, that is ~ 1800 $m^3$ $month^{-1}$.; the second period also had a positive sediment budget, but vertical variations smaller than the first period and most of them were lower than the error threshold of 0.10 – 0.15 m. Thus, only the threshold of 0.05 m was used. The sediment budget decreased to ~ 16800 $m^3$ $year^{-1}$, equivalent to ~ 1400 $m^3$ $month^{-1}$. Finally, the volumes derived from the last period can only be considered as a gross estimate of how the tidal flat is developing, considering that two different techniques were compared (DGPS *vs* Lidar). In these last 10 months the sediment gain was ~ 19000 $m^3$ $year^{-1}$, so 1600 $m^3$ $month^{-1}$; the sediment budget of the tidal flat is still positive and the orders of volume accretion are comparable.

The accretion occurs in different areas of the tidal flat but mostly in the creeks and at its edges. It is interesting to note that the sedimentation rate from the traps deployed during the Spring tidal cycle of June and the tidal cycle of May - June is quite the same (111.9 $g/m^2$ *vs* 117.7 $g/m^2$), adding reliability to the figures.

From a morphodynamics viewpoint, this “artificial” tidal flat presents an unusual behaviour compared to natural ones. The most evident difference is in the creeks. Natural creeks of young marshes are typically characterized by a deepening and enlarging phase, caused by the increase in flow resistance on the marsh platform which concentrates the flow in the channel (D’Alpaos et al., 2006). The opposite condition is found in this study area, where the creeks are filling up. This is clearly visible in Fig. 40, except for the cross section C4 which is located at the beginning of the creeks, where erosion is dominant, caused by high current velocities. On the other hand, the work of D’Alpaos et al. (2006) relates to an environment where vegetation starts to be present, while here there is no evidence of features (e.g. large bedforms, pioneering vegetation, bioconstructions) that could cause spatial changes in flow resistance. One could speculate that while the flow is inside the creek, velocities remain high, favouring the transit of consistent quantities of sediment. As the tide rises and overspills the creek banks, the expansion of the flow decreases its speed and the heaviest particles transported as bedload (e.g. sand) quickly settle inside the creek, while the fines are transported in suspension across the flat and settle in its upper part when slack tide occurs.

At last, on the basis of the inlet morphological analysis, the main channel that connects the tidal flat to the sea has become nearly stable, possibly providing a stable route for sediment input from the open estuary to the tidal flat. From a management viewpoint this is an important aspect as future design of similar schemes could benefit from this successful temptative to allow the system to reach an equilibrium with no intervention by man after the initial dredging.

### *5.5.3 Salt marsh formation*

According to Bakker (2014), the conventional limit between salt marsh and tidal flat is defined by the Mean High Tide, obtained by averaging between the Mean High Spring Tide and the Mean High Neap Tide. On the basis of the tidal records of the year 2016 at the Walsoorden tidal station, for this part of the estuary this limit can be identified at about +2.53 m NAP. All the Lidar maps showed that the highest elevation ranged between + 0.8 m NAP and + 1.10 m NAP, exception for small spots that reached +2.30 m NAP. Thus, the tidal flat has a low elevation and it is still far from becoming appropriate for salt marsh development as the basin is constantly submerged by the tide. If the highest elevation portions are masked after choosing an arbitrary value (e.g. elevation higher than 50 cm above NAP), and a specific accretion map of these areas is created (Fig. 46a), it becomes evident that the sediment is filling the lower areas, even if accretion values of Fig. 46b

are slighty smaller than the previous in Fig. 46a. This mechanism of growth is typical of tidal flat and salt marshes and it was described by previous studies (e.g. Leonard, 1997; Allen, 2000; Temmerman et al., 2004a).

The most elevated areas are located in the centre and at the borders (North-West and North-East principally) (Fig. 46b). In order to find how many years will be necessary for the tidal flat to reach the Mean High Tide at +2.53 m NAP, the best compromise was to consider the vertical accretion observed in these areas higher than 50 cm NAP. During the first period, from June 2015 to April 2016, the accretion rates of these areas was about 3.2 ± 1.7 cm $year^{-1}$.. During the second period, from April 2016 to February 2017, the average decreased to 2.6 ± 1.5 cm cm $year^{-1}$.. Furthermore, during the second period, the areas above 50 cm NAP became wider.

If the most elevated areas are taken into account (i.e. located in the northern areas at around 80 - 110 cm NAP), the highest rates of accretion are about 25 cm over 20 months, which means that these limited zones of the tidal flat will become a salt marsh not before a further 8 - 10 years, assuming that the sedimentation rate will remain constant in time. However, as already mentioned, the accretion of a salt marsh follows an asymptotic growth, consequently, the accretion will decrease in time. Considering now the whole areas above 50 cm NAP with an average of 3 ± 1.6 cm $year^{-1}$will become a marsh after approximately more than 50 years. The north-west zone could be a good candidate but it is still too exposed to high hydrodynamic conditions and it will probably take longer than the other two areas.

It should also be taken into account that every plant species has different vertical distribution above the high tide level. Gray et al. (1989) compared the vertical distribution of *Spartina anglica* along 107 transects across saltmarshes in 19 estuaries in south and west Britain, producing Eq. (6) that takes predicts the elevation limits for the existence of *Spartina*:

$$\mathbf{LL} = \mathbf{-0.805 + 0.366SR + 0.053F + 0.135Log_eA} \quad (6)$$

Where LL represents the lower limit of *Spartina* in meters above the NAP, SR is the Spring tidal Range (m), F is the fetch in the direction of the tidal flat transect (km) and $Log_eA$ is the area of the estuary ($km^2$). Perkpolder has a SR = 5.32 m, F = 3.30 km and the estuary area is 21863 $km^2$. Therefore, LL equals to 2.67 m. This value is slightly higher than the 2.53 m found by Gray et al. (1989) for British estuaries, meaning that here the condition for *Spartina* establishment could require the tidal flat to reach a higher elevation than the one identified along UK shores. It should be underlined that Gray's equation is based on data collected on natural salt marshes in Britain,

developed along open estuaries, while the tidal flat of Perkpolder is enclosed by dykes and has a limited tidal exchange through the inlet, subsequently this approach must be taken with caution and needs validation.

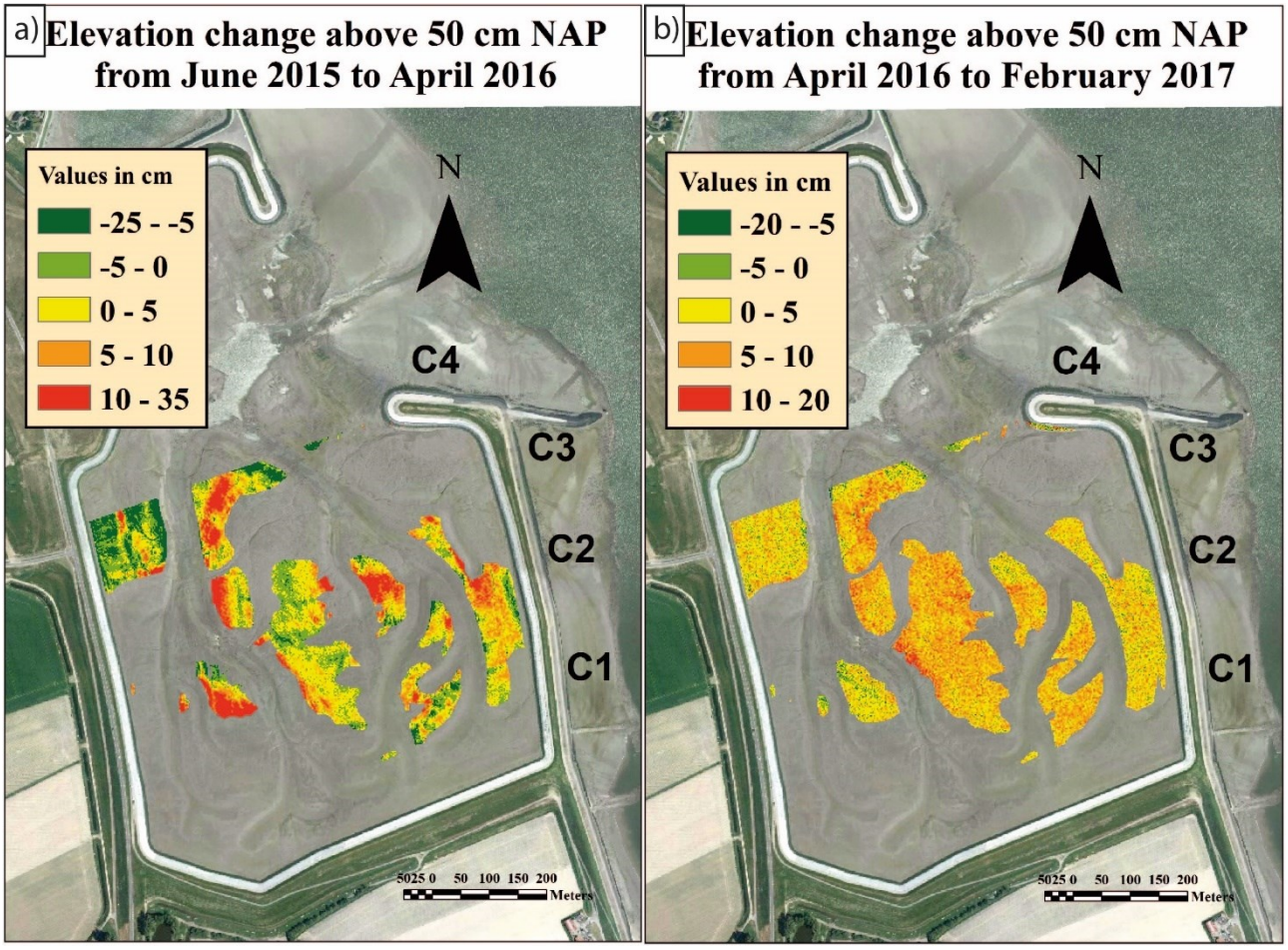


***Figure 46.*** *- On the left (a) elevation changes from June 2015 to April 2016 and on the right (b) from April 2016 to February 2017.*

### *5.5.4 Comparison with other case studies in the North Sea area*

Recent studies of other tidal flats showed how different accretion rates can occur despite similarities in tidal range. Widdows et al. (2004) described another tidal flat of the Westerschelde Estuary, Molenplaat, not so far from Perkpolder (around 6 km North-Westwards). This tidal flat has a sediment accretion of 2.4 cm year$^{-1}$, which is lower than the Perkpolder one. This could be related to granulometric differences between the two sites. The deposition rate is much lower on the open Molenplaat, with an average of 15 g/m² day$^{-1}$ while Perkpolder one has a much larger, higher than 100 g/m² day$^{-1}$. The Molenplaat tidal flat is characterized by a sand percentage between 61 – 99 %, while the tidal flat of Perkpolder is dominantly silty (as already mentioned,

most of the samples have less than 30% of sand; there are only 2 samples composed of more than 90% of sand). The causes of these differences, even if the tidal range and the elevation above mean sea level are the same, could be due to a different regime of tidal currents. Molenplaat is an open tidal flat located in the mid-part of the estuary and the hydrodynamic energy is probably higher than in the Perkpolder basin, which is, instead, enclosed by the dyke ring. According to Nihoul et al. (1978) Molenplaat is characterized by strong hydrodynamics.

A recent study by Oosterlee et al. (2017) studied another natural restoration project in the salt marsh of Lippenbroek, in the internal part of the Scheldt estuary. A long-term analysis of nine years of monitoring was performed for this 8 ha wetland, demonstrating that the rate of accretion was about 2.35 cm $year^{-1}$. Even in this case, the sedimentation rates are lower than Perkpolder. The reason behind this difference could be that Lippenbroek is a tidal flat that has developed into a proper salt marsh and a decrease in sedimentation is expected as high elevations are reached. Many authors (e.g. Pethick, 1981; Marani et al., 2007; Marani et al., 2010; D'Alpaos et al., 2011) showed that the accretion of a salt marsh follows an asymptotic growth that depends on sediment accretion, erosion, and biomass, if it is present. Besides, this site is a Controlled Reduced Tide (CRT) marsh, with an artificially controlled tidal range (1.30 m at Spring Tides instead of the expected 5.40 m). Nevertheless, the previous work of Vandenbruwaene et al. (2012) showed that the first year of this CTR marsh was characterised by an initial average sedimentation rate of about 6 cm $year^{-1}$, which is comparable with the 6 cm $year^{-1}$ observed during the first ten months of the evolution of Perkpolder. During the following four years, the rates of accretion of Lippenbroek decreased to less than 4 cm $year^{-1}$; similarly, the rate of accretion of the highest areas of Perkpolder after 20 months decreased to 4.8 cm $year^{-1}$. After nine years, the evolution and the accretion rates of the site of Lippenbroek become very similar to marshes in the UK, despite the different tidal regimes. On this basis, the accretion rates at Perkpolder could be expected to decrease in the future, reaching the values of natural marshes. An important difference is found in the mechanisms of channels formation. Vandenbruwaene et al. (2012) noticed that certain features influences channels formation, like low-elevated zones and area with compacted polder clay. In the tidal flat of Lippenbroek, channels were easily ditched in low-elevated zones but were hampered by compacted clay. In the tidal flat of Perkpolder, this statement seems not applicable. In fact, channels started to develop in the northern areas, even in high elevation zones, but, at the same time, they could not evolve in the southern areas, where silt-clay sediment is dominant but

not compacted, according to field observations by the authors. Mud here is at times liquid to the point that during field surveys by DGPS the authors were sinking to the waist.

Cousins et al. (2017) installed numerous experimental clay-terraces on engineered sea walls in the marshes of Tollesbury and Langenhoe (Essex, South-Eastern England) from October 2012 to July 2014. After 22 months, the terraces in Langenhoe gained sediment at a rate of 6 cm year$^{-1}$, while in Tollesbury the rate was 3.3 cm year$^{-1}$. Compared to the study case of this paper, the sediment accretion rates of the Perkpolder tidal flat are slightly higher than those of the UK sites. Furthermore, the sediment deposition in the UK cases could have been controlled by the presence of vegetation. The Perkpolder basin is instead a young tidal flat, surrounded by dykes and located at around mean sea level NAP where vegetation is not yet able to grow. In Tab. 14 the different average rates of accretion of the study cases previously discussed are summarized.

***Table 14*** *- Average rates of accretion of different study cases from the Western Scheldt (The Netherland) and South England. Next to each rate is expressed the elevation compared to the NAP in meters. *The total rate after 30 includes Lidar and DGPS surveys, so should be taken with attention as it might be overestimated for the last period.*

| **Location** | **Average rates (cm year$^{-1}$)** | | **Months** | **Tidal range (m)** |
|---|---|---|---|---|
| Perkpolder (NL) | 6 (Tot) | 3.2 (> 0.5 m MSL) | 10 | approx. 5 |
| | 4.8 (Tot) | 2.6 (> 0.5) | 20 | |
| | 5.7* (Tot) | | 30 | |
| Tollesbury (UK) | 3.3 | | 22 | approx. 5 |
| Langenhoe (UK) | 6 | | 22 | |
| Molenplaat (NL) | 2.4 (approx. 0) | | 432 | approx. 5 |
| Lippenbroek (NL) | 12.5 (0 - 0.3) | 4.8 (0.3 - 0.6) | 12 | 1.3 |
| | 8.5 (0 - 0.3) | 3.8 (0.3 - 0.6) | 48 | |
| | 2.35 (Tot) | | 108 | |

## *5.6 Conclusions*

The Perkpolder basin is a young artificial tidal flat that is still under development. Since the opening of the inlet on 25 June 2015, the site has been exposed to a semidiurnal tidal regime. Field surveys and sediment sampling proved that the basin is infilling by sand (small amounts), silty sand, sandy silt, loam, and clayey silt. Organic Carbon, determined as LOI varies from 1.9 % and 12.1 %. Between May and June 2017, during a whole Spring to Neap tidal cycle, the deposited sediment ranged from 6.3 g/m² $day^{-1}$ to a maximum of 355.5 g/m² $day^{-1}$. During the following tidal cycle up to the Spring tide at the end of June 2017, the sediment quantity varied from 4.7 g/m² $day^{-1}$ to 460.8 g/m² $day^{-1}$. The inlet morphology analysis proved that after a quick evolution following the opening, after 6-8 months the inlet stopped its morphodynamics and reached equilibrium conditions. The total sedimentary balance was about 22000 m³ during the first year of life of the tidal flat (1800 m³ per month) and 16800 m³ during the second year (1400 m³ per month). The average accretion rate of the whole study area was about 6 cm $year^{-1}$. The most elevated areas located 50 cm above NAP datum, like the central part of the flat and its borders, gained about 3 cm $year^{-1}$. Considering the highest regions of the study area, the conditions for initial salt marsh formation will not be established before a further 8-10 years. The portions of the tidal flat that will first become a salt marsh are mainly located in the central area, between the two artificial creeks, and in the Northeastern and Eastern areas. This study provides an indication for the ecosystem-based design of innovative coastal defences, giving indications of the time required by the scheme for reaching full efficiency. The establishment of an optimal height for colonisation by vegetation can be an important design guideline if a tidal flat is built by dumping of dredged material. Likewise, it provides an indication for optimal conditions if planting should be considered.

# *6. Sedimentological characteristics of young marshes in the Bay of Fundy (Canada).*

## *6.1 Introduction*

The management realignment policy is slowly becoming a well-accepted strategy to cope with sea level rise and protect the coastline (Masselink and Lazarus, 2019). Restoration projects are developing in several coastal wetlands around the globe, such as in Europe, America, and Canada. This Building-with-Nature approach is particularly important where large coastal wetlands dominate the environment; this is the case of the Bay of Fundy (eastern coast of Canada). This large bay is characterized by wide salt marshes that have decreased by an estimated 30,500 ha (~85% of the initial area) since European colonization in the 17th century (Thomas, 1983). Much of this loss was related to human intervention, in particular diking for agricultural land (Ganong, 1903). The whole region is subjected to one of the highest tidal ranges worldwide (between 5 to 16 m), which leads to a high diversification of the salt marshes. However, the transition from tidal flat to salt marsh is a process that needs more investigation, since the salt marshes that develop after a realignment usually present a different evolution and structure (Virgin et al., 2020). This study focuses on three young Canadian wetland environments that developed due to human intervention: i) the restoration project of Converse, located on the north side of the Bay (Cumberland Basin); ii) the transitional wetland of Halfway River, located in the southern side of the Bay (Minas Basin) that was born after the accidental breach of a dike; and iii) the salt marsh of Eldriken, which is part of the Windsor system located in the Minas Basin as well, that grew after the 1970s due to the construction of a railway.

## *6.2 Study site*

*Converse*

The study site is a management realignment project located in the Tantramar Marsh system, next to the Cumberland Basin (Fig. 47a, 47b), in the northern basin of the Bay of Fundy (East coast of Canada). This large basin (118 $km^2$) is characterized by a semi-diurnal macrotidal range of about 14 m and high sediment suspended concentrations (~0.3 g/L), mostly composed of coarse silt (van Proosdji et al., 1999). Sediment deposition is influenced by seasonal variations, and marshes are

usually covered by snow and ice during winter; storms have a minor control on sedimentation (Greenberg, 1984). This northern portion of the Bay of Fundy is characterized by expansive mudflats and higher concentrations of suspended sediments compared to the southern region (Chmura et al., 2001). The Tantramar marsh system includes a high variety of marshes, rivers, and lakes, that extends for about 230 ha, and it connects the provinces of New Brunswick (NB) and Nova Scotia (NS). This large wetland complex was highly reduced during the last 400 years, due to human intervention (e.g. dykes, transportation routes). The study site is located in the Missaguash River, one of the large tidal rivers that divides the two provinces (Fig. 47c). This restoration project, called the Converse Marsh, was developed due to a series of issues, which principally are the increasing salt marsh loss, strong erosion of the dykes at the mouth of the Missaguash River, and the unfeasibility of repairing and maintaining the dyke. The project aims to protect the transportation route of Fort Lawrence Road and the adjacent Parks Canada property by breaching the dyke in advance in order to flood the lower portion; the objective is to restore the historical salt marsh and increase the sustainability of dyke infrastructure. The project was applied in 2016 by the CB Wetlands & Environmental Specialists Inc. (CBWES), in partnership with the Nova Scotia Department of Agriculture (NSDA), to the Environment and Climate Change Canada's National Wetland Conservation Fund (NWCF). The final dyke realignment and salt marsh restoration design was completed in 2018 and a monitoring program was carried out based on the following points: i) to report the evolution of the habitat and to determine whether ecological benefits occur; ii) to describe the impacts of the tidal flow; iii) to define whether supplementary interventions are necessary.

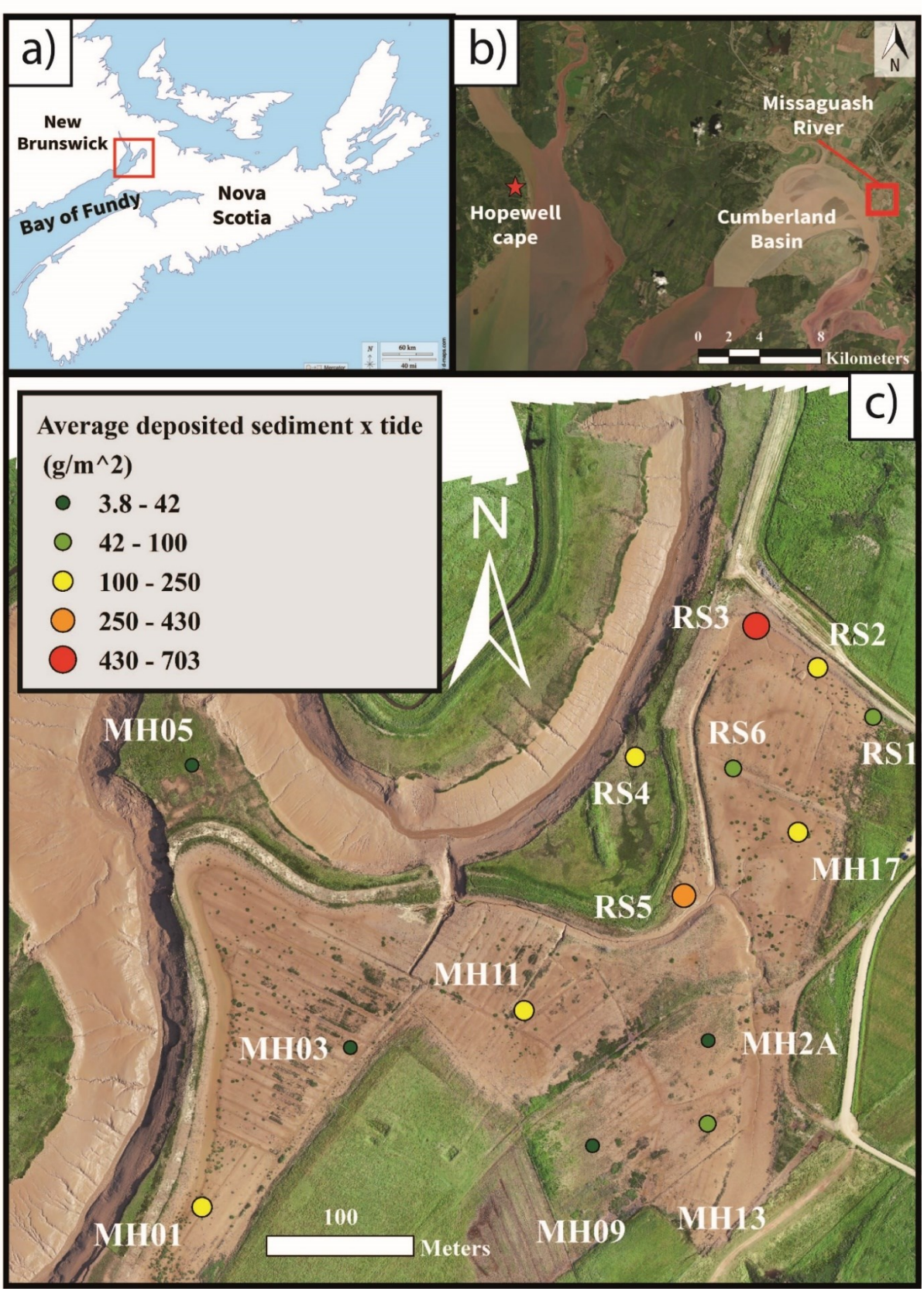


***Figure 47*** *– (a) The restoration project is located in the northern basin of the Bay of Fundy (Canada). (b) The Converse marsh is next to the mouth of the Missaguash river, on the eastern side of the Cumberland basin. In Figure (c) are shown the value of the average deposited sediment calculated from the surveys of July 2021. The orthophoto was obtained during the surveys as well.*

*Halfway River and Eldriken*

The Halfway River and the Eldriken study sites are located in Minas Basin, the southern basin of the Bay of Fundy (Fig. 48a, 48b). The basin is 124 km long, 30 km wide, and, compared to the northern side, this region of the bay is characterized by a sandier content and mostly sand flat and bars (Chmura et al., 2001). The sediment source derives glacial outwash deposits (Shaw et al., 2010), and they are the results of sandstone cliff erosion and resuspension of seabed material (Amos and Long, 1980). However, high concentrations of suspended sediment are caused mostly by the tidal flat sediment resuspension due to tidal currents and waves (Dalrymple et al., 1990). The Halfway River was historically and naturally a tidal river located in Hantsport (Nova Scotia) characterized by a wide wetland system in the lower flood plain (Fig. 48c). However, most of the marsh was lost due to the construction of barriers; in fact, the tidal inflow of the connected macrotidal Avon River was highly reduced by the historical construction and operation of a railway causeway across the mouth of the river. In 2017 the causeway breakdown reconnected the Avon and the Halfway River, resulting in a natural hydrological regime and a transition from land to marsh (Borown et al., 2018). Although the significant marsh recovery, the causeway was rebuilt in the following years and the system is now under pressure, since the tidal range and the sediment transport are highly reduced. The Eldriken study site is found about 6 km south-eastward to the Halfway River (Fig. 48d). This salt marsh composed principally of *Spartina alterniflora* and *Spartina patens* is part of a larger wetland that is recently forming next to the Windsor causeway of the Avon River. The system developed after 1968 – 1970 when the presence of the railway caused sediment accumulation. The presence of the tidal flat and the marsh attract a variety of birds for feeding and roosting purposes, including several that feed primarily on fish (Daborn et al., 2002).

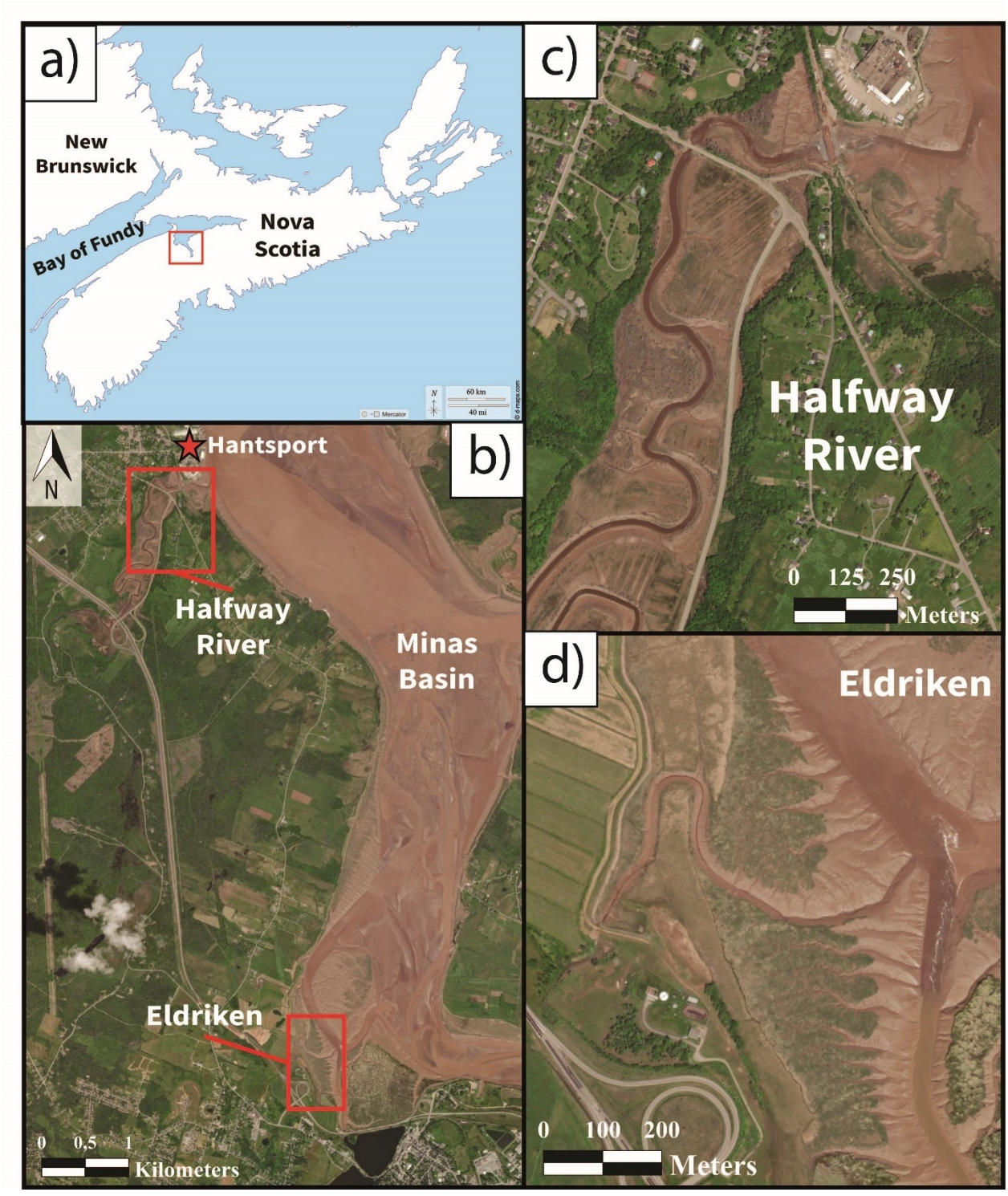


***Figure 48*** *– (a) Location of the study sites in the southern basin of the Bay of Fundy. (b) The two case study are both situated in the Minas Basin, about 6 km far from each other. (c) Halfway River study area in detail. (d) Eldriken study area in detail.*

## *6.3 Methodology*

### *6.3.1 Converse*

*Sediment traps*

A series of surveys that combine sediment traps, ADCP, and UAV were carried out between 23 and 26 July 2021 (Fig. 47c). Following the same methodology of the previous chapters, sediment deposition was measured using Polystyrene Petri dishes placed on the surface of the tidal flat. In this case, the structure of the Petri dish was the same as in Chapter 5, with an improvement; a Petri dish with a diameter of 10 cm and a border of 1.5 cm was glued to a wooden stick of about 10 cm and two hook-and-loop fasteners were attached in its internal border. A smaller Petri dish of 9.5 cm x 15 cm with two hook-and-loop fasteners attached to the external border was inserted on the larger one; this structure locks the upper Petri, which will become the actual sediment trap and can be easily removed. 14 stations distributed around the tidal flat were chosen for the analysis and 3 traps were placed in each station, following the same procedure of Chapter 3 (i.e. three traps spaced by 60 cm and oriented in the same direction). Since sedimentation in the Bay of Fundy is extremely high (i.e. high risk of overfilling) the traps were left in the tidal flat for a total of four tide events. One trap from all stations was collected and replaced with a new trap after the first tide, in order to measure the deposition of a single tide. Then, the second, the third, and the fourth tide were singularly measured by three traps only (RS1, RS2, RS3 in Fig. 47c). A total of 59 traps were submerged for four high tide events, from 24 to 26 of July 2021. The deposited sediment was then moved into beakers, dried at 70 C° for several days, and then weighted to measure the deposited sediment and the organic matter. This procedure was followed to determine if the organic matter amount could affect the deposited sediment weight only. In fact, the samples were then treated with hydrogen peroxide (30%) to remove the organic matter. The procedure was performed on hot plates set at 60 C° to accelerate the process. Once the organic matter was removed, the beakers were completely dried at 70° for several days and weighted to calculate the deposited sediment. As for Chapter 3, the location of the group of traps was measured using an RTK-GPS Leica (the receiver was a GS14, the controller a CS20); the centre of the three vertices represents the location and the elevation of the traps. The coordinate system used during the surveys is NAD83 (CSRS) UTM Zone 20N, while the vertical datum is CGVD2013, which is the most recent Canadian standard; however, the vertical datum is common for the whole State and needs to be corrected. Hence, the data measured by the GPS were rectified with the Chart Datum and the mean sea level of Hopewell Cape; despite this station being located next

to the Cumberland Basin, it was the nearest national tidal station available (Canadian Hydrographic Service) (Fig. 47b); the MHT and the tidal range was calculated through the tidal station of Hopewell Cape as well. This measurement was carried out in parallel with another type of sediment trap, made by a single filter paper placed in each station; the filters were replaced per each tide. Once collected, the filters were dried and weighed. This analysis was carried out by Megan Elliot (Saint Mary's University) and the data were used for validation of the Petri dish trap. The comparisons were made between traps that collected sediment during a single tide.

*Particle size analysis*

A granulometric analysis was carried out for one sample of each group of traps. Each sample was treated with isoton solution and sonified with a Misonix Sonicator Ultrasonic Processor in order to detach the particles; a Coulter Counter Multisizer 3 was used to measure the particle sizes. The process was divided into two phases: during the first phase, a 200 µm tube was used to measure the coarser sediment (i.e. from fine sand to coarse silt); during the second phase, a 30 µm tube was used to measure the finer particles (i.e. from coarser silt to clay). The granulometric distribution was processed using the Gradistat program (Grain Size Analysis Program v.8.0) made by Simon Blott (2010) in order to obtain the granulometric classes, using Stevens (1983) diagram.

*ADCP and submersion period calculation*

An ADCP was located and fixed on the surface of the central part of the inlet that connects the river to the tidal flat. The tool measured the water level variations, the current velocities, and it collected data for the whole survey (from 23 to 26 July 2021). The location of the sensor was measured with the GPS as well and the offset was considered in the correction. The current velocities were not processed for this PhD thesis, but the tidal variations were used to calculate the average submersion period and the total submersion period per each trap.

*UAV survey*

A drone survey was carried out the 25 July using a DJI Phantom 4. The fieldwork methodology and the data processing were the same as in paragraph 2.3.1 of Chapter 2 (i.e. GCP location, validation points, etc); however, the flying altitude was 120 m and the UAV was equipped with an RTK-GPS, which reduced the necessity of a high number of GCP (i.e. only 10 GCP were used for the whole study area). The data processing was carried out by Sam Lewis (Saint Mary's University) and a DSM was produced. A high number of validation points (i.e. more than 150) were measured on the surface of the tidal flat with the RTK-GPS in order to calculate the Root Mean Square Error (RMSE).

In addition, the DSMs from July 2019 and August 2020 were provided by Saint Mary's University; this dataset was processed through the GCD tool as well (Wheaton et al, 2010). As cited in chapters 2 and 5, when a DoD (Dem of Difference) is made, the individual errors of DSMs can propagate, following the equation (5):

$$\boldsymbol{\delta u_{DoD}} = \sqrt{(\boldsymbol{\delta z_{new}})^2 + (\boldsymbol{\delta z_{old}})^2} \quad (5)$$

Where $\delta u_{Dod}$ is the propagated error, while $\delta z_{New}$ and $\delta z_{Old}$ are the individual errors of each DTM (Brasington et al., 2003). The RMSE of the DSMs were calculated in order to obtain the TCD and define the significant vertical changes.

Two main areas were selected for the analysis: i) the tidal flat itself, and ii) the inlet area (Fig. 49). These areas were cropped in order to measure separately the volumes and the vertical changes, based on the morphological characteristics. The inlet area volume variations were studied considering the inlet itself, and the inlet area plus the nearby areas and the internal channels; the external area was chosen basing on the reliability of the DSMs area. Due to the presence of vegetated patches located in the southern-western area, the area was cropped out. The time intervals that were considered are: i) from July 2019 to August 2020, ii) from August 2020 to July 2021, and iii) the whole period, from July 2019 to July 2021. It is important to state that the DSM of 2020 focuses on the eastern section of the study site, ignoring the western part, meaning that the averages of volumes and vertical changes must be taken with caution. Furthermore, the DSM of 2019 was characterized by the presence of vegetation (i.e. plants from the previous agricultural fields) that could not be completely cropped out due to their extension; this aspect is discussed in paragraph 6.5.2.

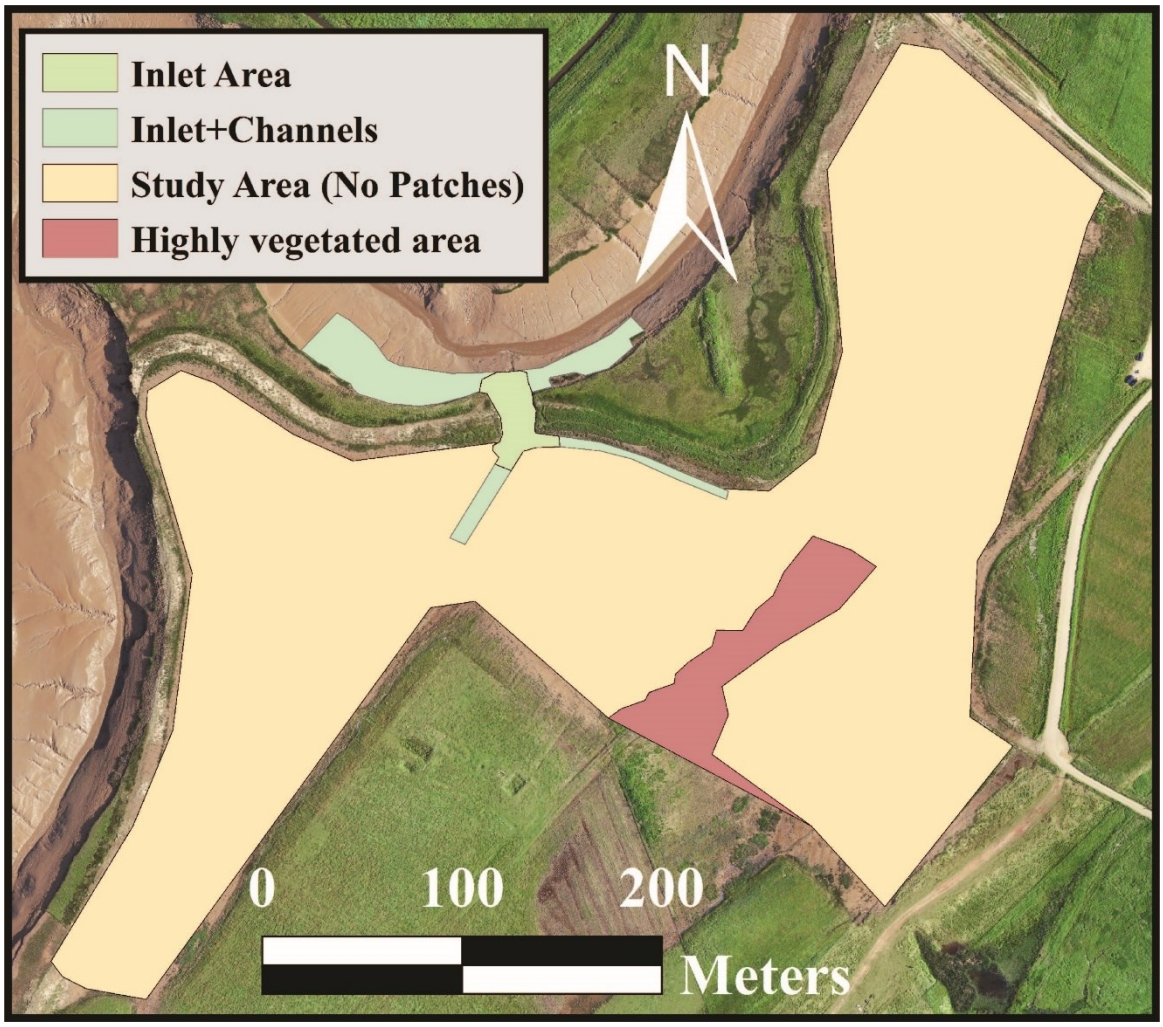


***Figure 49 –*** *Selected section for volumes and vertical changes analysis: the area concerning the inlet itself, the inlet area plus the channels and the nearby areas, the whole tidal flat area, and the highly vegetated area.*

### *6.3.2 Halfway River and Eldriken*

Fieldwork activities were carried out between 10 and 13 August 2021. The same methodology was applied to estimate the deposited sediment of Halfway River and Eldriken marsh. 10 stations were distributed between the two sites, with a total of 30 traps (no trap was replaced during this fieldwork). Three stations were located inside Halfway River, which is partially disconnected from the tidal basin; three were placed outside the river, which means inside the tidal basin; and four stations were located in the salt marsh of Eldriken. All traps collected sediment for two tidal events and the samples were processed following the procedure of the previous paragraph. Deposited sediment and granulometric distribution were obtained as well. The GPS position was corrected based on the Chart Datum and the mean sea level of the tidal station of Hantsport (Canadian Hydrographic Service) (Fig. 48b). However, tidal records were not available, so the rates

of deposition were calculated based on the tidal events only (i.e. g/m$^2$ per tide). Final considerations about vegetation distribution and marsh development were discussed using an orthophoto and a DSM provided by Saint Mary's University, which represents the Eldriken salt marsh during July 2019.

## *6.4 Results*

### *6.4.1 Sediment traps validation and rates of deposition*

All groups of traps from all study sites presented a consistent sediment deposition with a total average standard deviation of about 0.9 g. However, differences in standard deviation were found between the study sites; the Converse tidal flat presented a lower standard deviation (0.57 g), while in Halfway River the values were higher (2.7 g inside the River zone and 1.3 g in the basin); Eldriken values were similar to Converse (0.45 g). Comparisons between Petri dish traps of the Converse site and filter paper traps are shown in Fig. 50. Both methods denoted the same trend (i.e. as the elevation of the tidal flat increases, the rates of deposition decrease), with an average difference between traps of the same station of 117.2 g/m$^2$ per tide. Overall, the rates calculated from the Petri dishes are lower than the filter paper, but they showed a higher precision (i.e. lower discrepancies between traps of the same station). The sum of the rates calculated using the traps of the same station showed a lower difference between methods (about 70 g/m$^2$ per tide). It is interesting to note that the sum of the sediment weight collected during the single tide events (of a single station) is comparable with the traps that were submerged by the whole four tide events (i.e. 0.9 g of standard deviation), and the filter traps; this observation indicates the trap's design did not interfere with the sediment deposition, otherwise the traps of the single tide events would have collected a different sediment amount compared to the traps that were submerged for the whole four tide events.

The tidal flat of Converse (Bay of Fundy) presented rates of sedimentation that range from 3.8 to 703 g/m$^2$ per tide (average of 154.3 g/m$^2$ per tide), which have accumulated during 1 and 3 hours of submersion (Tab. 15). The salt marsh of Eldriken and the external part of the Halfway River (Minas Basin) presented similar rates (Fig. 51a, 51b), ranging from 25 to 1100 g/m$^2$ per tide (Eldriken: average of 230.4 g/m$^2$ per tide; Halfway River (Minas Basin): average of 431.1 g/m$^2$ per

tide). Lower values are found inside the Halfway River, which values range from 69 to 600 g/m$^2$ per tide (average of 197.7 g/m$^2$ per tide) (Tab. 16).

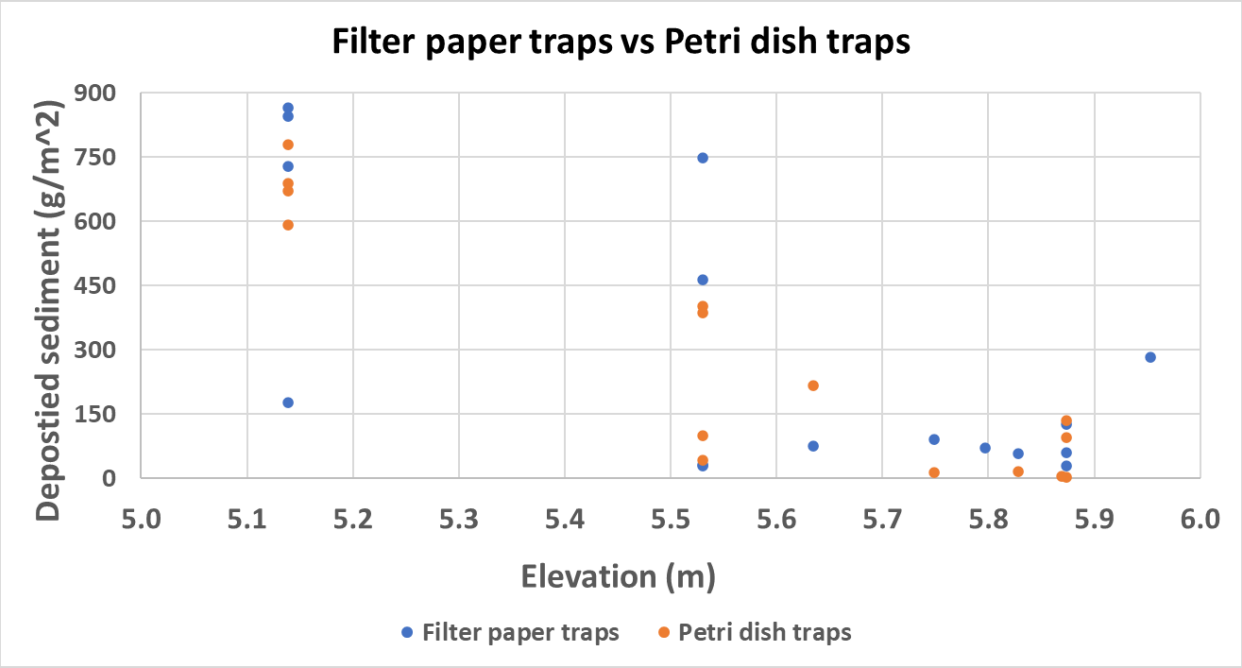


***Figure 50*** *– Comparison between filter paper traps and Petri dish traps from the case study of Converse.*

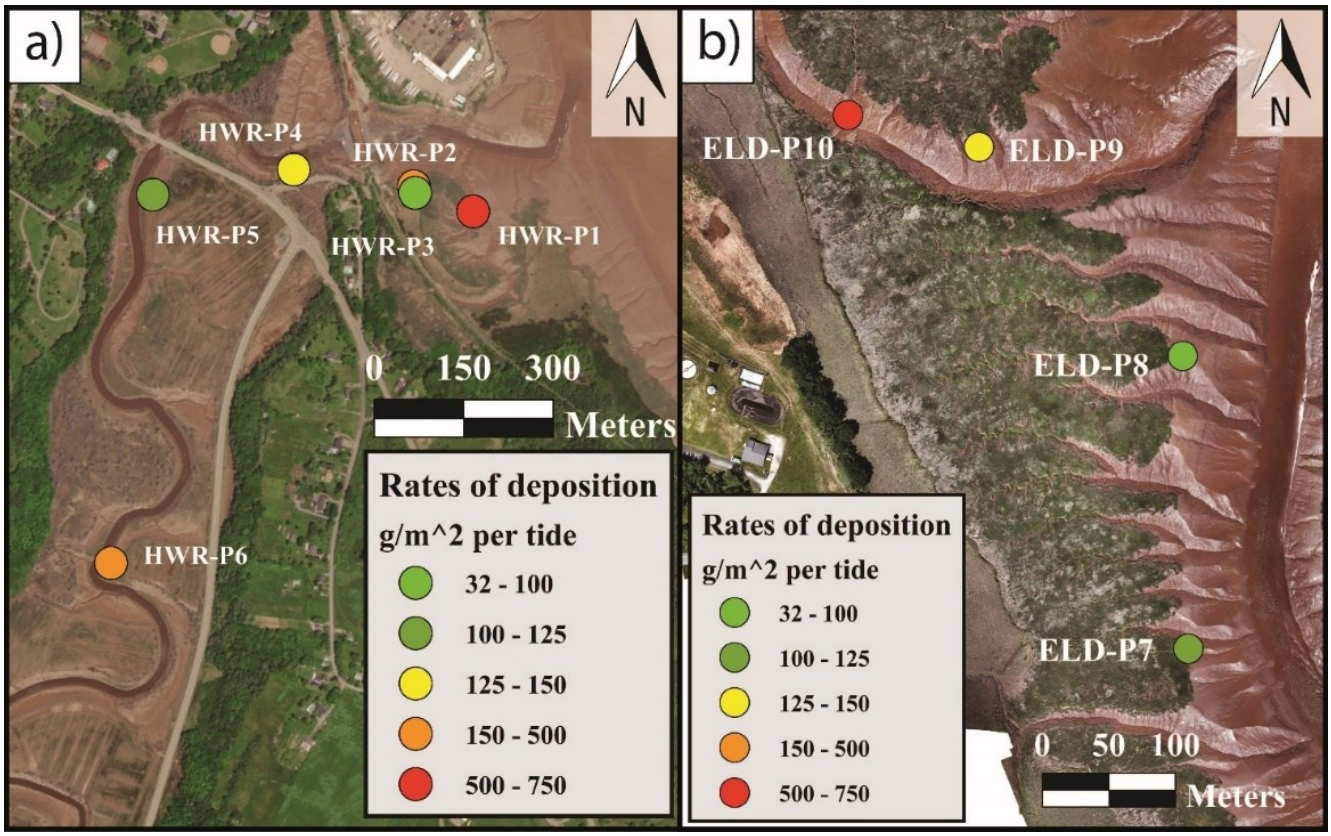


***Figure 51*** *– Rates of deposition of: (a) Halfway River, where P1-P1-P3 are located outside the river system; and (b) Eldriken*

***Table 15*** *– Deposited sediment and rates of deposition of Converse (Bay of Fundy).*

| Survey | ID | Weights | Avg. Weight | Average g/m$^2$ per tide | Average submersion period (hours) | Total submersion period (hours) |
|---|---|---|---|---|---|---|
| **July 2021 (3 days)** | RS1 | 54.77<br>46.28<br>25.83 | 0.300 | 42.29 | 1.96 | 7.82 |
| | RS2 | 227.29<br>267.90<br>252.41 | 1.765 | 249.20 | 2.30 | 9.21 |
| | RS3 | 673.84<br>708.12<br>726.46 | 4.979 | 702.80 | 2.65 | 10.58 |
| | RS4 | 82.66<br>124.02<br>101.58 | 0.728 | 102.76 | 1.82 | 7.28 |
| | RS5 | 372.09<br>333.02<br>579.07 | 3.033 | 428.06 | 2.23 | 8.91 |
| | RS6 | 85.99<br>72.33<br>91.55 | 0.590 | 83.29 | 2.03 | 8.13 |
| | MH 01 | 159.05<br>145.71<br>137.22 | 1.044 | 147.33 | 1.98 | 7.93 |
| | MH 03 | 21.13<br>33.66<br>30.75 | 0.202 | 28.51 | 1.98 | 7.93 |
| | MH 05 | 1.33<br>6.20<br>3.73 | 0.027 | 3.75 | 1.57 | 6.28 |

| | | | | | | |
|---|---|---|---|---|---|---|
| | MH 09 | 3.16<br>6.48<br>5.33 | 0.035 | 4.99 | 1.45 | 5.82 |
| | MH 11 | 155.22<br>120.73<br>158.00 | 1.025 | 144.65 | 2.14 | 8.55 |
| | MH 13 | 97.69<br>96.36<br>98.18 | 0.690 | 97.41 | 1.94 | 7.76 |
| | MH 17 | 99.02<br>116.75<br>107.81 | 0.764 | 107.86 | 2.08 | 8.30 |
| | MH 2A | 15.35<br>20.80<br>16.73 | 0.125 | 17.63 | 1.75 | 6.98 |

***Table 16*** *– Deposited sediment and rates of deposition of Halfway River and Eldriken (Bay of Fundy).*

| **Survey** | **Study site** | **ID** | **Weights** | **Avarage Weight** | **Average g/m² per tide** | **Average g/m² per tide (study site)** |
|---|---|---|---|---|---|---|
| **August 2021 (2 days)** | Halfway River (Minas Basin) | HWR -P1 | 7.133<br>16.175<br>8.574 | 10.63 | 750.02 | 431.13 |
| | | HWR -P2 | 4.690<br>10.198<br>5.076 | 6.65 | 469.66 | |
| | | HWR -P3 | 1.146<br>0.833<br>1.154 | 1.04 | 73.70 | |
| | Halfway River | HWR -P4 | 1.870<br>1.757<br>1.832 | 1.82 | 128.41 | 197.75 |

| | | | | | | |
|---|---|---|---|---|---|---|
| | (Internal part) | HWR -P5 | 1.378<br>1.483<br>0.984 | 1.28 | 100.93 | |
| | | HWR -P6 | 1.402<br>6.007<br>8.506 | 5.30 | 374.40 | |
| | Eldriken | ELD-P7 | 2.040<br>1.595<br>1.592 | 1.74 | 122.96 | 230.35 |
| | | ELD-P8 | 0.453<br>0.539<br>0.361 | 0.45 | 31.81 | |
| | | ELD-P9 | 1.800<br>1.943<br>2.055 | 1.93 | 136.38 | |
| | | ELD-P10 | 7.442<br>9.966<br>9.383 | 8.93 | 630.26 | |

### *6.4.2 Volumes and vertical changes of the tidal flat of Converse*

The RMSE values calculated from all the products are about ~0.03 m, which generates an error propagation of 0.04 m. Based on these results, the TCD chosen for the DoDs is 0.05 m. The differences between the calculations using no TCD and 0.05 m of TCD are highly restrained. Based on the results, the tidal flat was subjected to highly different rates of vertical changes throughout the study area.

During the first year (i.e. July 2019 – August 2020) the tidal flat was subjected to an erosional trend, with an average vertical variation of -2 cm (without TCD) and -4 ±4 cm (with TCD) (Fig. 52a). Consequently, the sediment loss was about 1300 $m^3$ (without TCD) and 860 ±800 $m^3$ (with TCD) (Fig. 53a). Most of the erosion focused inside the main channels, in particular next to the inlet where erosion reached values around 1 to 3 meters. Accretion focused in two zones: next to the

eastern channel bifurcation and inside the northern-eastern zone where accretion reached values higher than 10 cm.

A completely opposite trend is visible during the second year (i.e. August 2020 – July 2021). Strong accretion occurred throughout the whole area, with an average vertical change of 3 cm (without TCD) and 9 ±5 cm (with TCD) (Fig. 52b). Erosion is mostly absent, except for the inlet area which is still under strong erosion of more than 1 meter. The northern-eastern area presented trends that reached 18 cm of accretion. The sediment budget is positive with 2500 $m^3$ (without TCD) and 1900 ±1000 $m^3$ (with TCD) (Fig. 53b).

The sediment budget for the whole two years period (i.e. July 2019 – July 2021) is about 1550 $m^3$ (without TCD) and 1500 ±1200 $m^3$ (with TCD), suggesting that a positive trend is ongoing (Fig. 53c); however, the erosional and accretional trends seem to be relatively balanced. In fact, the average vertical changes are about 2 cm (without TCD) and 5 ±4 cm (with TCD) (Fig. 52c). Overall, the highest rates were found mostly in the eastern part of the study site, which is the lower zone (i.e. 5.1 – 5.8 m above m.s.l.) and next to the creeks. Vice versa, the western zone was characterized by lower rates, far from the creeks.

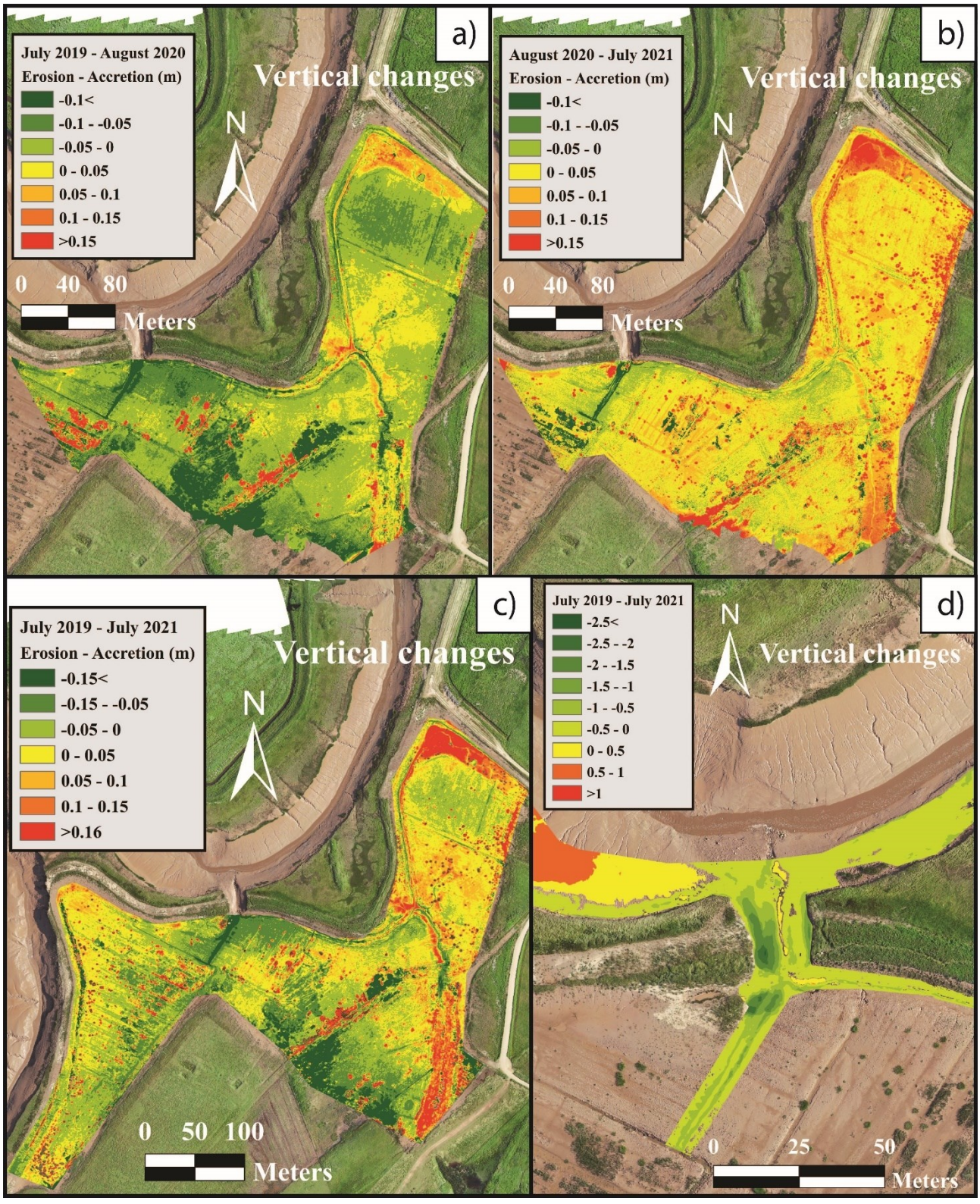


***Figure 52*** *– Vertical variations of the study area: (a) from July 2019 to August 2021, (b) from August 2020 and July 2021, and (c) the whole study period, from July 2019 to July 2021. The calculations of (a) and (b) have a lower extension because the DSM of 2020 covers the central-eastern area of the tidal flat only. Note that the DSMs shown in these figures were not filtered, hence the red dots represent patches of vegetation. (d) Vertical variations of the inlet area, the channels, and the nearby areas from July 2019 and July 2021.*

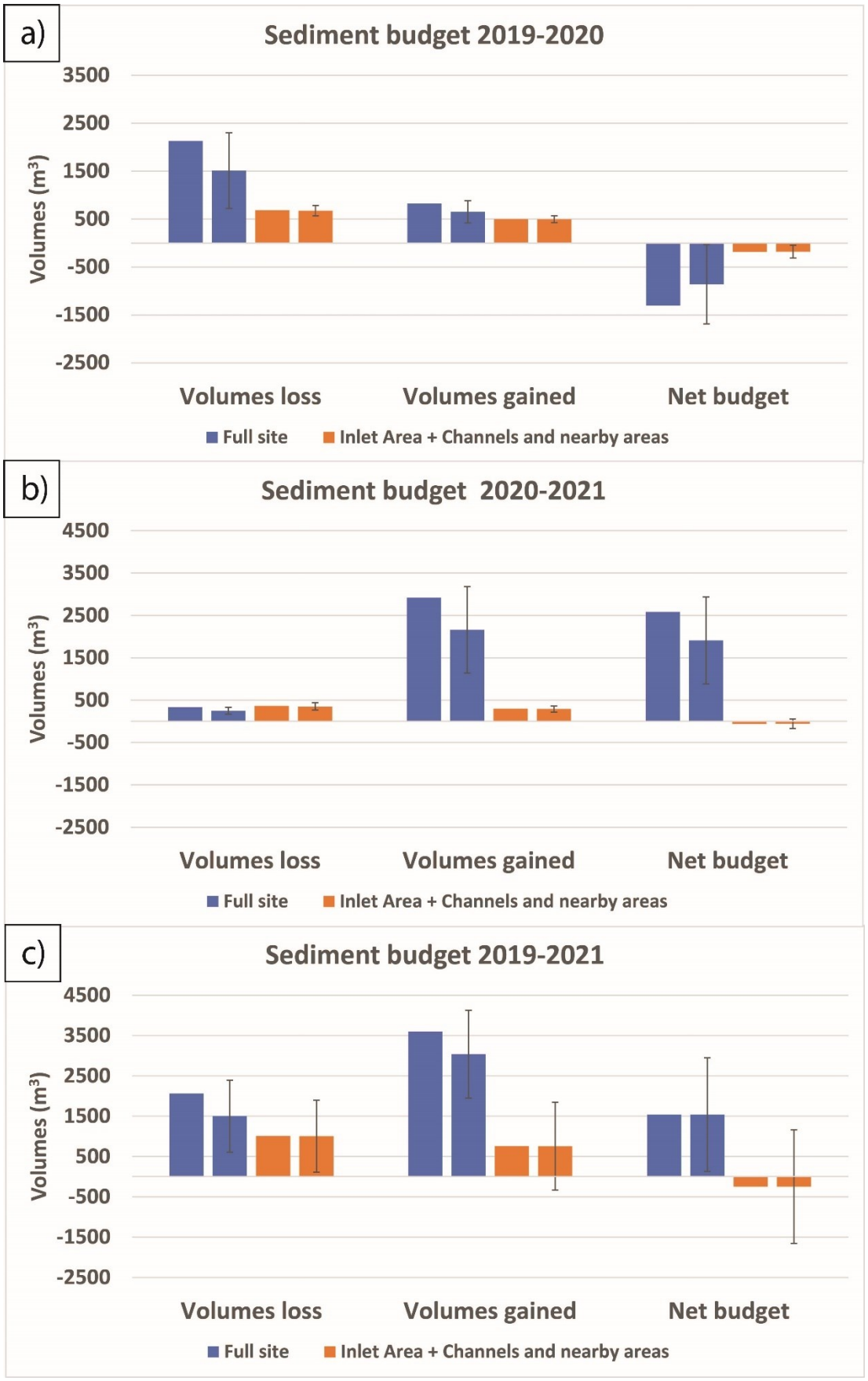


***Figure 53 –*** *Sediment budget calculated from (a) July 2019 to August 2020, (b) August 2020 to July 2021, and (c) the whole study period, from July 2019 to July 2021.*

*Inlet morphology*

The inlet underwent strong erosion since the breach of 2018. Between July 2019 and August 2020, the inlet was strongly eroded on the west side with rates of vertical changes that reached 2 m of erosion (Fig. 52d). The inlet became deeper and larger as well, extending for 4 m westward. The average vertical variations inside the inlet were about -50 cm (with TCD), with basically no accretion and a volume loss of 400 $m^3$. Erosion decreased during the second year (i.e. August 2020 – July 2021) to 150 $m^3$ and presented vertical variations of -20 cm; it is still focused on the west side and it is the dominant trend.

However, the external zones located inside the Missaguash river did not present only erosional trends. The western portion with respect to the inlet was characterized by accretion during both periods (i.e. 2019-2020 and 2020-2021) with an accretion rate that reached 45 cm/year; on the other side, the eastern part was under erosional trends, with rates of -50 cm/year. In this case, the volumes that were eroded and the volumes that were deposited are similar during both periods.

### *6.4.4 Granulometric distribution*

The particle size analysis showed that all samples from all sites of the Bay of Fundy are mainly composed of Silt (~85 - 90 %) (Fig. 54a). The sandy component is absent, except for one sample located inside the Halfway River (12% of sand) (Fig. 54b). Based on Stevens, (1983), the granulometric classes are mostly Clayey Silt. Although the coarser sediment was located on the lower surfaces and the clayer sediment on the highest, the granulometry of the sediment collected at the site of Converse is homogeneous and no variation of granulometry was detected during each tide. The site of Eldriken presented a similar granulometry as the Converse study site; on the other hand, the coarser sediment was located in the site of Halfway River only, in particular inside the river, rather than in the basin.

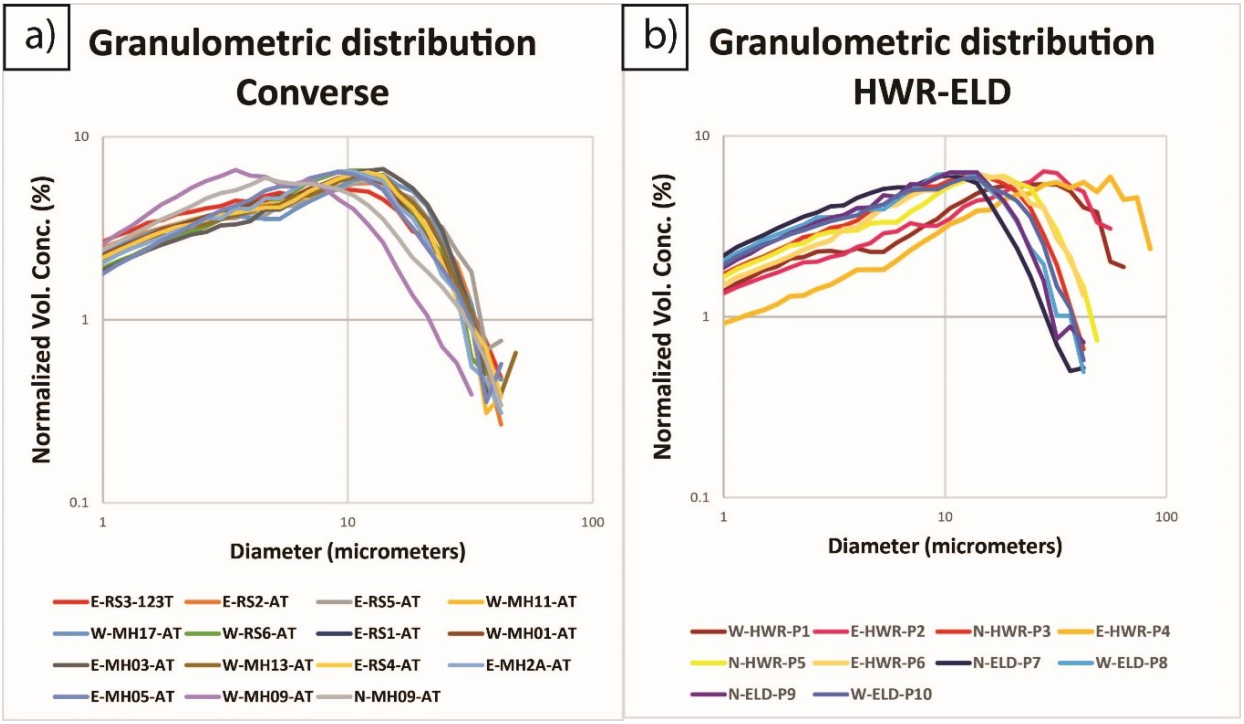


***Figure 54*** *– Granulometric distribution of (a) the site of Converse and (b) the site of Halfway River and Eldriken.*

## *6.5 Discussion*

### *6.5.1 Sediment deposition*

Although sediment deposition in the Bay of Fundy is generally high compared to worldwide intertidal areas, the Converse study site experienced short-terms high rates of deposition and rates of accretion compared to other coastal wetlands located nearby (i.e. average 150 g/m$^2$ per tide, ~10 cm/year). For example, lower rates of deposition (i.e. between 10 – 150 g/m$^2$ per tide) are found in the low marsh of Allen Creek (Fig. 55a), which is located in the same basin as the study site of Converse (van Proosdij et al., 2006) within similar elevation above m.s.l.. This difference in sedimentation might be due to the location of the sediment plume in the Cumberland basin, since the western section (i.e. Converse area) is commonly characterized by higher suspended sediment concentrations compared to the eastern side (Amos and Tee, 1989). Furthermore, Allen Creek is a marsh, which means that vegetation should increase deposition (Mudd et al., 2010) and it is directly connected with the estuary, which implies other factors that alter deposition, such as wave interaction and different tidal currents. Although these differences, this outcome seems unusual, suggesting that a local extra budget could be added to the sediment

input that derives from the suspended sediment; this interpretation is discussed in the following paragraph (6.5.2).

The Minas Basin showed similar rates as well. The external part of Halfway River and the Eldriken site are both low marsh environments subject to strong sedimentation, in particular Eldriken; in this case, the cause is highly related to the presence of the railway that stops the sediment path, forcing deposition (Daborn et al., 2002). It is interesting to note that all study sites experienced a decrease in deposition as elevation increases (Pethick, 1981), except the internal part of Halfway River (Fig. 55b), where the rates seem homogeneously constant. This behaviour enhances how the construction of the causeway changed the sediment transport, which is not following a regular trend of deposition.

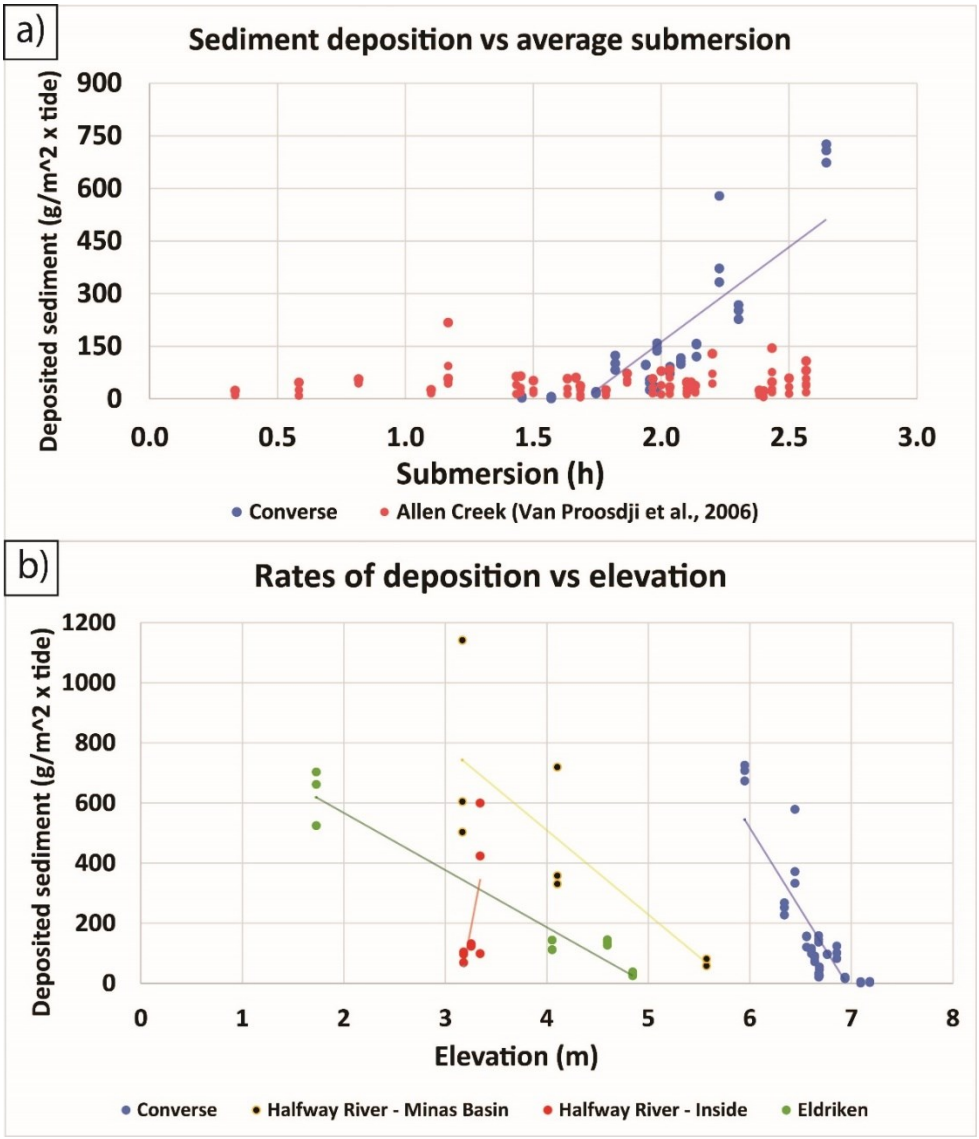


***Figure 55*** *– (a) Rates of deposition of all study sites in comparison to the elevation; (b) Comparison between the rates of deposition and the submersion period of the tidal flat of Converse.*

### *6.5.2 Morphological evolution of the tidal flat of Converse*

It is evident the difference between the first year results compared to the second year results. The first year is characterized by general erosion and sediment loss, while during the second year the trend inverts. However, it is plausible that the DSM of 2019 overestimates the actual surface of the tidal flat and underestimates deposition. In fact, after the opening, the tidal flat was an agricultural field characterized by inland plants; although they died during the salt water inundations, most of the old patches did not disappear completely and some have created several small domes of sediment and vegetation that increase the real surface of the tidal flat. During the fieldwork, most of these domes were visible in the western area of the site. In time, the patches have been consumed, lowering the elevation of certain areas. This process might have caused the first DSM of 2019 to overestimate the elevation and consequently to underestimate the vertical variations of the first year. This hypothesis could explain the balance between accretion and erosion at the end of the first two years, despite the high range of volumes and vertical variations. Since the DSM of 2020 is less influenced by vegetation, the calculations from 2020 to 2021 can be considered more reliable, despite it concerns the central-eastern area only (i.e. 60000 $m^2$ against 84000 $m^2$) and new patches of marsh plants have grown.

Overall, the tidal flat of Converse is under strong sedimentation and the vertical changes enhanced by the DSM analysis agree with the distribution of the rates of sediment deposition. It is important to note that the higher rates of accretion are located near the creeks in the most distant and lower zones of the tidal flat, which are mostly on the eastern side of the study area; instead, a strong erosional trend is occurring next to the inlet that connects the study site with the Missaguash River; erosion is also visible in the central channel. Although sedimentation is generally lower inside the creeks and higher next to the creeks of a developed marsh (D'Alpaos et al., 2006), sedimentation of this study site is higher inside the most distant portions of the creeks, similarly to other young tidal flats (e.g. Perkpolder (Brunetta et al., 2019)). This behaviour was found inside the lower creeks of the site of Eldriken as well. Field observations confirm that the creeks were composed of highly soft and not consolidated mud. Since Converse is a restoration project, and the channels and the inlet are man-made structures, this behaviour could be related to a morphodynamical disequilibrium between the tidal currents and the tidal flat, which means that the inlet and the channel will continue to be eroded until they reach a stable condition. Erosion is still undergoing after 2 years; however, the rates of vertical changes highly decreased during the second year (i.e. from 400 to 150 $m^3$, and from -50 cm to -20 cm), indicating that the inlet is slowly

reaching the equilibrium. Besides the high influence of the sediment concentration transported by the tide, the strong inlet erosion and the strong deposition suggest that deposition could be increased by a cannibalization process. In fact, in fact, the eroded sediment of the inlet could be transported by the flood tide, increasing the rates of accretion. During the whole period, the inlet itself (i.e. without considering the nearby areas and the channels) lost 600 $m^3$; if the nearby areas (i.e. channels and the external part of the Misseguash river) is considered, the whole sediment loss is about 1000 $m^3$. Assuming that the whole sediment eroded by the inlet and nearby areas was deposited inside the tidal flat and considering that the whole study period was subjected to a total gain of 1500 $m^3$, the erosion of the inlet could have supported from 36 % (considering the inlet area only) till 65% (considering also the nearby areas) of the whole budget of the system. However, it is important to remember that the DSM of 2019 is less reliable. Considering the period from August 2020 to July 2021, the inlet loss corresponds to 360 $m^3$, while the net gain of the whole tidal flat is about 2800 $m^3$. In this case, the budget received by the inlet to the system would be 14%. It is difficult to clearly state the proper sediment amount provided by the inlet erosion.

### *6.5.3 Future evolution of the salt marshes*

Only two species prevail in the marsh of Eldriken, which are *Spartina alterniflora* (the most common pioneer plant) and *Spartina patens*. The DSM of Eldriken showed that *Spartina* is located between ~4.5 and ~5.7 m above m.s.l., which values are confirmed by Porter et al. (2015). The strong deposition inside the creeks and the presence of two species only suggest that despite the Eldriken (and the Windsor system) being older than 50 years, it is still behaving like an unstable young tidal flat that is still building up and needs to develop diversification between species; for example, differences in community structures are found in realigned marshes by Mossman et al., (2012). Sedimentation inside the Halfway River is comparable with the other study sites (i.e. 197.7 $g/m^2$ per tide), probably because the traps were located next to the creeks; however deposition is lower than the outer zone (i.e. 431.1 $g/m^2$ per tide) and field observations make notice that vegetation is suffering the limited tidal range, due to the new causeway. As shown, the rates of deposition of the sites of Halfway River and Eldriken are higher than the site of Converse; despite the differences in suspended sediment concentrations, this difference could be caused by a difference in elevation, in fact, the Minas Basin sites are located below the MHT (5.7 m above m.s.l. in Hantsport), which increases the submersion period and deposition, while the site of Converse is located above the MHT (>4.8 m above m.s.l. in Hopewell Cape). The granulometry of the study sites follows the characteristics of the basin (i.e. coarser sediment in the Minas Basin,

finer sediment in the Cumberland Basin (Chmura et al., 2001)) confirming their origin. The sandier content of Halfway River suggests that it is subjected to stronger currents flood, probably induced by the causeway, compared to the outer zone of the basin. It is important to state that two years after the opening, vegetation manifested and several patches developed around the tidal flat. Since the MHT is about 4.8 m above m.s.l. and the average elevation of the tidal flat is around 5-6 m above m.s.l., the surface is located above the common level of marsh developing, from a morphological point of view. In fact, a salt marsh develops when the surface of the tidal flat reaches the MHT (De Vlas et al., 2013; Bakker, 2014), or is slightly lower for pioneer plants. This observation indicates that the tidal flat could be covered by pioneer plants after a few years.

## *6.6 Conclusions*

This study describes the sedimentological characteristics of three young wetland environments located in the Bay of Fundy (Eastern coast of Canada). A field campaign was carried out between 23 and 26 of July 2021 and a series of surveys that include sediment traps, ADCP, and UAV (then combined with granulometric analysis) allowed to investigate the recent evolution of the tidal flat of Converse, which is a restoration project that developed after the breach of the dike in the Missaguash River after 2018 (Cumberland Basin, northern side of the Bay of Fundy). Sediment traps and granulometric analysis were carried out in the study site of Halfway River and Edriken as well, both located in the Minas Basin (southern side of Bay of Fundy), between 10 and 13 of August 2021. All study sites were subject to high rates of deposition, prevalently characterized by a high silt content. The tidal flat of Converse experienced rates from 3.8 to 703 $g/m^2$ per tide (average of 154.3 $g/m^2$ per tide); these are in agreement with the vertical changes, which can reach more than 10 cm/year in the lower zones. Although the coarser silt was mostly located in the lower zones and the clayer content was located in the higher zone, no remarkable variation in granulometric distribution was found and no variation was found between single tidal events. The sediment budget for the whole study period is positive (i.e. about 1550 $m^3$) with an average vertical variation of about 2 – 5 cm/year. A strong erosional trend was found next to the inlet and inside the central channel (>1 m/year), while strong deposition occurred in the most distant areas (>10 cm/year); this behaviour suggests that the tidal flat needs to find a morphodynamic equilibrium and a cannibalization process might be ongoing, causing an increase in sedimentation inside the tidal flat.

Assuming that the whole sediment eroded by the inlet and nearby areas was deposited inside the tidal flat the erosion of the inlet could have supported from 14 to 36 % (till 65% considering also the nearby areas) of the whole budget of the system. The Minas Basin sites experienced rates between 230.4 g/$m^2$ per tide (Eldriken) and 431.1 g/$m^2$ per tide (outside Halfway River). However, the internal part of Halfway River collected lower values (197.7 g/$m^2$ per tide) with a coarser sediment content (slightly sandier); this behaviour was caused by the recent closure of the causeway that has reduced the tidal range and, as a consequence, the submersion period and the sediment transport. The Eldriken marsh is accreting inside the creeks as well, suggesting that after more than 50 years the marsh is still behaving like an unstable young tidal flat that is building up.

# *7. Evolution of coastal wetlands restoration projects: natural vs artificial tidal flats*

## *7.1 Introduction*

The practice of restoring lost or endangered ecosystems and services is a policy that has been carried out worldwide in recent decades (Masselink and Lazarus, 2019); the methods vary case-by-case basis. For what concerns coastal wetlands, the final aim is to obtain a salt marsh, which means to vegetate a pre-existing or newborn tidal flat. Vegetation survival is strongly dependent on the hydroperiod (French, 1993; Cahoon and Reed, 1995) which is in agreement with the elevation above m.s.l., in particular with reference to the MHT (De Vlas et al., 2013; Bakker, 2014). The most common strategy is to allow the sea water to submerge continental areas in order to restore coastal wetland environments (e.g. van der Deijl et al., (2018), Brunetta et al., (2019)). In most cases, this strategy necessarily needs a sediment income that enable the system to develop vegetation and cope with Sea Level Rise. This method consists in opening new connections between the sea and the inland or between a deltaic system in order to improve water circulation. However, the knowledge regarding the evolution of this young environments is still limited, in particular due to the small number of case studies and their youth.

In this study, three sites characterized by three different tidal regimes were investigated in order to determine their short-term morphological and sedimentological evolution, defining the differences and similarities of their trends. The case studies are: i) the tidal flat of the Barbamarco lagoon (Po River Delta, Italy) with a microtidal range; ii) the tidal flat of Perkpolder (The Netherlands) with a macrotidal range; iii) and the tidal flat of Converse (Bay of Fundy, Canada) with an ultratidal range. Despite these sites are located in highly different geographic areas characterized by diverse climate conditions, biological factors, and entity of the processes, they have a common origin; in fact, all sites are young tidal flats (i.e. few years since their birth) that developed after human interventions, specifically after a “breach”, which can be a dyke breach or a channel excavation; in short, a new connection between the study area and the sediment supplier is able to bring a high amount of sediment inside an area that previously was not a tidal flat (e.g. Cox et al., 2022). Besides, the sites have several environmental conditions in common, such as the absence of vegetation, highly reduced wave interaction, and a strong sedimentary input. The principal aims of this study are: i) to understand how the artificial structures (i.e.

channels and inlets) of restoration projects influence their evolution in comparison with natural or low human-influenced tidal flats; ii) to discuss how sediment deposition and accretion change in these artificial flats; iii) to discuss how fast a restoration project can reach its goal, which is the development of a salt marsh.

## *7.2 Study sites*

### *7.2.1 Barbamarco lagoon (Po River Delta, Italy)*

The Po Delta (Italy) is a microtidal deltaic system characterized by a mixed, mostly semi-diurnal, tide with an average spring-tidal range of about 0.5 m. Its evolution was highly influenced by both natural and anthropic processes (Bondesan et al., 1990; Cencini, 1998; Simeoni and Corbau, 2009), in particular, after the the "Porto Viro" bypass, a heavy human intervention made under the Venetian Republic in 1604, that diverted the delta to the current location (Stefani and Vincenzi, 2005) and making it one of the largest anthropic deltas in the world (Maselli and Trincardi, 2013). Strong erosion occurred between the 1930s-1940s and the 1970s-1980s, caused by heavy flooding and human interventions (e.g., dam construction, resource exploitation, agricultural reduction, etc. (Billi and Fazzini, 2017)), until 2010 when the trend reversed and now the delta is under progradation (Ninfo et al., 2018, Bezzi et al., 2021).

The Po Delta, which extends for 691 $km^2$ along 90 km of coastline (Fig. 2a, 4c), has five principal branches (from north to south, Po di Maistra, Pila, Tolle, Donzella or Gnocca, and Goro). The study case is located in the Southernmost part of the Barbamarco lagoon, which extends between the central branch of the Po della Pila and the Po di Maistra. The tidal flat is an ~8 ha young tidal flat that has been developing during the last 20 years after two channels were dug in order to connect the harbours of Pila. Both channels are separated from the tidal flat by the presence of wild reeds that have been established on the channels levees; two inlets on the east channel and one on the west channel connect the river to the flat. The study area is highly dependent on river floods, which caused several crevasse splays that originate from the inlets that connect the channels to the Barbamarco Lagoon (Brunetta et al., 2021).

### *7.2.2 Perkpolder (The Netherland)*

The tidal flat of Perkpolder is part of a restoration project located in the Scheldt estuary (province of Zeeland, The Netherlands) which aims to restore the natural wetlands and develop recreational

facilities in order to prompt the socio-economic development of the area (Fig. 2b, 36d). The estuary, characterized by a length of 355 km from source to mouth and a total catchment area of 22000 km², is characterized by a tidal range that varies from about 3.8 meters at Vlissingen (at the mouth) to about 5.2 meters at Antwerp (78 km upstream). However, the study site is macrotidal with a mean Spring tidal range of the study area is about 5 meters (Claessens and Belmans, 1984).

The tidal flat was born in June 2015, after 75 ha of agricultural fields were submerged by the salt water of the Western Scheldt. The water exchange is provided by the opening of an inlet of about 300 m that connects the tidal flat with the estuary, while two artificial creeks of about 40 meters in width and a total length of about 800 m were dug to facilitate water distribution. The location of the tidal flat is particularly convenient from a sedimentological point of view thanks to its proximity to the turbidity maxima caused by the mix of strong tidal currents and riverine water masses, as well as residual currents, that increase the residence time of the suspended material (Chen et al., 2005).

### *7.2.3 Converse (Bay of Fundy, Canada)*

The third study site is located in the northern basin of the Bay of Fundy (East coast of Canada), specifically in the Tantramar Marsh system, next to the Cumberland Basin (Fig. 2c, 47c). A semi-diurnal ultratidal range of about 14 m characterizes this large basin of about 118 $km^2$; the western side is generally subjected to higher sediment concentration compared to the eastern side (Amos and Tee, 1989) with an average of ~0.3 g/L, mostly composed of coarse silt (van Proosdji et al., 1999). The Tantramar marsh system is located on the western side of the basin, between the provinces of New Brunswick (NB) and Nova Scotia (NS), and it is composed of 230 ha of marshes, rivers, and lakes. The increasing marsh loss and the erosion of dykes lead to the development of restoration projects, such as in the Missaguash River, which is one of the large tidal rivers that divides the two provinces. The project under investigation, known as the Converse Marsh, was carried out in order to restore the historical salt marsh and increase the sustainability of dyke infrastructure since the strong erosion is threatening the near transportation route of Fort Lawrence Road and the adjacent Parks Canada property. The design of the management realignment included artificial channels and the breaching of the dyke, likewise for other restoration projects (e.g. van der Deijl et al., (2018), Brunetta et al., (2019)). The site was opened in 2018 and the evolution of the tidal flat was monitored since.

## *7.2 Methodology*

The data used in this study derive from the previous investigations carried out in the listed areas.

### *7.2.1 Po River Delta (Italy) and the Converse tidal flat (Canada)*

For what concerns the tidal flat of the Barbamarco lagoon (i.e. Po Delta, Italy), the dataset and the results that were used in this chapter are referred to chapter 2, 3, and 4. Specifically, the results and the interpretations that were obtained from DSMs analysis (between October 2018 and February 2020), granulometric analysis (from May 2019), sediment deposition analysis (between September 2019 and March 2021), and the historical review.

As for the Italian study site, the results and the interpretations concerning the restoration project of Converse (Canada) are referred to chapter 6. They include the volumes and the analysis of the vertical changes obtained through DSM analysis (between July 2019 and July 2021), the rates of deposition calculated through sediment traps (July 2021), and the granulometric analysis (July 2021).

### *7.2.2 Perkpolder (The Netherland)*

The analysis carried out at the study site of Perkpolder are described in Chapter 5. However, in order to compare the rate of deposition, the tide gauge of Walsordeen was obtained and the submersion period was calculated per each trap. As for Chapter 3, the rates were calculated as $g/m^2$ per tide. Note that these calculations are not discussed in Chapter 5 because the tidal record was not available before the publication.

Further datasets were used to improve the results and the interpretation of the previous chapter. The study area is extended to the whole restoration project and the areas in front of the inlet which are part of the Scheldt Estuary.

Two DSMs with a resolution of 2 x 2 m produced in June 2015 (the opening of the inlet) and in February 2017 were provided by the Dutch Ministry of Infrastructure and Environment (Rijwaterstaat); these two DSMs cover the internal areas of the system, which can be divided into two main zones: the proper tidal flat, which covers the southern part, and the pond, which is in front of the inlet (Fig. 56). In order to study the external area nearby the inlet, a series of multi-beam datasets were obtained from surveys undertaken by Rijkswaterstaat. Based on the analysis

of chapter 5, three DSMs out of seven were chosen (i.e. June 2015, April 2016, and January 2017) since these represent the most significant periods with the most important morphological changes; the Multibeam DSMs have a resolution of 1 x 1 m. The Geomorphic Change Detection (GCD) tool of Wheaton et al. (2010) was used for analysing the volumes variations; the study area was divided into four zones, based on the morphological characteristics (Fig. 56): i) Zone 1 – the proper tidal flat located in the southern part, ii) Zone 2 – the pond, which is on the west side of the inlet, iii) Zone–3 - the area located nearby the inlet, and iv) Zone 4 – which comprises the nearby areas of the inlet and the eastern external part. Based on the data available and the most relevant morphological changes, the time intervals chosen are: i) from June 2015 to April 2016, ii) from April 2016 to February 2017, and iii) from June 2015 to February 2017. As explained in chapter 5, since the point cloud of the DSMs was not supplied and the vertical accuracy could not be undertaken, several calculations were made considering different thresholds of detection (TCD) that allow to ignore variations that are considered meaningless. The most suitable thresholds chosen for the analysis are the same as in chapter 5, which are 0 m, 0.05 m, 0.1 m, and 0.15 m (Duo et al., 2021).

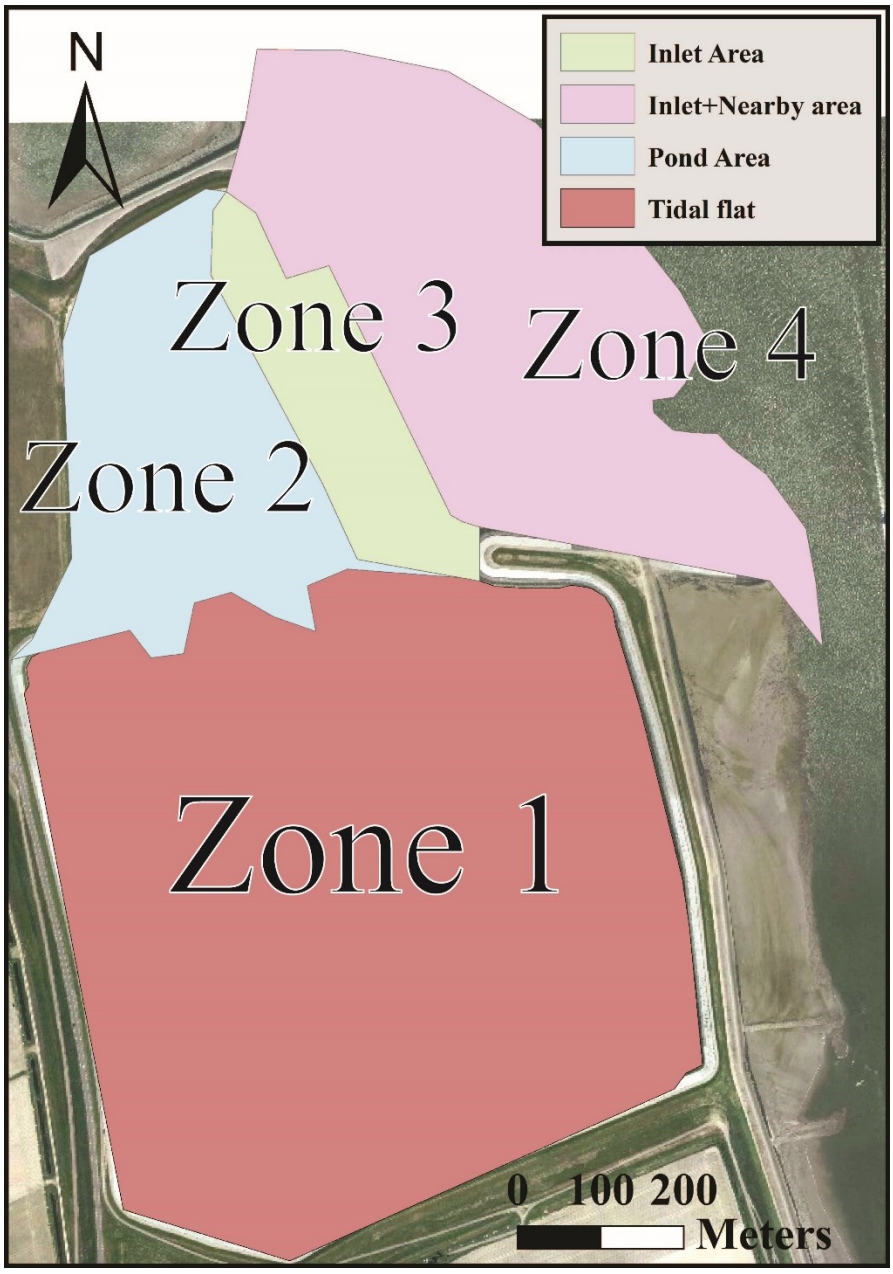


***Figure 56 -*** *Division of the morphological relevant areas in the restoration project of Perkpolder. Zone 1 represents the proper tidal flat; Zone 2 concerns the pond that connects the inlet with the tidal flat; Zone 3 regards the inlet area only; and Zone 4 concerns the inlet area and the external nearby areas.*

### *7.2.2 Tide gauge analysis and pioneer vegetation*

For each study site, the Mean High Tide (MHT) and the tidal range were calculated using annual tidal records retrieved from the nearest station: i) for the tidal flat of the Barbamarco lagoon, the tide gauge of Porto Garibaldi was chosen (coordinate system: WGS84 – UTM 33N; vertical datum: ETRF2000; see 4.3.2); ii) for the Perkpolder basin, the tide gauge of Walsordeen was chosen (Coordinate system: Amersfoort/RD new, vertical datum: NAP (Normaal Amsterdam Peil); iii) for

the tidal flat of Converse, the tide gauge of Hopewell Cape was chosen (Coordinate system: NAD83 (CSRS) UTM Zone 20N, vertical datum: CGVD2013; see 6.3.1).

A qualitative analysis of the distribution of the pioneer vegetation was carried out through GPS analysis and literature review in order to understand the spatial and vertical distribution of the early plants that cover the tidal flats, specifically the *Spartina* Spp. . *Spartina maritima* distribution was measured through GPS-RTK surveys in the Barbamarco lagoon (see 4.3.3). The Perkpolder and the Converse restoration projects did not present sufficient patches of vegetation, hence, literature research was carried out and, for the Canadian site, a DSM product that represents the morphology of the marsh of Eldriken (i.e. a southern study site compared to Converse) was investigated in order to measure the distribution of *Spartina alterniflora* (see 6.3.2).

## *7.3 Results*

### *7.3.1 Deposition and accretion of young tidal flats*

*Barbamarco lagoon (Po Delta)*

The tidal flat of the Barbamarco lagoon presented highly variable rates of accretion and deposition depending on the seasonality. The rates varied from ~ -2 cm/year (i.e. erosion) during spring-summer, to + 4.8 cm/year after the flood of November 2019; however, the average rate of vertical changes is 1.3 cm/year. Similarly, the average rate of deposition during the autumn-winter seasons is about 19 g/m$^2$ per tide and 67 g/m$^2$ per tide during the summer season. The average between all the traps from all the surveys carried out in the lagoon showed a total average sedimentation of 36.4 g/m$^2$ per tide; the average submersion period for all traps varies from 3.67 to 25 hours. In all surveys, sedimentation increases moving from the most elevated areas to the most depressed; no strong influence caused by other morphological structures (i.e. channels, inlets) has been observed. The rates of deposition and the vertical variations are discussed in detail in 2.4.5, 2.5.1, 3.4.2, and 3.5.2.

*Perkpolder (The Netherlands)*

The Perkpolder site (i.e. The Netherlands) was characterized by a wide range of rates of vertical changes. The overall average accretion during the first year after its opening was about 6 cm/year, and it slightly decreased to 5 cm/year during the second year. However, the most elevated areas (i.e. 0.5 m above m.s.l.) were characterized by lower rates of about 3.2 and 2.6 cm/year. Erosional

trends were visible in the areas nearby the inlet; strong erosion affected the area, enlarging and deepening the channels and the inlet itself, which after 8 months stopped its development. On the other hand, the internal areas were subjected to strong accretion, in particular inside the creeks, where the rates of vertical changes reached a maximum of 130 cm in 20 months. Although the rates of the Po Delta can reach comparable values with the tidal flat of Perkpolder (i.e. higher than 200 g/m$^2$ per tide), the macrotidal flat is subjected to higher average sedimentation of 64.1 g/m$^2$ per tide; the rates of deposition range from 2.3 to 265.5 g/m$^2$ per tide with a hydroperiod between 4 and 10 hours. As for the rates of vertical changes, deposition was higher inside and next to the creeks; in particular, it increased as the distance from the inlet increased, it decreased as the distance from the creeks increased, and as elevation increased. Detailed analysis can be found in 5.4.3 and 5.5.2.

*Converse (Canada)*

The highest range of deposition was found in the study site of Converse (i.e. Bay of Fundy, Canada), which experienced average rates of 154.3 g/m$^2$ per tide (from 3.8 to 703 g/m$^2$ per tide) during 1 and 3 hours of submersion. Similar to the Perkpolder tidal flat, the Converse tidal flat presented a generally positive trend of about 5 cm/year between August 2020 and July 2021; the most depressed areas next to the creeks are characterized by high rates of accretion higher than 10 cm/year. The inlet area is under a strong erosional trend, in particular, the inlet itself that is enlarging at a rate of 1 m/year and it has not found a morphodynamic equilibrium yet. More details can be found in 6.4.1, 6.4.2, 6.5.1, and 6.5.2.

The rates of deposition and the submersion period of the surveys of the study sites are shown in Fig. 57. The R values of the linear regression from all traps of the study sites are highly variable, depending on the site (from 0.7 for Converse to 0.2 for Perkpolder). Converse shows a high correlation between the sediment deposition and the submersion; however, Perkpolder is characterized by high dispersion and a low correlation. The traps from the Po Delta show an R of 0.5, but the values increase if traps from the same survey are chosen (R=0.6-0.8). In the case of Perkpolder, the R values are high only for the traps located in the most distant section with respect to the inlet (R=0.7) for both surveys; all the other sections have a low correlation between the sediment deposition and the submersion (R<0.2).

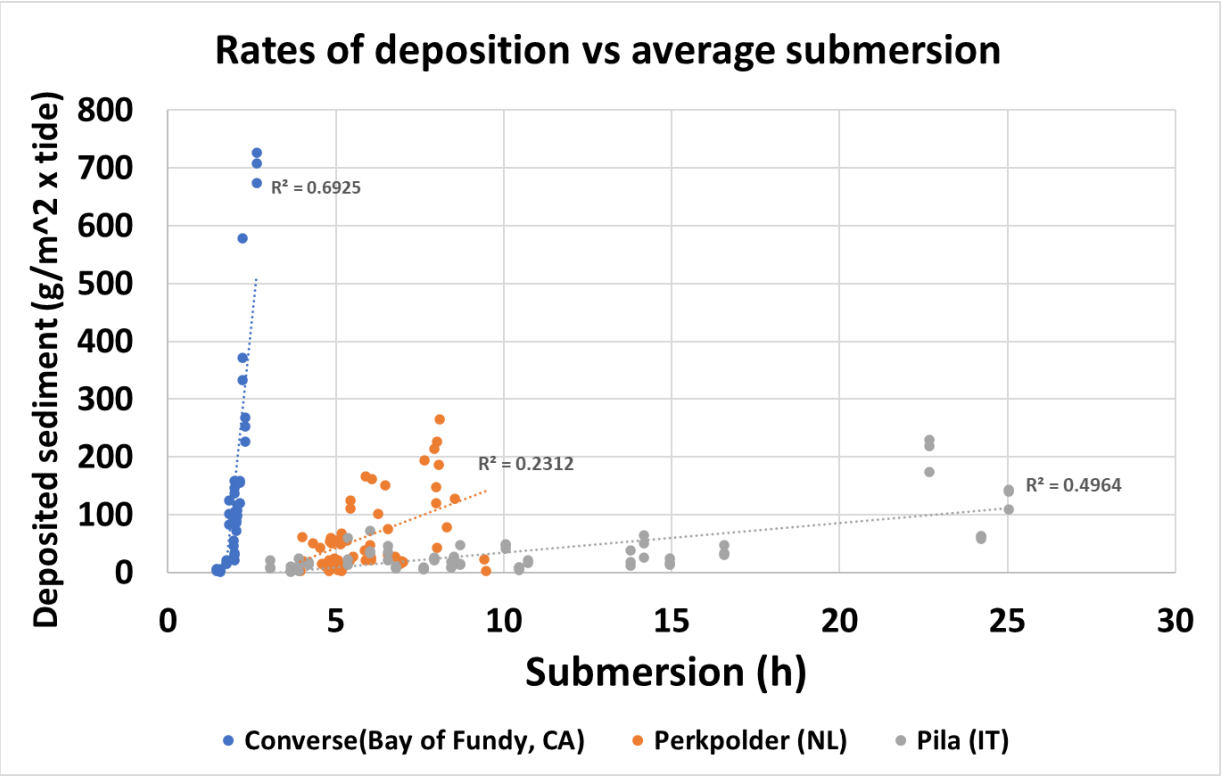


***Figure 57*** *– Sediment deposition and average hours of submersion calculated from all traps of all surveys from the Po Delta, Perkpolder, and Converse.*

## *7.3.2 Sediment budget and inlets erosion*

*Barbamarco lagoon (Po Delta)*

The tidal flat of the Barbamarco lagoon (i.e. Po Delta) started its development after the early 2000s when human intervention connected the Po River with the southern section of the lagoon. Between 2008 and 2012, vegetation established the small inlets that connect the channels to the tidal flat. The channel is the only artificial structure that is present inside the system and it did not show any instability. The study area has a positive sediment budget; between October 2018 and July 2019 the tidal flat maintained a relatively stable condition characterized by a partial erosion of 400 $m^3$. Between July 2019 and February 2020 strong floods occurred and an average of 1300 $m^3$ were deposited. During the whole study period, the sediment budget was about 800 $m^3$ per year. The results related to the sediment budget and the interpretations are discussed in 2.4.5 and 2.5.1.

*Perkpolder (The Netherlands)*

As shown in figure 58a and 58b, the volumes variations of the whole restoration project for all periods show clear trends, in spite of which TCD was chosen; however, in the case of the 0.15 m

TCD, the percentage of the area with detectable changes highly reduces, losing valuable information relative to the vertical variations. Since the trends are evident, the results with no TCD and with a TCD of 0.5 m or 0.1 m are reliable and the following volumes are referred to calculations without TCD. This section improves the results of paragraphs 5.4.1 and 5.4.5.

During the first period between June 2015 and April 2016, a net sediment budget of about 63000 $m^3$ were deposited inside the system; most of the budget was located inside the pond (Zone 2), with a net sediment of 44000 $m^3$, and the rest of the budget (20000 $m^3$) was located inside the tidal flat (Zone 1) (Fig. 59a). In the same period, the inlet area (Zone 3) lost about 4600 $m^3$; erosion highly increases if considered the inlet and the whole portion in front of the inlet (Zone 4) which was characterized by a sediment loss of 33000 $m^3$ (Fig. 60a).

A similar trend was found during the following period (i.e. April 2016 – February 2017) where the sediment budget was still positive but it decreased to 32000 $m^3$. However, most of the sediment deposited inside the tidal flat (Zone 1) reached 22400 $m^3$, while the pond collected 9000 $m^3$ (Fig. 59b). The inlet underwent erosion once again keeping very similar volumes; the inlet itself (Zone 3) lost the same sediment budget (4700 $m^3$), while the whole external area lost 24400 $m^3$ (Fig. 60b).

Overall, the system collected a net sediment budget of about 95000 $m^3$, where 42000 $m^3$ were deposited inside the actual tidal flat (Zone 1), and 53000 $m^3$ inside the pond (Zone 2) (Fig. 59c). The inlet (Zone 3) lost about 8400 $m^3$, while the external area was subject to a constant strong erosion that caused a sediment loss of about 49500 $m^3$ (Fig. 60c).

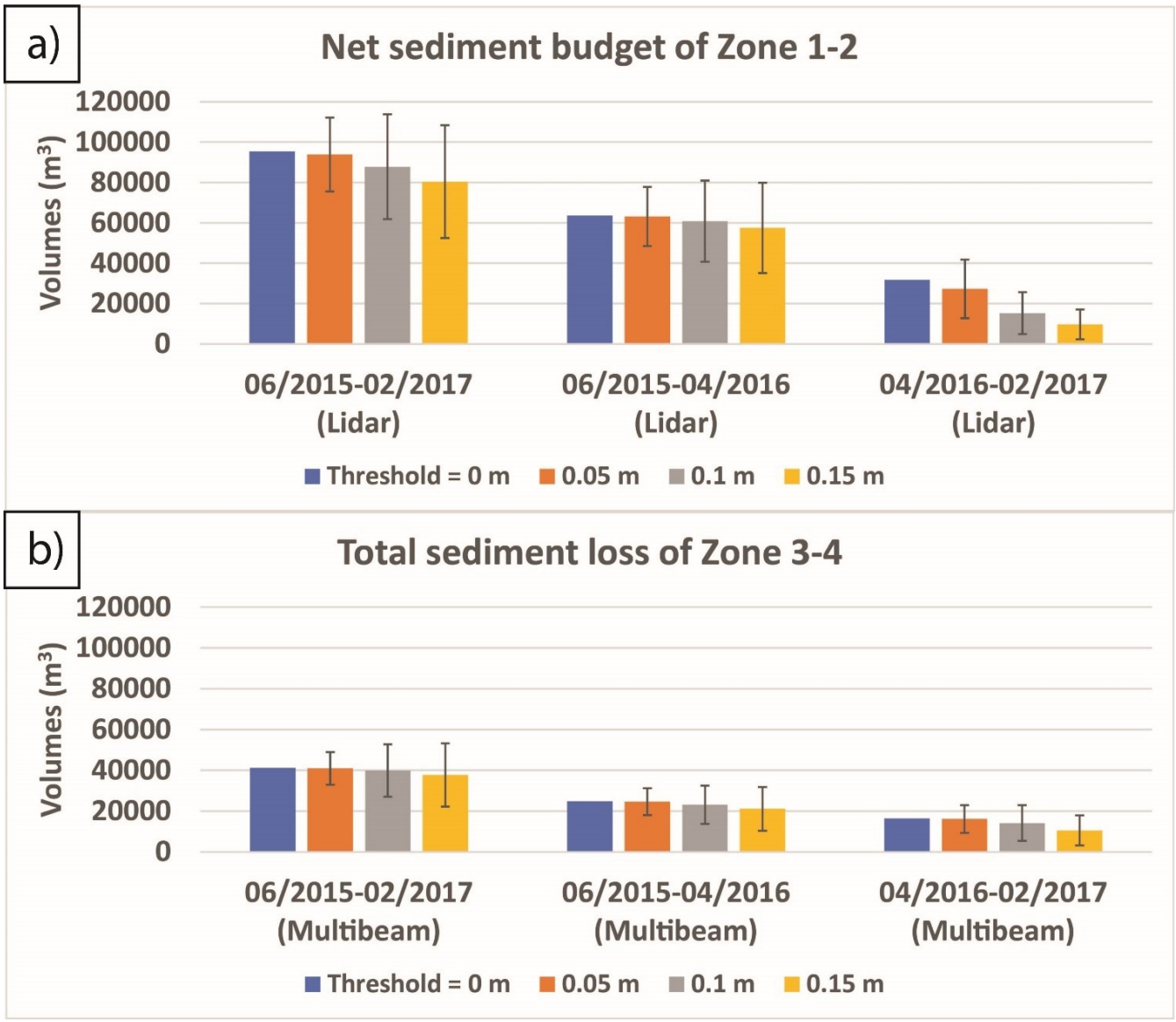


***Figure 58 –*** *(a) The net sediment budget of the whole restoration project of Perkpolder (Zone 1 and Zone 2). (b) Total sediment eroded from the external portion of the restoration project (Zone 3 and Zone 4).*

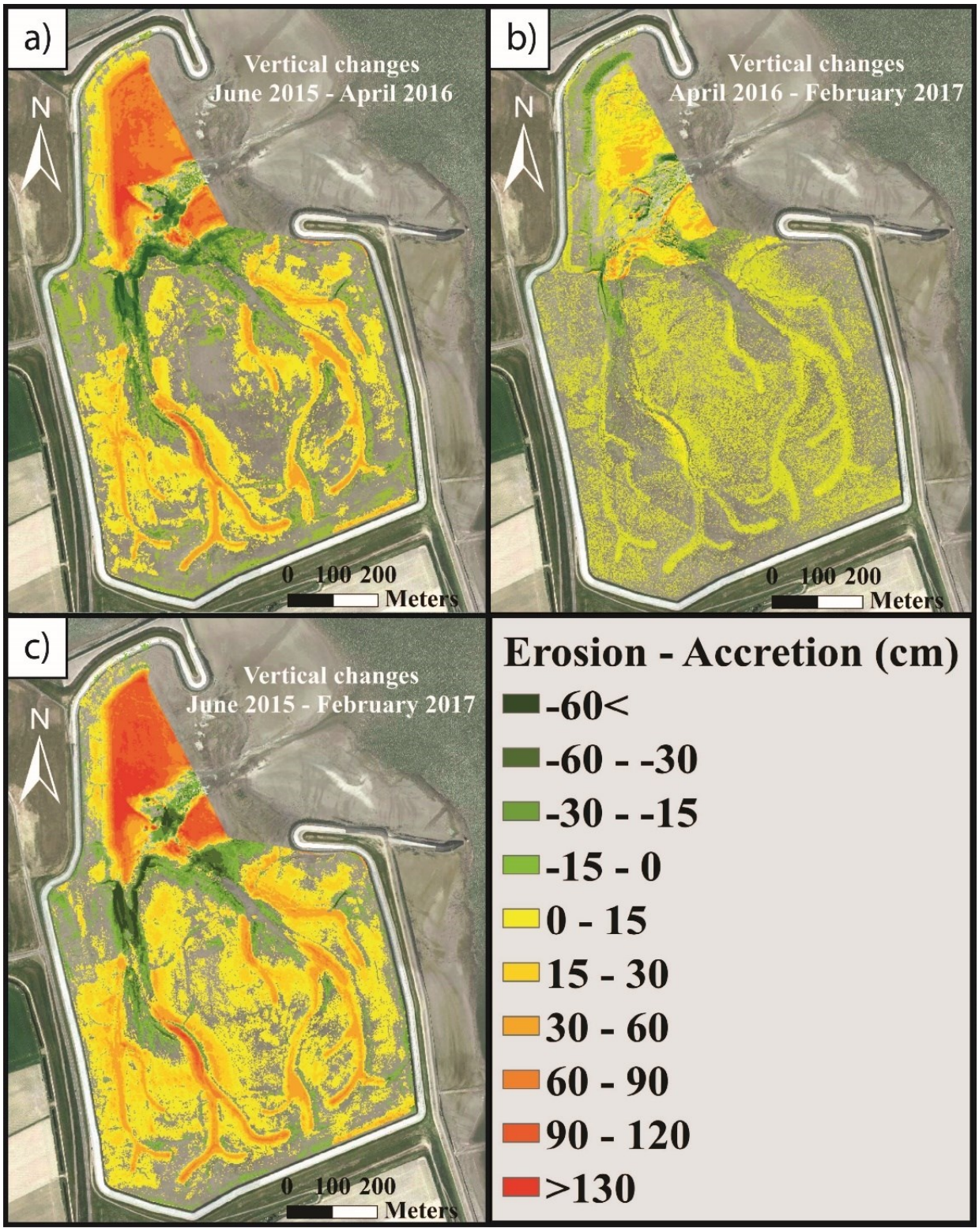


***Figure 59 –*** *Vertical changes of the restoration project of Perkpolder regarding the tidal flat (Zone 1) and the pond area (Zone 2) from (a) June 2015 to April 2016, (b) from April 2016 to February 2017, and (c) for the whole study period from June 2015 to February 2017. The DoDs shown in this figure are made with a TCD of 0.05 m.*

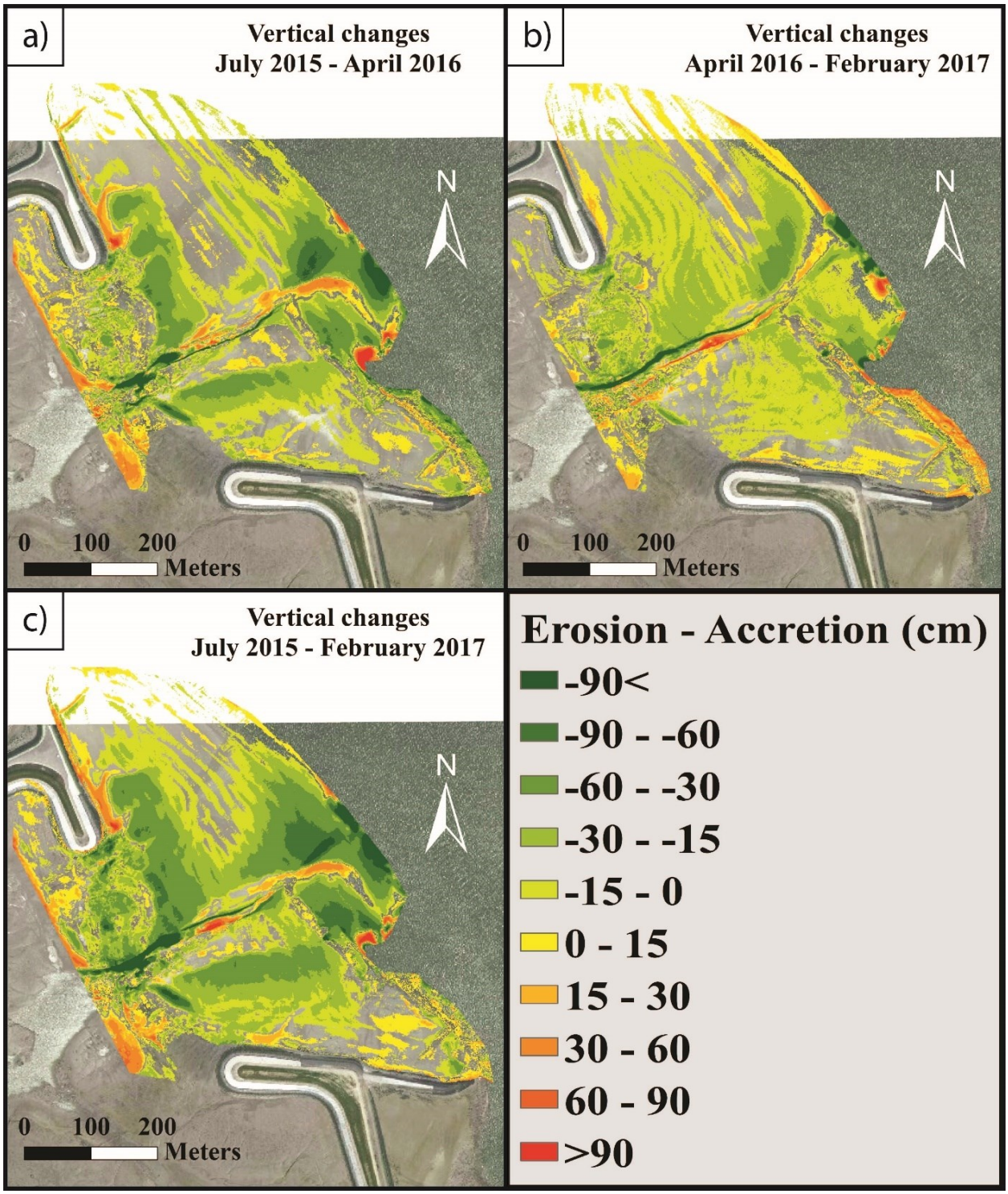


***Figure 60 –*** *Vertical changes of the restoration project of Perkpolder regarding the inlet area (Zone 3) and the external portion (Zone 4) from (a) July 2015 to April 2016, (b) from April 2016 to February 2017, and (c) for the whole study period from July 2015 to February 2017. The DoDs shown in this figure are made with a TCD of 0.05 m.*

*Converse (Canada)*

Between July 2019 and August 2020, the tidal flat of Converse underwent strong erosion (-2000 $m^3$, no TCD), in particular inside the main channels and the inlet; however, this erosional trend was

caused by the presence of pre-existent vegetation that overestimated the surface of the tidal flat (see 6.5.2). In the following period (i.e. August 2020 – July 2021) the trends were inverted and the sediment budget increased to 2800 $m^3$ (no TCD). The total sediment budget for the whole period (i.e. July 2019 – July 2021) is about 550 $m^3$ (no TCD), however, due to the overestimation, it is worth considering the total volume rising during the whole period and during the last period. The inlet area lost about 1000 $m^3$ during the whole period, while the whole study area was subjected to a total gain of 3900 $m^3$; during the last period (i.e. August 2020 – July 2021), the inlet lost 360 $m^3$ while the study area gained 3300 $m^3$. The detailed discussion can be found in 6.4.1 and 6.5.2.

### *7.3.3 Tide gauges and Spartina spp. distribution*

The calculated MHT and the tidal ranges of each study site are shown in Tab. 17. As described in4.4.2, the distribution of the *Spartina maritima* in the Po Delta is between 0.02 and 0.26 m above m.s.l., with a vertical distribution of 0.23 m. Van der Wal et al. (2008) showed that the most common pioneer plant that grows in the Scheldt Estuary is the *Spartina anglica*, whichtypically grows between 0.6 and 2 m above m.s.l.. The DSM of the salt marsh of Eldriken (Bay of Fundy) showed that the limit between *Spartina alterniflora* and bare ground is about ~4.5 m above m.s.l.. The presence of the species is found until the MHT, which is 5.73 m above m.s.l. (vertical distribution of 1.2 m). Above MHT the *Spartina* disappears and *Spartina patens* become dominant (i.e. above 5.73 m).

***Table 17*** *– Spartina spp. vertical distribution obtained from the study sites.*

| Study site | MHT (m) | Average Tidal range (m) | Spartina spp. Vertical range (m above m.s.l.) | Spartina spp. Distribution (m) |
|---|---|---|---|---|
| Po River Delta (Italy) | 0.38 | 0.51 | 0.04 – 0.26 | 0.23 |
| Perkpolder (The Netherland) | 2.53 | 4.6 | ~0.6 – ~2 (Van der Wal et al. (2008)) | / |
| Eldriken (Canada) | 5.73 | 13.22 | ~4.5 – ~5.7 | 1.2 |

## *7.4 Discussion*

### *7.4.1 Vertical variations and sediment deposition in human-induced tidal flats*

Despite the provenance of the sediment, tidal currents control the distribution of what the sediment supplier offers, depending on the study case. For example, the sediment transport in microtidal environments (i.e. Mediterranean Deltas) is mostly controlled by the river (e.g. Hensel et al., 1999; Ibáñez et al., 2010), and tidal currents commonly do not introduce sediment inside the system but redistribute the material brought by the river (i.e. Po Delta (Brunetta et al., 2021)) or storms (i.e. Venice lagoon (Ciavola et al., 2002)). For the tidal flat of the Barbamarco lagoon (i.e. Po Delta), important deposition and vertical variations focus during strong floods, which means that the rates of vertical changes are not consistent in time. However, the following discussion is based on the fact that the rates of deposition obtained during the fieldwork using the Petri dish traps depend entirely on tidal processes.

The average deposition of the Barbamarco lagoon is around 35 g/m$^2$ per tide; this value of deposition is lower than the other study sites, which is expected from a microtidal wetland (see 3.5.3), and the presence of crevasse splays, which are a typical morphological form caused by river floods, suggests that the river has a higher impact on the morphology and the tidal currents do not alter the structure of the tidal flat. In fact, the channels are not well developed, and they present an irregular shape caused by the floods (Brunetta et al., 2021). Due to the absence of complex morphologies and low current velocities, the elevation is the most predominant factor that influences deposition, which means that the higher the submersion period is, the higher is the deposited sediment going to be (Pethick, 1981). As shown in the results, a higher correlation for the traps of the Po Delta site is found when the traps from the same survey are chosen; higher values of R are found during the winter-spring surveys (R=0.7-0.8) while lower correlation is found during the summer survey (R=0.6). Since deposition varies during different seasons, the data dispersion increases when using all the data from the traps of all surveys.

A completely different situation is found in the tidal flat of Perkpolder. This artificial tidal flat is undergoing higher sediment deposition compared to the Po Delta, with average values of 65 g/m$^2$ per tide, and a shorter hydroperiod (i.e. between 4 and 10 hours of submersion). The complex morphology and the stronger currents widely influence deposition, which depends entirely on the tide; specifically, the rates increase with distance from the inlet and decrease moving away from the channels. Elevation in respect to the m.s.l. is less influential, meaning that for similar

submersion periods, the traps collected different sediment amounts. As a consequence, this leads to high dispersion of the data and it explains why correlation is lower for this dataset (R=0.2). In this study site, high amounts of sediment are transported by tidal currents due to the turbidity maxima hence when tidal and river currents collide (Chen et al., 2005); however, the high rates of deposition found in this restoration project (and in the Converse one as well) could depend on a local source linked to the morphodynamic instability of the system (see the next paragraph 7.4.2).

An intermediate condition is found in the tidal flat of Converse. Despite the site being characterized by exceptionally high rates of sedimentation (150 $g/m^2$ per tide between 1 to 3 hours of submersion), the channels do not develop through the whole tidal flat and the effect of the elevation in respect to the m.s.l. have higher control on sedimentation. In this case, the distance from the inlet seems to be less dominant on deposition; a possible hypothesis could be connected to the highly deep and vertically shaped channels. In fact, deep channels could slow down the current velocities before the water reaches the tidal flat, increasing the effect on sedimentation of the elevation and the distance from the creeks. As for the Perkpolder case, strong sedimentation could depend on the high concentration of sediment in the Cumberland Basin, but also on the lack of morphodynamic equilibrium (see the next paragraph 7.4.2).

The distribution of the rates of deposition of these study sites gives interesting hints about the sediment deposition collection procedure; in fact, the morphology and the seasonal variation highly influence the correlation between datasets. As morphology becomes more complex (i.e. high number of channels, distance from the inlet) elevation in respect to the m.s.l. loses its influence, resulting in an increase in dispersion (i.e. Perkpolder dataset). Data from different surveys increase dispersion as well, in particular, due to differences in seasonality (i.e. Po Delta dataset). These observations suggest that these factors should be considered for future surveys and data correlation, for example if high dispersion is expected in certain environments.

The tidal flats under investigation presented higher rates of vertical changes, compared to the average of other environments. As described in Chapter 2, microtidal flats with a positive dynamic are characterized by an average vertical increase of about 1-2 cm/year (Andersen et al., 2006; Brunetta et al., 2021), but in most cases, microtidal salt marshes are characterized by lower rates of accretion (i.e. 0.2 – 1 cm/year) (Hatton et al., 1983; Goodbred and Hine, 1995; Day et al., 1998; Scarton et al., 2000; Ciavola et al., 2002; White et al., 2002; Craft et al, 1993; Wood and Hine, 2003; Jankowski et al., 2017). Macrotidal flats with high sediment injection are commonly

characterized by higher rates of accretion compared to microtidal, with average values from 3 to 6 cm/year (Vandenbruwaene et al., 2012; Cousins et al., 2017; Oosterlee et al., 2017, 2018). Although the elevation with respect to the MHT affects sedimentation (i.e. as the surface gets lower, sedimentation increases) its effect is highly local, such as for the tidal range; each environment has different rates of deposition that are highly dependent on the sediment supplier. For example, Butzeck et al. (2015) studied the Elby Estuary (northern Germany) following the same methodology of this thesis (i.e. Petri dish trap). This macrotidal marsh (2.9 – 3.6 m of tidal range and MHT of 1.5 m) showed rates of deposition between ~1 and ~50 g/m$^2$ per tide (bi-weekly deposition between ~20 to ~1400 g/m$^2$) during 0.25 to 1.5 hours (7 to 43 hours bi-weekly) of submersion at an elevation of 1.6 to 2.3 m above m.s.l.; the accretion was between 0.1 and 2 cm/year. Although this is a macrotidal environment with strong sediment input, these values are rather similar to the Po Delta. This can be related to the low submersion period since the rates are referred to elevations higher than the MHT, while the Po Delta, and the other study cases, are located below the MHT. On the other side, the tidal flat of Converse, which surface is located higher than the MHT as well, has an extremely higher deposition, compared to the study site of Butzeck et al (2015).

### *7.4.2 Artificial morphologies affect the evolution of restoration projects*

Sedimentation depends on several bio-physical factors; however, one of the most influential is the effect of morphology. For what concerns the study sites under investigation, the distance from the creeks and their shape, the distance from the inlet, and the elevation in respect to the m.s.l., combined with the hydrodynamic conditions, had a strong control on sedimentation. These features of the morphology have changed the evolution of the tidal flats and the data collection as well. Before pursuing, it is important to state that in the following discussion it is considered only the deposition led by tidal influence (i.e. sediment transported and deposited by the tide, in spite of where the tide collected the sediment), without considering other processes (i.e. river floods).

One important difference between the tidal flat of the Barbamarco lagoon and the macrotidal study sites is that the flat has no artificial features. Besides the intervention that connected the Po della Pila branch with the tidal flat, the morphologies that developed during the years are natural, while the structure of the tidal flats of Perkpolder and Converse are mostly human-induced, especially the channels and the inlets. In the tidal flat of the Po Delta, the absence of artificial

creeks reduces its impact on deposition; the low tidal currents decrease the effect of the distance from the inlet as well and the elevation becomes the most influencing factor. This behaviour is highly in contrast with the evolution of artificial morphologies of restoration projects. In the case of Perkpolder, the distance from the inlet is a strong influencing factor, causing different rates of deposition and vertical variations among the same elevations. This behaviour is less evident in the site of Converse despite strong erosion in the central channel; the rates of deposition and vertical variation are strongly dependent on the distance from the creeks and elevation. This behaviour could be caused by the structure of the channel that has highly vertical levees next to the inlet; this structure might slow down the tidal currents and as a consequence it reduces the effect of the distance from the inlet.

Based on these studies, artificial tidal flats (i.e. Perkpolder, Converse) tend to have in common a strong morphological instability due to man-made channels and inlets that need to find a new equilibrium with the hydrodynamic forces of the tidal currents; hence, these currents erode the inlets and the channels in the nearby areas. On the other side, strong accretion occurs in the most distant areas of the tidal flat, where the elevation and the distance from the creeks become predominant. The channels act as a sediment sink and collect higher amounts with respect to the rest of the flat. Although the sites of Perkpolder and Converse were subjected to strong accretion because of the high concentration of sediment that the tidal currents offer, it is important to consider that part of the sediment could come from cannibalization due to the strong erosion that occurs in the inlets and the nearby areas.

For example, considering the Perkpolder case study, the inlet area lost 49500 $m^3$ of sediment during the whole study period, while the whole system gained 95000 $m^3$. Assuming that all the eroded sediment was moved inside the tidal flat, it would mean that the inlet could have provided 52% of the whole sediment budget. Considering the first year (i.e. 2015-2016), 63000 $m^3$ of net sediment were deposited inside the system, while 33000 $m^3$ eroded from the external area of the inlet; even in this case, the budget corresponds to 52%. During the last period (i.e. 2016-2017) the tidal flat gained 32000 $m^3$, while the external area lost 24500 $m^3$, meaning that 76% of the eroded sediment could have deposited inside the system. The inlet itself found a morphological equilibrium after 8 months (Brunetta et al., 2019), however, the external section might need more time to find stability. If this hypothesis is true, when the system finds a morphological equilibrium, deposition will drastically decrease, in particular if half of the budget derives from the inlet.

For what concerns the case of the tidal flat of Converse, the proportions between inlet erosion and tidal flat deposition are different. As explained in 6.5.2, the inlet erosion could have provided between 13 to 36 % (till 65%) of the whole budget. These percentages are highly lower than the sediment deposition in this system, suggesting that the tidal flat rather depends on the high concentration of the sediment plume of the Cumberland Basin. However, the erosion that is occurring in several sections of the Missaguash River was not considered, which means that the sediment provided could be higher.

If these systems are under cannibalization, the rates of deposition of Perkpolder and Converse will slowly decrease in time, flattening the linear regression shown in figure 57, reaching a natural behaviour (i.e. sediment does not derive from human structure, but only natural processes) similar to the tidal flat of the Po Delta, although the rates of the macrotidal environment will be higher than the Po Delta due to stronger deposition driven by higher sediment concentrations (example in Fig. 61). However, this hypothesis works only if the sediment transported by the tide derives entirely from the inlet or both the inlet and the sediment plume, which means the sediment concentration of the water. In fact, if the sediment derives entirely or mostly from the sediment plume, the linear regression of each environment should be considered as natural; furthermore, as the tidal range increases (i.e. Po Delta, Perkpolder, Converse) the average submersion period around the MHT (i.e. where the tidal flats develops) reduces and the linear regression increases the steepness (Fig. 61). Despite these considerations, the rates of deposition of Perkpolder and Converse are higher than several similar natural coastal wetlands (e.g. French et al. 1995; Leonard, 1997; Temmerman et al., 2003; Marion et al., 2009), suggesting that these restoration projects are experiencing an extra sediment input. Besides, it is found that in other systems characterized by similar submersion periods but lower deposition, such as Allen Creek (Van Proosji et al. 2006), where the linear regression is flat if compared to the Converse tidal flat (i.e. same submersion period, lower deposition; see fig. 56), or in the Authie Estuary (France), which is a macrotidal marsh (tidal range of 4.9-8.5 m) characterized by rates of deposition from ~2.5 to ~110 g/m$^2$ per tide during 0.25 to 1.8 hours of submersion (Marion et al., 2009).

One last consideration that must be taken into account is that as tidal flat increases in elevation, deposition decrease as well (e.g. Pethick, 1981; Marani et al., 2007), which means that the rates of vertical changes will decrease in time in any case; the cannibalization could speed up this process.

It is important to note that it is assumed that the whole sediment eroded from the inlet has been deposited inside the tidal flats. These datasets and analyses do not allow to clearly distinguish which percentage of sediment moved inside or outside the system. In most cases, the ebb currents have higher capability to shape tidal networks with respect to flood currents (Geng et al., 2020), hence if the erosion is driven by these currents, most of the sediment might have been transported out of the system, reducing the effect of the cannibalization. However, it depends on case by case basis. For example, in the tidal flat of Perkpolder the suspended concentration is usually higher during the flood and during Spring tides than during ebb and Neap tides (Fettweis et al., 1998). On the other side, external sediment banks not necessarily improve sediment incomes such as for the case of the Hesketh Out Marsh, in the Ribble Estuary (UK), where the presence of man-made embankments seemed to not feed and increase deposition inside the system (Pannozzo et al., 2022). An important future analysis could be the evaluation of the ebb current velocities in order to verify the entity of the erosion in the study cases.

If the cannibalization hypothesis is true or partially true, future analysis on deposition from this type of restoration project could consider the steepness of the dataset in order to define the evolution of the tidal flats. In any case, the time for the inlet to reach stability depends on specific conditions of the inlet and the current velocities. The inlet of Perkpolder stabilized after 8 months; the inlet of Converse is still under erosion after two years. This is an important aspect to consider for future restoration projects. Furthermore, it is important to note that the study sites of the Po Delta, Perkpolder, and the Bay of Fundy are young tidal flats located in favourable conditions for sedimentation at this moment in time (e.g. positive river transport (Brunetta et al., 2021), turbidity maxima for Perkpolder (Chen et al., 2005)), and their rates represent tidal flats that are evolving with a positive trend (i.e. high accretion). It is important to acknowledge, as well, that these observations are based on a single site from each type of environment; more study sites, in particular younger tidal flats, should be taken into account to validate these interpretations. Future studies should monitor and verify if positive trends strongly decrease in future years.

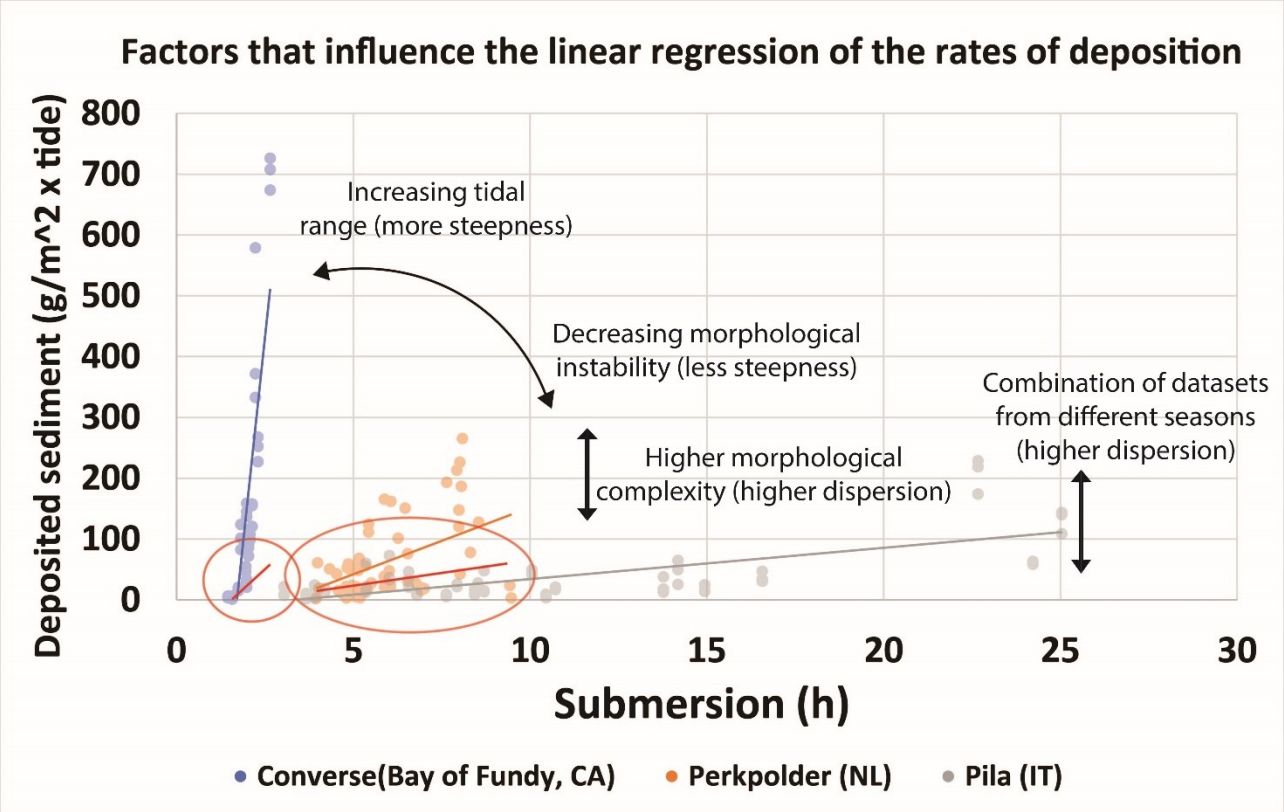


***Figure 61*** *– Example of future trends for deposition in restoration projects under morphological instability. As tidal range increases, the average submersion period decrease next to the MHT, increasing the steepness of the linear regression. If the cannibalization process decreases in time, the linear regression will flatten, and the rates of deposition will drastically reduce. If the study site is characterized by high morphological complexities (i.e. channels, strong local elevation variations, and strong hydrodynamics next to the inlets) the dispersion of the datasets might increase, reducing the effect of the surface elevation, hence the submersion period. Combining datasets from different seasons or surveys dispersion as well.*

### *7.4.3 Morphological evolution of restoration projects*

Cox et al. (2022) distinguish several strategies applied nowadays that improve the sediment injection in coastal wetlands; in the case of these studies, the main approaches can be summed up as river sediment diversion, and tidal flooding. They are based on the exploitation of the dominant sediment supplier using the same procedure, which consists in breaching a dyke or a levee to connect the sea or the river to the wetland. The sediment injection caused by river or tidal floods has the same outcome; what changes is the modality, which depends on the sediment supplier. The site of the Po Delta falls within the river diversion strategy since the opening of new channels allows the river to deposit sediment within areas that were previously not subjected to deposition. Since the river is the sediment supplier, strong accretion occurs during strong floods, while slow

deposition or erosion occurs during periods characterized by low hydrodynamics. There are several examples of case studies where river diversion was applied, such as the case of the Rheine-Meuse (NL) (van der Deijl et al., 2018), the Mississippi Delta (USA) (Boyer et al., 1997; Day et al. 2016), and the San Francisco Bay (USA) (Miller et al., 2008). The Mississippi case is particularly similar to the Po Delta case. The river diversions technique is highly used for crevasse development and land progradation; Day et al. (2016) emphasized that episodic strong river floods and large diversions lead to a rapid coastal restoration of the system. Since certain portions of the lagoons of the Po Delta are undergoing a similar evolution (see 4.5.2), this technique could be exploited and implemented in order to recover salt marsh loss.

On the other side, the sedimentation of the tidal flats of Perkpolder and Converse are fully controlled by the tidal currents, which cause constant deposition in time characterized by minor temporal variations, but strongly dependent on the hydroperiod, the distance from the creeks and the inlet. Tidal flooding restoration project are under developing in the recent years, such as the Lippenbroek marsh (NL) (Vandenbruwaene et al., 2012; Oosterlee et al., 2018), the Ems Estuary (DE) (Kwakernaak and Lenselink, 2015), and in Bangladesh (BGD) (Gain et al., 2017).

As described in the previous paragraph, morphological instability seems to affect the evolution of restoration projects, which follow an unnatural evolution during the first years after the opening. This behaviour is found in other artificial tidal flats, such as the Kleine Noordwaard restoration project, located in the lower Rhine-Meuse delta (The Netherlands) (Verschelling et al., 2017; van der Deijl et al., 2018). This microtidal wetland (tidal range of 0.2 – 0.4 m) is a restoration project with a similar design to the present studies (i.e. new connections between the sea and the inland areas, artificial channels) that started to be submerged by the tidal currents after 2008. The average rate of vertical variations is 0.6 cm/year, which is similar to the rates of the tidal flat of the Po Delta and it is a typical rate for a microtidal flat with a positive trend. During the following years, an overall morphodynamic instability characterized the system and strong accretion was found inside the creeks, while strong erosion was found inside the inlet and the channel that connects the river with the marsh system. A negative correlation between sedimentation and the elevation was found, similarly to the Perkpolder dataset obtained in this study. The authors suggest a hypothesis that is in accordance with the one proposed in this study, hence that the vertical variations do not have enough control on sedimentation if compared with the morphological complexity of the system. (Whitehouse et al., 2000; Takekawa et al., 2010; Fagherazzi and Mariotti, 2012). The case study of Perkpolder, Converse, and Rhein Meuse show

how artificial morphologies alter the natural deposition besides the hydrodynamic conditions and the tidal range.

Higher rates of deposition compared to natural sedimentation were detected in other restoration projects, such as in the Sacramento-San Joaquin Delta of the San Francisco Bay (California, USA), which was characterized by an average accretion of 4 cm/year, despite the system is a freshwater marsh (Miller et al., 2008). In certain cases, the restoration project is made in order to obtain unnatural deposition, such as for the case of Lippenbruek in the Netherlands (Oosterlee et al., 2018). Deposition, in this case, is controlled by a Controlled Reduced Tide (CRT), which means that the tidal range is limited to 1.3 m instead of 5.4 m; this strategy allows to maintain longer submersion periods at higher elevations in order to flatten the surface. The rates of accretion were higher than in natural marshes (12.5 – 5 cm/year during the first year) and decreased to 2.5 cm /year after 9 years. See 5.5.4 for more details.

### *7.4.4 The transition from tidal flat to salt marsh*

A wetland restoration project aims to develop a full tidal system and, most importantly, a full ecosystem, which is reached after the transition from tidal flat to salt marsh. A proper salt marsh develops around the MHT (De Vlas et al., 2013; Bakker, 2014), however, pioneer vegetation (e.g. *Spartina spp*.) typically colonizes at lower elevations, defining the low marsh. The *Spartina spp*. distribution identified during the fieldwork is comparable with the literature (Scarton et al. 2004; Porter et al., 2015) and, as expected, it showed that the vertical location and distribution of *Spartina spp*. increases as MHT and tidal range increase. However, as Balke et al., (2016) make notice, when the tidal range increases, the limit between tidal flat and salt marsh decreases (compared to the MHT) as well, widening the low marsh and decreasing the elevation necessary for vegetation to establish (in particular for macrotidal environments). The study sites discussed in this thesis are characterized by a general positive vertical accretion; however, the signs of a transition from tidal flat to salt marsh were not visible in all study sites. Salt marsh development can be addressed to several factors, such as tidal range, MHT, hydroperiod, salinity, the presence of nutrients, plant species requirements, and other geochemical parameters. However, most of these factors are linked to the elevation above m.s.l.. The vertical difference between the surface and the MHT was a highly influential factor for most of the study sites, but not for all of them.

As discussed in Chapter 4 (paragraph 4.5.2), in the Po Delta, the proximity to the freshwater flux and the strong deposition allowed the *Phragmites* to colonize the tidal flats of Burcio and the Basson lagoon; however, vegetation did not establish in the Barbamarco lagoon. Although the MHT is about 0.38 m and the higher surfaces of the tidal flat are between 0.2 and 0.3 m, the flat is located within the interval of *Spartina maritima* (Silvestri et al., 2005; Scarton et al. 2004) and *Phragmites australis* distribution. This limited colonization suggests that the MHT is influencing the growth, but the local conditions need to be taken into account.

The tidal flat of Perkpolder, as described in Chapter 5, has a MHT of 2.53 m and the highest surfaces are located around 5 – 1.1 m above m.s.l. (based on 2017 analysis). These areas are highly restrained (i.e. 14 hectares), compared to the 75 hectares of the whole system, and no vegetation appeared after its opening in 2015. Brunetta et al. (2019) used the equation of Gray et al. (1989) to calculate the lower level of *Spartina anglica;* however, Gray's formula is based on data collected on natural salt marshes in Britain and it needed validation. Van der Wal et al. (2008) demonstrated that this species, which is the most common species of Spartina in the estuary, typically grows between 0.6 and 2 m above m.s.l., which means that the result of the equation (2.67 m above m.s.l.) is incorrect. The vertical distribution of *Spartina anglica* indicates that the flat has barely reached the elevation for the pioneer plant to colonize. Furthermore, a study in the tidal flat of Perkpolder made by Cao et al., (2021) highlighted that poor drainage in fine sediment with high water content decreases the probability for seedlings to establish. They also noticed that the *Spartina anglica* survivance was enhanced by higher elevations above 0.6 m.

Vegetation was visible in the site of Converse (Bay of Fundy), where the first patches of *Spartina* appeared after 2 years. The MHT of this site is about 4.8 m above m.s.l. and the average elevation of the whole tidal flat is about 6 m above m.s.l., indicating that the condition for a salt marsh to develop is found, at least under the morphological point of view.

Overall, vegetation establishment occurred a few years after the breach of the dyke in the case of Converse, or the disappearance of the wall of vegetation in the case of the Po Delta (i.e. in the Burcio lagoon between 2011 and 2013; in the Basson lagoon between 1969 and 1977; in the tidal flat of Converse between 2020 and 2021). This condition was not found in the tidal flat of Perkpolder, due to its location with respect to the MHT. This observation indicates that if the conditions are favourable, a restoration project can quickly reach its goal. Although different species require different habitat conditions and the collected dataset needs additional case

studies and data, more importance should be attributed to the vertical distribution between the MHT and the low marsh *Spartina* spp. for salt marsh restoration in order to decrease the waiting time. It is not necessary to wait decades before reaching the transition of the environment. However, it is important to note that due to the reduced tidal range and the confined range of vertical distribution of the pioneer plants, elevation (i.e. compared to the MHT) is highly influential for macrotidal environments, rather than microtidal, which instead are more influenced by local factors.

### *7.4.5 Final considerations*

As seen in 7.4.2, the design of a restoration project influences the evolution of the future morphologies and, consequently, the colonization by vegetation. Based on the investigations carried out in this thesis and worldwide studies, the most important processes that change the results of a restoration project are: i) the connections between the sediment supplier, hence sediment availability, in particular if the surface of the new born tidal flat needs to reach higher elevations; ii) the geographical location of the project, which is strictly linked with the sediment supplier; iii) the design of the project, since morphological instability cause unusual trends of deposition that might change in time; surface elevation is part of the design as well and it defines the future vegetation colonization; iv) the hydrodynamics of the environment, which influences the sediment supplier and the design as well.

For what concerns the survival of these restoration projects against Relative Sea Level Rise, it is difficult to give a proper long-term prevision. Based solely on the rates of vertical variations, these young tidal flats are highly able to keep pace with sea level rise, at this moment in time. The tidal flat of the Barbamarco lagoon is accreting with 1.3 cm/year, while the long time series of the RLSR (1875-2017) is about 1.3 mm/year, and the short time series (1992-2017) show rates of 3.8 mm/years (Da Lio and Tosi, 2019); these values are highly lower than the rates of the tidal flat. The average accretion of the tidal flat of Perkpolder (6 cm/year) is higher than the whole range of RSLR of the Scheldt Estuary (0.3 - 1.5 cm/year) (Temmerman et al. 2004b). The same condition is found in the restoration project of Converse, where the positive trend overcomes the RSLR of 1 cm/year (Shaw et al. 1998; Greenberg et al 2012). The location with respect to the m.s.l. and the presence of a strong sediment input is not random; these sites were located and built in geographic zones that were affected by these positive trends of growth on purpose, which means it is difficult to define clearly the future development, although they are expected to be affected by positive

trends due to their strategic position. Plus, the possible cannibalization of these systems might give an overestimation of the rates of accretion for long-term evolution.

It is important to remember that the restoration projects under investigation have the same or similar design (i.e. dyke structure that defines the boundaries and one direct connection with the estuary); the effect of waves and storms are not discussed in these studies, since no analyses were carried out and wave action was assumed to be less relevant compared to other processes (i.e. river floods and tidal currents). However, it is known that the contribution of extreme storms to erosion of marshes is generally highly low (1%) if compared to moderate to gale wind waves (Leonardi et al., 2015). Since wind-wave erosion was observed in other case studies characterized by a small fetch, such as in the Kleine Noordwaard restoration project (NL), with a fetch of 400 m and an average depth of 0.2 m (van der Deijl et al., 2018), wave erosion cannot be completely excluded from the study cases. For example, the fetch inside the Barbamarco lagoon (Po Delta) can reach 2 km with respect to the tidal flat; 1 km of fetch is visible inside the tidal flat of Perkpolder; the Converse system is more complex and has a lower fetch, but it can reach 400 m at maximum. The effect can still be considered as low: i) although the tidal flat of the Barbamarco lagoon is exposed to a maximum fetch of 2 km, the major wind direction is from NNE and SSE (Bora and Sirocco) (Maicu et al., 2018); the tidal flat is protected by a wall of vegetation on the eastern side, suggesting a low effect due to wind waves. ii) the Perkpolder basin is exposed to 1 km of fetch at maximum but has a relatively high percentage of sand (40% on total average) that increases the critical bed shear stress necessary for waves to cause resuspension, which means that high wind speed is necessary to allow erosion (i.e. >13 m/s (Mitchener and Torfs, 1996)); iii) the Converse study case is highly silty, which mean finer than Perkpolder, but has a complex structure that makes the fetch smaller. A proper wind and wave direction and speed analysis would be necessary to define the contribution of this process on erosion and future analysis should be addressed in order to confirm the impact of possible resuspension.

# 8. Final conclusions

Sedimentological and morphological analyses combined with multi-disciplinary approaches were carried out in highly different coastal wetlands, specifically tidal flats that developed after human intervention (i.e. dyke breach or channel excavation), and characterized by different tidal range. The evolution of the tidal flats of the Po River Delta (Italy), Perkpolder (The Netherlands) and Converse (Bay of Fundy, Canada) were studied, implementing the analyses with the salt marshes of Halfway River, and Eldriken (Canada).

## 8.1 Restoration in the Po delta system

The Po Delta system underwent a severe transgression between the 1960s and the 1980s; agricultural fields were submerged, leading to the birth of new tidal flats. Three sections of the Delta were subject to interesting developments: the lagoon of Barbamarco, Burcio, and Basson. The tidal flat located in the southern part of the Barbamarco lagoon is experiencing a positive accretion trend during the last 20 years. Rates of accretion of 1.3 cm/year and rates of deposition of 36.4 g/m$^2$ per tide occurred between 2018 and 2021. Several cr*evasse splays* indicate that the tidal flat development is strictly related to sediment injection controlled by the Po River, in particular after 2010. *Spartina maritima* and *phragmites australis* are the only two marsh species that grow in the study site. However, their growth is highly limited in this area, and this might be caused by the low mixed salinity of the Barbamarco lagoon. A faster salt marsh development is found in the lagoon of Burcio and Basson. The historical review showed that agricultural fields of the Basson lagoon were submerged in 1969 and a strong recovery occurred in 1977 due to *phragmites* colonization. The Burcio lagoon presented a fast marsh development between 2011 and 2013, after a strong sediment injection as well. The proximity to the river is the most probable reason that caused a fast marsh restoration in these lagoons.

This study enhances that, although the Po Delta coastline is far from recovery in respect to the 1950s, controlled strong sediment input can improve marsh restoration. New inlets that connect the river (i.e. Po della Pila) directly with other sections of the lagoon could cause strong sedimentation, allowing vegetation to establish. This approach could be exploited to recover and restore portions of lagoons that were abandoned by man and have no purpose, such as the Burcio lagoon. It is important to remember that these connections between river and lagoon could increase sedimentation inside the lagoon but decrease the sediment budget outside the Delta, hence this aspect needs to be investigated.

## *8.2 The restoration project of Perkpolder (The Netherlands)*

The Perkpolder tidal flat is a restoration project located in the Scheldt Estuary (The Netherlands) that was opened the 25 June 2015. Analyses showed that the study area is undergoing strong sedimentation; the rates of deposition range from 2.3 to 265.5 g/m$^2$ per tide with a hydroperiod between 4 and 10 hours (average deposition of 64.1 g/m$^2$ per tide). The whole system collected a net sediment budget of about 95000 m$^3$, where 42000 m$^3$ were deposited inside the proper tidal flat. However, the external portion of the inlet was subject to a constant strong erosion that caused a sediment loss of about 49500 m$^3$. After 6-8 months the inlet channel stopped its morphological evolution and reached equilibrium conditions, but this did not happen inside the external area. If portions of the sediment that was eroded from the external area entered the system, a process of cannibalization might be ongoing and the inlet erosion could provide till the 52% of the whole sediment budget. The average accretion rate of the whole study area was about 6 cm year$^{-1}$. The highest regions of the tidal flat are mostly under 1 m NAP and the conditions for initial salt marsh formation will not be established before a further 8-10 years.

## *8.3 The restoration project of Converse (Canada)*

The tidal flat of Converse is a restoration project that developed after the breach of the dike in the Missaguash River after 2018 (Cumberland Basin, northern side of the Bay of Fundy, Canada). This system, prevalently characterized by a high silt content, experienced rates of deposition from 3.8 to 703 g/m$^2$ per tide (average of 154.3 g/m$^2$ per tide), which have accumulated during 1 and 3 hours of submersion. Overall, the sediment budget is positive (i.e. about 1550 m$^3$) and the vertical variations are about 2-5 cm/year. On the other hand, a strong erosional trend was found next to the inlet and inside the central channel (>1 m/year); the strong deposition inside the tidal flat and the strong erosion of the inlet suggest that the tidal flat is under a morphodynamic instability and part of the eroded sediment could be feeding the tidal flat. Assuming that the whole sediment eroded by the inlet and nearby areas was deposited inside the tidal flat the erosion of the inlet could have supported from 14 to 36 % (till 65% considering also the nearby areas) of the whole budget of the system. The surface of the flat is located above the MHT and, as expected, vegetation started to develop quickly (i.e. 2 years after the opening); suggesting that the mudflat can shortly become a salt marsh.

## *8.4 Restoration projects from microtidal to macrotidal environments*

Coastal wetlands restoration projects are efficient approaches that aim to recover the ecosystem that man has reclaimed in the past. The artificial tidal flats that have been studied experienced an overall high deposition: the microtidal flat of the Po Delta experienced an average rate of deposition around 35 g/m$^2$ per tide; the macrotidal flat of Perkpolder (The Netherlands) was subjected to an average rate of 60 g/m$^2$ per tide; the ultratidal flat of Converse (Canada) presented an average deposition of 150 g/m$^2$ per tide. However, a strong morphological instability was found in the tidal flats that were characterized by artificial features (i.e. Perkpoder and Converse). The artificial channels are subjected to strong erosion in the initial section, nearby the inlet, and strong sediment deposition in the most distant portion of the tidal flat. The inlets are affected by a strong erosion as well and their rates are slowly reducing during the first years after the breach. Due to the high sediment deposition (in comparison with other study sites), the tidal flats may receive extra input from the local erosion of the external part of these systems. The volumes of sediment eroded from the inlet may be part of the sediment budget that has been deposited after the opening of each restoration project, suggesting that a cannibalization process might be ongoing and that the strong accretion that was detected may decrease drastically in the future, when the tidal flat will find a proper morphological equilibrium. Hence, the design of a restoration project is highly influential on future developments and makes it difficult to predict long-term evolution. The design influences the transition from tidal flat to marsh as well. In fact, the elevation of the surfaces with respect to the MHT showed that the transition from tidal flat to salt marsh can occur within a few years, as for the restoration project of Converse, or the Po Delta lagoons, but it can take decades if the tidal flat elevation is mostly under the MHT, in particular under the pioneer plant vertical range, such as for the case of Perkpolder.

## *8.5 Future improvements*

After the results and the discussion that this study allowed to achieve, new research questions arise:

i) How much time a wetland restoration project needs before becoming a natural tidal flat and then salt marsh (i.e. to present natural processes and evolution)? The transition from unstable to natural conditions and from tidal flat to salt marsh can occur simultaneously since these processes

need different requirements, besides the strong interconnectivity. Each environment presents local conditions that change the time of transition; it is important to monitor these and more study cases for longer periods in order to define when these restoration projects will reach a natural behaviour and obtain an estimation of the timing.

ii) How is the project affecting the nearby environment and which consequences the morphodynamic instability has brought in and outside the system?

iii) What is the entity of the cannibalization process? Does it provide a consistent amount of sediment or is it negligible for the evolution of the system?

iv) Can the "breach" technique be improved by mixing other types of techniques that increase sedimentation inside the system?

Future analyses on the Po Delta should focus on sediment deposition inside the lagoons that have recently been connected to the Po River (e.g. Burcio lagoon), and on reeds distribution in order to apply for a restoration project which aims to recover the unused section of the Po Delta and increase low marsh cover. These studies should investigate how the opening of new breaches, or the closure of channels, could influence sedimentation inside the lagoons and outside the Delta.

A higher number of cases of restoration projects should be compared and longer monitoring programs need to be carried out to confirm the early and long-term evolution of these environments and more importance should be given to features that characterize artificial tidal flats, such as the residues of the previous condition of the tidal flat (e.g. non-marsh plants, soil, different granulometry) that influence their evolution (e.g. vegetation establishment, changes in sediment deposition). More analyses should focus on breached inlets and artificial channels, in order to avoid long-term equilibrium of the system. Future restoration projects should take into account the elevation of the tidal flats and the sediment supplier as a preliminary measure to define the location of the realignment and estimate the time for the transition.

## 9. References


Adam, E., Mutanga, O., and Rugege, D. (2010). Multispectral and hyperspectral remote sensing for identification and mapping of wetland vegetation: a review. *Wetlands Ecol Manage* 18, 281–296. doi:10.1007/s11273-009-9169-z.

Adam, P. (2011). *Saltmarsh Ecology.* Cambridge, GBR: Cambridge University Press Available at: http://public.ebookcentral.proquest.com/choice/publicfullrecord.aspx?p=4641474 [Accessed January 10, 2020].

Adams, J. B., and Bate, G. C. (1995). Ecological implications of tolerance of salinity and inundation by Spartina maritima. *Aquatic Botany* 52, 183–191. doi:10.1016/0304-3770(95)00496-3.

Allen, J. R. L. ed. (1992). *Saltmarshes: morphodynamics, conservation and engineering significance*. Cambridge: Cambridge Univ. Press.

Allen, J. (2000). Morphodynamics of Holocene salt marshes: a review sketch from the Atlantic and Southern North Sea coasts of Europe. *Quaternary Science Reviews* 19, 1155–1231. doi:10.1016/S0277-3791(99)00034-7.

Allen, J. R. L., and Pye, K. eds. (1992). *Saltmarshes: morphodynamics, conservation, and engineering significance*. Cambridge [England] ; New York, NY, USA: Cambridge University Press.

Andersen, T. J., Pejrup, M., and Nielsen, A. A. (2006). Long-term and high-resolution measurements of bed level changes in a temperate, microtidal coastal lagoon. *Marine Geology* 226, 115–125. doi:10.1016/j.margeo.2005.09.016.

Amos, C.L., Long, B.F.N., 1980. The sedimentary character of the Minas Basin, Bay of Fundy. Littoral Processes and Shore Morphology — Geological Survey of Canada Papers. 80-10, pp. 123–152.

Amos, C. L., and Tee, K. T. (1989). Suspended sediment transport processes in Cumberland Basin, Bay of Fundy. *J. Geophys. Res.* 94, 14407. doi:10.1029/JC094iC10p14407.

Amos, C. L. (1995). “Siliciclastic tidal flats,” in Geomorphology and Sedimentology of Estuaries, ed. G. M. E. Perillo (Amsterdam: Elsevier), 273–306. doi: 10.1016/ s0070-4571(05)80030-5

Bakker, J. P. (2014). Ecology of salt marshes: 40 years of research in the Wadden Sea. *Wadden Academy.* 53. Downloadable from: https://www.waddenacademie.nl/en/organisation/publications list/eng/news/detail/ecology-of-salt-marshes-40-years-of-research-in-the-wadden-sea/.

Balke, T., Stock, M., Jensen, K., Bouma, T. J., and Kleyer, M. (2016). A global analysis of the seaward salt marsh extent: The importance of tidal range: The Global Seaward Salt Marsh Extent. *Water Resour. Res.* 52, 3775–3786. doi:10.1002/2015WR018318.

Barbier, E. B., Koch, E. W., Silliman, B. R., Hacker, S. D., Wolanski, E., Primavera, J., et al. (2008). Coastal Ecosystem-Based Management with Nonlinear Ecological Functions and Values. *Science* 319, 321–323. doi:10.1126/science.1150349.

Barbier, E. B., Hacker, S. D., Kennedy, C., Koch, E. W., Stier, A. C., and Silliman, B. R. (2011). The value of estuarine and coastal ecosystem services. *Ecological Monographs* 81, 169–193. doi:10.1890/10-1510.1.

Bassoullet, P., and Bacher, C. (2000). Characterization of intertidal hydrodynamics. *Continental Shelf Research*, 27.

Benito, X., Trobajo, R., and Ibáñez, C. (2014). Modelling Habitat Distribution of Mediterranean Coastal Wetlands: The Ebro Delta as Case Study. *Wetlands* 34, 775–785. doi:10.1007/s13157-014-0541-2.

Bezzi, A., Pillon, S., Popesso, C., Casagrande, G., Da Lio, C., Martinucci, D., et al. (2021). From rapid coastal collapse to slow sedimentary recovery: The morphological ups and downs of the modern Po Delta. *Estuarine, Coastal and Shelf Science* 260, 107499. doi:10.1016/j.ecss.2021.107499.

Billi, P., and Fazzini, M. (2017). Global change and river flow in Italy. *Global and Planetary Change* 155, 234–246. doi:10.1016/j.gloplacha.2017.07.008.

Bloesch, J., and Burns, N. M. (1980). A critical review of sedimentation trap technique. *Schweiz. Z. Hydrologie* 42, 15–55. doi:10.1007/BF02502505.

Boavida, M. J. (1999). Wetlands: Most relevant structural and functional aspects. *Limnetica* 17: 57-63. Downloadable from: https://www.limnetica.com/en/node/860.

Boersema, M. (2016). Perkpolder tidal restoration: one year after realisation draft progress report. *Centre of expertise Delta Technology*. 53. Downloadable from: https://www.zeeweringenwiki.nl/wiki/index.php/PP_Morphology_and_water_movement_processes_VN.

Boesch, D. F., and Turner, R. E. (1984). Dependence of Fishery Species on Salt Marshes: The Role of Food and Refuge. *Estuaries* 7, 460. doi:10.2307/1351627.

Bondesan M., Castiglioni G. B., Elmi C., Gabbianelli G., Marocco E., Pirazzolift P. A., & Tomasin A. (1995). Coastal Areas at Risk from Storm Surges and Sea-Level Rise in Northeastern Italy. *Journal of Coastal Research*, *11*(4), 1354–1379. http://www.jstor.org/stable/4298437

Bondesan, M. (1990). L'area deltizia padana: Caratteri geografici e geomorfologici. In: *Il Parco del Delta del po. Studi e Immagini. L'ambiente Come Risorsa*; Spazio Libri: Ferrara, Italy; Volume 16, pp. 10–48.

Borsje, B. W., van Wesenbeeck, B. K., Dekker, F., Paalvast, P., Bouma, T. J., van Katwijk, M. M., et al. (2011). How ecological engineering can serve in coastal protection. *Ecological Engineering* 37, 113–122. doi:10.1016/j.ecoleng.2010.11.027.

Boyer, M. E., Harris, J. O., and Turner, R. E. (1997). Constructed Crevasses and Land Gain in the Mississippi River Delta. *Restor Ecology* 5, 85–92. doi: 10.1046/j.1526-100X.1997.09709.x.

Bouma, T. J., van Belzen, J., Balke, T., Zhu, Z., Airoldi, L., Blight, A. J., et al. (2014). Identifying knowledge gaps hampering application of intertidal habitats in coastal protection: Opportunities & steps to take. *Coastal Engineering* 87, 147–157. doi:10.1016/j.coastaleng.2013.11.014.

Boutwell, J. L., and Westra, J. V. (2015). Evidence of Diminishing Marginal Product of Wetlands for Damage Mitigation. *NR* 06, 48–55. doi:10.4236/nr.2015.61006.

Bowron, T.M.; Graham, J.; van Proosdij, D. (2018). A River in Transition – the Restoration of the Halfway River and its Tidal Wetlands. Report of CBWES Inc. for NS Department of

Transportation and Infrastructure Renewal (NSTIR). Downloadable at: https://www.halifaxexaminer.ca/wp-content/uploads/2019/08/attachment-1.pdf

Brooks, H., Möller, I., Spencer, T., Royse, K., and Price, S. J. (2018). Geotechnical proprierties of salt marsh and tidal flat substrates at Tillingham, Essex, UK. *Int. Conf. Coastal. Eng.*, 55. doi:10.9753/icce.v36.papers.55.

Brooks, H., Moeller, I., Spencer, T., Royse, K., Price, S., and Kirkham, M. (2022). How strong are salt marshes? Geotechnical properties of coastal wetland soils. *Earth Surf Processes Landf*, esp.5322. doi:10.1002/esp.5322.

Brown, S. L. (1998). Sedimentation on a Humber saltmarsh. *Geological Society, London, Special Publications* 139, 69–83. doi:10.1144/GSL.SP.1998.139.01.06.

Brasington, J., Langham, J., and Rumsby, B. (2003). Methodological sensitivity of morphometric estimates of coarse fluvial sediment transport. *Geomorphology* 53, 299–316. doi:10.1016/S0169-555X(02)00320-3.

Brinke, W. B. M. 1994 The mixing of marine and riverine mud in the Scheldt estuary. *ESTUCON*, 14 pp. (in dutch).Brown, S. L. (1998). Sedimentation on a Humber saltmarsh. *Geological Society, London, Special Publications* 139, 69–83. doi:10.1144/GSL.SP.1998.139.01.06.

Brunetta, R., de Paiva, J. S., and Ciavola, P. (2019). Morphological Evolution of an Intertidal Area Following a Set-Back Scheme: A Case Study From the Perkpolder Basin (Netherlands). *Front. Earth Sci.* 7, 228. doi:10.3389/feart.2019.00228.

Brunetta, R.; Duo, E.; Ciavola, P. (2021). Evaluating Short-Term Tidal Flat Evolution Through UAV Surveys: A Case Study in the Po Delta (Italy). Remote Sens., 13, 2322. https://doi.org/10.3390/rs13122322;

Brunier, G., Michaud, E., Fleury, J., Anthony, E. J., Morvan, S., and Gardel, A. (2020). Assessing the relationship between macro-faunal burrowing activity and mudflat geomorphology from UAV-based Structure-from-Motion photogrammetry. *Remote Sensing of Environment* 241, 111717. doi:10.1016/j.rse.2020.111717.

Butzeck, C., Eschenbach, A., Gröngröft, A., Hansen, K., Nolte, S., and Jensen, K. (2015). Sediment Deposition and Accretion Rates in Tidal Marshes Are Highly Variable Along Estuarine Salinity and Flooding Gradients. *Estuaries and Coasts* 38, 434–450. doi:10.1007/s12237-014-9848-8.

Cahoon, D. R., Reed, D. J. (1995). Relationships among Marsh Surface Topography, Hydroperiod, and Soil Accretion in a Deteriorating Louisiana Salt Marsh. *J. Coast. Res.* 11, 15. Downloadable from: https://www.jstor.org/stable/4298345?origin=JSTOR-pdf.

Cahoon, D. R., Perez, B. C., Segura, B. D., and Lynch, J. C. (2011). Elevation trends and shrink–swell response of wetland soils to flooding and drying. *Estuarine, Coastal and Shelf Science* 91, 463–474. doi:10.1016/j.ecss.2010.03.022.

Cahoon, D.R.; Hensel, P.F.; Spencer, T.; Reed, D.J.; McKee, K.L.; Saintilan, N. (2016). Coastal wetland vulnerability to relative sea-level rise: Wetland elevation trends and process controls. In Wetlands and Natural Resource Management; Verhoeven, J.T.S., Beltman, B., Bobbink, R., Whingham, D.F., Eds.; Springer: Berlin, Germany; pp. 271–292.

Canali L. e Allodi G. (1963) - Contributo di studio sul trasporto in sospensione dei corsi d'acqua padani e sulla degradazione del suolo nel bacino del Po. *Giornale del Genio Civile*, 5: 252-272.

Campbell, A., and Wang, Y. (2019). High Spatial Resolution Remote Sensing for Salt Marsh Mapping and Change Analysis at Fire Island National Seashore. *Remote Sensing* 11, 1107. doi:10.3390/rs11091107.

Cao, H., Zhu, Z., Belzen, J., Gourgue, O., Koppel, J., Temmerman, O. S., et al. (2021). Salt marsh establishment in poorly consolidated muddy systems: effects of surface drainage, elevation, and plant age. *Ecosphere* 12. doi:10.1002/ecs2.3755.

Capobianco, M., and Stive, M. J. F. (2000). Soft intervention technology as a tool for integrated coastal zone management. *J Coast Conserv* 6, 33–40. doi:10.1007/BF02730465.

Casella, E.; Rovere, A.; Pedroncini, A.; Mucerino, L.; Casella, M.; Cusati, L.A.; Vacchi, M.; Ferrari, M.; Firpo, M. (2014). Study of wave runup using numerical models and low-altitude aerial

photogrammetry: A tool for coastal management. *Estuarine, Coastal and Shelf Science* 149, 160–167. doi:10.1016/j.ecss.2014.08.012.

Casella, E.; Rovere, A.; Pedroncini, A.; Stark, C.P.; Casella, M.; Ferrari, M.; Firpo, M. (2016). Drones as tools for monitoring beach topography changes in the Ligurian Sea (NW Mediterranean). *Geo-Mar Lett* 36, 151–163. doi:10.1007/s00367-016-0435-9.

Casella, E., Drechsel, J., Winter, C., Benninghoff, M., and Rovere, A. (2020). Accuracy of sand beach topography surveying by drones and photogrammetry. *Geo-Mar Lett* 40, 255–268. doi:10.1007/s00367-020-00638-8.

Cencini, C. (1998). Physical Processes and Human Activities in the Evolution of the Po Delta, Italy. *J. Coast. Res.*, *14*, 774–793, doi:10.2307/4298834.

Chen, M. S., Wartel, S., Eck, B. V., and Maldegem, D. V. (2005). Suspended matter in the Scheldt estuary. *Hydrobiologia* 540, 79–104. doi:10.1007/s10750-004-7122-y.

Cheng Wang, Menenti, M., Stoll, M.-P., Feola, A., Belluco, E., and Marani, M. (2009). Separation of Ground and Low Vegetation Signatures in LiDAR Measurements of Salt-Marsh Environments. *IEEE Trans. Geosci. Remote Sensing* 47, 2014–2023. doi:10.1109/TGRS.2008.2010490.

Christiansen, T., Wiberg, P. L., and Milligan, T. G. (2000). Flow and Sediment Transport on a Tidal Salt Marsh Surface. *Estuarine, Coastal and Shelf Science* 50, 315–331. doi:10.1006/ecss.2000.0548.

Chmura, G. L., Coffey, A., and Crago, R. (2001). Variation in Surface Sediment Deposition on Salt Marshes in the Bay of Fundy. *Journal of Coastal Research* 17, 221–227.

Ciabatti, M., (1967). *Ricerche sull'evoluzione del delta padano*. G. Geol. 34/1966, 381–410. CIESM, 2006. Fluxes of small and medium-size Mediterranean rivers: impact on coastal areas. CIESMWorkshop Monographs, No. 30, Trogir, 29 March–1st April 2006. 16 pp.

Ciavola, P., Organo, C., Vintró, L. L., and Mitchell, P. I. (2002). Sedimentation Processes on Intertidal Areas of the Lagoon of Venice: Identification of Exceptional Flood Events (Acqua

Alta) Using Radionuclides. *Journal of Coastal Research* 36, 139–147. doi:10.2112/1551-5036-36.sp1.139.

Claessens, J., and Belmans, H. (1984). Overview of the tidal observations in the Scheldt basin during the decennium 1971–1980. Tijdschrift der Openbare Werken van Belgie, No. 3.

Coco, G., Zhou, Z., van Maanen, B., Olabarrieta, M., Tinoco, R., and Townend, I. (2013). Morphodynamics of tidal networks: Advances and challenges. *Marine Geology* 346, 1–16. doi:10.1016/j.margeo.2013.08.005.

Colombo, C.; Tosini, L. (2009). Sessant'anni di bonifica nel delta del Po. Padova (IT): Papergraf S.p.a. Italian.

Corbau, C., Zambello, E., Nardin, W., Simeoni, U., Secular diachronic analysis of coastal marshes and lagoons evolution: Study case of the Po river delta (Italy), *Estuarine, Coastal and Shelf Science* (2022), doi: https://doi.org/10.1016/j.ecss.2022.107781.

Correggiari, A., Cattaneo, A., and Trincardi, F. (2005). The modern Po Delta system: Lobe switching and asymmetric prodelta growth. *Marine Geology* 222–223, 49–74. doi:10.1016/j.margeo.2005.06.039.

Cortese, L., and Fagherazzi, S. (2022). Fetch and distance from the bay control accretion and erosion patterns in Terrebonne marshes (Louisiana, USA). *Earth Surf Processes Landf*, esp.5327. doi:10.1002/esp.5327.

Cousins, L. J., Cousins, M. S., Gardiner, T., and Underwood, G. J. C. (2017). Factors influencing the initial establishment of salt marsh vegetation on engineered sea wall terraces in south east England. *Ocean & Coastal Management* 143, 96–104. doi:10.1016/j.ocecoaman.2016.11.010.

Cox, J. R., Paauw, M., Nienhuis, J. H., Dunn, F. E., van der Deijl, E., Esposito, C., et al. (2022). A global synthesis of the effectiveness of sedimentation-enhancing strategies for river deltas and estuaries. *Global and Planetary Change* 214, 103796. doi: 10.1016/j.gloplacha.2022.103796.

Crosby, S. C., Sax, D. F., Palmer, M. E., Booth, H. S., Deegan, L. A., Bertness, M. D., et al. (2016). Salt marsh persistence is threatened by predicted sea-level rise. *Estuarine, Coastal and Shelf Science* 181, 93–99. doi:10.1016/j.ecss.2016.08.018.

Culberson, S. D., Foin, T. C., and Collins, J. N. (2004). The Role of Sedimentation in Estuarine Marsh Development within the San Francisco Estuary, CA, USA. *Journal of Coastal Research* 20, 13.

Da Lio, C., and Tosi, L. (2019). Vulnerability to relative sea-level rise in the Po river delta (Italy). *Estuarine, Coastal and Shelf Science* 228, 106379. doi:10.1016/j.ecss.2019.106379.

Dąbski, M., Zmarz, A., Pabjanek, P., Korczak-Abshire, M., Karsznia, I., and Chwedorzewska, K. J. (2017). UAV-based detection and spatial analyses of periglacial landforms on Demay Point (King George Island, South Shetland Islands, Antarctica). *Geomorphology* 290, 29–38. doi:10.1016/j.geomorph.2017.03.033.

Daborn G. R., Brylinsky M., and van Proosdij D. (2002). Ecological Studies of the Windsor Causeway and Pesaquid Lake. Acadia Centre for Estuarine Research Publication No. 69. Downloadable at:https://novascotia.ca/tran/highways/3_Mile_Plains_to_Falmouth/ACER_69_2003%20Avon%20Report.pdf

Dai, W., Li, H., Zhou, Z., Cybele, S., Lu, C., Zhao, K., et al. (2018). UAV Photogrammetry for Elevation Monitoring of Intertidal Mudflats. *Journal of Coastal Research* 85, 236–240. doi:10.2112/SI85-048.1.

Dal Cin, R. (1983). I litorali del delta del Po e alle fois dell' Adige e del Brenta; caratteri tessiturali e dispersione dei sedimenti, cause dell'arretramento e perisioni sull' evoluzione futura. *Italian Journal of Geosciences* 102, 9–56.

Dalrymple, R.W., Knight, R.J., Zaitlin, B.A., Middleton, G.V., (1990). Dynamics and facies model of a macrotidal sand-bar complex, Cobequid Bay Salmon River estuary (Bay of Fundy). Sedimentology 37 (4), 577–612.

Dal Cin R. e Simeoni U. (1984). *Variazioni volumetriche del delta padano nell'ultimo secolo, distribuzione dei sedimenti nei rami deltizi e caratteri granulometrici dei materiali cavati nel basso Po*. In: Atti del 2° Convegno di Idraulica Padana, Tecnografica, Parma, I. pp. 255-279.

D'Alpaos, A., Lanzoni, S., Mudd, S. M., and Fagherazzi, S. (2006). Modeling the influence of hydroperiod and vegetation on the cross-sectional formation of tidal channels. *Estuarine, Coastal and Shelf Science* 69, 311–324. doi:10.1016/j.ecss.2006.05.002.

D'Alpaos, A., Mudd, S. M., and Carniello, L. (2011). Dynamic response of marshes to perturbations in suspended sediment concentrations and rates of relative sea level rise. *J. Geophys. Res.* 116, F04020. doi:10.1029/2011JF002093.

Day, J. W., Pont, D., Hensel, P. F., Ibañez, C. (1995). Impacts of Sea-Level Rise on Deltas in the Gulf of Mexico and the Mediterranean: The Importance of Pulsing Events to Sustainability. *Estuaries* 18, 636. doi:10.2307/1352382.

Day, J. W., Rismondo, A., Scarton, F., Are, D., and Cecconi, G. (1998). Relative sea level rise and Venice lagoon wetlands. *J Coast Conserv* 4, 27–34. doi:10.1007/BF02806486.

Day, J., Ibáñez, C., Scarton, F., Pont, D., Hensel, P., Day, J., et al. (2011). Sustainability of Mediterranean Deltaic and Lagoon Wetlands with Sea-Level Rise: The Importance of River Input. *Estuaries and Coasts* 34, 483–493. doi:10.1007/s12237-011-9390-x.

Day, J. W., Lane, R. R., D'Elia, C. F., Wiegman, A. R. H., Rutherford, J. S., Shaffer, G. P., et al. (2016). Large infrequently operated river diversions for Mississippi delta restoration. *Estuarine, Coastal and Shelf Science* 183, 292–303. doi: 10.1016/j.ecss.2016.05.001.

de Vet, P. L. M., van Prooijen, B. C., and Wang, Z. B. (2017). The differences in morphological development between the intertidal flats of the Eastern and Western Scheldt. *Geomorphology* 281, 31–42. doi:10.1016/j.geomorph.2016.12.031.

De Vlas, J., Mandema, F.S., Nolte, S., Van Klink, R. & Esselink, P. (2013). Nature conservation of salt marshes – The influence of grazing on biodiversity. *Report It Fryske Gea, Olterterp.*

Doughty, C., and Cavanaugh, K. (2019). Mapping Coastal Wetland Biomass from High Resolution Unmanned Aerial Vehicle (UAV) Imagery. *Remote Sensing* 11, 540. doi:10.3390/rs11050540.

Duarte, B., Santos, D., Marques, J. C., and Caçador, I. (2014). Biophysical probing of Spartina maritima photo-system II changes during prolonged tidal submersion periods. *Plant Physiology and Biochemistry* 77, 122–132. doi:10.1016/j.plaphy.2014.01.023.

Duffy, J. P., Pratt, L., Anderson, K., Land, P. E., and Shutler, J. D. (2018). Spatial assessment of intertidal seagrass meadows using optical imaging systems and a lightweight drone. *Estuarine, Coastal and Shelf Science* 200, 169–180. doi:10.1016/j.ecss.2017.11.001.

Duo, E., Trembanis, A. C., Dohner, S., Grottoli, E., and Ciavola, P. (2018). Local-scale post-event assessments with GPS and UAV-based quick-response surveys: a pilot case from the Emilia–Romagna (Italy) coast. *Nat. Hazards Earth Syst. Sci.* 18, 2969–2989. doi:10.5194/nhess-18-2969-2018.

Duo, E., Fabbri, S., Grottoli, E., and Ciavola, P. (2021). Uncertainty of Drone-Derived DEMs and Significance of Detected Morphodynamics in Artificially Scraped Dunes. *Remote Sensing* 13, 1823. doi: 10.3390/rs13091823.

Duvall, M. S., Wiberg, P. L., and Kirwan, M. L. (2019). Controls on Sediment Suspension, Flux, and Marsh Deposition near a Bay-Marsh Boundary. *Estuaries and Coasts* 42, 403–424. doi:10.1007/s12237-018-0478-4.

Dyer, K. R., Christie, M. C., and Wright, E. W. (2000). The classification of intertidal mudflats. *Continental Shelf Research*, 22.

Evans, B. R., Möller, I., Spencer, T., and Smith, G. (2019). Dynamics of salt marsh margins are related to their three-dimensional functional form. *Earth Surf. Process. Landforms*, esp.4614. doi:10.1002/esp.4614.

Fabris, M. (2019). Coastline evolution of the Po River Delta (Italy) by archival multi-temporal digital photogrammetry. *Geomatics, Natural Hazards and Risk* 10, 1007–1027. doi:10.1080/19475705.2018.1561528.

Fagherazzi, S., Carniello, L., D'Alpaos, L., and Defina, A. (2006). Critical bifurcation of shallow microtidal landforms in tidal flats and salt marshes. *Proceedings of the National Academy of Sciences* 103, 8337–8341. doi:10.1073/pnas.0508379103.

Fagherazzi, S., Kirwan, M. L., Mudd, S. M., Guntenspergen, G. R., Temmerman, S., D'Alpaos, A., Koppel, J., Rybczyk, J. M., Reyes E., Craft C., Clough J. (2012). Numerical models of salt marsh evolution: Ecological, geomorphic, and climatic factors. *Rev. Geophys.* 50, RG1002. doi:10.1029/2011RG000359.

Fagherazzi, S. and Mariotti, G. (2012). Mudflat runnels: Evidence and importance of very shallow flows in intertidal morphodynamics, Geophys. Res. Lett., 39, L14402, https://doi.org/10.1029/2012GL052542.

Fernandez-Nunez, M., Burningham, H., and Ojeda Zujar, J. (2017). Improving accuracy of LiDAR-derived digital terrain models for saltmarsh management. *J Coast Conserv* 21, 209–222. doi:10.1007/s11852-016-0492-2.

Ferrari, C., Gerdol, R., and Piccoli, F. (1985). The halophilous vegetation of the Po Delta (northern Italy). *Vegetatio* 61, 5–14. doi:10.1007/BF00039805.

Fettweis, M., Sas, M., and Monbaliu, J. (1998). Seasonal, Neap-spring and Tidal Variation of Cohesive Sediment Concentration in the Scheldt Estuary, Belgium. *Estuarine, Coastal and Shelf Science* 47, 21–36. doi:10.1006/ecss.1998.0338.

Fonstad, M. A., Dietrich, J. T., Courville, B. C., Jensen, J. L., and Carbonneau, P. E. (2013). Topographic structure from motion: a new development in photogrammetric measurement: Topographic structure from motion. *Earth Surf. Process. Landforms* 38, 421–430. doi:10.1002/esp.3366.

Francis P. Shepard (1954). Nomenclature Based on Sand-silt-clay Ratios. *SEPM JSR* Vol. 24. doi:10.1306/D4269774-2B26-11D7-8648000102C1865D.

French, J.R. (1993), *Numerical simulation of vertical marsh growth and adjustment to accelerated sea-level rise, North Norfolk, U.K.. Earth Surf. Process. Landforms, 18: 63-81. https://doi.org/10.1002/esp.3290180105*

French, J. R., Spencer, T., Murray, A. L., and Arnold, N. S. (1995). Geostatistical Analysis of Sediment Deposition In Two Small Tidal Wetlands, Norfolk, U.K. *Journal of Coastal Research* 11, 14.

Friedrichs, C. T. (2011). “Tidal Flat Morphodynamics,” in *Treatise on Estuarine and Coastal Science* (Elsevier), 137–170. doi:10.1016/B978-0-12-374711-2.00307-7.

Frostick, L.E.; McCave, I. *Seasonal shifts of sediment within an estuary mediated by algal growth. Estuar. Coast. Mar. Sci.* ***1979****, 9, 569–576, doi:10.1016/0302-3524(79)90080-x.*

Gadow, S., 1970. Sedimente und chemismus. In: Reineck, H.E., (Ed.), Das Watt, Ablagerungs- und Lebensraum. Waldemar Kramer, Frankfurt, pp. 23–35.

Gaglio, M., Aschonitis, V. G., Gissi, E., Castaldelli, G., and Fano, E. A. (2017). Land use change effects on ecosystem services of river deltas and coastal wetlands: case study in Volano–Mesola–Goro in Po river delta (Italy). *Wetlands Ecol Manage* 25, 67–86. doi:10.1007/s11273-016-9503-1.

Gain, A. K., Benson, D., Rahman, R., Datta, D. K., and Rouillard, J. J. (2017). Tidal river management in the south west Ganges-Brahmaputra delta in Bangladesh: Moving towards a transdisciplinary approach? *Environmental Science & Policy* 75, 111–120. doi: 10.1016/j.envsci.2017.05.020.

Galliniani, P., (1985). *Sedimentazione recente ed attuale nei fondali antistanti il delta del Po*. Atti Tav. rot. “Il Delta del Po – Sezione Geologica – Bologna 24 Novembre 1982. Acc. Sc. Ist., Bologna, pp. 85–99.

Galloway W. (1975). Process framework for describing the morphologic and stratigraphic evolution of deltaic depositional system. Society of Economic Paleontologists and Mineralogist (SEPM), Special Publication No. 31. 127-156.

Ganju, N. K., Defne, Z., Kirwan, M. L., Fagherazzi, S., D’Alpaos, A., and Carniello, L. (2017). Spatially integrative metrics reveal hidden vulnerability of microtidal salt marshes. *Nat Commun* 8, 14156. doi:10.1038/ncomms14156.

Ganong, W.F., 1903. The vegetation of the Bay of Fundy salt and diked marshes: an ecological study. Bot. Gaz. 36, 161–186.

Greenberg, D.A. (1984). A review of the physical oceanography of the Bay of Fundy. In: Gordon, D.C. JR. and Dadswell, M.J. (eds.), Update on the Marine Environmental Consequences of

Tidal Power Development in the Upper Reaches of the Bay of Fundy Canadian Technical Report of Fisheries and Aquatic Sciences No. 1256. pp. 9-31.

Greenberg, D. A., Blanchard, W., Smith, B., and Barrow, E. (2012). Climate Change, Mean Sea Level and High Tides in the Bay of Fundy. *Atmosphere-Ocean* 50, 261–276. doi: 10.1080/07055900.2012.668670.

Gedan, K. B., Kirwan, M. L., Wolanski, E., Barbier, E. B., and Silliman, B. R. (2011). The present and future role of coastal wetland vegetation in protecting shorelines: answering recent challenges to the paradigm. *Climatic Change* 106, 7–29. doi:10.1007/s10584-010-0003-7.

Geng, L., Gong, Z., Zhou, Z., Lanzoni, S., and D'Alpaos, A. (2020). Assessing the relative contributions of the flood tide and the ebb tide to tidal channel network dynamics. *Earth Surf. Process. Landforms* 45, 237–250. doi:10.1002/esp.4727.

Ghosh, S., and Mishra, D. (2017). Analyzing the Long-Term Phenological Trends of Salt Marsh Ecosystem across Coastal Louisiana. *Remote Sensing* 9, 1340. doi:10.3390/rs9121340.

Gindraux, S., Boesch, R., and Farinotti, D. (2017). Accuracy Assessment of Digital Surface Models from Unmanned Aerial Vehicles' Imagery on Glaciers. *Remote Sensing* 9, 186. doi:10.3390/rs9020186.

Goodbred, S. L., and Hine, A. C. (1995). Coastal storm deposition: Salt-marsh response to a severe extratropical storm, March 1993, west-central Florida. *Geology*; v. 23; no. 8; p. 679–682.

Grabemann, H.-J., Grabemann, I., and Eppel, D. P. (2004). Climate Change and Hydrodynamic Impact in the Jade-Weser Area: a Case Study, Coastline Report, 1. Warnemunde: Geographie Der Department of Drainage and Irrigation, Kuala Meere Und Küste, 9.

Gray, A. J., Clarke, R. T., Warman, E. A., and Johnson, P. J. (1989). Prediction of marginal vegetation in a post-barrage environment. Energy Technology Support Unit Report ETSU-TID-4070.

Gray, A. J. (1992). Saltmarsh plant ecology: zonation and succession revisited. *Cambridge University Press – Saltmarshes: Morphodynamics, Conservation and Engineering Significance. Chapter 4:* pp. 63 – 79.

Green, M. O., and Hancock, N. J. (2012). Sediment transport through a tidal creek. *Estuarine, Coastal and Shelf Science* 109, 116–132. doi:10.1016/j.ecss.2012.05.030.

Green, M. O., and Coco, G. (2014). Review of wave-driven sediment resuspension and transport in estuaries: Wave-driven sediment transport. *Rev. Geophys.* 52, 77–117. doi:10.1002/2013RG000437.

Green, D., Mauquoy, D., Hagon, J., Angus, S., Hansom, J., Rennie, A., et al. (2017). Monitoring, mapping and Modelling saltmarsh: the UAV way. *GIS Professional* August 2017, 22–28.

Gunnell, J. R., Rodriguez, A. B., and McKee, B. A. (2013). How a marsh is built from the bottom up. *Geology* 41, 859–862. doi:10.1130/G34582.1.

Harrison, E. Z., and Bloom, A. L. (1977). Sedimentation rates on tidal salt marshes in Connecticut. *Journal of Sedimentary Research* 47, 1484–1490. doi:10.1306/212F739C-2B24-11D7-8648000102C1865D.

Hatton, R. S., DeLaune, R. D., and Patrick, W. H. (1983). Sedimentation, accretion, and subsidence in marshes of Barataria Basin, Louisiana1: Marsh accretion, subsidence. *Limnol. Oceanogr.* 28, 494–502. doi:10.4319/lo.1983.28.3.0494.

Heiri, O., Lotter, A. F., and Lemcke, G. (2001). Loss on ignition as a method for estimating organic and carbonate content in sediments: reproducibility and comparability of results. *Journal of Paleolimnology* **25:** 101–110.

Hensel, P. E., Jr., J. W. D., and Pont, D. (1999). Wetland Vertical Accretion and Soil Elevation Change in the Rhône River Delta, France: The Importance of Riverine Flooding. *Journal of Coastal Research* 15, 668–681.

Hladik, C., and Alber, M. (2012). Accuracy assessment and correction of a LIDAR-derived salt marsh digital elevation model. *Remote Sensing of Environment* 121, 224–235. doi:10.1016/j.rse.2012.01.018.

Ibáñez, C., Sharpe, P. J., Day, J. W., Day, J. N., and Prat, N. (2010). Vertical Accretion and Relative Sea Level Rise in the Ebro Delta Wetlands (Catalonia, Spain). *Wetlands* 30, 979–988. doi:10.1007/s13157-010-0092-0.

ICRAM (2004). Ministero Dell'ambiente e Della Tutela del Territorio. Servizion Difesa Mare. Metodologie Analitiche di Riferimento. Programma di Monitoraggio per il Controllo Dell'ambiente Marino-Costiero (triennio 2001-2003). Available at: http://www.isprambiente.gov.it/it/pubblicazioni manuali-e-linee-guida/ (accessed August 29, 2019).

Idroser (1994) - *Aggiornamento ed integrazione del Piano progettuale per la difesa della costa adriatica emilianoromagnola. Relazione generale*. Regione Emilia-Romagna, Bologna. pp. 276.

James, M. R., Robson, S., d'Oleire-Oltmanns, S., and Niethammer, U. (2017). Optimising UAV topographic surveys processed with structure-from-motion: Ground control quality, quantity and bundle adjustment. *Geomorphology* 280, 51–66. doi:10.1016/j.geomorph.2016.11.021.

Jankowski, K. L., Törnqvist, T. E., and Fernandes, A. M. (2017). Vulnerability of Louisiana's coastal wetlands to present-day rates of relative sea-level rise. *Nat Commun* 8, 14792. doi:10.1038/ncomms14792.

Jaud, M., Grasso, F., Le Dantec, N., Verney, R., Delacourt, C., Ammann, J., et al. (2016). Potential of UAVs for Monitoring Mudflat Morphodynamics (Application to the Seine Estuary, France). *IJGI* 5, 50. doi:10.3390/ijgi5040050.

Javernick, L., Brasington, J., and Caruso, B. (2014). Modeling the topography of shallow braided rivers using Structure-from-Motion photogrammetry. *Geomorphology* 213, 166–182. doi:10.1016/j.geomorph.2014.01.006.

Johnson, T. C. (1981). Origin of sedimentary rocks (Second edn.), H. Blatt, G. Middleton, and R. Murray, Prentice-Hall, Inc., 1980. *Earth Surface Processes and Landforms* 6, 97–97. doi:10.1002/esp.3290060115.

Joyce, K. E., Duce, S., Leahy, S. M., Leon, J., and Maier, S. W. (2019). Principles and practice of acquiring drone-based image data in marine environments. *Mar. Freshwater Res.* 70, 952. doi:10.1071/MF17380.

Kalacska, M., Chmura, G. L., Lucanus, O., Bérubé, D., and Arroyo-Mora, J. P. (2017). Structure from motion will revolutionize analyses of tidal wetland landscapes. *Remote Sensing of Environment* 199, 14–24. doi:10.1016/j.rse.2017.06.023.

Kwakernaak, C., & Lenselink, G. (2015). Economische en ecologische perspectieven van een dubbele dijk langs de Eems-Dollard.

Kim, K.-L., Kim, B.-J., Lee, Y.-K., and Ryu, J.-H. (2019). Generation of a Large-Scale Surface Sediment Classification Map using Unmanned Aerial Vehicle (UAV) Data: A Case Study at the Hwang-do Tidal Flat, Korea. *Remote Sensing* 11, 229. doi:10.3390/rs11030229.

Kirwan, M. L., Guntenspergen, G. R., D'Alpaos, A., Morris, J. T., Mudd, S. M., and Temmerman, S. (2010). Limits on the adaptability of coastal marshes to rising sea level: Ecogeomorpgic limits to wetland survival. *Geophysical Research Letters* 37, n/a-n/a. doi:10.1029/2010GL045489.

Kirwan, M. L., and Megonigal, J. P. (2013). Tidal wetland stability in the face of human impacts and sea-level rise. *Nature* 504, 53–60. doi:10.1038/nature12856.

Kirwan, M. L., Temmerman, S., Skeehan, E. E., Guntenspergen, G. R., and Fagherazzi, S. (2016). Overestimation of marsh vulnerability to sea level rise. *Nature Clim Change* 6, 253–260. doi:10.1038/nclimate2909.

Klemas, V. V. (2014). "Remote Sensing of Coastal Ecosystems and Environments," in *Remote Sensing and Modeling* Coastal Research Library., eds. C. W. Finkl and C. Makowski (Cham: Springer International Publishing), 3–30. doi:10.1007/978-3-319-06326-3_1.

Koch, E. W., Barbier, E. B., Silliman, B. R., Reed, D. J., Perillo, G. M., Hacker, S. D., et al. (2009). Non-linearity in ecosystem services: temporal and spatial variability in coastal protection. *Frontiers in Ecology and the Environment* 7, 29–37. doi:10.1890/080126.

Lenstra, K. J. H., Ridderinkhof, W., and Vegt, M. (2019). Unraveling the Mechanisms That Cause Cyclic Channel-Shoal Dynamics of Ebb-Tidal Deltas: A Numerical Modeling Study. *J. Geophys. Res. Earth Surf.* 124, 2778–2797. doi:10.1029/2019JF005090.

Leonard, L. A., Hine, A. C., and Luther, M. E. (1995). Surficial Sediment Transport and Deposition Processes in a Juncus roemerianus Marsh, West- Central Florida. *Journal of Coastal Research* 11, 322–336.

Leonard, L. A. (1997). Controls of sediment transport and deposition in an incised mainland marsh basin, southeastern North Carolina. *Wetlands* 17, 263–274. doi:10.1007/BF03161414.

Leonard, L. A., Wren, P. A., and Beavers, R. L. (2002). Flow dynamics and sedimentation in Spartina alterniflora and Phragmites australis marshes of the Chesapeake Bay. *Wetlands* 22, 415–424. doi:10.1672/0277-5212(2002)022[0415:FDASIS]2.0.CO;2.

Leonardi, N., and Fagherazzi, S. (2015). Effect of local variability in erosional resistance on large-scale morphodynamic response of salt marshes to wind waves and extreme events: Resistance Variability Affects Marsh. *Geophys. Res. Lett.* 42, 5872–5879. doi: 10.1002/2015GL064730.

Leonardi, N., Carnacina, I., Donatelli, C., Ganju, N. K., Plater, A. J., Schuerch, M., et al. (2018). Dynamic interactions between coastal storms and salt marshes: A review. *Geomorphology* 301, 92–107. doi:10.1016/j.geomorph.2017.11.001.

Letzsch, S,W. and R.W. Frey. 1980. *Deposition and erosion in a Holocene salt marsh, Sapelo Island, Georgia. JoumM of Sedimentary Petrology 50:529-542.*

Long, N., Millescamps, B., Guillot, B., Pouget, F., and Bertin, X. (2016). Monitoring the Topography of a Dynamic Tidal Inlet Using UAV Imagery. *Remote Sensing* 8, 387. doi:10.3390/rs8050387.

Ludwig, W., Dumont, E., Meybeck, M., and Heussner, S. (2009). River discharges of water and nutrients to the Mediterranean and Black Sea: Major drivers for ecosystem changes during past and future decades? *Progress in Oceanography* 80, 199–217. doi:10.1016/j.pocean.2009.02.001.

MacKenzie, R., and Dionne, M. (2008). Habitat heterogeneity: importance of salt marsh pools and high marsh surfaces to fish production in two Gulf of Maine salt marshes. *Mar. Ecol. Prog. Ser.* 368, 217–230. doi:10.3354/meps07560.

Maicu, F., De Pascalis, F., Ferrarin, C., and Umgiesser, G. (2018). Hydrodynamics of the Po River-Delta-Sea System. *J. Geophys. Res. Oceans* 123, 6349–6372. doi:10.1029/2017JC013601.

Mancini, F., Dubbini, M., Gattelli, M., Stecchi, F., Fabbri, S., and Gabbianelli, G. (2013). Using Unmanned Aerial Vehicles (UAV) for High-Resolution Reconstruction of Topography: The Structure from Motion Approach on Coastal Environments. *Remote Sensing* 5, 6880–6898. doi:10.3390/rs5126880.

Marani, M., D'Alpaos, A., Lanzoni, S., Carniello, L., and Rinaldo, A. (2007). Biologically-controlled multiple equilibria of tidal landforms and the fate of the Venice lagoon. *Geophys. Res. Lett.* 34, L11402. doi:10.1029/2007GL030178.

Marani, M., D'Alpaos, A., Lanzoni, S., Carniello, L., and Rinaldo, A. (2010). The importance of being coupled: Stable states and catastrophic shifts in tidal biomorphodynamics. *J. Geophys. Res.* 115, F04004. doi:10.1029/2009JF001600.

Marchi, E., Roth, G., and Siccardi, F. (1995). The Po: Centuries of River Training. *Phys. Chem. Earth,* Vol. 20, No. 5-6, pp. 475-478.

Marion, C., Anthony, E. J., and Trentesaux, A. (2009). Short-term (≤2 yrs) estuarine mudflat and saltmarsh sedimentation: High-resolution data from ultrasonic altimetery, rod surface-elevation table, and filter traps. *Estuarine, Coastal and Shelf Science* 83, 475–484. doi:10.1016/j.ecss.2009.03.039.

Maselli, V., and Trincardi, F. (2013). Man made deltas. *Sci Rep* 3, 1926. doi:10.1038/srep01926.

Masselink, G., and Lazarus, E. D. (2019). Defining Coastal Resilience. *Water* 11, 2587. doi:10.3390/w11122587.

Mayor, J. R., and Hicks, C. E. (2009). "Potential impacts of elevated CO2 on plant interactions, sustained growth, and carbon cycling in salt marsh ecosystems," in Human Impacts on Salt Marshes: A Global Perspective, eds B. R. Silliman, E. D. Grosholz, and M. D. Bertness (Berkeley, CA: University of California Press), 207–228.

McHone, J. G. (1977). Triplot: an APL program for plotting triangular diagrams. *Computers & Geosciences* 3, 633–635. doi:10.1016/0098-3004(77)90044-9.

Mckee, K.L., Patrick, W.H. (1988). The relationship of smooth cordgrass (Spartina alterniflora) to tidal datums: a review. *Estuaries* 11, 143-151.

Meire, P., Ysebaert, T., Damme, S. V., Bergh, E. V. den, Maris, T., and Struyf, E. (2005). The Scheldt estuary: a description of a changing ecosystem. *Hydrobiologia* 540, 1–11. doi:10.1007/s10750-005-0896-8.

Mfikili, A. N., Bornman, T. G., and du Preez, D. R. (2022). Sediment deposition and its implications for vertical accretion in an intertidal salt marsh—A case study of a microtidal estuary along the southeast coast of South Africa. *Regional Studies in Marine Science* 51, 102203. doi:10.1016/j.rsma.2022.102203.

Millard, K., Redden, A. M., Webster, T., and Stewart, H. (2013). Use of GIS and high resolution LiDAR in salt marsh restoration site suitability assessments in the upper Bay of Fundy, Canada. *Wetlands Ecol Manage* 21, 243–262. doi:10.1007/s11273-013-9303-9.

Millennium Ecosystem Assessment. (2005). Ecosystems and human well-being: synthesis. *Washington, DC: Island Press*. Downloadable from: https://www.millenniumassessment.org/en/Framework.html.

Miller, R. L, Fram, M., Fujii, R., & Wheeler, G. (2008). Subsidence Reversal in a Re-established Wetland in the Sacramento-San Joaquin Delta, California, USA. *San Francisco Estuary and Watershed Science*, 6(3). doi:https://doi.org/10.15447/sfews.2008v6iss3art1

Mitchener, H. and Torfs, H.: Erosion of mud/sand mixtures, Coast. Eng., 29, 1–25, 1996.

Möller, I., Kudella, M., Rupprecht, F., Spencer, T., Paul, M., van Wesenbeeck, B. K., et al. (2014). Wave attenuation over coastal salt marshes under storm surge conditions. *Nature Geosci* 7, 727–731. doi:10.1038/ngeo2251.

Moloney, J. G., Hilton, M. J., Sirguey, P., and Simons-Smith, T. (2018). Coastal Dune Surveying Using a Low-Cost Remotely Piloted Aerial System (RPAS). *Journal of Coastal Research* 345, 1244–1255. doi:10.2112/JCOASTRES-D-17-00076.1.

Morris, J. T., Porter, D., Neet, M., Noble, P. A., Schmidt, L., Lapine, L. A., et al. (2005). Integrating LIDAR elevation data, multi-spectral imagery and neural network modelling for marsh

characterization. *International Journal of Remote Sensing* 26, 5221–5234. doi:10.1080/01431160500219018.

Morton R. A. and White W. A. (1997). Characteristics of and Corrections for Core Shortening in Unconsolidated Sediments. *Journal of Coastal Research* 13, 3, 761-769. https://www.jstor.org/stable/4298671.

Mossman, H. L., Davy, A. J., and Grant, A. (2012). Does managed coastal realignment create saltmarshes with 'equivalent biological characteristics' to natural reference sites? *J Appl Ecol* 49, 1446–1456. doi:10.1111/j.1365-2664.2012.02198.x.

Mount, R. Acquisition of Through-water Aerial Survey Images: Surface Effects and the Prediction of Sun Glitter and Subsurface Illumination. *Photogrammetric Engineering*, 9.

Mudd, S. M., D'Alpaos, A., and Morris, J. T. (2010). How does vegetation affect sedimentation on tidal marshes? Investigating particle capture and hydrodynamic controls on biologically mediated sedimentation. *J. Geophys. Res.* 115, F03029. doi:10.1029/2009JF001566.

Murray, A. B., Knaapen, M. A. F., Tal, M., and Kirwan, M. L. (2008). Biomorphodynamics: Physical-biological feedbacks that shape landscapes: Opinion. *Water Resour. Res.* 44. doi:10.1029/2007WR006410.

Nardin, W., and Edmonds, D. A. (2014). Optimum vegetation height and density for inorganic sedimentation in deltaic marshes. *Nature Geosci* 7, 722–726. doi:10.1038/ngeo2233.

Nelson, B. W. (1970). "Hydrography, Sediment Dispersal, and Recent Historical Development of the Po River Delta, Italy1," in *Deltaic Sedimentation, Modern and Ancient*, eds. J. P. Morgan and R. H. Shaver (SEPM Society for Sedimentary Geology), 0. doi:10.2110/pec.70.11.0152.

Neumeier, U., and Ciavola, P. (2004). Flow Resistance and Associated Sedimentary Processes in a Spartina maritima Salt-Marsh. *Journal of Coastal Research* 202, 435–447. doi:10.2112/1551-5036(2004)020[0435:FRAASP]2.0.CO;2.

Nihoul, J. C. J., Ronday, F. C., Peters, J. J., and Sterling, A. (1978). "Hydrodynamics of the Scheldt Estuary," in *Elsevier Oceanography Series* (Elsevier), 27–53. doi:10.1016/S0422-9894(08)71270-4.

Ninfo, A., Ciavola, P., and Billi, P. (2018). The Po Delta is restarting progradation: geomorphological evolution based on a 47-years Earth Observation dataset. *Sci Rep* 8, 3457. doi:10.1038/s41598-018-21928-3.

Nolte, S., Koppenaal, E. C., Esselink, P., Dijkema, K. S., Schuerch, M., De Groot, A. V., et al. (2013). Measuring sedimentation in tidal marshes: a review on methods and their applicability in biogeomorphological studies. *J Coast Conserv* 17, 301–325. doi:10.1007/s11852-013-0238-3.

Odum, W. E., McIvor, C. C., and Smith, T. J. (1982). The Ecology of the Mangroves of South Florida: A Community Profile. U.S. Fish and Wildlife Service, Office of Biological Services, Washington, 156.

Oosterlee, L., Cox, T. J. S., Vandenbruwaene, W., Maris, T., Temmerman, S., and Meire, P. (2017). Tidal Marsh Restoration Design Affects Feedbacks Between Inundation and Elevation Change. *Estuaries and Coasts*. doi:10.1007/s12237-017-0314-2.

Orson R., Panageotou W. and Leatherman S. P. (1985). Response of Tidal Salt Marshes of the U.S. Atlantic and Gulf Coasts to Rising Sea Levels. Journal of Coastal Research, Vol. 1, No., pp. 29-37. Downloadable from: https://www.jstor.org/stable/4297007.

Ozesmi, S. L., and Bauer, M. E. (2002). Satellite remote sensing of wetlands. *Wetlands Ecology and Management. Kluwer Academic Publishers. Printed in the Netherlands.*10: 381–402.

Pannozzo, N., Smedley, R. K., Chiverrell, R. C., Carnacina, I., and Leonardi, N. (2022). An Integration of Numerical Modeling and Paleoenvironmental Analysis Reveals the Effects of Embankment Construction on Long-Term Salt Marsh Accretion. *JGR Earth Surface* 127. doi: 10.1029/2021JF006524.

Paola, C., Twilley, R. R., Edmonds, D. A., Kim, W., Mohrig, D., Parker, G., et al. (2011). Natural Processes in Delta Restoration: Application to the Mississippi Delta. *Annu. Rev. Mar. Sci.* 3, 67–91. doi:10.1146/annurev-marine-120709-142856.

Perini, L., Calabrese, L., Deserti, M., Valentini, A., Ciavola, P., and Armaroli, C. (2011). *Le mareggiate e gli impatti sulla costa in Emilia-Romagna. Project: Micore; Arpa Emilia-Romagna; 1946-2010. ISBN: 88-87854-27-5*.

Pethick (1981). Long-term Accretion Rates on Tidal Salt Marshes. *SEPM JSR* Vol. 51. doi:10.1306/212F7CDE-2B24-11D7-8648000102C1865D.

Phillips, J. D. (2018). Coastal wetlands, sea level, and the dimensions of geomorphic resilience. *Geomorphology* 305, 173–184. doi:10.1016/j.geomorph.2017.03.022.

Porter, C., Lundholm, J., Bowron, T., Lemieux, B., van Proosdij, D., Neatt, N., et al. (2015). Classification and environmental correlates of tidal wetland vegetation in Nova Scotia, Canada. *Botany* 93, 825–841. doi:10.1139/cjb-2015-0066.

Pratolongo, P., Leonardi, N., Kirby, J. R., and Plater, A. (2019). "Temperate coastal wetlands," in Coastal Wetlands, eds G. Perillo, E. Wolanski, D. Cahoon, and M. Brinson (Amsterdam: Elsevier), 105–152. doi: 10.1016/b978-0-444-63893- 9.00003-4

Price, D. C. (2016). Influence of vegetation on sediment accumulation in tidal saltmarshes: An integrated field and modelling study. Ph.D. thesis. *Coastal and Estuarine Research Unit UCL Department of Geography.*

Ramirez, I., and Imberger, J. (2002). The numerical simulation of the hydrodynamics of Barbamarco Lagoon, Italy. *Applied Numerical Mathematics* 40, 273–289. doi:10.1016/S0168-9274(01)00079-4.

Ramsar Convention Secretariat (2012) Information sheet on Ramsar wetlands (RIS)—2009-2014 version. https://rsis. ramsar.org/RISapp/files/RISrep/ES1265RIS.pdf. Accessed 28 May 2016

Redfield, A. C. (1972). Development of a New England Salt Marsh. *Ecological Monographs* 42, 201–237. doi:10.2307/1942263.

Reed, D. J. (1989). Patterns of Sediment Deposition in Subsiding Coastal Salt Marshes, Terrebonne Bay, Louisiana: The Role of Winter Storms. *Estuaries* 12, 222. doi:10.2307/1351901.

Reef, R., Schuerch, M., Christie, E. K., Möller, I., and Spencer, T. (2018). The effect of vegetation height and biomass on the sediment budget of a European saltmarsh. *Estuarine, Coastal and Shelf Science* 202, 125–133. doi:10.1016/j.ecss.2017.12.016.

Reimer, J., Schuerch, M., and Slawig, T. (2015). Optimization of model parameters and experimental designs with the Optimal Experimental Design Toolbox (v1.0) exemplified by

sedimentation in salt marshes. *Geoscientific Model Development* 8, 791–804. doi:10.5194/gmd-8-791-2015.

Rosso, P. H., Ustin, S. L., and Hastings, A. (2006). Use of lidar to study changes associated with Spartina invasion in San Francisco Bay marshes. *Remote Sensing of Environment* 100, 295–306. doi:10.1016/j.rse.2005.10.012.

Ryan, J. C., Hubbard, A. L., Box, J. E., Todd, J., Christoffersen, P., Carr, J. R., Holt T. O., and Snooke N. (2015). UAV photogrammetry and structure from motion to assess calving dynamics at Store Glacier, a large outlet draining the Greenland ice sheet. *The Cryosphere* 9, 1–11. doi:10.5194/tc-9-1-2015.

Sadeghi, S., and Sohrabi, H. (2019). The effect of UAV Flight Altitude on Accuracy of Individual Tree Height Extraction in a Broad-Leaved *Ukr. J. For. Wood Sci.*, *42*, 1168–1173, doi:10.5194/isprs-archives-xlii-4-w18-1168-2019.

Sanz-Ablanedo, E., Chandler, J. H., Ballesteros-Pérez, P., and Rodríguez-Pérez, J. R. (2020). Reducing systematic dome errors in digital elevation models through better UAV flight design. *Earth Surf. Process. Landforms* 45, 2134–2147. doi:10.1002/esp.4871.

Scarton, F., Day, J. W., Rismondo, A., Cecconi, G., and Are, D. (2000). Effects of an intertidal sediment fence on sediment elevation and vegetation distribution in a Venice (Italy) lagoon salt marsh. *Ecological Engineering* 16, 223–233. doi:10.1016/S0925-8574(00)00045-8.

Scarton, F., Ghirelli, L., Cavalli, I., Cazzin, M., and Scattolin, M. (2004). Spartina x Towsendii H. and J. groves, nuova alofita per la laguna di Venezia: distribuzione al 2003. *Bollettino del Museo Civico di Storia Naturale di Venezia, vol. 55.*

Shaw, J., Amos, C.L., Greenberg, D.A., O'Reilly, C.T., Parrott, D.R., Patton, E. (2010). Catastrophic tidal expansion in the Bay of Fundy, Canada. Can. J. Earth Sci. 47, 1079–1091.

Schmid, K. A., Hadley, B. C., and Wijekoon, N. (2011). Vertical Accuracy and Use of Topographic LIDAR Data in Coastal Marshes. *Journal of Coastal Research* 275, 116–132. doi:10.2112/JCOASTRES-D-10-00188.1.

Schuerch, M., Rapaglia, J., Liebetrau, V., Vafeidis, A., and Reise, K. (2012). Salt Marsh Accretion and Storm Tide Variation: an Example from a Barrier Island in the North Sea. *Estuaries and Coasts* 35, 486–500. doi:10.1007/s12237-011-9461-z.

Schuerch, M., Vafeidis, A., Slawig, T., and Temmerman, S. (2013). Modeling the influence of changing storm patterns on the ability of a salt marsh to keep pace with sea level rise: Salt marsh accretion and storm activity. *J. Geophys. Res. Earth Surf.* 118, 84–96. doi:10.1029/2012JF002471.

Schuerch, M., Dolch, T., Reise, K., and Vafeidis, A. T. (2014). Unravelling interactions between salt marsh evolution and sedimentary processes in the Wadden Sea (southeastern North Sea). *Progress in Physical Geography* 38, 691–715. doi:10.1177/0309133314548746.

Schuerch, M., Spencer, T., Temmerman, S., Kirwan, M. L., Wolff, C., Lincke, D., McOwen C. J., Pickering M. D., Reef R., Vafeidis A. T., Hinkel J., Nicholls R. J., and Brown S. (2018). Future response of global coastal wetlands to sea-level rise. *Nature* 561, 231–234. doi:10.1038/s41586-018-0476-5.

Shepard F. P.(1954). Nomenclature Based on Sand-silt-clay Ratios. *SEPM J. Sediment. Res.* Vol. 24. doi:10.1306/D4269774-2B26-11D7-8648000102C1865D.

Shepard, C. C., Crain, C. M., and Beck, M. W. (2011). The Protective Role of Coastal Marshes: A Systematic Review and Meta-analysis. *PLoS ONE* 6, e27374. doi:10.1371/journal.pone.0027374.

Silvestri, S., Defina, A., and Marani, M. (2005). Tidal regime, salinity and salt marsh plant zonation. *Estuarine, Coastal and Shelf Science* 62, 119–130. doi:10.1016/j.ecss.2004.08.010.

Simeoni, U., Fontolan, G.; Dal Cin, R.; Calderoni, G.; Zamariolo, A. (2000). Dinamica sedimentaria dell'area di Goro (Delta del Po). *Studi Costieri*, *2*, 139–151.

Simeoni, U.; Gabbianelli, G.; Tessari, U.; Calderoni, G.; Grande, C. (2000). Un Bacile di nome Delta. La Sacca di Goro. Studi Costieri, 2, 31–44.

Simeoni, U., and Corbau, C. (2009). A review of the Delta Po evolution (Italy) related to climatic changes and human impacts. *Geomorphology* 107, 64–71. doi:10.1016/j.geomorph.2008.11.004.

Slobbe, E., Vriend, H. J., Aarninkhof, S., Lulofs, K., Vries, M., and Dircke, P. (2013). Building with Nature: in search of resilient storm surge protection strategies. *Nat Hazards* 65, 947–966. doi:10.1007/s11069-012-0342-y.

Smits, A. J. M., Nienhuis, P. H., and Saeijs, H. L. F. (2006). Changing estuaries, changing views. Living Rivers: Trends and Challenges in Science and Management, 565:339–355, DOI 10.1007/s10750-005-1924-4

Smith, A.E. (1966). Modern deltas: Comparison maps. In *Deltas in Their Geologic Framework, Houston*; Shirley, M.L., Ed.; Houston Geological Society: Houston, TX, USA; p. 223.

Smolders, S., Plancke, Y., Ides, S., Meire, P., and Temmerman, S. (2015). Role of intertidal wetlands for tidal and storm tide attenuation along a confined estuary: a model study. *Natural Hazards and Earth System Sciences* 15, 1659–1675. doi:10.5194/nhess-15-1659-2015.

Spencer, T., Schuerch, M., Nicholls, R. J., Hinkel, J., Lincke, D., Vafeidis, A. T., et al. (2016). Global coastal wetland change under sea-level rise and related stresses: The DIVA Wetland Change Model. *Global and Planetary Change* 139, 15–30. doi:10.1016/j.gloplacha.2015.12.018.

Stark, J., Van Oyen, T., Meire, P., and Temmerman, S. (2015). Observations of tidal and storm surge attenuation in a large tidal marsh: Tidal and Storm Surge Attenuation in a Marsh. *Limnology and Oceanography* 60, 1371–1381. doi:10.1002/lno.10104.

Stark, J., Meire, P., and Temmerman, S. (2017). Changing tidal hydrodynamics during different stages of eco-geomorphological development of a tidal marsh: A numerical modeling study. *Estuarine, Coastal and Shelf Science* 188, 56–68. doi:10.1016/j.ecss.2017.02.014.

Stefani, M., and Vincenzi, S. (2005). The interplay of eustasy, climate and human activity in the late Quaternary depositional evolution and sedimentary architecture of the Po Delta system. *Marine Geology* 222–223, 19–48. doi:10.1016/j.margeo.2005.06.029.

Stevens, R. (1983). A new sand-silt-clay triangle for textural nomenclature. *Geologiska Föreningen i Stockholm Förhandlingar* 105, 245–250. doi:10.1080/11035898309452593.

Stevens, R. L. (1991). Triangle plots and textural nomenclature for muddy sediments. *Geo-Marine Letters* 11, 166–169. doi:10.1007/BF02431005.

Stevenson, J. C., Ward, L. G., and Kearney, M. S. (1986). "Vertical accretion in marshes with varying rates of sea level rise" in *Estuarine Variability* (Elsevier), 241–259. doi:10.1016/B978-0-12-761890-6.50020-4.

Stutz, M.L., Pilkey, O.H., (2002). Global distribution and morphology of deltaic barrier island systems. Journal of Coastal Research 36, 694-707.

Syvitski, J. P. M., Kettner, A. J., Correggiari, A., and Nelson, B. W. (2005). Distributary channels and their impact on sediment dispersal. *Marine Geology* 222–223, 75–94. doi:10.1016/j.margeo.2005.06.030.

Syvitski, J. P. M., Kettner, A. J., Overeem, I., Hutton, E. W. H., Hannon, M. T., Brakenridge, G. R., et al. (2009). Sinking deltas due to human activities. *Nature Geosci* 2, 681–686. doi:10.1038/ngeo629.

Swart, J. P. (1987). Research on the Ratio Marine/Riverine Mud in the Western Scheldt Estuary. Nota NXL-97.015. Utrecht: Rijkswaterstaat, 14.

Takekawa, J. Y.,Woo, I., Athearn, N. D., Demers, S., Gardiner, R. J., Perry, W. M., Ganju, N. K., Shellenbarger, G. G., and Schoellhamer, D. H. (2010). Measuring sediment accretion in early tidal mars restoration, Wet. Ecol. Manag., 18, 297–305.

Temmerman, S., Govers, G., Wartel, S., and Meire, P. (2003). Spatial and temporal factors controlling short-term sedimentation in a salt and freshwater tidal marsh, Scheldt estuary, Belgium, SW Netherlands. *Earth Surf. Process. Landforms* 28, 739–755. doi:10.1002/esp.495.

Temmerman, S., Govers, G., Wartel, S., and Meire, P. (2004a). Modelling estuarine variations in tidal marsh sedimentation: response to changing sea level and suspended sediment concentrations. *Marine Geology* 212, 1–19. doi:10.1016/j.margeo.2004.10.021.

Temmerman, S., Govers, G., Meire, P., and Wartel, S. (2004b). Simulating the long-term development of levee–basin topography on tidal marshes. *Geomorphology* 63, 39–55. doi: 10.1016/j.geomorph.2004.03.004.

Temmerman, S., De Vries, M. B., and Bouma, T. J. (2012). Coastal marsh die-off and reduced attenuation of coastal floods: A model analysis. *Global and Planetary Change* 92–93, 267–274. doi:10.1016/j.gloplacha.2012.06.001.

Temmerman, S., Meire, P., Bouma, T. J., Herman, P. M. J., Ysebaert, T., and De Vriend, H. J. (2013). Ecosystem-based coastal defence in the face of global change. *Nature* 504, 79–83. doi:10.1038/nature12859.

Tesi, T., Miserocchi, S., Goñi, M. A., Turchetto, M., Langone, L., De Lazzari, A., et al. (2011). Influence of distributary channels on sediment and organic matter supply in event-dominated coastal margins: the Po prodelta as a study case. *Biogeosciences* 8, 365–385. doi:10.5194/bg-8-365-2011.

Thomas, M.L.H. (1983). Salt marsh systems. In: Thomas, M.L.H. (Ed.), Marine and Coastal Systems of the Quoddy Region, New Brunswick. Department of Fisheries and Oceans, Ottawa, Ontario, pp. 107–118.

Thomas, S., and Ridd, P. V. (2004). Review of methods to measure short time scale sediment accumulation. *Marine Geology* 207, 95–114. doi:10.1016/j.margeo.2004.03.011.

Thorne, K., MacDonald, G., Guntenspergen, G., Ambrose, R., Buffington, K., Dugger, B., et al. (2018). U.S. Pacific coastal wetland resilience and vulnerability to sea-level rise. *Sci. Adv.* 4, eaao3270. doi:10.1126/sciadv.aao3270.

Trincardi, F.; Cattaneo, A.; Correggiari, A. (2003) Mediterranean Prodelta, Systems Natural Evolution and Human Impact. *Oceanography*, *17*, 37–45.

van der Deijl, E. C., van der Perk, M., and Middelkoop, H. (2018). Establishing a sediment budget in the newly created “Kleine Noordwaard” wetland area in the Rhine–Meuse delta. *Earth Surf. Dynam.* 6, 187–201. doi: 10.5194/esurf-6-187-2018.

Van der Wal, D., Wielemaker-Van den Dool, A., and Herman, P. M. J. (2008). Spatial patterns, rates and mechanisms of saltmarsh cycles (Westerschelde, The Netherlands). *Estuarine, Coastal and Shelf Science* 76, 357–368. doi:10.1016/j.ecss.2007.07.017.

van Loon-Steensma, J. M. (2014). Salt marshes for flood protection. Ph.D. *Wageningen University*.

van Proosdij, D., Ollerhead, J., Davidson-Arnott, R.G.D., Schostak, L.E., (1999). Allen Creek marsh, Bay of Fundy: a macro-tidal coastal salt marsh. The Canadian Geographer 43, 316e322.

van Proosdij, D., Davidson-Arnott, R. G. D., and Ollerhead, J. (2006). Controls on spatial patterns of sediment deposition across a macro-tidal salt marsh surface over single tidal cycles. *Estuarine, Coastal and Shelf Science* 69, 64–86. doi:10.1016/j.ecss.2006.04.022.

van Wijnen, H. J., and Bakker, J. P. (2001). Long-term Surface Elevation Change in Salt Marshes: a Prediction of Marsh Response to Future Sea-Level Rise. *Estuarine, Coastal and Shelf Science* 52, 381–390. doi:10.1006/ecss.2000.0744.

Vandenbruwaene, W., Maris, T., Cox, T. J. S., Cahoon, D. R., Meire, P., and Temmerman, S. (2011). Sedimentation and response to sea-level rise of a restored marsh with reduced tidal exchange: Comparison with a natural tidal marsh. *Geomorphology* 130, 115–126. doi:10.1016/j.geomorph.2011.03.004.

Vandenbruwaene, W., Meire, P., and Temmerman, S. (2012). Formation and evolution of a tidal channel network within a constructed tidal marsh. *Geomorphology* 151–152, 114–125. doi:10.1016/j.geomorph.2012.01.022.

Van Koningsveld, M., Mulder, J. P. M., Stive, M. J. F., VanDerValk, L., and VanDerWeck, A. W. (2008). Living with Sea-Level Rise and Climate Change: A Case Study of the Netherlands. *Journal of Coastal Research* 242, 367–379. doi:10.2112/07A-0010.1.

Veggiani, A. (1994). I deterioramenti climatici dell'Età del Ferro e dell'Alto MedioEvo. Boll. Soc. Torricelliana 45, 1–80.

Vella, C., Fleury, T.-J., Raccasi, G., Provansal, M., Sabatier, F., Bourcier, M., (2005). *Evolution of the Rhône delta plain in the Holocene. Marine Geology 222, 235-265.*

Verney, R., Deloffre, J., Brun-Cottan, J.-C., and Lafite, R. (2007). The effect of wave-induced turbulence on intertidal mudflats: Impact of boat traffic and wind. *Continental Shelf Research* 27, 594–612. doi:10.1016/j.csr.2006.10.005.

Verschelling, E., van der Deijl, E., van der Perk, M., Sloff, K., and Middelkoop, H. (2017). Effects of discharge, wind, and tide on sedimentation in a recently restored tidal freshwater wetland. *Hydrol. Process.* 31, 2827–2841. doi: 10.1002/hyp.11217.

Verza E. and Catozzo L. (2015). *Atlante Lagunare Costiero del Delta del Po*. Consorzio di Bonifica del Delta del Po. Link: https://www.bonificadeltadelpo.it/wp-content/uploads/2016/10/atlante-lagune_ott.pdf

Virgin, S. D. S., Beck, A. D., Boone, L. K., Dykstra, A. K., Ollerhead, J., Barbeau, M. A., et al. (2020). A managed realignment in the upper Bay of Fundy: Community dynamics during salt marsh restoration over 8 years in a megatidal, ice-influenced environment. *Ecological Engineering* 149, 105713. doi:10.1016/j.ecoleng.2020.105713.

Visentini, M. (1940). *Ricerche Idrografiche nel Delta del Po. Ufficio Idrografico del Po-Parma*; Istituto Poligrafico Dello Stato: Roma, Italy; Volume, 14, pp. 175.

Vuik, V., Jonkman, S. N., and van Vuren, S. (2016). Nature-based flood protection: using vegetated foreshores for reducing coastal risk. *E3S Web of Conferences* 7, 13014. doi:10.1051/e3sconf/20160713014.

Wang, Z. B., Van Maren, D. S., Ding, P. X., Yang, S. L., Van Prooijen, B. C., De Vet, P. L. M., et al. (2015). Human impacts on morphodynamic thresholds in estuarine systems. *Continental Shelf Research* 111, 174–183. doi:10.1016/j.csr.2015.08.009.

Wartel, S., Keppens, E., Nielsen, P., Dehairs, F., Van Den Winkel, P. & Cornand, L. 1993. Determination of the ratio marine to terrestrial mud in the Belgian part of the Scheldt estuary. *KBIN and VUB report*. 16 pp.Wehr, A., and Lohr, U. (1999). Airborne laser scanning—an introduction and overview. *ISPRS Journal of Photogrammetry and Remote Sensing* 54, 68–82. doi:10.1016/S0924-2716(99)00011-8.

Weis, P. (2016). “Salt Marsh Accretion,” in *Encyclopedia of Estuaries*, ed. M. J. Kennish (Dordrecht: Springer Netherlands), 513–515. doi:10.1007/978-94-017-8801-4_28.

Wentworth, C. K. (1922). A Scale of Grade and Class Terms for Clastic Sediments. *The Journal of Geology* 30, 377–392. doi:10.1086/622910.

Westoby, M. J., Brasington, J., Glasser, N. F., Hambrey, M. J., and Reynolds, J. M. (2012). 'Structure-from-Motion' photogrammetry: A low-cost, effective tool for geoscience applications. *Geomorphology* 179, 300–314. doi:10.1016/j.geomorph.2012.08.021.

Wehr, A., and Lohr, U. (1999). Airborne laser scanning—an introduction and overview. ISPRS J. Photogramm. Remote Sens. 54, 68–82. doi: 10.1016/S0924-2716(99)00011-8

Wheaton, J. M., Brasington, J., Darby, S. E., and Sear, D. A. (2009). Accounting for uncertainty in DEMs from repeat topographic surveys: improved sediment budgets. *Earth Surf. Process. Landforms*, n/a-n/a. doi:10.1002/esp.1886.

White, W. A., Morton, R. A., and Holmes, C. W. (2002). A comparison of factors controlling sedimentation rates and wetland loss in fluvial–deltaic systems, Texas Gulf coast. *Geomorphology* 44, 47–66. doi:10.1016/S0169-555X(01)00140-4.

Whitehouse, R., Bassoullet, P., Dyer, K., Mitchener, H., and Roberts, W. (2000). The influence of bedforms on flow and sediment transport over intertidal mudflats, Cont. Shelf Res., 20, 1099–1124.

Widdows, J., Brinsley, M., Salkeld, P., and Lucas, C. (2000). Influence of biota on spatial and temporal variation in sediment erodability and material flux on a tidal flat (Westerschelde, The Netherlands). *Mar. Ecol. Prog. Ser.* 194, 23–37. doi:10.3354/meps194023.

Widdows, J., Blauw, A., Heip, C., Herman, P., Lucas, C., Middelburg, J., et al. (2004). Role of physical and biological processes in sediment dynamics of a tidal flat in Westerschelde Estuary, SW Netherlands. *Marine Ecology Progress Series* 274, 41–56. doi:10.3354/meps274041.

Wood, N., and Hine, A. C. (2007). Spatial Trends in Marsh Sediment Deposition Within a Microtidal Creek System, Waccasassa Bay, Florida. *Journal of Coastal Research* 234, 823–833. doi:10.2112/04-0243.1.

Wood, N. J., and Hine, A. C. (2003). Sediment Dynamics of a Sediment-Starved, Open-Marine Marsh Embayment: Waccasassa Bay, Florida. *Journal of Coastal Research* 19, 574–583.

Yellen, B., Woodruff, J., Ladlow, C., Ralston, D. K., Fernald, S., and Lau, W. (2021). Rapid tidal marsh development in anthropogenic backwaters. *Earth Surf. Process. Landforms*, esp.5045. doi:10.1002/esp.5045.

Zhang, K., Liu, H., Li, Y., Xu, H., Shen, J., Rhome, J., et al. (2012). The role of mangroves in attenuating storm surges. *Estuarine, Coastal and Shelf Science* 102–103, 11–23. doi:10.1016/j.ecss.2012.02.021.

Zonta, R., Cassin, D., Pini, R., and Dominik, J. (2019). Assessment of heavy metal and As contamination in the surface sediments of Po delta lagoons (Italy). *Estuarine, Coastal and Shelf Science* 225, 106235. doi:10.1016/j.ecss.2019.05.017.